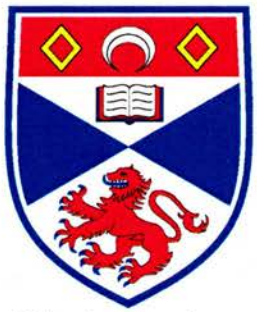

University
of
St Andrews

Exploring Recognition-Mediated Acceleration of Chemical Reactions

Rosalyne Marie Cowie MChem (Hons)

A Thesis Presented for the Degree of

Doctor of Philosophy

in the

School of Chemistry

University of St Andrews

St Andrews **January 2005**

(i) I, Rosalyne Cowie, hereby certify that this thesis, which is approximately 50 000 words in length, has been written by me, that it is the record of work carried out by me and that it has not been submitted in any previous application for a higher degree.

Signature of candidate Date 3/5/05

(ii) I was admitted as a research student in September 2001, and as a candidate for the degree of Doctor of Philosophy in September 2001; the higher study for which this is a record was carried out in the University of St Andrews between 2001 and 2004.

Signature of candidate . Date 3/5/05

(iii) I hereby certify that the candidate has fulfilled the conditions of the Resolution and Regulations appropriate for the degree of Doctor of Philosophy in the University of St Andrews and that the candidate is qualified to submit this thesis in application for that degree.

Signature of supervisor .Date 3/5/05

In submitting this thesis to the University of St Andrews I understand that I am giving permission for it to be made available for use in accordance with the regulations of the University Library for the time being in force, subject to any copyright vested in the work not being affected thereby. I also understand that the title and abstract will be published, and that a copy of the work may be made and supplied to any *bona fide* library or research worker.

Signature of candidate . Date 3/5/05

Abstract

There are many different theories which attempt to rationalise the mechanisms used by enzymes to achieve catalysis. It is difficult to determine exactly which, if any, are the most important factors for catalysis because it is not possible to investigate each one independently. However, small molecule organic catalysts or 'organocatalysts' can be developed which can be used to test different aspects of enzyme catalysis. For example intramolecularity, or the proximity effect, where a reaction is catalysed by locating the reactants close together and thereby rendering the reaction *pseudo*-intramolecular, can be mimicked in a chemical system using recognition-mediated processes.

This thesis describes three different systems developed to test the ability of organocatalysts to accelerate different reaction types. These range from non-polar reactions such as the Diels-Alder reaction through to polar reactions, such as conjugate addition.

Chapter 2 describes an organocatalyst which activates the substrate by polarising it through hydrogen bonding. This organocatalyst was then tested for three different reaction types and was most effective when catalysing a polar reaction.

Chapter 3 describes a system whereby rate acceleration of a Diels-Alder reaction is achieved by holding the reactants in close proximity. This proximity also leads to control of the stereochemistry of the reaction.

Chapter 4 was designed to combine both ideas to create an organocatalyst capable of holding reactants together whilst also activating one of the reactants through polarisation.

The results demonstrate clearly that it is more difficult to accelerate non-polar reactions with simple organocatalysts when compared with polar reactions.

Abbreviations

AIBN	2,2'-azobisisobutyronitrile
Ar	aryl
assoc	association
bi	bimolecular reaction
Boc	*tert*-butoxycarbonyl
Bu	butyl
cat	catalysed reaction
CBz	benzyloxycarbonyl
CIMS	chemical ionisation mass spectrometry
DCM	dichloromethane
DDG	2-dehydro-3-deoxygalactarate
dissoc	dissociation
DMF	*N*,*N*-dimethylformamide
DMSO	dimethyl sulfoxide
DNA	deoxyribonucleic acid
dr	diastereomeric ratio
EDCI	1-(3-dimethylaminopropyl)-3-ethyl carbodiimide hydrochloride
EDTA	ethylenediamine-*N*,*N*,*N'*,*N'*-tetraacetic acid
ee	enantiomeric excess
EIMS	electron impact mass spectrometry
ESMS	electrospray mass spectrometry
FABMS	fast atom bombardment mass spectrometry
FMO	Frontier Molecular Orbital
fwd	forward reaction
gem	geminal
HOMO	highest unoccupied molecular orbital
HPLC	high-pressure liquid chromatography
HRMS	high-resolution mass spectrometry
HSQC	heteronuclear single quantum correlation
Ig	immunoglobulin
IR	infra red
K_a	association constant
KIE	kinetic isotope effect
LNKS	lovastatin nonaketide synthase
LUMO	lowest unoccupied molecular orbital
NAC	near attack conformation
N-AC	*N*-acetylcysteamine thioester
NMR	nuclear magnetic resonance
Pg	protecting group
PMA	phosphomolybdic acid
quant.	quantitative
rev	reverse reaction
t or *tert*	tertiary

THF	tetrahydrofuran
TS	transition state
uncat	uncatalysed reaction
uni	unimolecular reaction
UV	ultra violet

Contents

Acknowledgements

The past three years have not been easy and I would not have been able to complete my PhD without the support and understanding of a lot of great people. Firstly, I would like to thank all the staff in the School of Chemistry for creating a friendly department and maintaining an open doors policy. Without them I would not have been encouraged to stay in St Andrews after finishing my undergraduate degree.

In particular I would like to thank my supervisor Dr Douglas Philp for creating interesting projects for me to work on and providing me with many words of wisdom throughout the years. I would also like to thank the Philp group members past and present: Dr Russell Pearson, Dr Julie Quayle, Dr Simon Turega, (Dr) Eleftherios Kassianidis, (Dr) Mairead Minto, (Dr) Peter Donnelly, and (Dr) Evan Wood. I would particularly like to thank the rest of the "Dream Team": Russell, Elef and Mairead who have been a constant source of support, inspiration and knowledge. I'm sure that the image of Elef and Russell body checking for motivation will stay with us all forever! I would also like to thank our honorary group member (Dr) Gareth Knight for joining us at cake times and teaching me to play the Himalayas!

I would like to thank Melanja Smith for her assistance in NMR, for running all my kinetic experiments and for always being so cheerful and willing to help. I would also like to thank Caroline Horsburgh for running all my mass spec samples extremely quickly, Sylvia Williamson for elemental analysis and Alex Slawin for advice on crystallography.

We have had some wonderful project students over the years who have all done some great work and kept us entertained in the lab. Summer students: Amy Gradwell and Neil Keddie. Honours students: Angus Roy and Ewan "Puppy" M^{c}Neil, have all helped maintain a great atmosphere in the lab. Final year would have been a lot more stressful without Puppy providing some light relief by dancing round the lab!

I have lived with some fantastic people over the past three years who have put up with my moans and complaints whilst also reminding me that there is life outside of chemistry! Amanda (my academic daughter), Tabbie and Keith were all fantastic housemates and friends – even if they thought I was crazy for being a scientist. I would also like to thank my summer housemate Helena who is the most enthusiastic person I know – even about sea lice! Writing

up would not have been possible without the generous hospitality of many people: Russell, Keith, Peter, Calum, Mairead (before she joined the ranks of the homeless!), Amanda, Iain and especially my Grandparents.

During my undergraduate degree I spent 6 months on placement working for DSM in the Netherlands where I actually spent time socialising with chemists – and Walter Broek! Amrish Bohara, Dr Tim Kidd, Dr Lavinia Panella, Dr Lowri Cochlin, Dr Hefziba ten Brink-Ayres and Dr Lee Ayres have always been willing to give me advice on life, chemistry and surviving a PhD!

Back in this country I have very supportive friends who have known me long enough not to take my bad moods personally. I am extremely grateful to Sophie for putting up with me for the last 20 years and for being willing to proof read my thesis despite not having studied chemistry since Higher and hating it with a passion! I would also like to thank Craig for driving me crazy during physics at school, but also for always keeping me entertained and living in fear of the elbow! I must also thank Claire for always being on the other end of the phone and providing me with a place to visit whenever escape from St Andrews was necessary. I also have to thank Mairead again, for not only being a great colleague but also for being a fantastic friend on a daily basis – we've been through a lot together since our carefree undergrad days!

Last but definitely not least I have to thank all my family. I would not have had the opportunity to continue my education without their unfailing support. In particular I would like to thank my wee brothers, Martin and Jonathan, for being my bodyguards all their lives, for being proud of their big sis (some of the time!) and not forgetting about me now that they're high flying finance professionals.

I could never have achieved any of this without my parents, Julian and Anne Marie. They have always believed that I can do anything I put my mind to and have always been there to support me through it. I am also extremely grateful that they realised that constantly wearing pyjamas was a necessary feature of writing up!

This thesis is dedicated to my parents and my brothers.

"'Rabbit's Clever,' said Pooh thoughtfully.
'Yes,' said Piglet. 'Rabbit's clever.'
'And he has Brain.'
... 'I suppose,' said Pooh
'that that's why he never understands anything.' "
-A. A. Milne

"... what can be imagined can be achieved.
That you must dare to dream,
but there is no substitute for
perseverance, hard work... and teamwork.
Because no one gets there alone."
-Chris Carter

1. Introduction

1.1 Preamble

Catalysts are essential in allowing many chemical reactions to proceed at acceptable reaction rates with the desired selectivity. The chemical industry is dependent upon catalysis, and it has been estimated that as many as 80% of industrial processes use catalysts. Consequently the development of new catalysts, or the refinement of existing ones, is big business. It has been suggested that a small increase in selectivity – just 1% – can lead to an increase of operating profits of up to one million dollars.

Many of the catalytic processes require catalysts containing metals and there are concerns about their impact on the environment. Even with careful controls, there is still a risk of releasing chemicals into the atmosphere or into rivers and seas leading to pollution. These catalysts are also often air and water sensitive which means that large volumes of organic solvents are required. Many industrial processes involve toxic solvents, gases and metals, and research into new "green catalysts" is becoming increasingly important. Focus has shifted towards using aqueous systems with non-toxic catalysts.

Naturally, attention turns to biological catalysts because many biological processes are controlled by catalysts. Enzymes are highly evolved, specialised catalysts for a wide variety of reactions. They catalyse reactions with total regio- and stereochemical control at high turnover rates. In the development of new catalysts, enzymes are an ideal model system because reactions are accelerated under mild conditions with high substrate specificity. In order to replicate this efficiency, it is first necessary to understand how enzymes are able to achieve these impressive results. Many investigations have been carried out into the mechanism of enzyme action and there is great debate as to the most important factors.

1.2 Mechanism of Enzyme Catalysis

The first hypothesis to describe an enzyme's ability to catalyse a reaction was proposed by Fischer[1] in 1894. The lock-and-key model was used to explain enzyme specificity whereby the enzyme active site acts as the "lock" which only works when the correct substrate or "key" is present. The active site was viewed as a rigid arrangement of amino acids unaffected by the substrate. This model did not make any provision for product inhibition because it was assumed that product release was automatic as it could no longer fit in the active site.

Koshland[2] recognised the limitations of the lock-and-key model and went on to develop the induced fit theory. In this case, the flexibility of enzymes is acknowledged. In fact, it is a requirement for catalysis to occur. Induced fit proposes that there is a conformational change of the enzyme upon substrate binding which brings the catalytic groups into the correct alignment. Koshland likens the flexibility of the system to a "hand in glove" using Fisher's idea of enzyme and substrate complementarity, but also incorporates the idea of a flexible active site.

Pauling[3] postulated that enzymes achieve catalysis through stabilisation of an activated complex. The activated complex was defined as "the molecular configuration that is intermediate between the reacting substances and the products of reaction for these catalysed processes". This activated complex is now referred to as the transition state of a reaction and it is accepted that stabilisation of the transition state is very important in enzyme catalysis.[4-7] Many different theories have been presented as to the mechanism of rate accelerations achieved by enzymes. Several of the most common will be presented here.

The simplest explanation for the large rate accelerations exhibited by enzymes, is the proximity or approximation effect.[8-13] Enzymes are different from all other catalysts due to their ability to bind the reaction substrates in close proximity to each other, and the catalytic groups within the active site of the enzyme. It is accepted that intramolecular reactions, where reactive sites are covalently bonded, are faster than the analogous intermolecular reactions. Enzymes effectively create a situation whereby the reaction becomes *pseudo*-intramolecular leading to rate enhancement. The debate arises when considering the magnitude[8] of this contribution towards rate enhancement in relation to other factors.

Rate enhancement[14] is calculated by comparing the rate of the intermolecular reaction with the intramolecular reaction or enzyme catalysed reaction (Equation 1). It is expressed in units of concentration because it is a comparison between a bimolecular and a unimolecular reaction. For this reason, rate enhancement is often referred to as the "effective concentration" or "effective molarity". Effective molarity has been formally defined as "the concentration of the catalytic group required to make the intermolecular reaction proceed at the rate of the intramolecular process".[15] Measured values for effective molarity range from 10^{-3} to 10^{16} M.

$$EM = \frac{k_{cat}}{k_{uncat}}$$

Equation 1 Effective molarity can be defined as the ratio of the rates of catalysed and uncatalysed reactions.

Given the wide range of values for rate enhancement, it is natural to ask how much of this can be attributed solely to proximity without considering other factors such as strain or solvation effects. It had been accepted that proximity gave small rate enhancements, and values of 55 M[16] were commonly used. This value was obtained by assuming that reactants A and B are the size and molecular weight of water molecules. Thus, if A is dissolved in neat B, the *pseudo* first order rate constant cannot exceed 55.5 times the rate constant when B is at 1.0 M.[17]

However, it was later proposed by Page and Jencks[18] that large rate enhancements should be expected from proximity alone, and it is actually low values of effective molarities that require further explanation. In order to examine if enzymes produce large rate accelerations through only proximity, comparisons between inter- and intramolecular reactions of simple organic molecules were conducted. From the results obtained, Page and Jencks state that rate enhancements of around 10^8 should be expected for intramolecular reactions, purely on the basis of differences in entropy change. Rate enhancements of less than this value are predicted to arise from unfavourable entropy changes, such as loss of internal rotations and/or potential energy changes in the intramolecular reactions. This theory has been termed "entropy trap" which essentially means that translational and rotational freedom observed in a bimolecular reaction has been "frozen out" in a one-substrate enzymatic or intramolecular reaction.[19,20]

It is suggested that proximity alone is not enough for reaction to occur, but that instead there must be the correct orientation of the orbitals of the reactive sites. This hypothesis led to the introduction of the term "orbital steering".[21-25] There has been evidence[26] for many years

showing an angular component in the wave functions of p, d, and hybrid orbitals; what was not proven was the importance of this in chemical reactivity. Experiments on the rates of acid catalysed lactonisation were conducted using several small organic molecules. Results suggested that the correct orientation of reactants can influence the rate of the reaction by a factor of 10^4 excluding other factors such as proximity. It was calculated that an overlap window of 10° exists, and that outside of this, great rate reductions are observed. The probability of two reactants colliding at precisely the required geometry is small. This theory has been widely disputed.[18,27,28]

Experiments by Menger[29] on the lactonisation rates of rigid bicyclic compounds (Figure 1) with different angles between reactive groups gave very different results. Comparisons between reaction rates for compound **1** with **2**, where the $O_1C_2C_3$ angles are 70° and 80° respectively; and **3** with **4**, where the $O_1C_2C_3$ angles are 76° and 85° respectively, were carried out. According to Koshland, an angle misalignment of 10° could give a 10^4 difference in reaction rates. However, this was not the case. On the contrary, the reaction rates for **1** and **2** or **3** and **4** proved to be virtually identical, showing that an angle displacement of 10° is not kinetically significant.

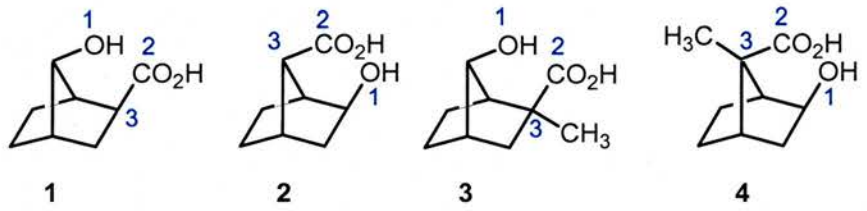

1 **2** **3** **4**

Figure 1 Structures of rigid bicyclic compounds used to investigate angle dependence ($O_1C_2C_3$ angle) upon reactivity. The reactivity of compounds **1** and **2**, with $O_1C_2C_3$ angles of 70° and 80°, were compared and found to be virtually identical. Similarly, the reactivities of **3** and **4** were also virtually identical despite having $O_1C_2C_3$ angles of 76° and 85° respectively.

Instead, Menger gives a different explanation for the rate enhancements observed in intramolecular and enzyme catalysed reactions, known as the "spatiotemporal postulate". It is assumed that the rate of reaction between A and B is proportional to the time that A and B are at a critical distance to each other. This distance is defined as "van der Waals contact distances"[30] which means the distance is too small for solvent molecules to be between A and B. The postulate is similar to the proximity theory, but in this case time is included as a factor and the distances involved are clearly defined.

The energy of desolvation becomes an important consideration in this postulate. In order to bring two reactants within bonding distances, solvent must first be extruded which requires a

significant amount of energy. Thermal energy in a bimolecular reaction is responsible for desolvating reactants, bringing them into close contact, and allowing the complex to proceed to the transition state of the reaction. On the other hand, an intramolecular reaction is accelerated as a result of "covalent energy", which is the energy given to a molecule during synthesis. Consequently, intramolecular reactions are rapid, because the van der Waals complex is already present and does not require energy for its formation.

There is one specific example, the *gem*-dialkyl effect,[31] where there is an angular dependence on rate acceleration. An intramolecular cyclisation reaction is accelerated by replacing hydrogen atoms with alkyl groups on the carbon backbone linking the two reacting groups. It was first postulated in 1915 that the addition of alkyl substituents to a central methylene would lead to angular deformation bringing the two ends of the chain closer together, thus favouring ring closure. This hypothesis was later termed the 'Thorpe-Ingold effect' and was largely forgotten until after the 1950s[32,33] when experimental techniques were refined and unambiguous studies could be carried out. Studies by P. von R. Schleyer[34] have shown that angle deformation does indeed play a minor role within the *gem*-dialkyl effect.

An alternative explanation for the *gem*-dialkyl effect is the "reactive rotamer effect"[35-37] whereby rate enhancement is achieved by the higher population of reactive *syn* rotamers as a result of alkyl substitution. Figure 2 shows Newman projections for two molecules, A and B, which both contain reactive groups, X and Y, which could be diene and dienophile, electrophile and nucleophile, *etc.* In order for reaction to occur, groups X and Y must be close together which requires rotation about the central C-C bonds. Formation of a five-membered ring requires the rotation of two bonds, whereas the formation of a six-membered ring requires the rotation of three bonds. For molecule A, the most stable conformation, and therefore the most populated conformation, is the *anti* conformation where the reactive groups are not in close proximity, thus reaction cannot occur. On the other hand, in molecule B, depending on the size of the alkyl groups, the *anti* conformation is essentially equienergetic with the *gauche* conformation. Consequently, the *gauche* conformation is more populated which favours cyclisation.

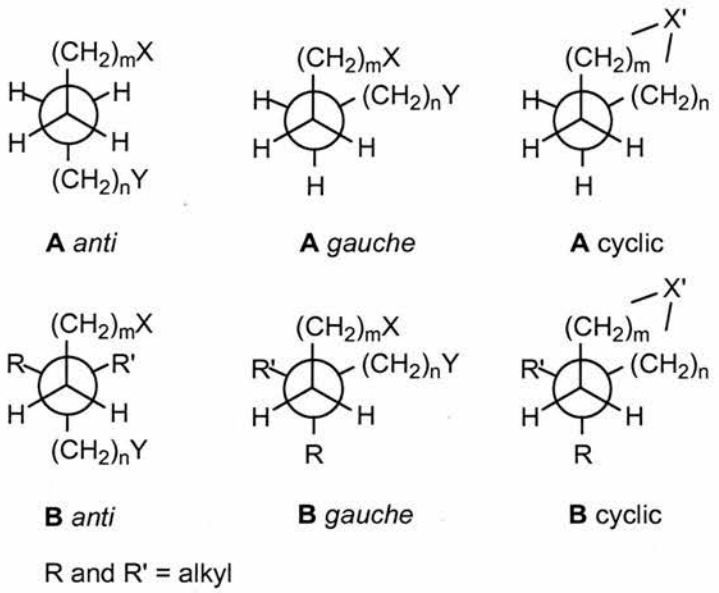

Figure 2 In order for reaction between reactive groups X and Y to occur, the *gauche* conformation must first be adopted. The most stable conformation of molecule A is the *anti* conformation which means that reaction cannot occur. In the case of molecule B, depending on the size of the alkyl groups, the *anti* and *gauche* conformations are equienergetic. Adapted from ref 36.

One hypothesis presented by Bruice[19,38] attempts to incorporate several factors in an attempt to explain the rate enhancements observed in enzymes. Studies were carried out on nucleophilic ester hydrolysis. Bruice proposed that in order for a reaction to proceed to the transition state, a specific ground state conformation must first be achieved. This structure is known as the near-attack conformation (NAC).[39-41] NACs have a specific set of criteria. The conformation occurs when the approaching nucleophile is at a distance of about 3 Å, which is before van der Waals overlap has begun, therefore no bond making or breaking has occurred. The approaching nucleophile must also be within a 30° cone which has an axis 15° off the normal carbonyl plane (Figure 3). The population of the NACs determines the reaction rate – the greater the proportion of NACs in solution, the faster the reaction proceeds.

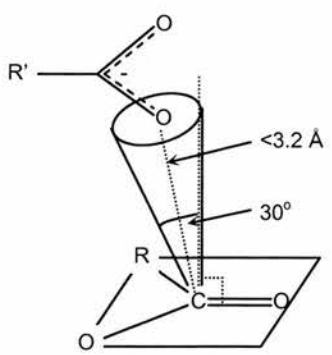

Figure 3 The near attack conformation (NAC) is a ground state conformation where the approaching nucleophile is within a 30° cone with an axis 15° off the normal carbonyl plane. The nucleophile is at a distance of around 3 Å, before van der Waals overlap has begun. Adapted from ref 38.

Molecular modelling calculations were performed on the conformers of selected dicarboxylic acid monoesters. Experiments were carried out by conducting stochastic searches combined with molecular mechanics to identify the ground state conformational equilibria and formation of the NAC. Consequently, quantum mechanics was used to locate the transition state during conversion of the NAC to the product. The energies of the conformations identified were then used in the Boltzmann equation in order to determine the mole fraction of NACs present. Calculations show[41] that a rate enhancement of 10^8 can be expected when the ground state is entirely comprised of NACs.

This theory was later discussed in terms of structural preorganisation,[42] whereby the better the preorganisation of the substrate, the greater the population of NACs. Experiments showed[40] that it was the enthalpy for NAC formation that determined the extent of preorganisation as opposed to entropy. These results contradict the proposal by Page and Jencks that entropy trap is significant in rate enhancement.

One very simple way for an enzyme to catalyse a reaction is to use hydrogen bonding for the activation of the substrate. This process is known as polarisation.[43] Specific amino acid residues within the active site are capable of hydrogen bonding to the substrate in such a way as to withdraw electron density away from the molecule. Consequently, the substrate is activated towards reaction or, in the case of chorismate mutase (discussed in detail in Section 1.4.4), polarisation leads to the stabilisation of charges which develop in the transition state of the reaction.

The difficulty with assessing the significance of any of these hypotheses comes when calculating the effects of other factors. It is not possible to study each effect in isolation, so it is often dependent on which models have been used for calculations. Different values have been suggested for the contributions from entropy, proximity, angular dependence, reactive rotamers, solvent and strain *etc.* To date there is still no satisfactory explanation, taking all data into consideration, for the large rate accelerations observed in enzyme catalysed reactions. What is clear is that no single effect appears to be responsible for the rate enhancements observed, rather that a combination of factors is required.

1.3 Classification of Reaction Types

Before discussing specific examples of reactions catalysed by enzymes, it is necessary to define different reaction types. There are three mechanisms by which organic reactions can occur:[44] radical reactions, polar reactions or pericyclic reactions. Before discussing the different reaction mechanisms, it is useful to consider covalent bonding. All reactions involve bond making and bond making steps. There are two ways in which a covalent two-electron bond can be formed or broken, in an electronically symmetrical or unsymmetrical manner.

Firstly, when examining bond breaking (Figure 4) it can be seen that homolytic, or symmetrical, cleavage can occur to leave each fragment with one electron. Homolytic cleavage results in the production of radical species which contain an unpaired electron. Conversely, heterolytic, or unsymmetrical, cleavage can occur to produce one fragment with both electrons and one with no electrons from the covalent bond. This cleavage produces an anion and a cation.

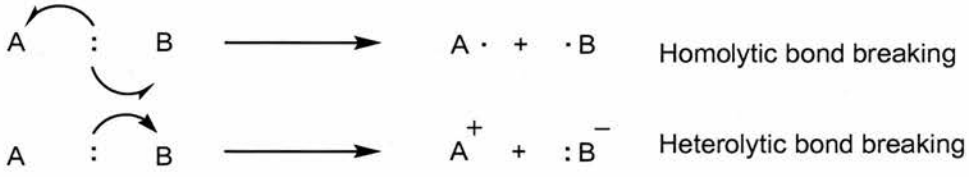

Figure 4 There are two ways a bond can be broken: homolytically or heterolytically. In homolytic cleavage, one electron is donated to each fragment, whereas in heterolytic cleavage, one fragment retains both electrons from the bond. Adapted from ref 44.

Similarly, bond making (Figure 5) can occur in a homogenic, or symmetrical, manner where both fragments donate a single electron, or it can occur in a heterogenic, or unsymmetrical, manner with one fragment donating both electrons. Reactions involving homolytic or homogenic processes are radical reactions because they involve species containing an unpaired electron. Polar reactions arise from heterolytic or heterogenic processes and involve charged species. The most common type of reaction in organic chemistry involves polar species and are therefore heterogenic processes.

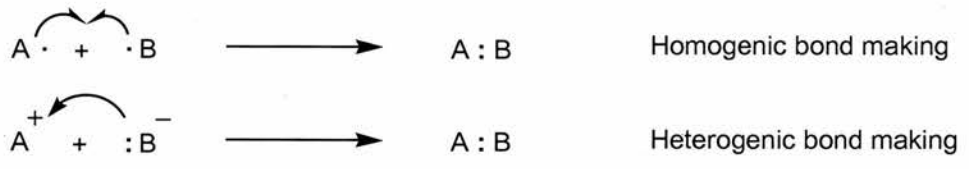

Figure 5 There are two ways a bond can be broken: homogenically or heterogenically. In homogenic bond formation, one electron is donated from each fragment, whereas in heterogenic bond formation, the anion donates both electrons. Adapted from ref 44.

Radical reactions involve species which are electrically neutral, but which are highly reactive as a consequence of the odd number of electrons present. Many different reactions can be carried out using radical processes; however these will not be discussed in detail here. From our perspective, it is more worthwhile to compare polar reactions and pericyclic, or non-polar, reactions.

1.3.1 Polar Reactions

Polar reactions occur as a consequence of the electrostatic attraction between a positive electrophile and a negative nucleophile. The nucleophile donates both electrons to form the bond as shown in Figure 5. Polar reactions are also identified by reaction intermediates or transition states possessing full positive or negative charges.

1.3.2 Pericyclic Reactions

Pericyclic reactions occur as concerted processes *via* cyclic transition states (Figure 6). 'Concerted' indicates that no intermediates are formed in the reaction; instead bond making and breaking steps occur within the same kinetic step. There are three main classes of pericyclic reactions: cycloadditions, sigmatropic rearrangements and electocyclic reactions.

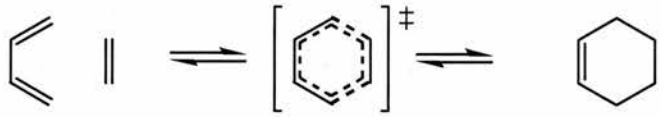

Figure 6 Pericyclic reactions occur in a concerted manner where bond making and bond breaking steps occur within one kinetic step.

Pericyclic reactions are non-polar reactions. However, depending upon the sequence of events within the transition state, it is possible for partial charges to be formed. A synchronous concerted process involves a symmetrical transition state where bond making and bond breaking steps progress to the same degree. The symmetrical nature of the transition state means that unbalanced partial charges do not form and the reaction is truly non-polar. Figure 7 shows the transition state of a synchronous, concerted reaction.

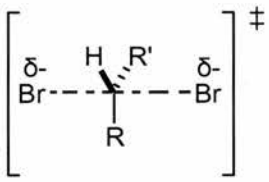

Figure 7 The transition state for a synchronous, concerted S_N2 reaction. The transition state is symmetrical, the approaching nucleophile and the leaving group are identical in shape and charge which means there are no overall partial charges because the bond making and breaking steps proceed at the same time.

In contrast, it has been suggested[45,46] that no Diels-Alder reactions are ever synchronous because they contain unsymmetrical transition states. One C-C bond is formed more rapidly than the other, leading to the formation of one short and strong bond at the same time as the other C-C bond is long and weak. The example shown in Figure 6 could also be depicted as shown in Figure 8.

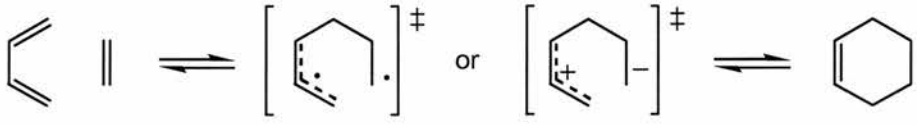

Figure 8 The Diels-Alder reaction is asynchronous which means one C-C bond forms before the second C-C bond is formed so the transition state could be represented as a biradical or a zwitterion. Adapted from ref 45.

This asynchrony is important when considering ways to accelerate a Diels-Alder reaction. If the process was truly non-polar then there would be no possibility of achieving catalysis by simply stabilising partial charges with carefully positioned complementary functionality. The Diels-Alder reaction can be considered a two-stage reaction because it is a concerted reaction with no stable intermediates and it is also asynchronous. Moving from a two-stage reaction towards a stepwise reaction leads to an increase in transition state charge which increases the possibility of catalysis through stabilisation of charges.

1.3.3 Cycloaddition Reactions

Cycloaddition reactions involve two unsaturated molecules reacting to form a cyclic product. The Diels-Alder reaction is one of the most well known cycloaddition reactions. It is known as a [4+2] cycloaddition because it involves 4π electrons from a diene reacting with 2π electrons from a dienophile to form a cyclohexene product. Diels-Alder reactions often proceed under mild conditions and are stereospecific reactions. For example, in the room temperature reaction between 1,3-butadiene **5** and the alkene isomers, **6** and **8**, shown in Scheme 1, the stereochemistry of the starting material is retained in the product. *Cis* alkene **6**

always produces *cis* cyclohexene **7**, likewise *trans* alkene **8** always yields *trans* cyclohexene **9**.

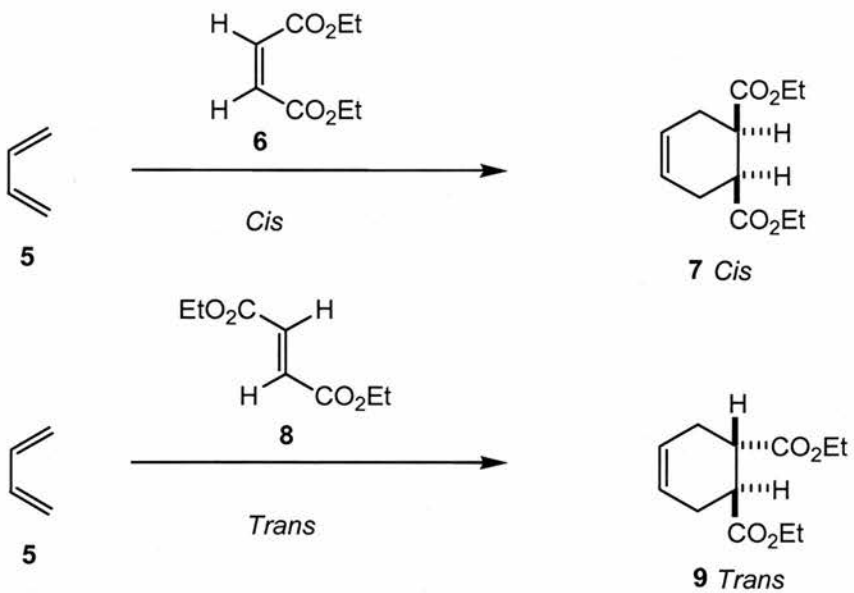

Scheme 1 The stereochemistry of a substrate is always retained in the product of a Diels-Alder reaction. Therefore, reaction of **5** with **6** always produces **7**, and reaction with **8** always produces **9** as the only product. Adapted from ref 44.

1.3.4 Sigmatropic Rearrangement Reactions

A sigmatropic rearrangement reaction is one where a σ-bonded substituent migrates across a π electron system. The transition state for the rearrangement involves breaking one σ bond, moving π bonds and forming a new σ bond, for example a [3,3] sigmatropic rearrangement reaction is shown in Scheme 2.

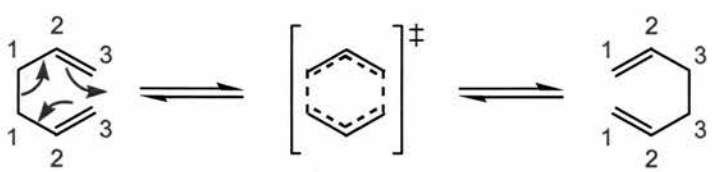

Scheme 2 A [3,3] sigmatropic rearrangement showing the cyclic transition state. Adapted from ref 44.

The Claisen rearrangement reaction is also an example of a [3,3] sigmatropic rearrangement which will be discussed in more detail in Section 1.4.4.

1.3.5 Electrocyclic Reactions

Electrocyclic reactions involve the cyclisation of polyenes where a cyclic product is obtained through breaking one π bond, rearranging the other π bonds and forming a new σ bond. Two

examples of these reactions are shown in Scheme 3. In both cases the conjugated polyene and cyclic product are in equilibrium. The position of the equilibrium depends on the molecules in question. Generally, a triene *e.g.* **10** will favour cyclised product **11**, whereas a diene *e.g.* **5** will favour the linear ring-opened product instead of cyclised product **12**.

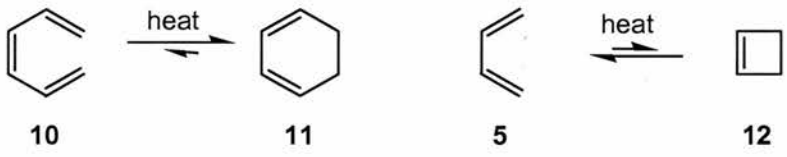

Scheme 3 The thermal products of electrocyclic cyclisation reactions of conjugated dienes and trienes lead to different product distributions at equilibrium. At equilibrium, the cyclisation of conjugated triene **10** favours cyclohexadiene **11**, whereas the reaction for diene **5** favours the starting material instead of cyclobutene **12**.

Electrocyclic reactions can be carried out under thermal or photochemical conditions. There are interesting differences in the stereochemical outcome of thermal and photochemical reactions (Scheme 4). Under thermal conditions (2*E*, 4*Z*, 6*E*)-octatriene **13** will only give the *cis*-cyclohexadiene product **14** whereas under photochemical conditions only *trans*-cyclohexadiene **15** will be produced.

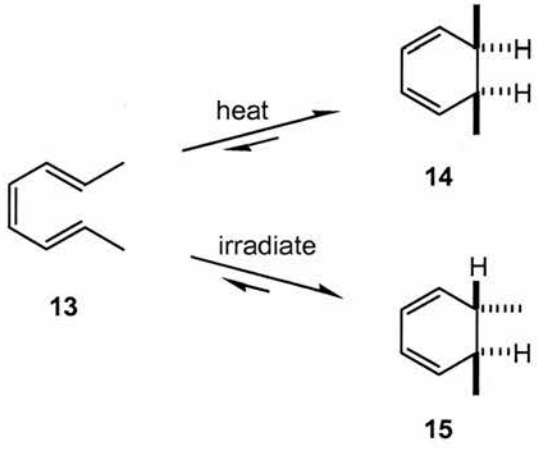

Scheme 4 The stereochemical outcome of electrocyclic reactions are dependent upon reaction conditions. Thermal cyclisation of **13** only produces *cis* isomer **14**, whereas irradiation only gives *trans* isomer **15**.

There is also an interesting difference when comparing the number of natural catalysts and the rate accelerations achieved for polar and non-polar reactions. There are fewer enzymes or catalytic antibodies capable of catalysing non-polar reactions than polar reactions. The rate accelerations achieved are also two orders of magnitude lower for non-polar reactions, as will be discussed in more detail.

1.4 Non-Polar Enzyme Catalysis

In organic synthesis, some of the most useful reactions are non-polar reactions. For example, the Diels-Alder reaction is used extensively for creating multiple ring systems particularly for the total synthesis of natural products. It is therefore surprising that Nature does not also exploit the potential of these reaction types. To date, there have been few enzymes discovered, and still fewer characterised fully, capable of catalysing non-polar reactions.[47,48]

1.4.1 Solanapyrone Synthase

(-)-Solanapyrones A **18** and D **19**, optically active diastereomers, were isolated as phytotoxic substances produced by the fungus *Alternaria solani*.[47,49-51] Isolation of these substances strongly indicated the presence of an enzyme catalysed Diels-Alder reaction in the biosynthetic pathway. Extensive studies conducted using cell-free extracts from *A. solani* failed to lead to the isolation of biosynthetic intermediates from the culture broth. However, studies conducted using isotopically labelled prosolanapyrone II **16** unambiguously confirmed the biosynthetic pathway shown in Scheme 5.

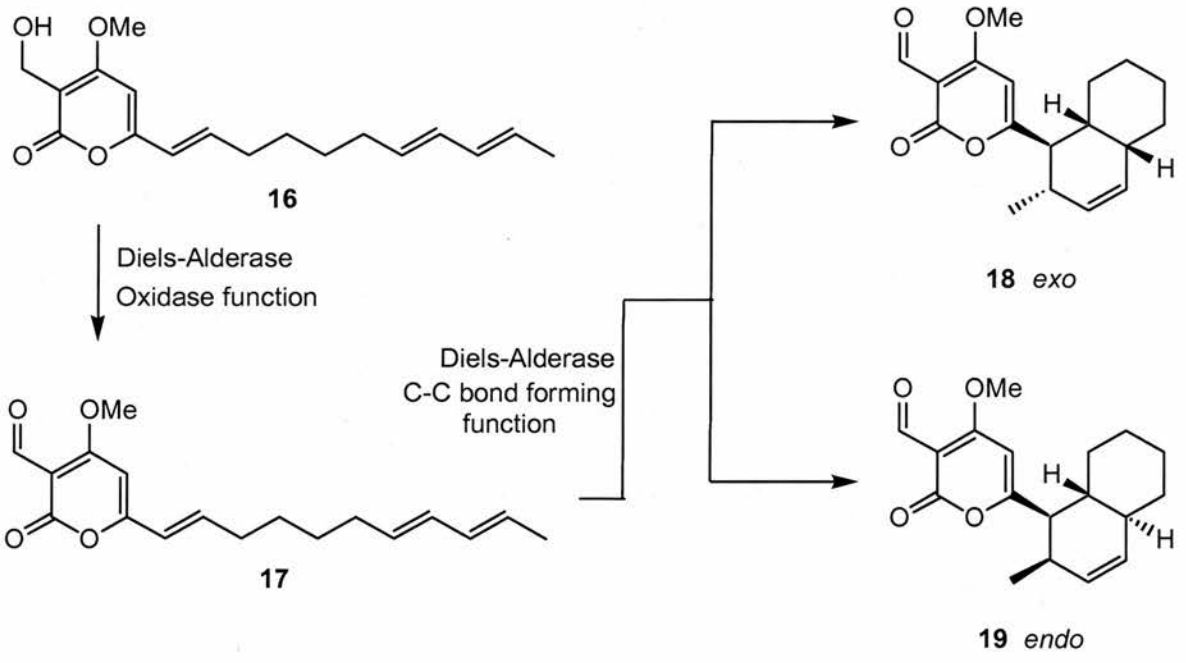

Scheme 5 The proposed mechanism for the two step reaction catalysed by solanapyrone synthase whereby the enzyme first oxidises prosolanapyrone II **16** to prosolanapyrone III **17** before catalysing the cyclisation reaction to form (-) solanapyrone A **18** and (-) solanapyrone D **19**. Adapted from ref 47.

The enzyme first catalyses the oxidation of **16** to prosolanapyrone III **17**, before catalysing the cyclisation reaction to form **18** (*exo*) and **19** (*endo*). The cell free extract was found to give greater *exo* selectivity than the control reaction. It was confirmed that the enzyme is responsible for the oxidation of **16** to **17** by carrying out reactions under an argon atmosphere which led to total suppression of the cycloaddition reaction.

Comparisons of the reaction rates of the non-enzymatic and enzymatic reactions show that the non-enzymatic reaction is in competition with the enzymatic reaction. From these observations it has been proposed that the major role of solanapyrone synthase is in the oxidation of **16** to more reactive **17**, and in stabilisation of the *exo*-transition state.

Studies also show that the enzyme preferentially selects the disfavoured diastereomer. The non-enzymatic Diels-Alder reaction of **17** gives no reaction in organic solvents but favours **19** in aqueous media. There are different theories as to why **19** is the favoured product. It has been suggested by Breslow[52] that hydrophobic effects are responsible; water forces the substrate to adopt the more compact *endo*-transition state to minimise the surface exposed to the aqueous media. It has also been proposed that hydrogen-bonding between the water and dienophile carbonyl group acts to reduce the energy of the LUMO which enhances the reactivity of the substrate.

1.4.2 Lovastatin Nonaketide Synthase

Lovastatin nonaketide synthase[47,53-57] (LNKS) was the first purified enzyme proven to catalyse a Diels-Alder reaction. The enzyme is found on the biosynthetic pathway for the production of the fungal polyketide lovastatin **22** (also known as mevinolin, monacolin K or Mevacor). Polyketide **22** is a powerful inhibitor of the biosynthetic pathway for cholesterol in humans and is therefore used as a treatment for coronary heart disease. Scheme 6 shows the proposed biosynthetic pathway for **22**, where the decalin ring system is produced *via* the [4+2] cycloaddition of an intermediate hexaketide **20**.

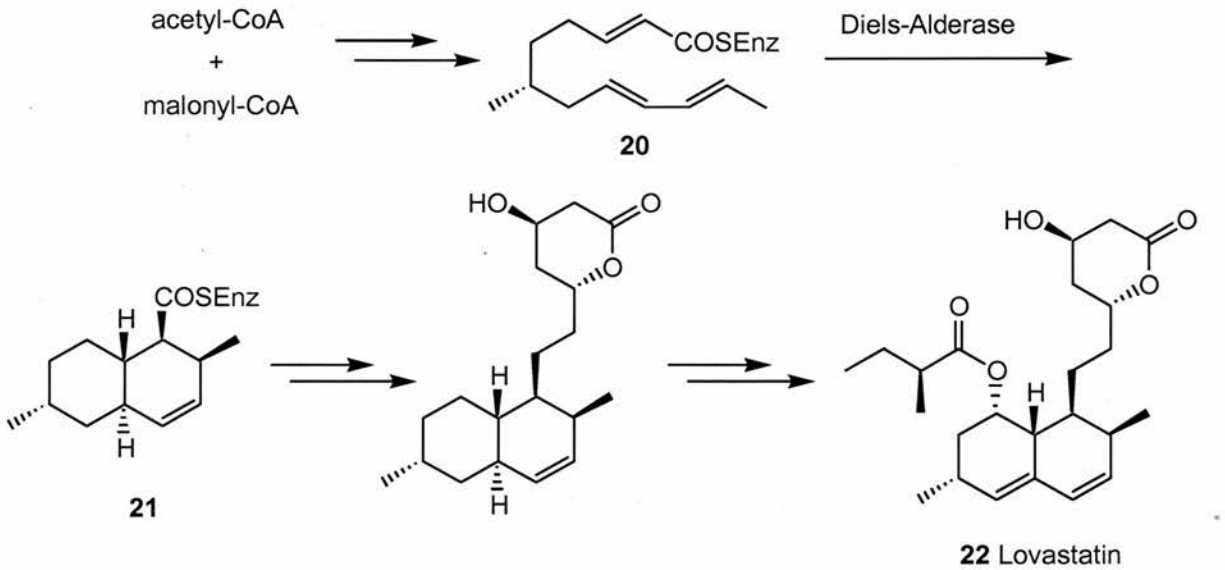

Scheme 6 The proposed biosynthetic pathway for the production of lovastatin **22**. The key step involves the intramolecular Diels-Alder cyclisation of **20** to form intermediate **21** catalysed by lovastatin nonaketide synthase. Adapted from ref 58.

Studies[58] using the substrate analogue (*E*,*E*,*E*)-(*R*)-6-methyl-dodecatri-2,8,10-enoic acid *N*-acetylcysteamine (*N*-AC) thioester **23**, shown in Scheme 7, with the four possible isomeric products from a Diels-Alder reaction have shown that a sample of purified LNKS does indeed catalyse an intramolecular Diels-Alder reaction. The resulting bicyclic system has the same stereochemistry as **22** which is different to those products obtained by the nonenzymatic cyclisation.

Experiments have shown that in the absence of LNKS, a 1:1 mixture of **25**:**26** is formed. In contrast, addition of purified LNKS shows a 15:15:1 ratio of isomers **25**:**26**:**27**. Denaturing the enzyme and repeating the experiment led to the formation of only isomers **25** and **26** as in the case of nonenzymatic cyclisation. In order to form product **27**, the starting material must adopt a sterically hindered transition state with the C-6 methyl group in a *pseudo*axial conformation.

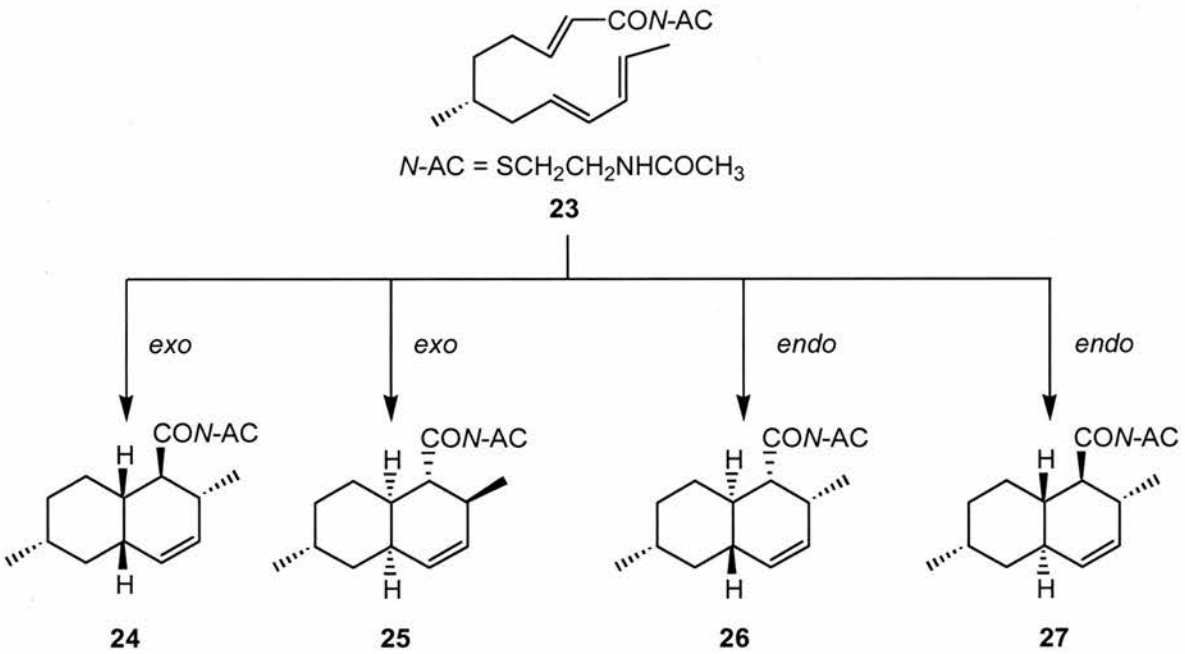

Scheme 7 The Diels-Alder reaction of **23**, a substrate analogue of **20**, leads to the formation of four possible isomeric products **24**, **25**, **26** and **27** in different ratios.

It appears that LNKS binds the substrate in the correct conformation to produce the desired stereochemistry of the unfavoured *endo* isomer. It is also suggested that the enzyme acts as a Lewis acid through hydrogen bonding to the carbonyl group in order to activate the dienophile towards attack.

1.4.3 Macrophomate Synthase

Macrophomate synthase[59] is another enzyme categorised as a Diels-Alderase. The enzyme is from the fungus *Macrophoma commelinae* which is capable of catalysing a five-step transformation from 2-pyrone derivatives *e.g.* **29** and oxalacetate **28** to benzoate derivatives *e.g.* **30** (Scheme 8). Macrophomate synthase is an Mg^{2+}-dependent enzyme which catalyses three separate chemical steps: a decarboxylation reaction, C-C bond formation and dehydration. The C-C bond formation reaction is of particular interest because it is proposed that the enzyme uses a Diels-Alder reaction to obtain the bicyclic intermediate. The mechanisms of the three chemical steps have been extensively studied.[60,61]

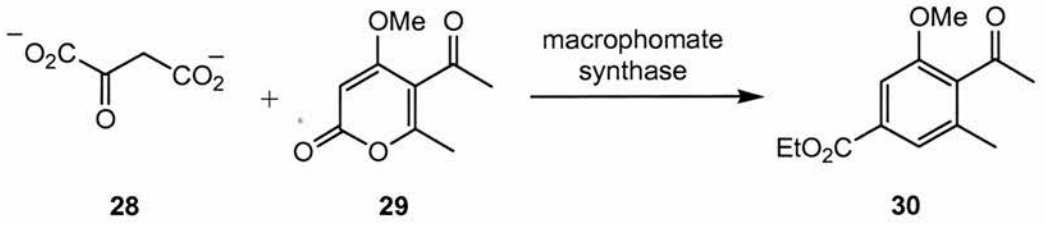

28 **29** **30**

Scheme 8 The enzyme macrophomate synthase catalyses the reaction between oxalacetate **28** and 2-pyrone derivatives *e.g.* **29** in a five step transformation. One step is reported as a Diels-Alder reaction.

The first step involving the decarboxylation of **28**, is Mg^{2+}-dependent. Experiments were conducted to replace Mg^{2+} with other divalent metal cations. Firstly, the enzyme was incubated with EDTA to remove Mg^{2+} before other metals were tested. Decarboxylation activity was only restored when Mg^{2+} was added. Atomic absorption and titration experiments also showed that the stoichiometry of magnesium:enzyme is 1:1. In the absence of **29**, the enzyme acts solely as a decarboxylase with high catalytic efficiency.

The final step is the decomposition of the bicyclic intermediate *via* a dehydration reaction involving *anti*-elimination with concomitant decarboxylation. Kinetic analysis has shown that the final step is in fact the rate limiting step of the reaction pathway.

The most interesting step is the C-C bond formation reaction. The mechanism has been studied extensively and following publication of the crystal structure[62] of the enzyme it has been proposed that the enzyme utilises a Diels-Alder reaction to form the bicyclic intermediate **31** as shown in Scheme 9.

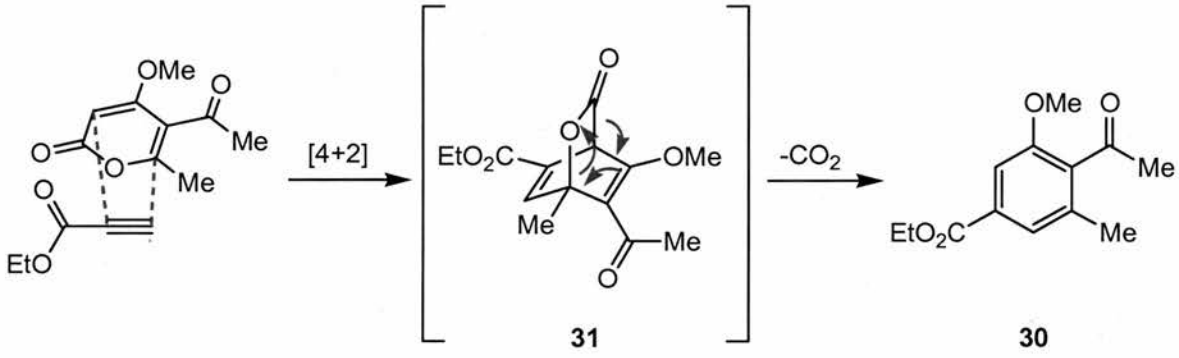

31 **30**

Scheme 9 The proposed reaction mechanism for the [4+2] cycloaddition reaction catalysed by macrophomate synthase involving a Diels-Alder reaction. Adapted from ref 58.

The crystal structure of macrophomate synthase complexed with Mg^{2+} and pyruvate shows that the enzyme is comprised of three dimers forming a hexameric molecule with the active site at the interface. The tertiary and quaternary structures are comparable with the structure of 2-dehydro-3-deoxygalactarate (DDG) aldolase. DDG aldolase catalyses the transformation

of DDG to pyruvate and tartronic semialdehyde *via* a reversible aldol reaction. The authors state that the catalytic activities of both enzymes are very different so no conclusions can be drawn about similarities in the mechanism of the reactions. However, it is possible to draw the mechanism of formation of **31** *via* a Diels-Alder reaction or *via* a Michael-aldol reaction (Scheme 10). The authors have been unable to prove to date that the reaction is concerted and does not occur by stepwise reaction.

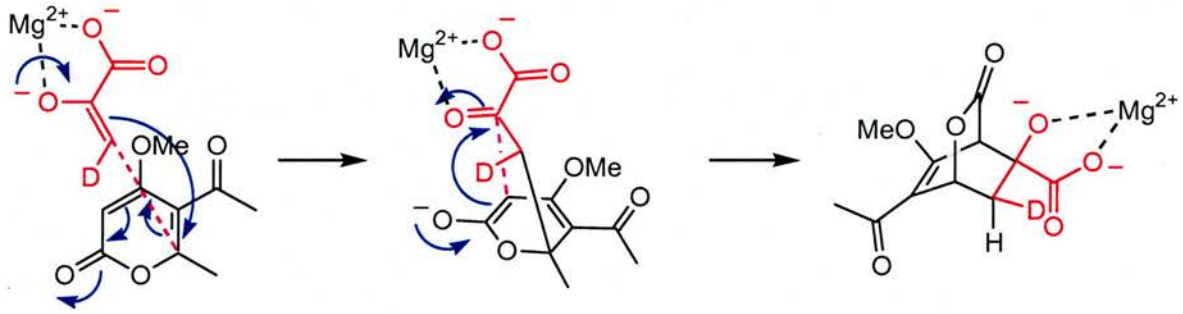

Scheme 10 The alternative Michael-aldol mechanism for the reaction catalysed by macrophomate synthase. Adapted from ref 59.

1.4.4 Chorismate Mutase

The conversion of (-)-chorismate **32** to prephenate **33** is a key step in the shikimate pathway[63] for the biosynthesis of the aromatic amino acids tyrosine and phenylalanine in higher plants, bacteria and fungi (Scheme 11). The enzyme responsible for this process is chorismate mutase, and thus, the enzyme is an ideal target for developing herbicides and antibacterial therapeutics. Chorismate mutase is one of the few characterised naturally occurring enzymes to catalyse a pericyclic reaction – an intramolecular Claisen-type rearrangement – from **32** to **33**. The reaction is very interesting to study because intramolecularity plays no role in the method of enzyme catalysis. The reaction is already intramolecular, so the enzyme cannot accelerate the reaction simply by holding the reactants in close proximity. There must be other factors involved in catalysis. Extensive studies have been conducted to try to probe the mechanism of this enzyme capable of catalysing an unusual rearrangement.[64-80]

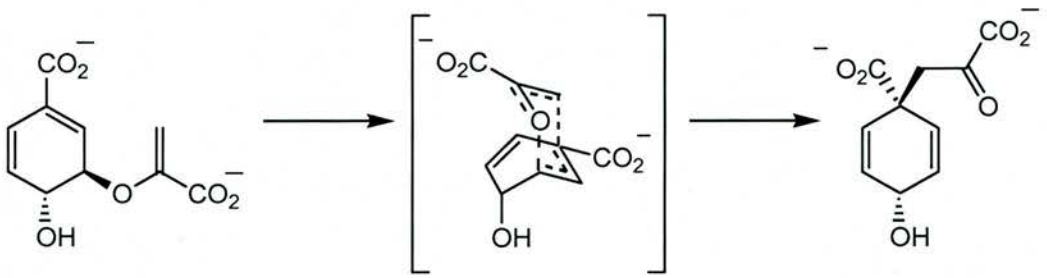

32 **33**

Scheme 11 The rearrangement of (-)-chorismate **32** to prephenate **33** *via* the *pseudo* axial conformation.

There is poor sequence homology in chorismate mutases from different organisms which gives the potential for the development of specific inhibitors for particular plants or micro organisms. The crystal structure of chorismate mutase from wild type *Bacillus subtilis*[69-88] has been obtained (Figure 9). The enzyme from *B. subtilis* is the smallest natural chorismate mutase and is easier to use in mechanistic studies because it is monofunctional, unaffected by product amino acids and also displays Michaelis-Menten kinetics. The crystal structure shows that the enzyme is a homotrimer with three equivalent active sites found at the interfaces of two adjacent subunits.

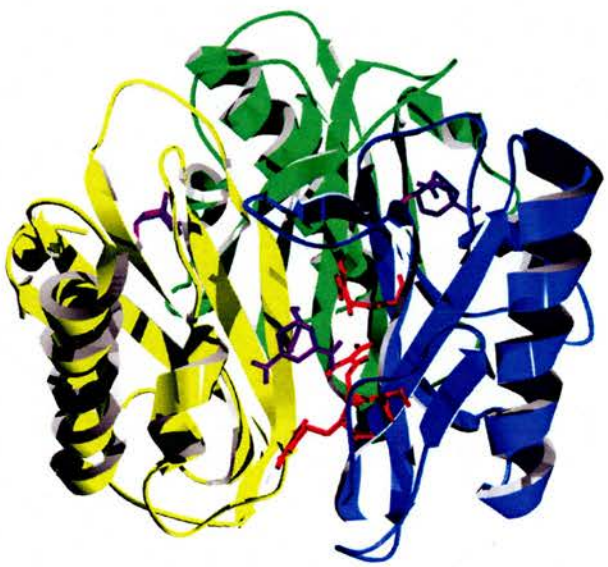

Figure 9 Crystal structure of chorismate mutase from *Bacillus subtilis*, the three subunits are shown in yellow, blue and green. The three active sites are indicated by the three inhibitor molecules shown in purple. Arginine residues, shown in red, hold the substrate in the active site and activate it through polarisation.

The location of the active site was also obtained by solving the crystal structure of the enzyme complexed with a transition state mimic that acts as an inhibitor. This structural study has established the presence of arginine residues in the active site capable of forming hydrogen

bonds to the ether and carbonyl oxygens (shown in detail in Figure 10). The structure of the active site gives further proof of the mechanism of the reaction. There are no functional groups in the region of the ether oxygen capable of proton transfer. This observation suggests a pericyclic reaction is occurring in a similar manner to the uncatalysed reaction. Chorismate is inherently capable of undergoing a rearrangement reaction and the enzyme acts as a template. Rate acceleration occurs through stabilising the transition state of the reaction by holding chorismate in the active conformation.

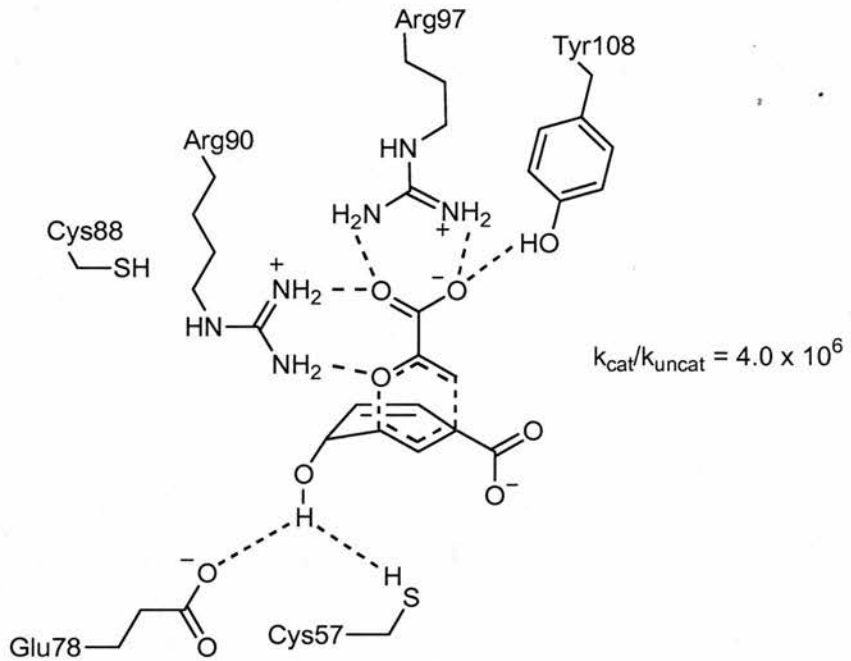

Figure 10 Diagrammatic representation of the active site of chorismate mutase from *Bacillus subtilis* showing key active site residues.

In order to probe the activity of the enzyme, mutation experiments[71] were performed which involved randomising key sequences in the active site. It was found that the only active mutants were those containing a positively charged residue in the region of the ether oxygen.

Kinetic isotope effect (KIE) studies,[72] using chorismate labelled with ^{13}C and ^{18}O as a substrate for chorismate mutase from *B. subtilis*, have shown that the Claisen rearrangement proceeds through an asynchronous and concerted transition state (see Section 1.3.2).

It has been shown both experimentally[73-75] and also through molecular modelling[76-79] that breaking of the C-O bond occurs more rapidly than C-C bond formation in the transition state for the catalysed and uncatalysed reactions. This sequence is important for the enzyme to stabilise the transition state because breaking of the ether bond leads to negative charge

developing on the oxygen and can therefore be stabilised by a positively charged amino acid residue within the active site.

The structure of chorismate mutase from *Escherichia coli*[80] shows very different secondary and tertiary structures to chorismate mutase from *B. subtilis*. The different chorismate mutases also bind chorismate in different ways; although both create a highly charged active site to hold chorismate in the reactive conformation. Crucially, *E. coli* chorismate mutase also contains a charged residue at the ether oxygen position to activate chorismate in a similar manner to chorismate mutase from *B. subtilis*.

It is assumed that rate acceleration arises from preorganisation of the substrate by the enzyme, known as an "entropy trap". The substrate exists as a mixture of conformations[81] in equilibrium (Figure 11) however, only one is reactive. The enzyme selectively binds the *pseudo* axial conformation – the reactive but less populated conformation.

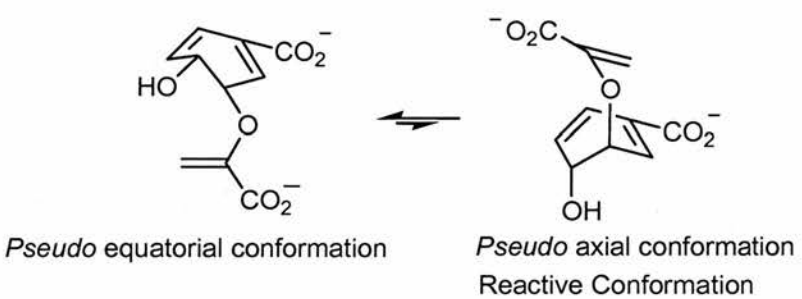

Figure 11 The *pseudo* equatorial and *pseudo* axial conformations of chorismate **33** exist in equilibrium.

Chorismate mutase has also been the subject of extensive computational studies[82-89] into the source of catalytic efficiency. There is debate over the most important factor in catalysis. Some studies[82] have shown that a small deformation in the enzyme leads to the increased stabilisation of this conformation within the enzyme. This deformation was believed to be the main reason for the large rate accelerations observed in the enzyme reaction when compared to the uncatalysed reaction. It is believed that the distortion leads to preferential binding of the near attack conformations (NACs, p.6).

Experiments by Bruice[14,18,87] and co-workers have shown that rate acceleration by the enzyme arises from the greater NAC population within the enzyme compared to in solution. Molecular dynamics simulations have shown that the mole fraction of NAC in water is

0.00007% whereas the mole fraction of NAC found within the active site is 34%. It is claimed that 90% of the kinetic advantage of chorismate mutase when compared to the reaction in water comes from the enzyme's ability to support the NAC in the active site, and only 10% is as a result of its the ability to bind the transition state of the reaction.

Simulations by Lipscomb and co-workers[85] show a close correlation with the transferred nuclear Overhauser effects for chorismate in solution described[86] by Hilvert and co-workers. There is no evidence that the reactive chair-like conformation of chorismate exists in solution for the enzyme to bind. Instead it is proposed that the enzyme binds the more abundant conformations from the solution and converts them into the reactive conformation in the active site. The molecular modelling results show that within the active site unreactive conformations are converted into the chair-like conformation within 50 ps at 300 K.

Recent computational studies[83] have shown that results obtained vary depending upon the type of molecular modelling experiments conducted. Using advanced software to simulate the enzyme catalysed and uncatalysed rearrangement reaction of chorismate in both the gas phase and solvent, is believed to give the most accurate results. In this case, it is proposed that transition state stabilisation plays a major role in rate acceleration. The transition state is stabilised as a consequence of the strengthening of hydrogen bonds to charged residues in the active site. Hydrogen bonds are observed to shorten when binding the transition state which indicates a stronger bond.

Comparisons between chorismate in gas and solution phases with chorismate bound to the enzyme have shown the geometry of the substrate is significantly altered in the enzyme complex. Depending on the modelling method, the distortion or compression of the substrate can have a significant factor in rate acceleration or a minor one. Studies by Martí and co-workers[65,82] have shown that this distortion of the substrate is the determining factor in rate acceleration, whereas recent results by Mulholland and co-workers[83] have shown this distortion to be much smaller and less significant.

In all cases – formation of the NAC or transition state – chorismate is required to form a conformation where two carboxylate groups are held in close proximity. This arrangement is very unfavourable as a result of electrostatic repulsion which means it is difficult for the

substrate to achieve this conformation in water. Conversely, the active site of chorismate mutase is ideal for the formation of the reactive conformation as a result of the alignment of positively charged active site residues. These residues lead to binding of chorismate and the reaction transition state in the most reactive conformation.

Both chorismate mutase and solanapyrone synthase catalyse intramolecular C-C bond formation reactions. Comparing the two enzymes[50] reveals several differences. For example, the K_m values vary from 16 μM in solanapyrone synthase to 100 μM in chorismate mutase obtained from *B. subtilis*. The most interesting difference arises when comparing the reaction rate of the catalysed and uncatalysed reactions. In the case of solanapyrone synthase, the control reaction competes with the catalysed reaction, whereas for chorismate mutase the catalysed reaction proceeds a million times faster than the control reaction.

1.5 Catalytic Antibodies

Antibodies[63,90] are a class of proteins, known as immunoglobulins, produced by the immune system in response to the presence of a foreign substance called an antigen. The immune system cannot elicit a response against a small molecule, but instead reacts with larger molecules such as proteins or polysaccharides. All antibodies have the same general structure (Figure 12), a dimeric Y-shaped assembly composed of a pair of identical light chains and a pair of identical heavy chains connected by disulfide bridges. Both chains are comprised of a variable domain and a constant domain. The variable domain provides diversity to allow the production of large numbers of antibodies to bind to a wide range of antigens. There are five different constant domains which correspond to the five different classes of mammalian immunoglobulins: IgM, IgG, IgA, IgD and IgE.

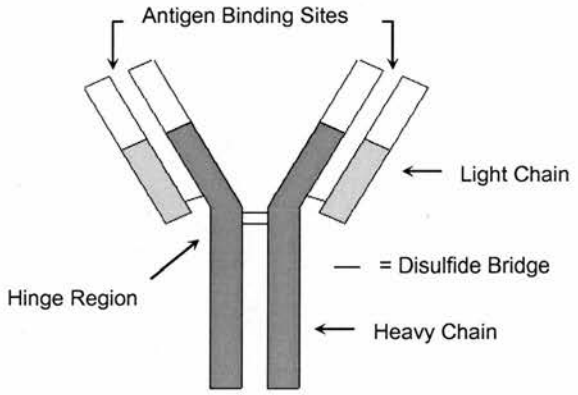

Figure 12 Diagrammatic representation of a typical IgG antibody. Variable domains are shown in white and the constant domains are shown in grey. Adapted from ref 90.

The structure of the constant domain allows the different immunoglobulin classes to perform their specific functions. IgM exists as a pentamer and is the first circulating antibody found in the serum following exposure to an antigen. The pentameric structure allows it to effectively agglutinate antigens. IgA exists as a dimer capable of being transported across epithelia. It is the major class found in external secretions whose main function is to prevent bacteria and viruses attaching to epithelial surfaces. IgD is found on the surface of cells and is membrane bound where it acts as a receptor for antigens to trigger an immune response. IgE comprises the smallest fraction of the total antibodies in the blood and is involved in allergic reactions. The primary class of circulating antibody is IgG, which protects against the circulation of toxins in the blood.

In 1948, Pauling reported[3] that investigations had shown the immune system was capable of producing antibodies against chemical functional groups not found in nature. This flexibility within the immune system gives the potential to create vast numbers of unique antibodies to bind various synthetic or biological molecules with high affinity. It is the exploitation of this ability that has led to the creation of catalytic antibodies.[91-101]

When the immune system is exposed to antigenic material then large numbers of antibodies with different variable regions are produced. From this large pool, a few antibodies with high affinity for the antigenic material will bind and be copied by the immune system to give large numbers of antibodies specific for the antigen. By controlling the structure of the antigen it is possible to screen for specific antibodies with a high affinity for that material.

It is possible to create a transition state analogue for a specific reaction, bind it to a carrier protein (together known as a hapten) and expose it to the immune system to produce antibodies with a high binding affinity for the analogue. It is hoped that these antibodies can then be used to catalyse the reaction. The main aim is to use catalytic antibodies to accelerate reactions for which there are no catalysts known.

For example, the synthesis of the natural product 1-deoxy-L-xylulose[102] **36** has been shortened as a result of antibody catalysis (Scheme 12). Antibody 38C2 was isolated and it was found to be the only known catalyst to accelerate the aldol addition of unprotected hydroxyacetone to an aldehyde *e.g.* **34**. The product dihydroxyketone **35** is isolated in 37% yield with 97% enantiomeric excess (*ee*) after 48 hours with 0.04 mol% antibody catalyst added.

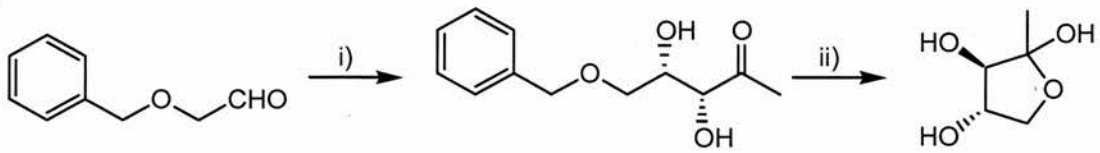

34 **35** **36**

Scheme 12 i) IgG 38C2, hydroxyacetone; ii) $Pd(OH)_2/C$, H_2 (g).

Antibody 38C2[103,104] is unusual when compared to natural enzymes and other catalytic antibodies because it accepts a wide variety of substrates. Unlike transition metal catalysts, the antibody efficiently catalyses both the aldol-addition reaction and the retro-aldol reaction

which allows both aldol enantiomers to be prepared using a single catalytic antibody (Scheme 12).

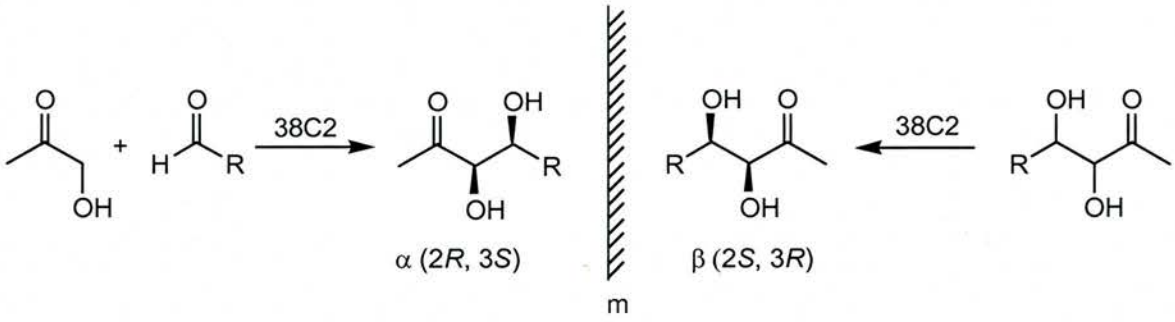

Scheme 13 Antibody 38C2 is unusual because it can be used to form both enantiomers by catalysing both an aldol addition reaction and also the corresponding retro aldol reaction. Adapted from ref 103.

It has already been shown that few enzymes catalyse pericyclic reactions. These reaction types are ideal targets for catalysis by catalytic antibodies. It is difficult to engineer enzymes which catalyse new reactions and accept new substrates[105-113] whereas catalytic antibodies only require the design of an appropriate transition state analogue. Theoretically it should be more straightforward to produce tailor-made catalysts for any reaction using catalytic antibodies. It is interesting to collate the data available on rate accelerations for different reaction types using catalytic antibodies. The graphs in Figure 13 show the number of catalytic antibodies versus rate acceleration for four different reaction types, three polar and one non-polar.

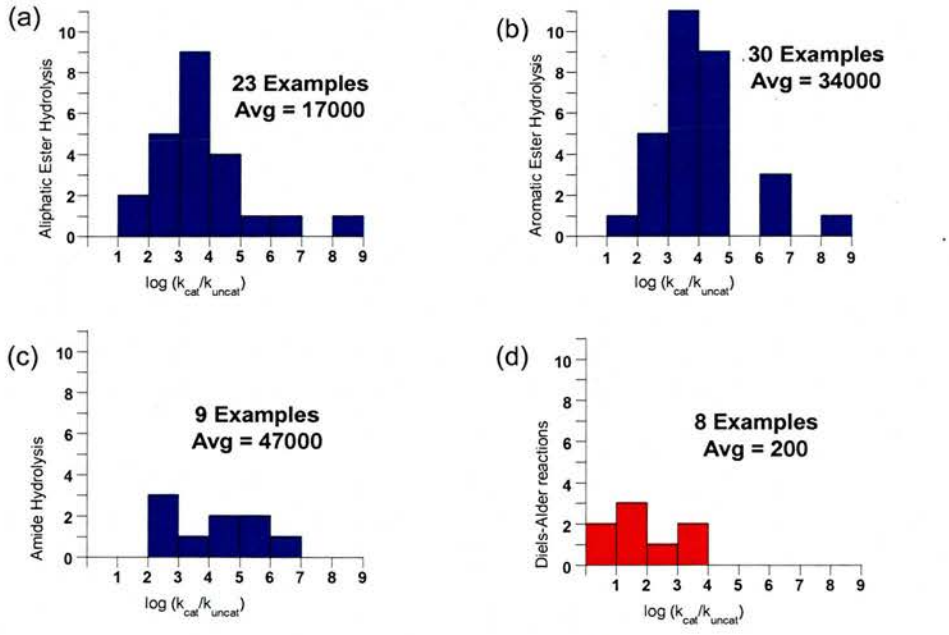

Figure 13 Graphs showing rate acceleration vs number of catalytic antibodies for four different reaction types: (a) aliphatic ester hydrolysis, (b) aromatic ester hydrolysis, (c) amide hydrolysis and (d) Diels-Alder reactions. The polar reactions are shown in blue and non-polar reaction in red. Data from ref 114.

From these graphs, it is clear that there are fewer antibodies which catalyse the Diels-Alder reaction compared to other polar reactions. The rate accelerations recorded for Diels-Alder reactions are also two orders of magnitude lower than polar reactions. There could be many different explanations for these observations.

It is difficult to design transition state analogues for a Diels-Alder reaction because of the inherently product-like transition state. If the transition state analogue binds too tightly to the transition state then it will also bind tightly to the product, which will lead to inhibition and poor turnover.

The first Diels-Alder cycloaddition reaction catalysed by an antibody[115] was reported by Hilvert and co-workers. The reaction used is the cycloaddition reaction between tetrachlorothiophene dioxide **37** and *N*-ethylmaleimide **38** to give tetrachlorodihydrophthalimide **40** *via* an unstable bicyclic intermediate **39** with the release of SO_2 (Scheme 14). This reaction is ideal for demonstrating the feasibility of using antibodies to accelerate Diels-Alder cycloadditions because the product and transition states are very different. It is an unusual reaction in that gas is lost, preventing the product from undergoing the retro Diels-Alder reaction. This feature allows bicyclic transition-state analogue **41** to be used and prevents product inhibition of the catalyst.

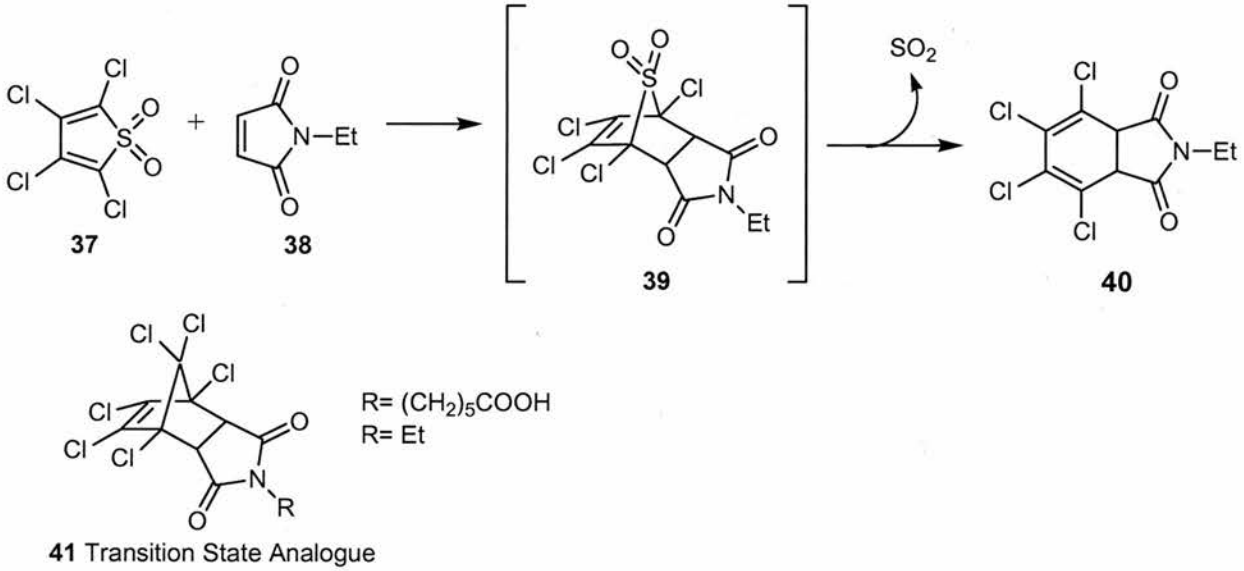

Scheme 14 Antibody 1E9 catalyses the Diels-Alder reaction between **37** and **38**. Transition state analogue **41** is used to elicit an immune response.

Five high-affinity monoclonal antibodies were raised against the transition state analogue hapten and then methylated. Methylation was required to prevent reaction between lysine residues of the antibody and **37**. The methylated antibodies were then tested and it was found that antibody 1E9 gave rate acceleration. The effective molarity for this antibody[116] was determined to be in excess of 10^2 M.

Values for other Diels-Alderases rarely exceed 10 M,[114] making 1E9 one of the most efficient catalytic antibodies for a Diels-Alder reaction. Structural information shows that the antibody is acting as an entropy trap.

Schultz and co-workers[117] used the same hapten to produce catalytic antibodies for this reaction. In this case, k_{cat} values of 0.072 min^{-1} were obtained as opposed to 2.7 min^{-1} in the case of antibody 1E9. This result illustrates a potential problem in using catalytic antibodies – as a result of the vast numbers of antibodies produced there is no guarantee of isolating identical antibodies after exposure to the same antigen.

1.6 Supramolecular Catalysis

Supramolecular chemistry[118-120] is defined as "chemistry beyond the molecule" and exploits covalent and non-covalent interactions to create more complicated systems. One of the most well-known uses for supramolecular chemistry is in self-assembly,[121-127] where larger structures are created using smaller building blocks in a similar way to natural systems such as viruses, DNA or proteins.

Supramolecular catalysis[128] involves using non-covalent interactions, such as hydrogen bonds, to accelerate reactions. There are many different ways in which this goal can be achieved. Three methods will be highlighted here because of their relevance to what follows but the reader is directed to the literature[129,130] for more comprehensive coverage.

1.6.1 AB Methodology

As previously discussed in Section 1.2, intramolecular reactions proceed faster than the corresponding intermolecular reactions. AB methodology aims to take advantage of this information by converting a bimolecular reaction into a *pseudo*-unimolecular reaction through non-covalent interactions. This effect can be more clearly understood by examining the schematic shown in Figure 14. Molecules **A** and **B** have reactive sites, shown in blue and green, which are connected *via* a spacer unit to complementary recognition sites shown in red and yellow. There are two possible reaction pathways available. Firstly, there is the bimolecular pathway where reaction occurs between **A** and **B** to form product **P'** in an uncatalysed reaction. Alternatively, **A** and **B** can associate through the complementary recognition sites to form an **[A•B]** complex which makes the reaction *pseudo*-unimolecular to form product **P** *via* the catalytic **[A•B]** complex-mediated pathway.

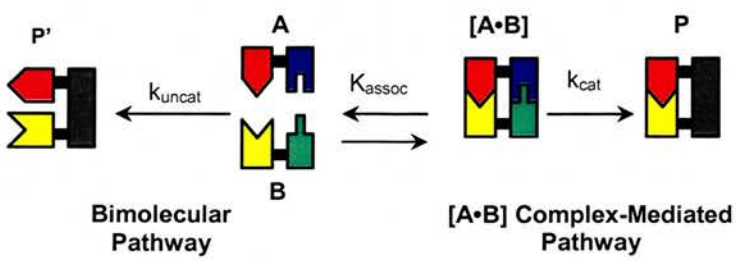

Figure 14 Schematic representation of an **AB** mediated reaction. The bimolecular pathway is the uncatalysed reaction between the blue and green reactive sites. In the **[A•B]** complex-mediated pathway, molecules **A** and **B** first bind through the complementary recognition sites shown in red and yellow, making the reaction *pseudo*-intramolecular.

Several examples[131-135] of systems utilising AB methodology have been reported. Hamilton and co-workers[136,137] developed a system to accelerate acyl transfer reactions. Receptor **42** containing a thiol group was developed with complementary recognition sites to barbiturate acetate derivatives *e.g.* **43**, as shown in Scheme 15.

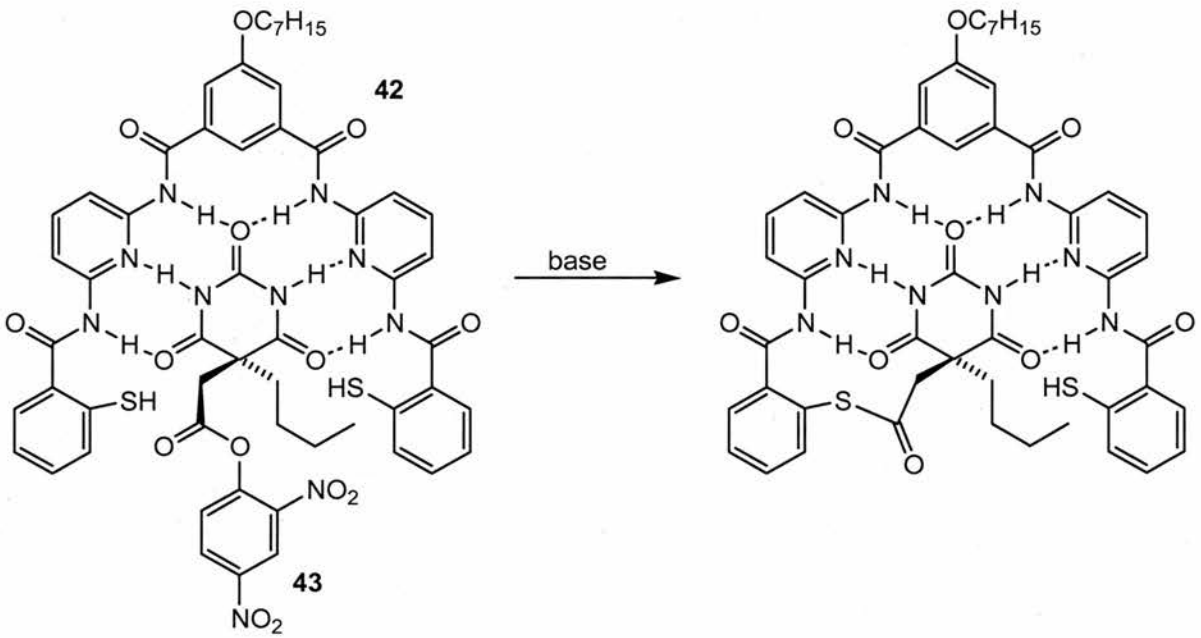

Scheme 15 AB methodology leads to the acceleration of an acyl transfer reaction as a consequence of the complementarity between receptor **42** and the barbiturate derivative **43**.

The system was developed following molecular modelling studies which showed the thiol and carbonyl reactive groups were 3.5 Å apart. Receptor **42** gives a rate acceleration of more than 10^4 as a result of the reaction becoming *pseudo*-intramolecular.

Recently, Philp and co-workers have published[138] an example of a completely selective and strongly accelerated Diels-Alder cycloaddition using AB methodology. The reaction pathway used is shown in Scheme 16. In order to measure the bimolecular rate of the reaction, control compounds were also synthesised and in this case the methyl ester of 3-maleimidopropanoic acid **45** was used.

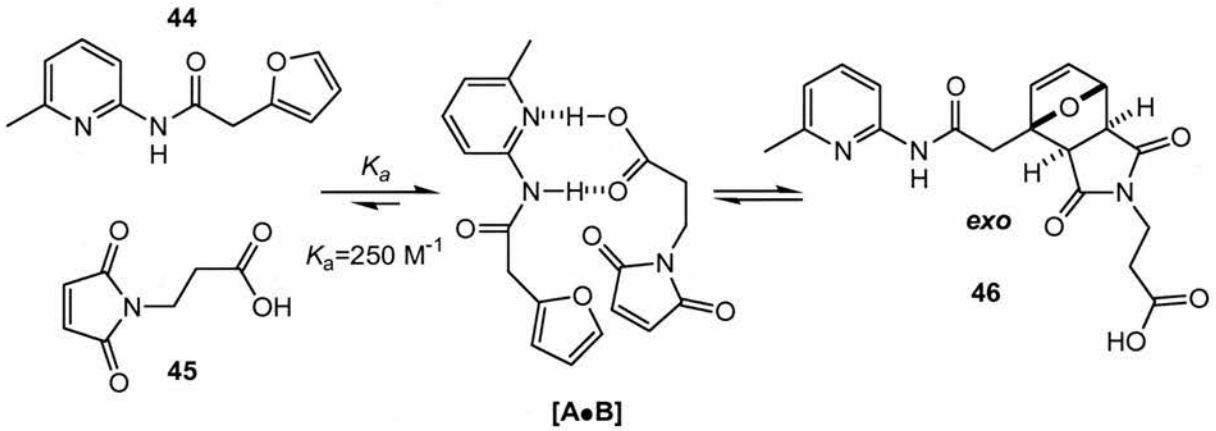

Scheme 16 Reaction between **44** and **45** is accelerated by the formation of an **[A•B]** complex which also controls the stereochemical outcome of the Diels-Alder reaction to form only the *exo* cycloadduct.

Reactions were carried out using 25 mM solutions of **44** and **45** in $CDCl_3$ at 35 °C. The bimolecular reaction led to the formation of both *exo* and *endo* cycloadducts in a ratio of approximately 2:1. A combined conversion of 4% was achieved after 5 hours for the bimolecular reaction; in contrast, the recognition-mediated reaction reached over 80% conversion in the same time period and gave the *exo* cycloadduct **46** as the only product.

This result shows the advantages of this type of methodology where large rate enhancements with stereoselective control can be achieved through a simple hydrogen bonding recognition motif. The main disadvantage of AB methodology is that systems must be designed carefully to ensure that binding occurs between the two building blocks, and that the spacers are the correct length to hold reactive groups in the correct orientation. However, excellent results can be achieved with careful design.

1.6.2 ABC Methodology

Another method of achieving rate acceleration through recognition is to use a bisubstrate reaction template, also known as ABC methodology which is shown schematically in Figure 15. In this case, substrates **A** and **B** are once again comprised of reactive sites and recognition sites separated by a spacer unit. The difference now is that the recognition sites, shown in yellow, are identical as opposed to complementary. The complementary recognition sites are now found on **C**, the reaction template. There are two possible reactive pathways possible depending upon the presence or absence of reaction template. In the uncatalysed reaction, **A** and **B** react *via* the bimolecular pathway to form product **P'**. In the presence of **C**, recognition promotes the formation of an **[A•B•C]** complex to give a **[P•C]** complex *via* a *pseudo*-unimolecular reaction. If dissociation of **C** from **P** occurs then the catalytic cycle is complete.

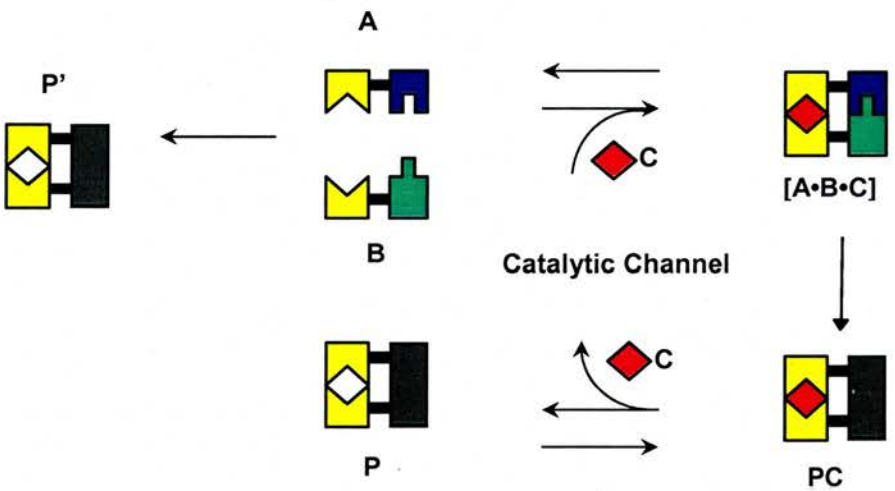

Figure 15 Schematic representation of an **ABC** mediated reaction. In the absence of reaction template **C**, the bimolecular reaction occurs. In the presence of **C**, which has complementary recognition sites to molecules **A** and **B**, the **[A•B•C]** complex is formed to make the reaction *pseudo*-intramolecular. If **C** can dissociate from the product then the catalytic channel is completed.

The **[A•B•C]** complex is not the only ternary complex which will be formed in solution. Clearly, there is also the possibility of forming the unproductive **[A_2•C]** and **[B_2•C]** complexes. The system relies on fast exchange between the **[A•B•C]**, **[A_2•C]** and **[B_2•C]** complexes which means Cutin-Hammett-Winstein-Holness kinetics[139,140] apply. Fast exchange means the **[A•B•C]** complex does not have to be the dominant complex in solution, because any that is present will react, and the rate limiting step is not the formation of the reactive ternary complex.

ABC reactions[141-143] can be carried out using a variety of different types of molecules. The first example[144] of a bisubstrate reaction template accelerating a reaction that would otherwise be intermolecular is reported by Kelly. The mechanistically straightforward S_N2 alkylation of amine **48** by alkyl halide **49** was used in initial investigations. The structure of the productive ternary complex is shown in Figure 16.

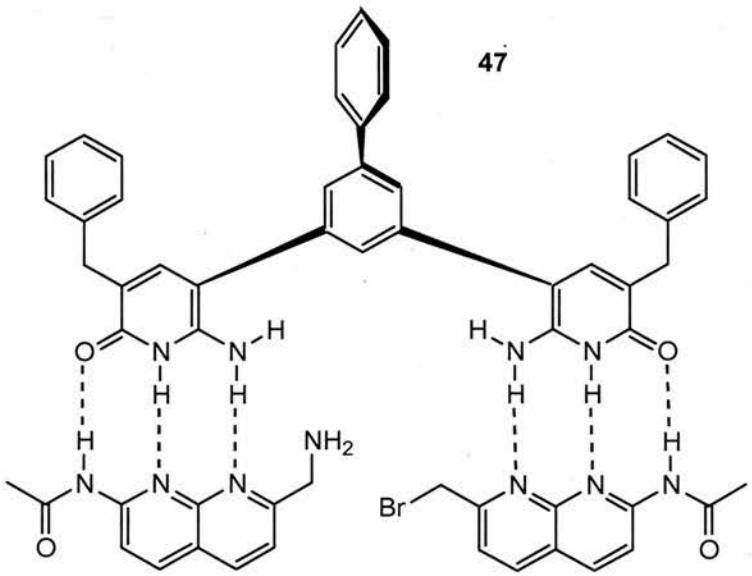

Figure 16 Structure of the ternary complex between Kelly's reaction template **47** and the two substrates **48** and **49** which leads to rate acceleration of an S_N2 alkylation reaction.

Addition of one equivalent (4 mM) of the bisubstrate reaction template **47** gives a 6-fold rate increase for the reaction. ^{1}H NMR titration studies demonstrated that the template is capable of simultaneously binding both substrates. The advantage of this system is that the product precipitates as the hydrobromide salt which prevents product inhibition. A control compound with only one binding site has no effect on the rate of the intermolecular reaction, suggesting that hydrogen bonding has no role in rate acceleration but instead it is proximity that is responsible.

Previously within our group,[145] ABC methodology has been applied using complexes of crown ether derivatives. Experiments were carried out on the base-catalysed aldol reaction between formylbenzo-15-crown-5 **50** and acetylbenzo-15-crown-5 **51**, shown in Scheme 17.

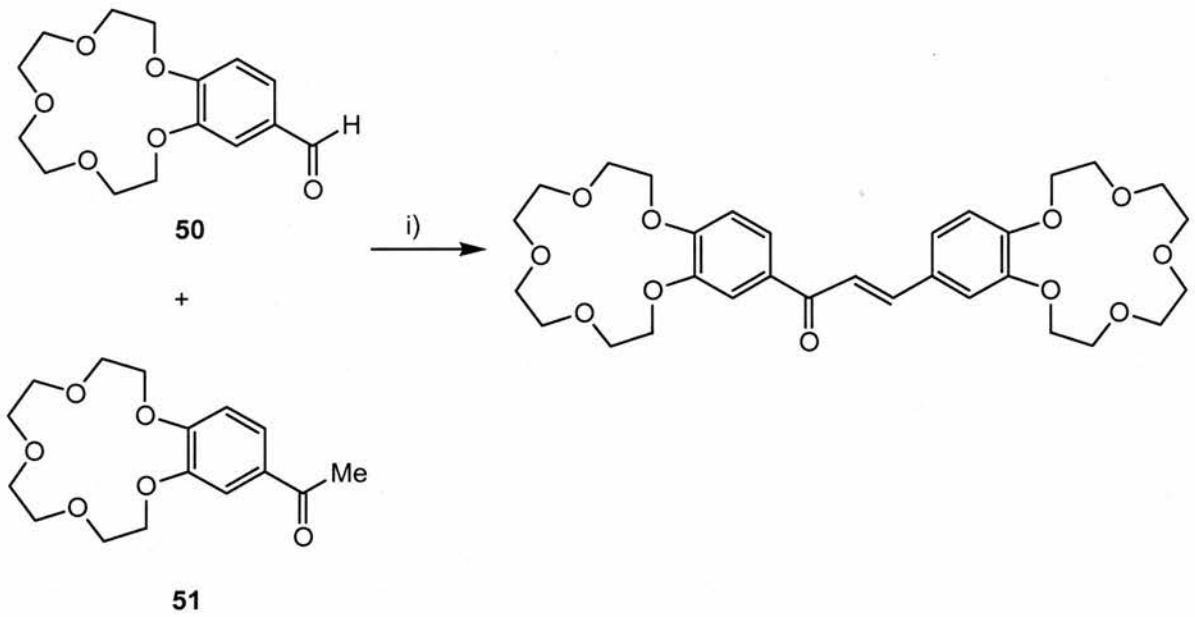

Scheme 17 i) KOMe, MeOH, 50 °C.

The reactive sites on molecules **50** and **51** are held in close proximity by utilising the ability of crown ethers to bind metal cations, in this case K^+ ions. The success of this strategy is dependent on fast exchange between the different crown ether compounds and potassium cation so that Curtin-Hammett kinetics applies as previously described. A schematic of the different complexes involved is shown in Figure 17. Analysis by fast atom bombardment mass spectrometry (FABMS) showed the presence of all three expected complexes with 2:1 stoichiometry for crown ether:metal ion. This result is not sufficient to prove that the system is following Curtin-Hammett kinetics so further experiments were carried out using 300 MHz ^{1}H NMR spectroscopy. Results show that sandwich complexes are indeed formed.

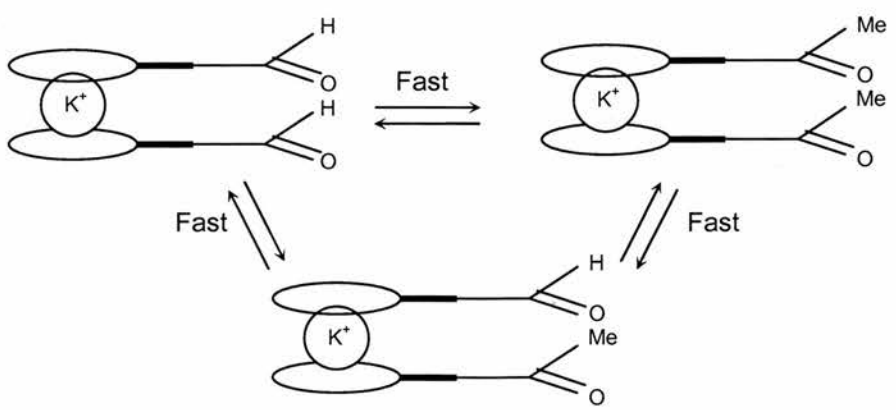

Figure 17 Schematic representation of all complexes in solution: **[A_2•C]**, **[B_2•C]** and **[A•B•C]**. For Curtin-Hammett kinetics to apply all species must be in fast exchange.

The NMR studies were carried out by observing the chemical shift changes in the aromatic protons using solutions of **50** and **51** in d_4-MeOH with varying concentrations of KBF_4. For all concentrations of K^+, upfield shifts of the aromatic protons were observed which strongly suggests that the aromatic rings in **50** and **51** are stacked in a sandwich-type arrangement. When the experiments were repeated using Li^+ or Na^+ ions, only downfield shifts were observed which is consistent with the deshielding effect of the electrophilic cation.

Interestingly, the NMR experiments did not result in the observation of bound and unbound species when KBF_4 was added. This observation would suggest that the complexes are in fast exchange in solution on the NMR time scale, giving rise to a time-averaged spectrum. Therefore, as long as the aldol reaction is much slower than the rate of exchange, the use of Curtin-Hammett kinetics in this system is valid.

The importance of recognition upon the rate of reaction was also determined by repeating experiments using control compounds **52** and **53** (Figure 18). These compounds lack the crown ether recognition sites and will not be affected by the presence or absence of K^+. These compounds can only react *via* a bimolecular pathway.

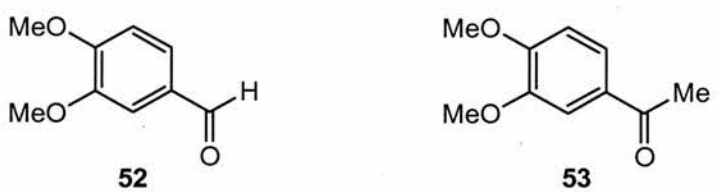

52 **53**

Figure 18 Structure of the control compounds used to determine the importance of recognition on reaction rate. These molecules do not possess the crown ether recognition sites and will be unaffected by the presence or absence of K^+.

Results show that the reaction goes to around 75% completion after 24 hours at 50 °C using 25 mM solutions of **50** and **51** with 1 equivalent of KOMe, whereas under the same conditions using compounds **52** and **53** with 1 equivalent of KOMe, the reaction only goes to around 10% completion. Clearly, recognition is very important in achieving rate acceleration for these reactions. It also shows that the Curtin-Hammett principle can be applied to supramolecular assemblies to achieve rate acceleration.

1.6.3 Organocatalysis

There are many advantages to using organic catalysts[146-153] as opposed to traditional organometallic catalysts. Metals are frequently expensive, toxic, air sensitive and give problems with leaching making it difficult to guarantee that products are free from all traces of metal and leading to difficulties with catalyst separation for recycling. In pharmaceutical processes there is a restriction on the metals, if any, which can be used safely. Therefore, metal-free catalysts are required. Organocatalysts can also be easily attached onto solid support[154] which minimises loss and makes separation trivial.

Combining supramolecular recognition with catalysis leads to more efficient systems and product inhibition is rarely a problem as a consequence of using weaker binding interactions such as hydrogen bonds. There have been many different types of organocatalysts reported which have been developed for various reaction types.

There are four different mechanisms[155] through which organic molecules can be used to catalyse reactions:

1. Activation of the reaction, similar to Lewis acid/base activation where the catalyst is not consumed in the reaction.
2. Formation of reactive intermediates where the catalyst is consumed in the reaction, therefore requiring regeneration through a parallel catalytic cycle.
3. Phase-transfer reactions where the catalyst is used to transport the substrate between the organic solvent and second phase through the formation of a host-guest complex.
4. Molecular-cavity-accelerated reactions where the catalyst is used to select between competing substrates depending on the size and structure of the cavity within the catalyst.

These four different mechanisms will be discussed in more detail with respect to both enantioselective and achiral organocatalyts. The majority of achiral organocatalysts which have been developed to date operate *via* the first mechanism.

The most interesting organocatalysts utilise hydrogen bonding in a similar method to enzyme catalysis. Consequently, theories of enzyme catalysis can be applied to these simple organic catalysts in an attempt to learn more about the mechanism of enzyme action. By examining

simple systems it is hoped to separate out the different factors important in enzyme catalysis to investigate their magnitude. The use of hydrogen bonding to alter the electronic distribution in a complex is known as "polarisation". Rate enhancements obtained are not always impressive and there is a long way to go before enzyme-like rate accelerations are achieved. However, each system provides valuable information required to achieve the long-term goal of enzyme-like activity. Catalysis of non-polar reactions is of particular interest – therefore organocatalysts which have been developed to accelerate pericyclic reactions will be discussed separately.

1.6.3.1 Catalysis based on Nucleophilic/Electrophilic Properties

The first mechanism, where activation is achieved through the nucleophilic/electrophilic properties of the organocatalyst, can be compared to Lewis acid/base catalysis.[156,157] An interesting feature of organocatalysts is their ability to have the same reactive centre acting as both a Lewis acid and base depending on the reaction conditions. For example, it is well known in biological systems that certain amino acid residues, such as histidine, can act as general bases or acids depending on protonation.

Morán and co-workers[158] have developed organocatalysts based upon guanidinium salts, for example **54**, for the acceleration of the Michael addition of amines *e.g.* **56** to α,β-unsaturated lactones *e.g.* **55** (Scheme 18). Formation of β-aminolactones *e.g.* **57** from α,β-unsaturated lactones is of synthetic interest as it provides a flexible route for the formation of β-lactams, β-aminoesters and β-aminoalcohols.

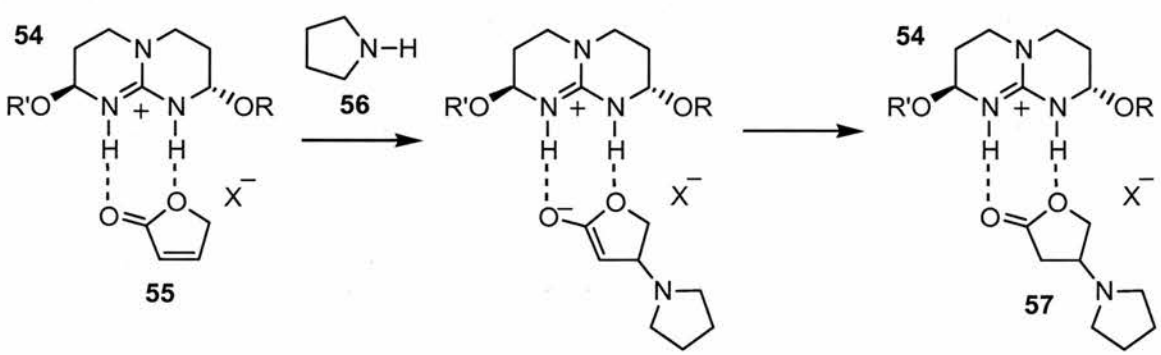

R' = *t*BuMe$_2$SiO, R = *t*BuPh$_2$SiO, X = Ph$_4$B

$t_{1/2}$ uncatalysed = 184 minutes
$t_{1/2}$ catalysed = 22 minutes

Scheme 18 The Michael addition of amines to α,β-unsaturated esters is catalysed by the presence of the guanidinium salt organocatalyst **54**.

Guanidinium salts are used in the recognition of carboxylates or phosphonates as a consequence of their ability to form two strong zwitterionic hydrogen bonds. Organocatalyst **54** works well as a result of its positive charge, which forms a non-charged saturated compound in the transition state to give added stability.

An interesting reaction to catalyse is H/D exchange. It is possible for a catalytic group on an enzyme of pK_a less than 8 to abstract a substrate proton with pK_a of more than 20. Two very different approaches have been taken. Macrocyclic polyamine organocatalysts *e.g.* **58** capable of binding malonate ions **59** were used by Lehn[159,160] whereas cleft type organocatalysts *e.g.* **60** capable of amide deuteration were prepared by Morán.[161] Both systems are shown in Figure 19.

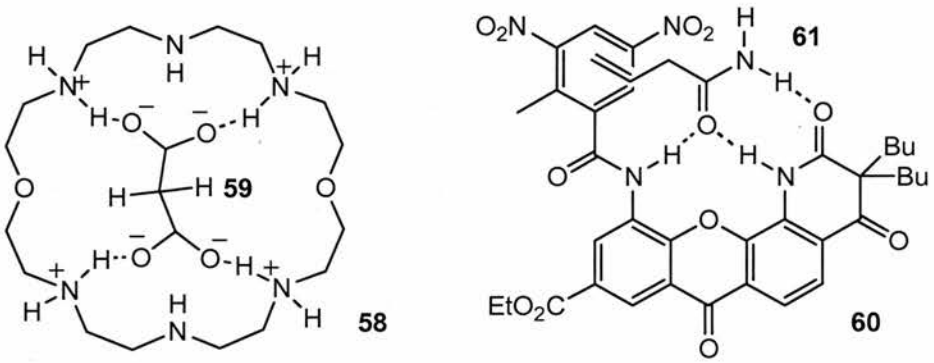

Figure 19 Two different approaches to organocatalysts capable of accelerating H/D exchange: macrocyclic polyamine **58** developed by Lehn and **60**, a cleft type receptor developed by Morán.

Organocatalyst **58** gave k_{cat}/k_{uncat} values of approximately 1.4 x 10^3 in D_2O at 25 °C but this is pH dependent. At low pH values **59** is protonated and is therefore unable to complex with **59**, whereas at high pH values **58** is unprotonated and does not bind **59**.

Organocatalyst **60** operates by binding **61** *via* hydrogen bonds and stabilising the intermediate enolate through charge transfer to the electon deficient aromatic ring on **60**. Addition of **60** reduces the half-life of the deuteration reaction of **61** from 535 to 160 minutes which is impressive.

Crabtree and Kavallieratos[162] used a simple disulfonamide organocatalyst **62** to catalyse imine formation between an aldehyde and an amine. This reaction was chosen because the imine product is not expected to bind to **62** as strongly as the aldehyde starting material which should prevent product inhibition of the organocatalyst. Figure 20 shows **62** binding the transition state of the reaction **63**.

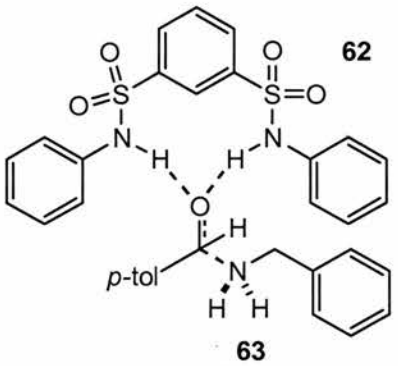

Figure 20 Disulfonamide organocatalyst **62** bound to transition state **63** of the imine formation reaction.

Organocatalyst **62** is capable of increasing the reaction rate by a factor of 6 at a catalyst concentration of 8 mol%. Clearly the prediction that the product would be bound less tightly is correct as **62** can have a large effect at a small concentration.

Some organocatalysts are derived from natural products such as alkaloids or amino acids. The main natural organocatalysts used are amino acids, such as proline **64** and phenylalanine **65**; more recently oligopeptides *e.g.* **66** have also been used (Figure 21). There are several advantages when using oligopeptides as opposed to single amino acids. The efficiency of the catalyst can be improved by varying the amino acid sequences by utilising combinatorial synthesis. There is also great flexibility within the system, which is essential in enantioselective organocatalysis because it is easy to prepare the peptide sequence that produces the opposite enantiomer or its epimer. It is almost always not possible to do this with enzymes. The main disadvantage of using natural products is that few possess a naturally occurring enantiomeric counterpart.

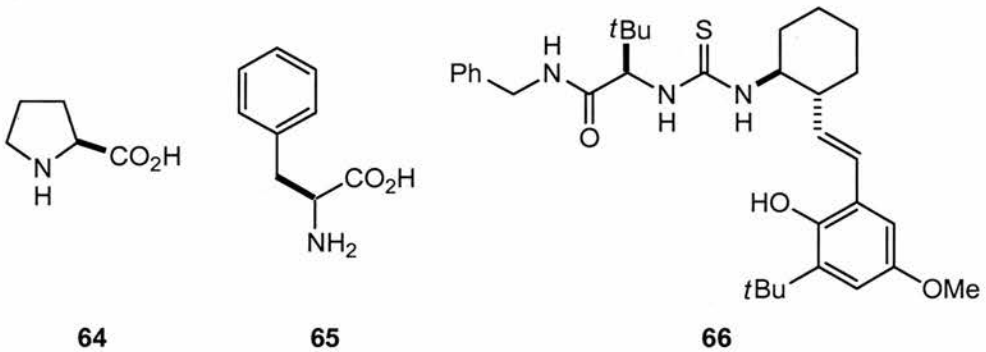

Figure 21 Structures of the amino acids proline **64**, phenylalanine **65** and an oligopeptide **66** which have all been successfully used as organocatalysts.

Proline **64** is very effective as an enantioselective organocatalyst for use in aldol condensation reactions. Work by Barbas and co-workers has shown[163,164] excellent results when **64** is used to catalyse the condensation reaction between acetone **68** and selected aldehydes *e.g.* **67**

(Scheme 19). The best yields are observed for α-unsubstituted aldehydes because selfcondensation side reactions are minimised.

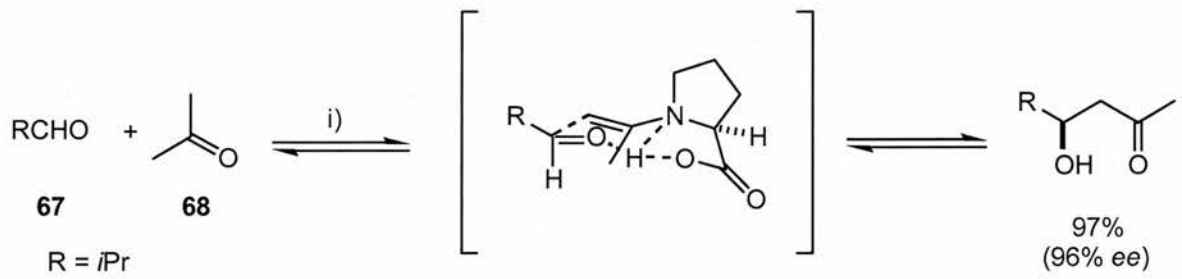

Scheme 19 i) L-proline **64**.

Synthetic organocatalysts are more versatile than those derived from natural products because both enantiomers are readily available and modification of structures is trivial. Many of the synthetic organocatalysts were originally developed as ligands for use in organometallic chemistry, hence many contain phosphorus. Phosphorus-containing organocatalysts are advantageous as a result of their potential for complexation through the phosphorus atom and, more importantly, its ability to act as both a stereogenic centre and as a nucleophilic site. A selection of nitrogen (**69-71**) and phosphorus-containing (**72-74**) organocatalysts is shown in Figure 22.

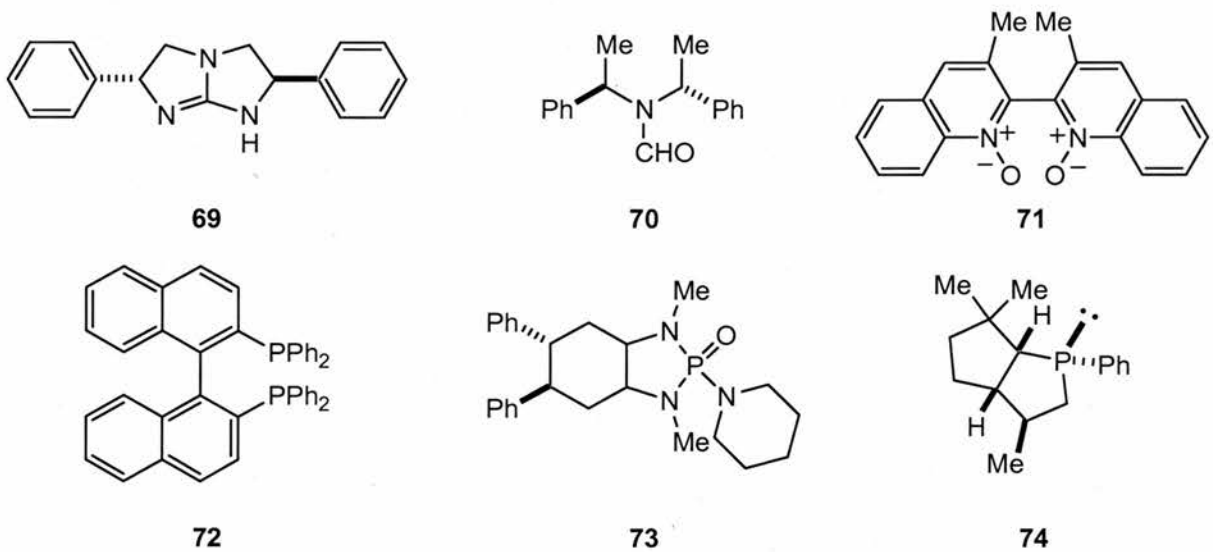

Figure 22 Examples of N- and P-containing organocatalysts.

1.6.3.2 Formation of Reactive Intermediates

Enantioselective protonation is the main reaction type utilising enantioselective organocatalysis with organic molecules which form reactive intermediates and are therefore consumed during the reaction. The exact role of chiral additives in enantioselective protonations has yet to be fully eludidated. One proposed mechanism[149] for catalysis, including regeneration of the chiral organocatalyst, is shown in Scheme 20.

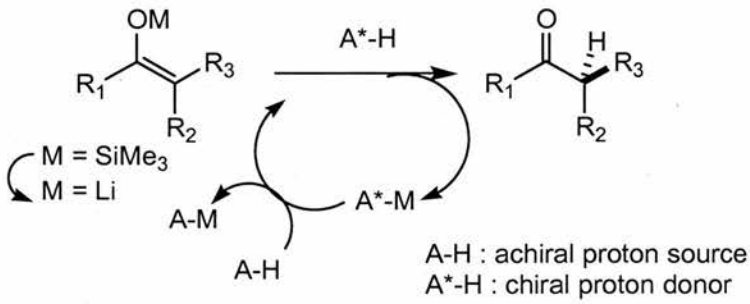

Scheme 20 One mechanism proposed for the enantioselective catalytic protonation of lithium enolates. Adapted from ref 149.

This catalytic cycle is dependent upon the achiral proton source (A-H) reacting with the deprotonated chiral proton donor (A*-H) more rapidly than with the metal enolate starting material. In order to diminish competition between the chiral and achiral proton sources, the chiral organocatalyst is added to the reaction first.

There are several chiral organocatalysts available for the reaction, a selection of which is shown in Figure 23 **75-78**. The achiral proton source should be carefully selected to promote products with high *ee* values. The highest *ee* values are obtained when moderately acidic, rigid and sterically hindered proton sources are used. Those commonly used are: cyclic imides, such as succinimide and phthalamide; dipivaloylmethane; moderately acidic carbonyl compounds, such as phenyl-2-propanone; or non-activated phenol derivatives, such as catechols. The enantioselectivity increases with higher concentrations of organocatalysts although in some cases 0.01 equivalents of catalyst can give acceptable *ee* values.

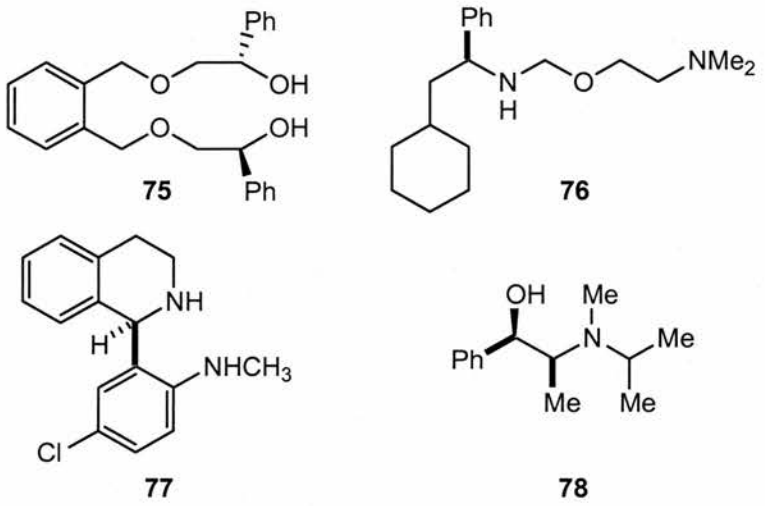

Figure 23 Examples of chiral organocatalysts used in enantioselective catalytic protonation.

1.6.3.3 Phase Transfer Catalysis

Chiral quaternary ammonium salts are used to mediate phase-transfer catalysis as a consequence of their unique mechanism of action. The mechanism was proposed[165,166] to occur in three main steps:

1. Deprotonation of the active methylene compound by a base at the layer interface.
2. The anion of the quaternary ammonium salt is extracted into the organic phase by ion exchange whilst the cation forms a lipophilic ion pair.
3. The ion pair is alkylated by the reagent with concomitant regeneration of the catalyst.

Cinchonium derivatives *e.g.* **79** have been shown to be effective quaternary ammonium salt catalysts. The structure of one such derivative is shown below (Figure 24). The key feature of the structure is the β-hydroxyammonium fragment which is found, for example, in ephedra alkaloid catalysts such as **80**.

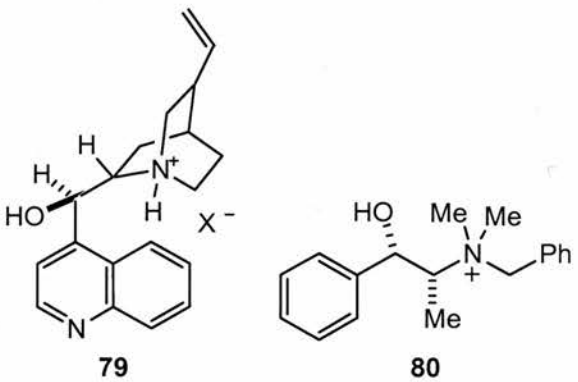

Figure 24 Structures of two effective naturally occurring quaternary ammonium salt catalysts containing the key β-hydroxyammonium fragment.

Quaternary ammonium salts are not the only phase transfer organocatalysts available. Page and co-workers have reported[167,168] promising results for asymmetric epoxidation reactions using iminium salts. Two examples of the iminium salt organic catalysts which have been developed are shown in Figure 25.

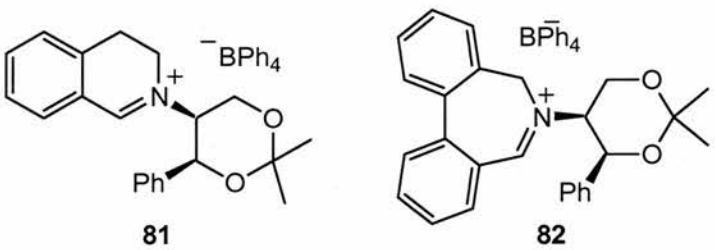

Figure 25 Structures of iminium salts used as organocatalysts for asymmetric epoxidation.

These organocatalysts were tested for their ability to catalyse asymmetric epoxidation of a range of unfunctionalised alkenes using Oxone™. Table 1 shows a comparison of the results obtained for both organocatalysts.

Table 1 Comparison of two organocatalysts, **81** and **82**, capable of asymmetric epoxidation. Yields are calculated by ^{1}H NMR spectroscopy by integration of alkene versus epoxide.

	81			**82**		
Epoxide	Yield / %	*ee* / %	Reaction time / min	Yield / %	*ee* / %	Reaction time / min
	64	20	5	100	24	10
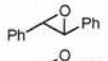	56	15	120	90	15	10
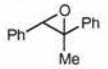	52	52	60	95	37	5
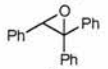	54	59	40	90	59	3
	55	41	5	100	60	3
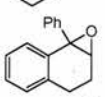	64	49	5	90	41	3
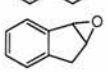	52	17	5	100	10	3

Results show that organocatalyst **82**, containing a seven-membered ring, is more reactive than organocatalyst **81** which only contains six-membered rings, significantly reducing reaction times. The enantioselectivities recorded for each organocatalyst are similar with a maximum value of 60% *ee*.

1.6.3.4 Molecular-Cavity-Accelerated Transformations

Chiral host-guest chemistry is becoming increasingly important, however, there are still few examples where an enantioselective catalytic transformation[169-171] occurs. The main reason for this is that the host-guest complexes formed are often too stable which inhibits catalytic turnover. There are two main categories of materials with chiral cavities: cyclodextrins and molecularly imprinted polymers.

1.6.3.4.1 Cyclodextrins

Cyclodextrins[172-179] are macrocyclic oligosaccharides made from glucopyranose molecules containing a hydrophobic cavity. There are three well-known and industrially available cyclodextrins, α **83**, β **84** and γ **85**, which differ by the number of glucose units in the ring (Figure 26).

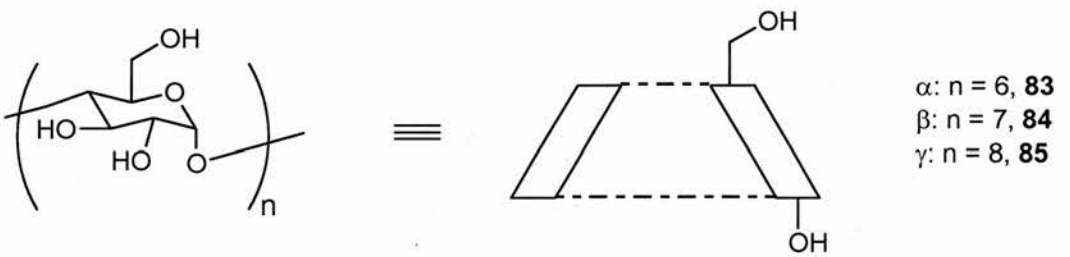

Figure 26 Two representations of cyclodextrins known as α **83**, β **84** or γ **85**, depending upon the number of glucose units in the ring.

In aqueous solutions, the cyclodextrin cavity contains energetically unfavourable water molecules that can be easily displaced by a guest molecule. The reactivity of the guest is altered when it is within the cavity. Usually activity is reduced, but in some cases the cyclodextrin behaves like an artificial enzyme to accelerate reactions.

Cyclodextrin acts as a chiral host molecule which allows guests to bind in the cavity. The size of the guest molecule is restricted by the size of the cavity within the cyclodextrin. γ-Cyclodextrin **85** is attractive for the development of an organocatalyst because the chiral cavity is able to accommodate two molecules of aromatic compounds. This effect is clearly demonstrated in studies by Inoue and Nakamura[180] into the photocyclodimerisation of 2-anthracenecarboxylic acid **86**.

A titration experiment was carried out to measure the decrease in fluorescence intensity with increasing concentrations of **85** which showed the formation of a 1:1 complex of **86**:**85** when **85** is added to a dilute solution of **86**. At a higher concentration of **86**, the major species in solution is the 2:1 complex of **86**:**85**. The 2:1 inclusion complex was also studied by ^{1}H NMR spectroscopy to analyse the 3D structure. Results show that all aromatic signals for **86** are shifted upfield upon complexation. The shift arises from the ring current of nearby **86** and provides clear evidence for the co-inclusion of two molecules of **86** within the same cavity. Depending upon the orientation of **86** within the cavity of **85**, four different regioisomers are obtained. Formation of two of the regioisomers is illustrated in Figure 27.

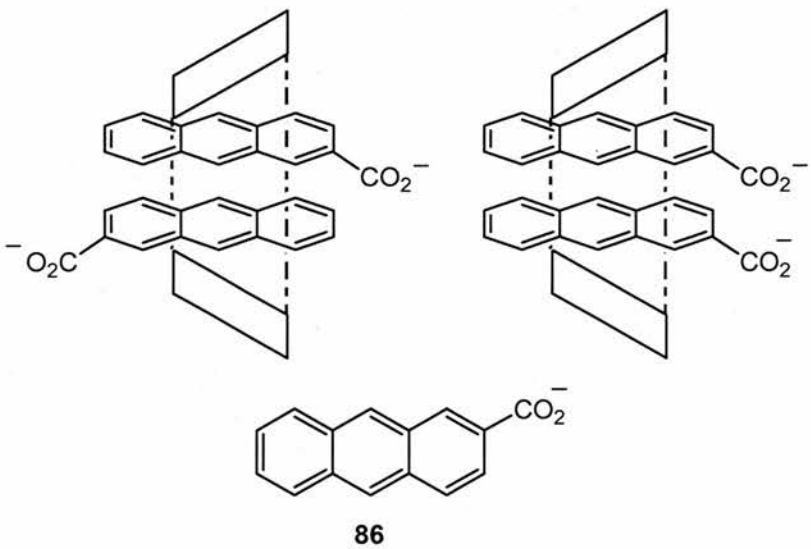

86

Figure 27 Different regioisomers of the product of the photodimerisation reaction are obtained depending on the orientation of the two molecules of 2-anthracenecarboxylic acid **86**. Two examples of different orientations within γ-cyclodextrin **85** are shown.

With this evidence in hand, aqueous solutions of **86** were irradiated at 366 nm in the presence and absence of **85** to determine the effect of **85** on the photocyclodimerisation reaction. Results were analysed by HPLC using an achiral reverse-phase column. The four different product regioisomers were identified, two of which are chiral, giving a total of six product isomers. The structures of the four regioisomers are shown in Figure 28.

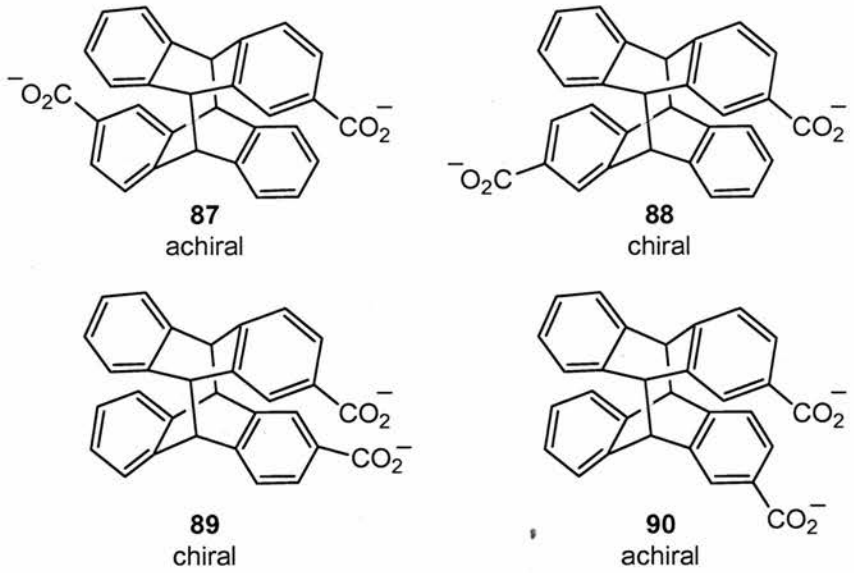

Figure 28 Regioisomers formed upon the photodimerisation of 2-anthracenecarboxylic acid **86**.

In the absence of **85**, all six isomers are formed with a preference for achiral isomer **87** whereas in the presence of **85** the distribution of isomers changes leading to a greater yield of isomer **88** at the expense of **89** and **90**. A racemic mixture of isomers **88** and **89** is formed in the absence of **85** but enantiodifferentiating photocyclodimerisation is induced by **85**. The enantiomeric excess is dependent upon temperature, ranging from 21% *ee* at 60 °C to 41% *ee* at 0 °C for isomer **88** and 5% *ee* to 1% *ee* for isomer **89** over the same temperature range. In addition to lower temperatures improving the enantiomeric excess for isomer **88**, the yields are also improved at the expense of other isomers, especially isomers **89** and **90**.

1.6.3.4.2 Molecularly Imprinted Polymers

A molecularly imprinted polymer[181-187] is created using a reaction template which, when later removed, forms a cavity within the polymer capable of binding a specific substrate.

The synthetic strategy for making the imprinted polymer is shown in Figure 29, whereby the template is first mixed with vinyl monomers, specially selected for their ability to bind the template, and cross-linking monomers. The copolymerisation reaction is then carried out, either thermally or photochemically, before the template is removed. Removal of the template results in a polymeric species containing sites that are complementary in shape to the template and also carry functionality in a specific arrangement to bind the reaction substrate.

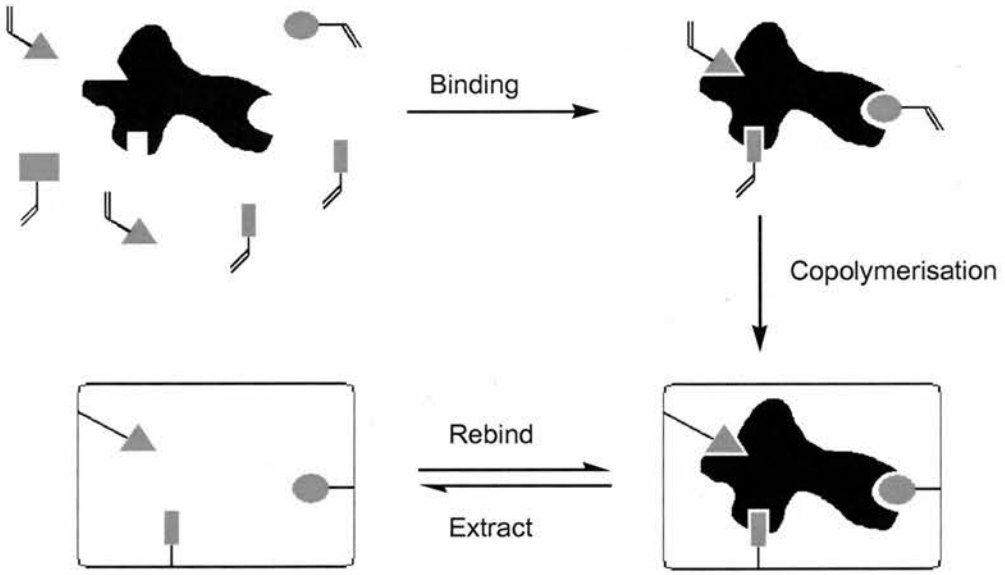

Figure 29 Diagrammatic representation of the imprinting process. A template binds the monomer units in the correct orientation before polymerisation occurs. The template is then removed from the polymer to leave polymeric material with functionality correctly aligned in the active site.

The process of molecular imprinting has been applied to many different reactions. Investigations have been carried out to discover the synthetic feasibility of using imprinted polymers as "microreactors" for chiral synthesis.[188,189] They have also been used as protecting groups with the potential of recycling[190] and as catalysts[191-194] for various reactions.

An example of enantioselective ester hydrolysis catalysed by an imprinted polymer by Sellergren and co-workers shows[195] the potential of using polymers as specific heterogeneous catalysts. The polymer in this case was designed as a mimic for the enzyme chymotrypsin to catalyse the ester hydrolysis reaction of BOC-D(L)-PheONP **91**, shown in Scheme 21.

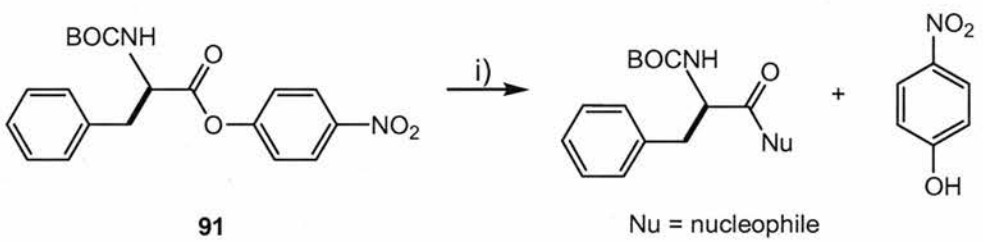

Scheme 21 i) imprinted polymer.

The key requirements for the active site in this case are: a stereoselective binding site capable of stabilising a tetrahedral intermediate, a nucleophile in the region of the reactive carbonyl group, along with an imidazole and a carbonyl group within hydrogen bonding distance of the nucleophile. The polymer is created using the monomer units shown in Figure 30, **92**

contains a phosphate group to mimic the tetrahedral nature of the transition state and also leads to the correct orientation of the "active site residues", the carboxylate groups on **93**.

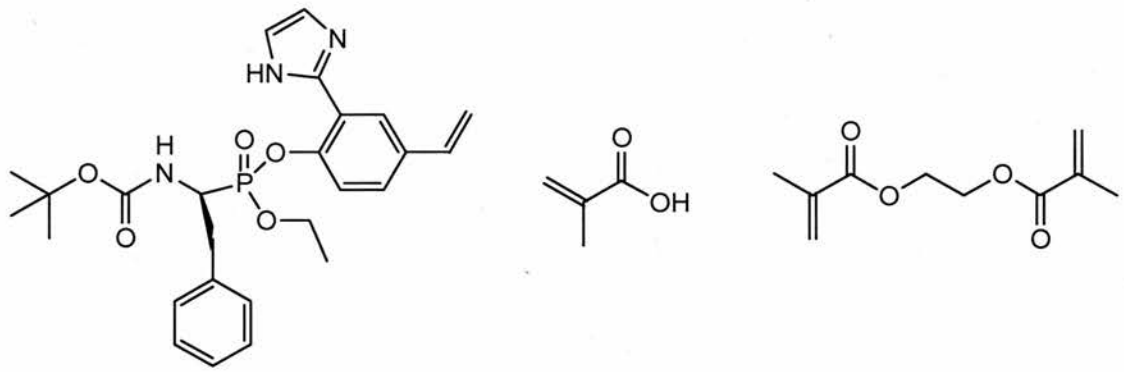

92 0.5 mol%

93 10 mol%

94 90 mol%

Figure 30 Structures of the monomer units used to make the imprinted polymer. The tetrahedral nature of the transition state is mimicked by the phosphate group in **92**.

The monomers are polymerised by photolysis using AIBN as the initiator to produce polymer **95**. The template is then removed (Scheme 22) by cleaving the phosphate group using CsF to give the imprinted polymer **96** containing a chymotrypsin mimic active site. The efficiency of the polymer as a catalyst is dependent upon different factors. The nucleophile chosen to cleave the template, the solvents used and the temperature the hydrolysis reaction is conducted at all affect the rate acceleration and enantioselectivity.

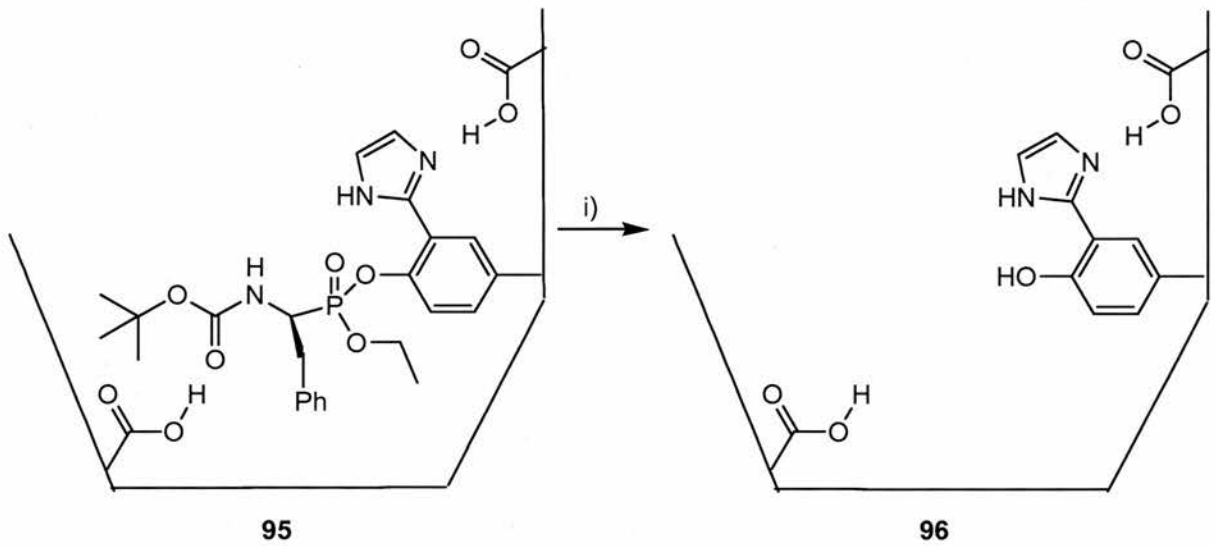

95 **96**

Scheme 22 i) CsF.

1.6.4 Organocatalysts for Pericyclic Reactions

1.6.4.1 Diels-Alder Reaction Catalysis

Several different strategies have been used to accelerate Diels-Alder reactions using metal-free catalysts.[196-200] Traditionally Lewis acids such as $AlCl_3$ and $TiCl_4$ have been used to accelerate the Diels-Alder reaction. Frontier Molecular Orbital (FMO) theory[201] is used to explain the mechanism through which Lewis acids achieve rate enhancements. Coordination of the Lewis acid to the dienophile leads to a withdrawal of electron density which lowers the LUMO energy of the system. This decrease in energy gives an improved $HOMO_{Diene}$-$LUMO_{Dienophile}$ interaction. One problem with Lewis acid catalysts is product inhibition and reactions often have to be carried out with stoichiometric amounts of "catalyst".

It is established that solvent effects[146,202] can lead to an increase in reaction rate for the Diels-Alder reaction. Jørgensen and co-workers have shown[203] that two water molecules can hydrogen bond to a carbonyl group of the dienophile leading to activation. Consequently, bidentate hydrogen-bond donor systems have been developed.

Kelly and co-workers developed[204] substituted biphenylenediol **97** shown in Figure 31 to accelerate the Diels-Alder reaction. Addition of 40 mol% of **97** to reactions between cyclopentadiene **99** and α,β-unstaurated carbonyl compounds *e.g.* **98** leads to an increase in yields by a factor of 12.

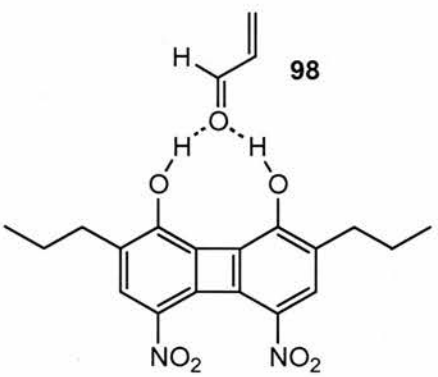

98

97

Figure 31 Structure of organocatalyst **97** developed by Kelly which binds **98**, a dienophile, leading to activation.

It was first shown by Etter[205,206] that diaryl ureas with electron-withdrawing substituents form cocrystals with various proton acceptors including carbonyl compounds. These results led to

the development of organocatalysts based upon the bidentate hydrogen bonding capability of ureas and thioureas to accelerate the Diels-Alder reaction. Schreiner and co-workers have tested[146,207] a wide variety of diaryl thiourea organocatalysts to catalyse the Diels-Alder reaction between **99** and **100** with varying degrees of success (Figure 32). It was found that those diaryl thioureas with electron-withdrawing groups in the *meta* positions gave the greatest rate enhancements because the hydrogen bonding ability of the amide groups was enhanced.

The reaction chosen and a selection of the best organocatalysts are shown in Figure 32; for comparisons the dialkyl thiourea **101** is also included. The catalyst was added at a concentration of 1 mol%. Addition of **102** gives a relative rate (k_{rel}) of 1.8 showing that it has a minimal effect on the reaction rate. The mono-trifluoromethyl substituted catalyst **102** increases the reaction rate by a factor of approximately 4 (k_{rel} = 3.9) whereas for the di-trifluoromethyl substituted catalyst **102** this increases to k_{rel} = 8.8. Chloride is also electronegative enough to increase the reaction rate by a factor of 5 (k_{rel} = 5.1) when **104** is added. It is also important to note that there appears to be little product inhibition of the organocatalyst because there is still activity observed even after the reaction has gone to 80% completion.

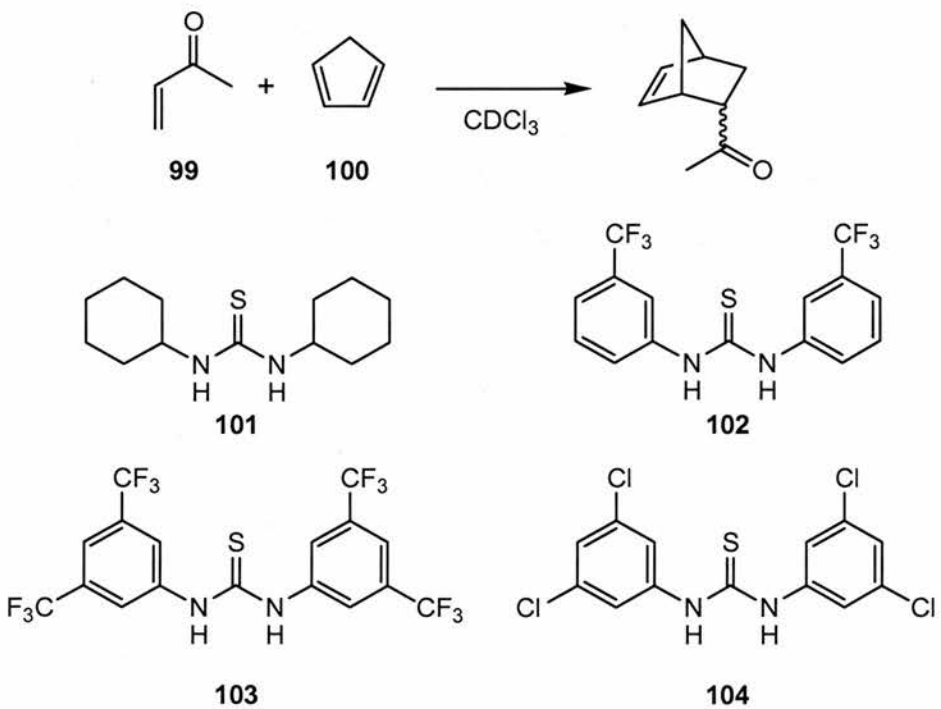

Figure 32 Structures of four organocatalysts tested for their ability to accelerate the Diels-Alder reaction between cyclopentadiene **100** and but-3-en-2-one **99**.

The total synthesis of the natural product (+)-hapalindole Q **107** *via* Diels-Alder reaction[208] was possible thanks to organocatalyst **105** (Scheme 23). The hapalindoles are a group of structurally related tri- and tetracyclic alkaloids first isolated from the terrestrial blue-green alga *Hapalosiphon fontinalis* which display anti-algal and antimycotic activity. Organocatalyst **105** was developed by MacMillan[209] and after screening different solvent conditions, it was found that the optimum results were obtained when using a 1:1 mixture of DMF and methanol containing 5% water. This mixture gave the desired *exo* cycloadduct **106** in 35% yield and 93% *ee* with a catalyst loading of 40 mol%. The reaction yields are poor, but excellent selectivity is achieved using this method. Catalyst recovery yields of 85-90% were also achieved. This route is considered desirable because it allows "the rapid and enantioselective assembly of the complex intermediate from readily accessible achiral starting materials".[208]

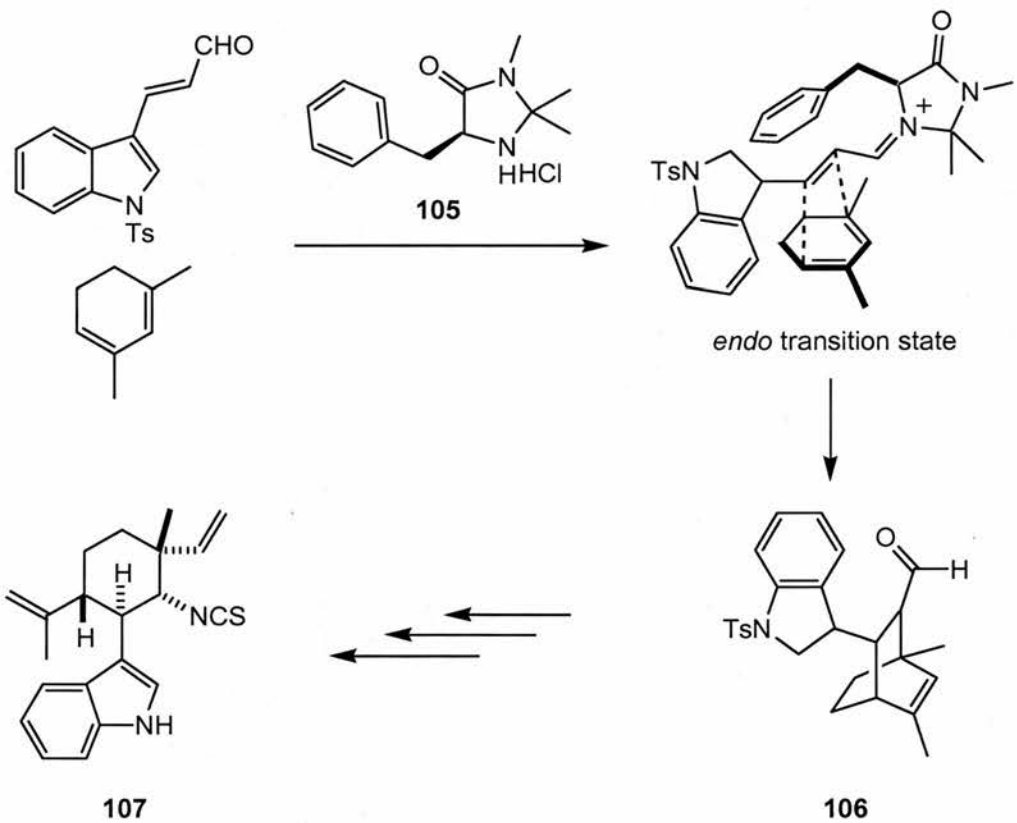

Scheme 23 The proposed transition state in the key Diels-Alder step in the total synthesis of (+)-hapalindole Q **107** mediated by MacMillan's organocatalyst **105**. Adapted from ref 208.

Organocatalyst **105**[209] leads to rate acceleration by lowering the energy of the LUMO of the α,β-unsaturated aldehyde dienophile. Instead of specific lone pair coordination, as in the case of Lewis acid catalysis, selective π-bond formation is used.

1.6.4.2 Dipolar Cycloaddition Reaction Catalysis

Cucurbituril ($C_{36}H_{36}N_{24}O_{12}$) **108**[210] is a nonadecacyclic cage structure with hexagonal symmetry. It is a relatively rigid structure with a hollow core capable of forming tight complexes with alkylammonium ions. A schematic representation of cucurbituril is shown in Figure 33.

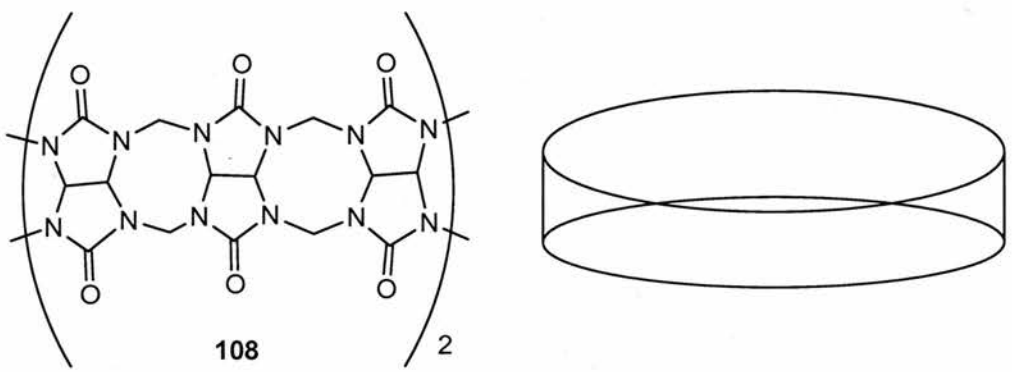

Figure 33 Schematic representation of the nonadecacyclic cage structure of cucurbituril ($C_{36}H_{36}N_{24}O_{12}$) **108**.

It has been shown that **108** not only acts as a host molecule for binding alkylammonium ions, but can also be used to accelerate the 1,3-dipolar cycloaddition reaction[211] between an alkyne *e.g.* **109** and an alkyl azide *e.g.* **110**. The reaction chosen is shown in Scheme 24.

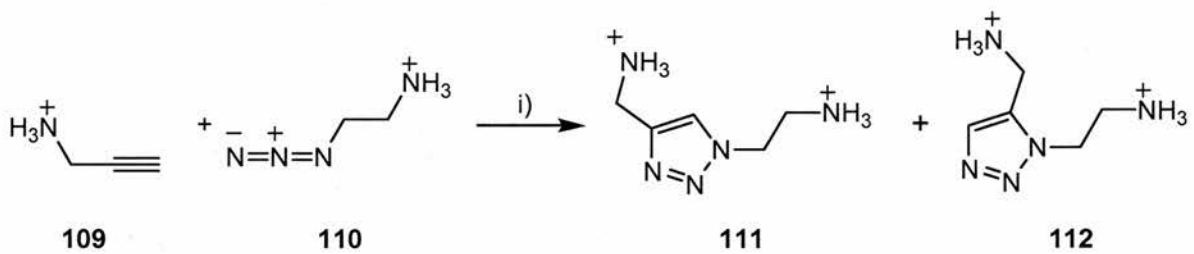

Scheme 24 i) **108**.

In the absence of **108** the reaction is slow, k = 1.16 x 10^{-6} M^{-1} s^{-1} in aqueous formic acid at 40 °C, producing both regioisomers, **111** and **112**. Addition of a catalytic amount of **108** leads to the reaction becoming regiospecific for the production of **111** and the rate is enhanced by a factor of 5.5 x 10^4.

It is believed that there is the formation of a transient ternary complex where **109** and **110** are both bound to **108**. The alkylammonium groups on both substrates bind to the urea carbonyl

groups of **108** to give the correct alignment of the reactive groups within the cavity and hence rate acceleration.

It is also possible to accelerate other types of dipolar cycloaddition reactions. The [3+2] dipolar cycloaddition reaction between diphenyl nitrone **113** and maleimide **114** (Scheme 25) can be accelerated by a simple organocatalyst.

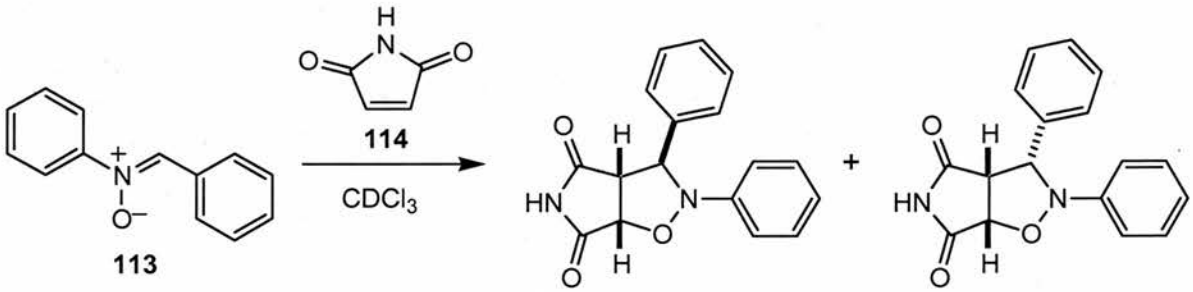

Scheme 25 [3+2] Dipolar cycloaddition reaction between diphenyl nitrone **113** and maleimide **114**.

The simple bisamide organocatalyst **115** shown in Figure 34 has been developed in the Philp group[212] to catalyse the reaction shown in Scheme 25. In order to probe the effect of the organocatalyst, control receptor **116** was also developed which is incapable of hydrogen bonding to maleimide.

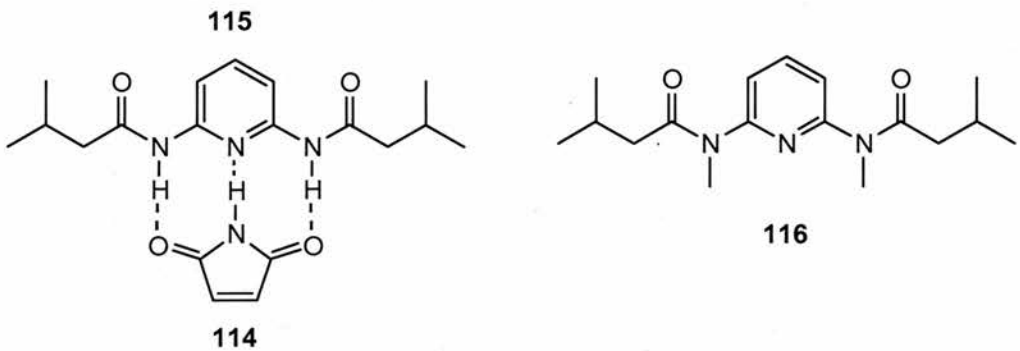

Figure 34 Organocatalyst **115** binds maleimide **114** to accelerate the [3+2] dipolar cycloaddition reaction with diphenyl nitrone **113**. The effect of control organocatalyst **116**, which has the hydrogen bond donor sites blocked by methyl groups, was also tested.

Addition of **115** leads to a five-fold increase in reaction rate when compared with the reaction rate in the absence of **115** or in the presence of **116**. These results show that a simple organocatalyst can be used to obtain rate accelerations by careful design of hydrogen bonding motifs.

1.7 Aims and Objectives

Many investigations have been carried out into the mechanisms used by enzymes to catalyse chemical reactions. It is clear that a variety of factors must be considered and it is not possible to study them in isolation. Using small organic molecules as model systems it is possible to explore individual factors more systematically. By carefully designing systems it should be possible to investigate factors such as polarisation and proximity using simple hydrogen bonding recognition motifs.

It is also clear from reviewing the literature that there are marked differences observed when catalysing different reaction types. There are few examples of natural systems capable of catalysing non-polar reactions, and the rate accelerations observed are much smaller than those observed for polar reactions. It is worthwhile exploring the effects of transition state charge upon rate acceleration. One possible explanation for the discrepancies observed in rate acceleration for the different reaction types is that it is more difficult to accelerate non-polar reactions because it cannot be achieved simply by stabilising charges.

A valuable investigation would be to conduct a systematic study involving one organocatalyst across a range of reaction types. Designing a system where only the reaction type and therefore, transition state charge changes and all other factors remain constant is a challenge that has not been fully addressed to date. Ultimately, the challenge is to design an organocatalyst capable of giving good rate accelerations for non-polar reactions due to the synthetic utility of these catalysts. The aim is to understand effects, such as polarisation and proximity, thought to be important in enzyme catalysis in simple chemical systems. The results obtained should allow us to develop organocatalysts that give good rate acceleration by exploiting recognition-mediated processes. Comparing the results obtained for different reaction types should also give an indication of the most important factors required for accelerating a non-polar reaction and if this can be achieved using recognition processes.

The first system discussed has been developed to investigate the effects of polarisation on rate acceleration for three different reaction types. Secondly, the effects of proximity on the reaction rate and stereochemical outcome of a Diels-Alder reaction are described. Finally, a system has been developed to investigate the effect of combining polarisation and proximity across different reaction types.

2. Rate Acceleration through Polarisation

2.1 Introduction

The work described in the Introduction has shown that several factors are involved in enzyme catalysis and some advances have been made to incorporate these into organocatalysis with promising results. The main factors important in enzyme catalysis that we wanted to investigate are: activation of a substrate through polarisation, and rate acceleration through proximity. It is clear that nature has found biosynthetic pathways to produce complex natural products without exploiting the potential of non-polar reactions. In order to investigate if there is a simple explanation for this observation – if it is simply easier to accelerate polar reactions – it is necessary to develop an organocatalyst that can be used with one substrate across a range of different reaction types.

In order to investigate the conditions required for rate acceleration, it is necessary to determine the role of transition state charge. If there is a simple function relating transition stage charge with rate acceleration, then its functional form can be one of three possibilities (Figure 35(a)).

(i) The rate acceleration may be directly proportional to transition state charge, shown in black.

(ii) A small increase in charge may give a disproportionately large rate acceleration, shown in red.

(iii) Or significant transition state charge may be required before any rate acceleration is observed, shown in blue.

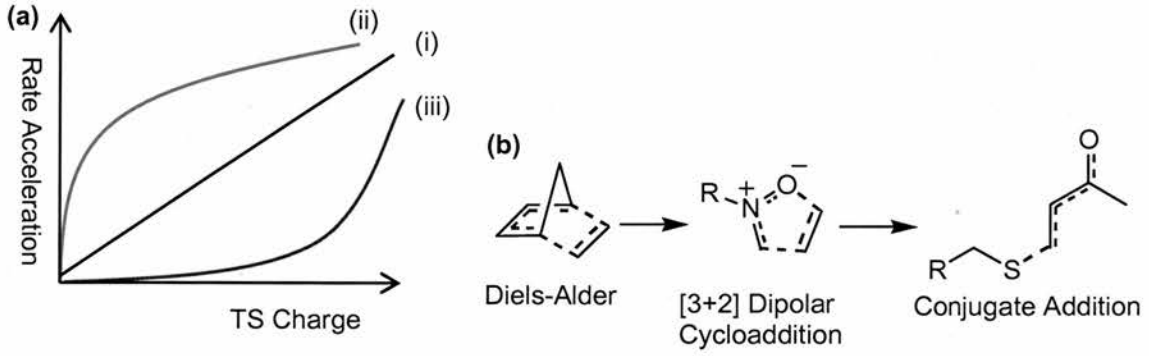

Figure 35 **(a)** A graphical representation to show the predicted relationships between transition state charge and rate acceleration. **(b)** Examples of reaction types with differing transition state charges.

Three possible reactions types are shown in Figure 35(b):

(i) The Diels-Alder reaction which is a non-polar reaction containing no charges in the ground or transition states.

(ii) [3+2] Dipolar cycloaddition involves an uncharged transition state but reactants which may possess a formal charge.

(iii) Conjugate addition is a polar reaction involving a charged substrate.

Organic receptors have been shown to polarise substrates using hydrogen bonding. However, to date there has been no systematic study carried out using the same receptor and substrate across a range of reaction types with differing transition state polarity, such as those shown in Figure 35(b). Several organocatalysts have been developed to probe the different reaction types based purely on polarisation of a substrate.

Organocatalysts **117** and **118**[213] shown in Figure 36(a) were developed to accelerate the three reaction types shown in Figure 35(b). Organocatalysts **117** and **118** were tested for these reactions with promising results; however, the association constant obtained for **117** and **118** binding to substrate **119** is low. Maleimide **119** does not fit well into the organocatalysts which means that the spacing between the carboxylic acid binding sites and the urea polarisation site is not correct. These organocatalysts are expected to give more impressive results if the organocatalyst and substrate can be altered to give the optimum spacing for hydrogen bonding.

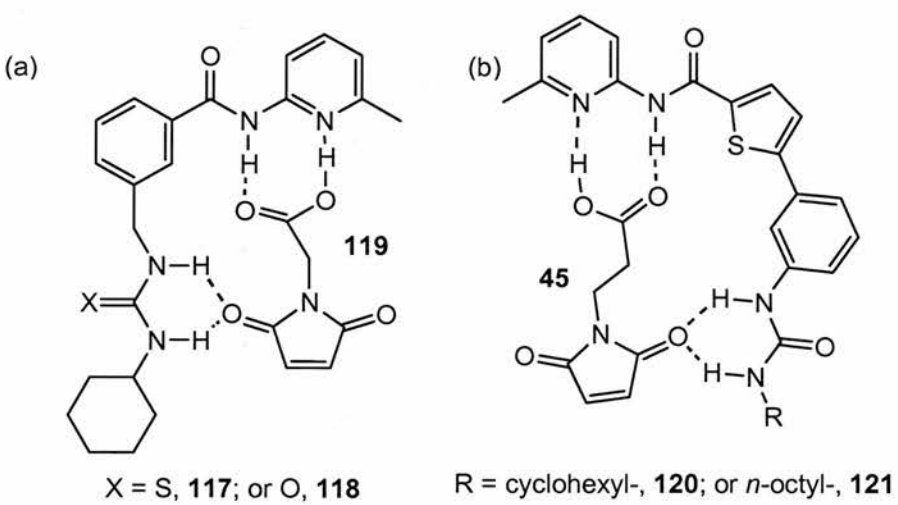

Figure 36 Examples of two types of organocatalysts previously developed within the Philp group, with different limitations.

Alternatively, organocatalysts **120** and **121**,[214] shown in Figure 36(b) were developed. Organocatalysts **120** and **121** contain a thiophene unit attached onto a phenyl ring giving rigidity to the spacer unit which should lead to effective binding of substrate **45**. Unfortunately, **120** and **121** are insoluble in non-polar solvents. In order to conduct binding studies and kinetic experiments using the organocatalysts, all molecules must be soluble in a non-polar solvent such as $CDCl_3$ to prevent disruption to the hydrogen bonds between the organocatalyst and the reagent. Therefore, we decided to develop a new system in order to try to address these problems.

Molecular modelling studies were conducted on target organocatalyst **122** and **45** shown schematically in Figure 37. Organocatalyst **122** was expected to be a good candidate for polarisation, as a consequence of the presence of an internal hydrogen bond between the carbonyl group 1 and amide 5. This internal hydrogen bond leads to activation of amide 2, the polarisation site amide. The internal hydrogen bond leads to removal of electron density from amide 2. Upon hydrogen bonding to **45**, the internal hydrogen bond leads to electron density being withdrawn through the conjugated system resulting in activation of the substrate double bond through lowering of the LUMO energy.

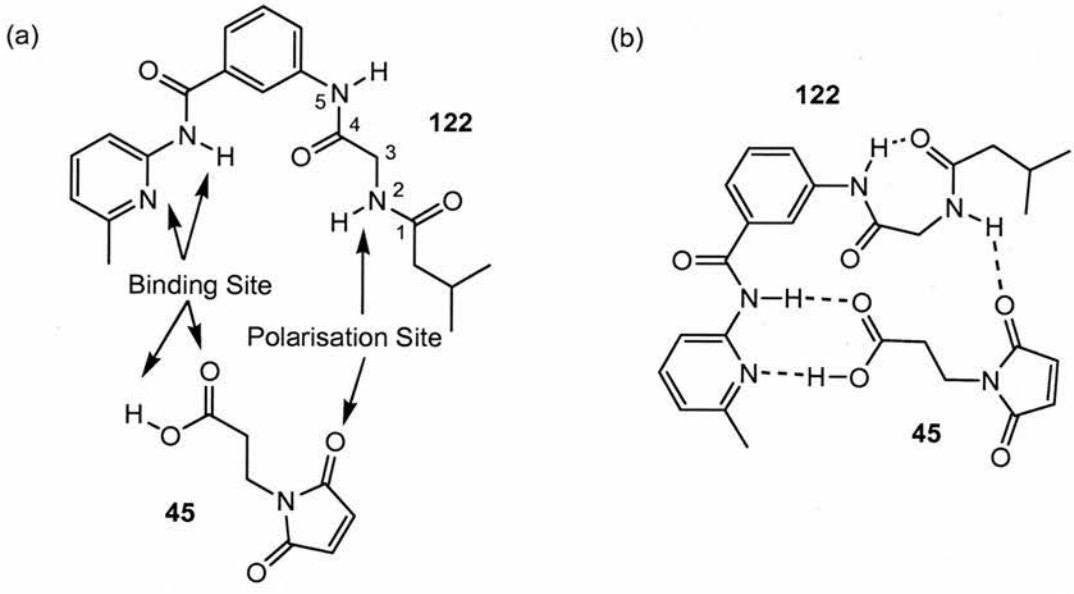

Figure 37 **(a)** Structure of organocatalyst **122** and substrate **45** showing binding and polarisation sites. **(b)** The conformation of **122** adopted upon binding **45** containing an internal hydrogen bond.

The effect of the internal hydrogen bond can be seen more clearly when examining the electrostatic potential surfaces obtained by molecular modelling. The electrostatic potential surfaces show a map of charges with electron rich areas, such as oxygen atoms, shown in red, and electron deficient areas shown in blue. When examining the conformation without the

internal hydrogen bond (Figure 38) it can be seen that the polarisation site amide is already blue, ESP_{max} = +23 kJ mol^{-1}, indicating it is electron deficient, which is necessary for a polarisation site. However, this is not the lowest energy conformation for the organocatalyst.

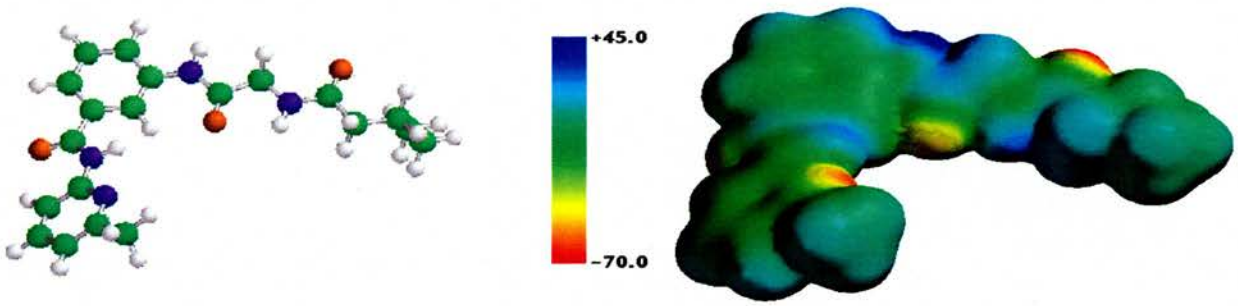

Figure 38 Electrostatic potential surface of receptor without the internal hydrogen bond. ESP_{max} = +23 kJ mol^{-1}

The lowest energy conformation for the organocatalyst contains the internal hydrogen bond (Figure 39). From the electrostatic potential surface obtained in this case, it can be seen that the polarisation site is now much more blue (ESP_{max} = +45 kJ mol^{-1}) indicating that it is more electron deficient and will therefore be a much better polarisation site. The internal hydrogen bond means that the polarisation site amide is activated by a factor of two when compared with the conformation lacking this hydrogen bond.

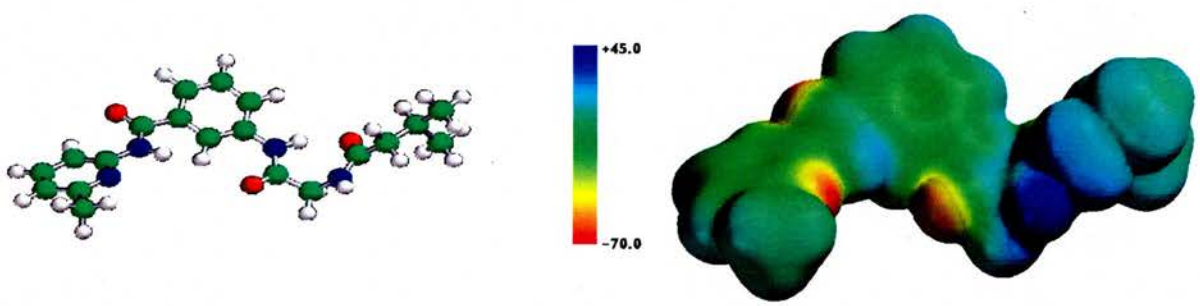

Figure 39 Electrostatic potential surface of receptor with the internal hydrogen bond. ESP_{max} = +45 kJ mol^{-1}

It is not only the polarisation site which is important. The binding site must also be carefully considered. It is well established that carboxylic acid groups and amidopyridine derivatives hydrogen bond.[205,206] In some cases high binding constants have been recorded. For this reason 3-maleimidopropanoic acid **45** was identified as a good substrate.

Maleimide **45** is an ideal substrate because it is easily synthesised from a coupling reaction between maleic anhydride and the amino acid β-alanine. Maleimides are known to act as dienophiles, dipolarophiles and Michael acceptors which means that a single substrate can be

used across all reaction types. This use of a *single* substrate is essential in order to compare only transition state charge and rate acceleration. Organocatalyst **122** polarises **45** equally in all three cases – the only difference is transition state charge.

2.2 Synthesis of Organocatalyst

2.2.1 Retrosynthetic Analysis

Retrosynthetic analysis shows that synthesis of **122** can be easily achieved by breaking three amide bonds (Figure 40).

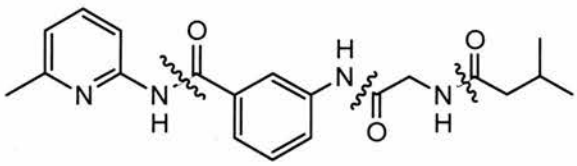

Figure 40 Retrosynthetic analysis of **122** showing the disconnection of three amide bonds.

The left hand part of the molecule arises from synthesising the aromatic amine 3-amino-*N*-(6-methylpyridin-2-yl) benzamide **123**. The middle section introduces flexibility within the synthetic strategy because it can be derived from various different starting materials. For example, it could be derived from the amino acid glycine **124** or from chloroacetylchloride **125**. The right hand part of the molecule is a capping group derived from isovaleric acid. Incorporating an amino acid in the middle section also allows the potential for creating diversity. The introduction of different amino acids introduces chirality into the organocatalyst, which allows the effect of chirality on product distribution to be investigated in reactions that produce more than one isomer. For example, it may be that one face of the substrate is obscured leading to the selection of the unfavourable isomer.

Introducing amino acids also allows great synthetic flexibility because the chain length can be easily extended. Other amino acids can be incorporated to move the polarisation site to different positions and allow different substrates to be used.

2.2.2 Synthesis of 3-Amino-*N*-(6-methylpyridin-2-yl) benzamide 123

Amine **123** has been previously synthesised within the group following the reaction sequence shown in Scheme 26.

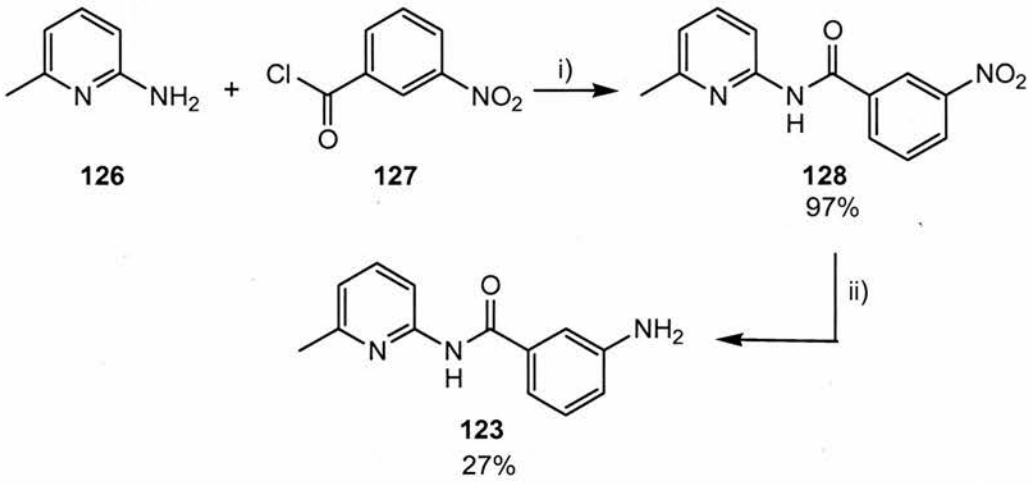

Scheme 26 i) Et_2O; ii) $Cu(acac)_2$, $NaBH_4$, MeOH.

2-Amino-6-methylpyridine **126** and 3-nitrobenzoyl chloride **127** were reacted at room temperature in diethyl ether for 18 hours. After subsequent work-up, the resulting product was purified by recrystallisation from v/v 1:10 DCM:hexane to give **128** in 97% yield.

Nitro **128** was then reduced using $Cu(acac)_2$ and $NaBH_4$. The reaction was monitored by tlc to detect disappearance of **128** before work-up and purification *via* recrystallisation to give **123** in 27% yield. The first time the reaction was carried out the product was easily obtained through recrystallisation from v/v 1:5 chloroform:hexane as a pale yellow solid. When the reaction was repeated, however, frequently the only product isolated was an impure brown oil that could not be purified. This method proved unreliable so reduction was attempted using another method.

The second method of reduction chosen involved the use of 5% Pd/C under hydrogenation conditions in methanol. Progress of the reaction was again monitored using tlc and removal of the starting material was slow. The reaction was left overnight under hydrogen, however, **123** could not be isolated from the crude product after work-up. From the ^1H NMR spectrum recorded in $CDCl_3$, it could be seen that the crude product was a mixture of product and starting material. Tlc results revealed two spots which stained with ninhydrin, one corresponding to **123** and the other postulated to be an intermediate hydroxylamine.

It was then decided to follow a different synthetic strategy (Scheme 27) to obtain **123**. This strategy proved more reliable and resulted in higher yields of the desired product being isolated.

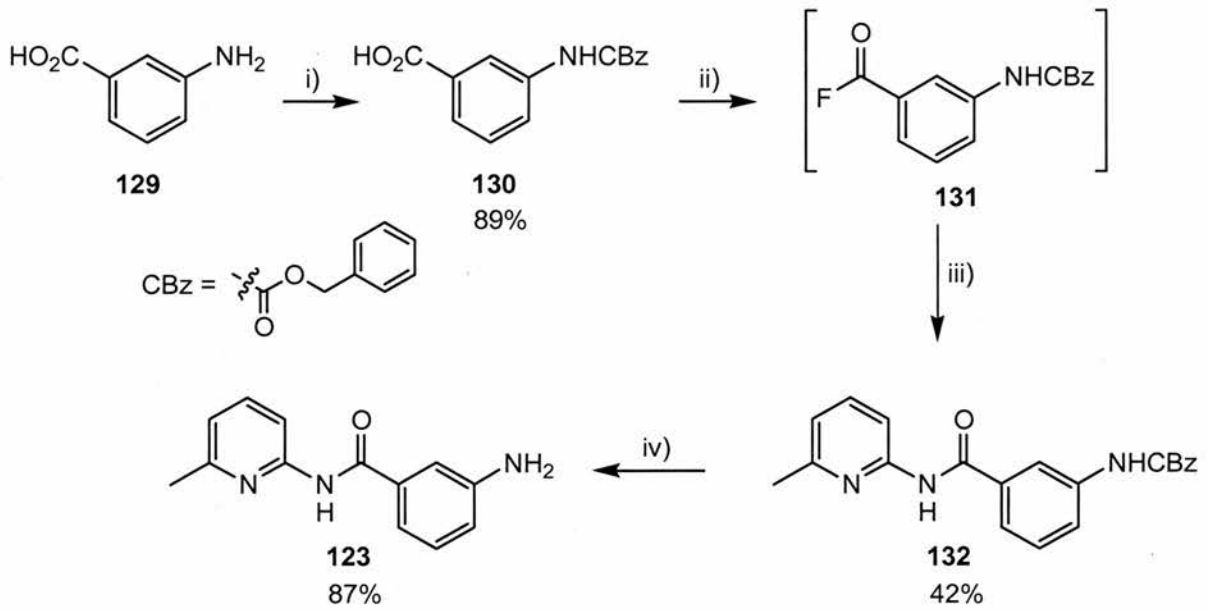

Scheme 27 i) Benzyl chloroformate, THF; ii) Cyanuric fluoride, pyridine, EtOAc, 0 °C; iii) **126**, DCM; iv) 30% HBr in AcOH.

3-Aminobenzoic acid **129** was protected using benzyl chloroformate under standard conditions to afford **130** in 89% yield before it was converted into acid fluoride **131** using cyanuric fluoride. Acid fluorides are easily decomposed; thus, after a quick work-up, **131** was reacted with **126** directly for 18 hours. After purification by column chromatography, **132** was obtained in 42% yield. Deprotection was carried out using 30% hydrogen bromide in acetic acid to give **123** in 87% yield.

This reaction was first carried out in acetonitrile or acetone but it was found that the best results were obtained using ethyl acetate as a consequence of the insolubility of **130**. When the coupling reaction was purified *via* column chromatography, it was possible to recover a large amount of unreacted starting material. It was assumed that the coupling reaction between **126** and **131** was quantitative, but solubility problems inhibited formation of **131**. The yield for this reaction was calculated after accounting for recovered, unreacted **130**.

2.2.3 Amino Acid Coupling

In order to couple **123** with **124**, it was first necessary to protect the amino acid. This coupling was carried out under standard conditions using BOC-ON [(2-*tert*-butoxycarbonyloxyimino)-2-phenylacetonitrile] to afford *N*-Boc-protected glycine **133** in 81% yield. Standard peptide couplings involve the use of 1-(3-dimethylaminopropyl)-3-ethyl carbodiimide hydrochloroide (EDCI) in DMF. However, when a coupling reaction between

123 and **133** was carried out using EDCI, it did not yield any of the desired product. Instead, the synthetic strategy shown in Scheme 28 was chosen.

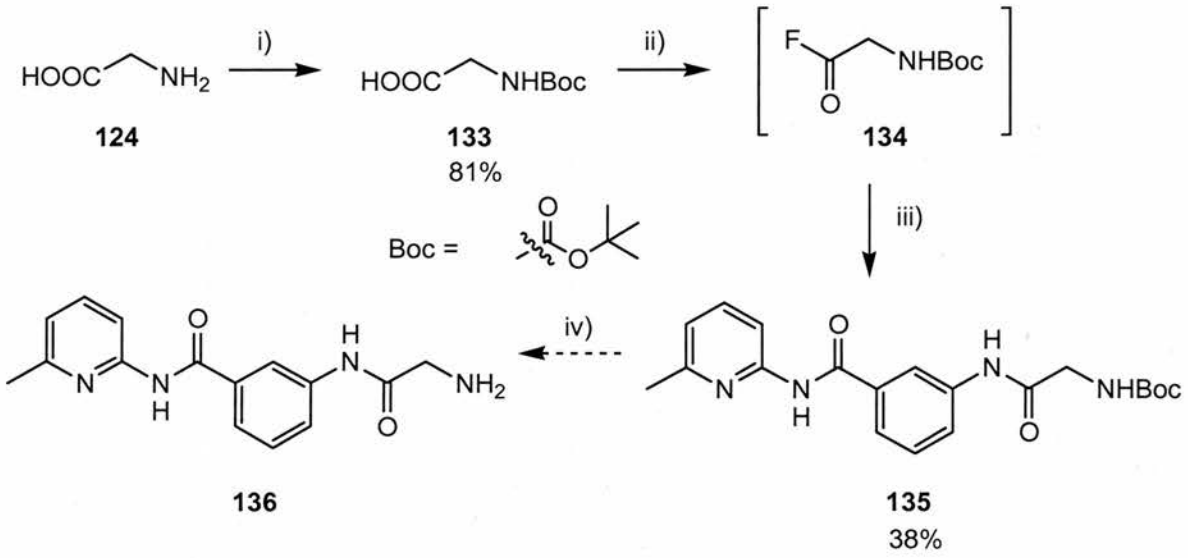

Scheme 28 i) BOC-ON, NEt_3, dioxane, H_2O; ii) Cyanuric fluoride, pyridine, MeCN, 0 °C; iii) **123**, DCM; iv) HCl (aq), dioxane.

Acid fluoride **134** was prepared using standard conditions for cyanuric fluoride reactions and reacted with **123** for 18 hours. The product obtained was sparingly soluble in chloroform. From the 300 MHz ^{1}H NMR spectrum recorded in d_6-acetone, it appeared that it was the correct product, although it was masked by the presence of the large *t*-butyl peak from the Boc group. It was decided to carry out the Boc deprotection reaction using HCl on the isolated product regardless. The product obtained from this reaction was soluble in chloroform – however, the ^{1}H NMR spectrum recorded in $CDCl_3$ still showed the presence of the Boc group. It was postulated that the product obtained from the fluoride coupling reaction was in fact the fluoride salt, which would account for the solubility problems.

In order to complete the synthesis of **122**, it was decided not to incorporate any amino acids at this time. Scheme 29 was developed instead in order to complete the coupling of the middle section. Chloride **137** was obtained in 75% yield following a standard amide coupling reaction between chloroacetylchloride **125** and **123**. Chloride **137** was then converted into **138** by heating to reflux with sodium azide overnight. Azide **138** was obtained in 66% yield and directly reduced using triphenylphosphine and water. The product was isolated by filtration as hydrochloride salt **139** in quantitative yield and used without further purification.

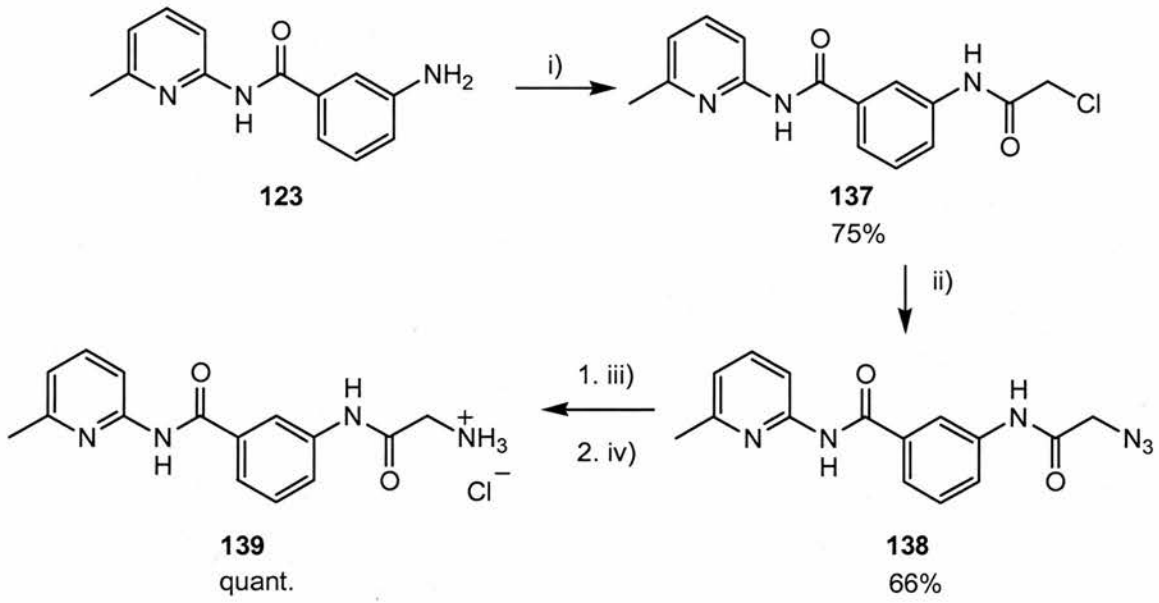

123 **137** 75% **138** 66% **139** quant.

Scheme 29 i) **124**, DCM; ii) NaN_3, acetone, Δ; iii) PPh_3, THF, H_2O; iv) HCl (aq), EtOH.

Having successfully coupled **125** to **123**, target **122** was obtained *via* a coupling reaction between isovaleryl chloride and **139,** as shown in Scheme 30. After purification through recrystallisation from v/v 5:1 DCM:hexane, **122** was obtained in 57% yield.

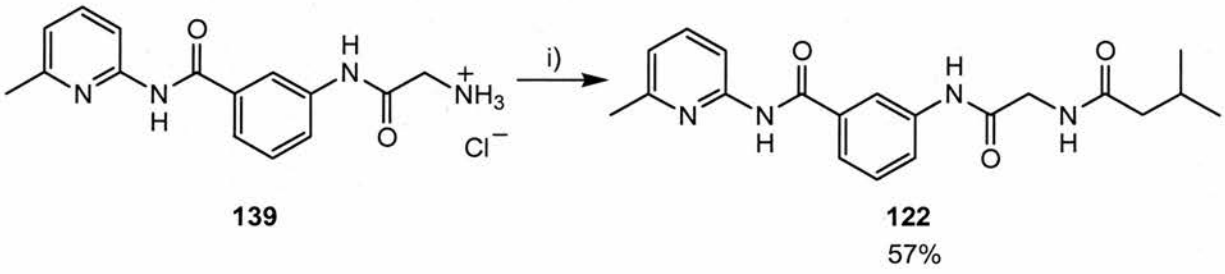

139 **122** 57%

Scheme 30 i) isovaleryl chloride, NEt_3, DCM.

2.3 Synthesis of 3-Maleimidopropanoic acid 45

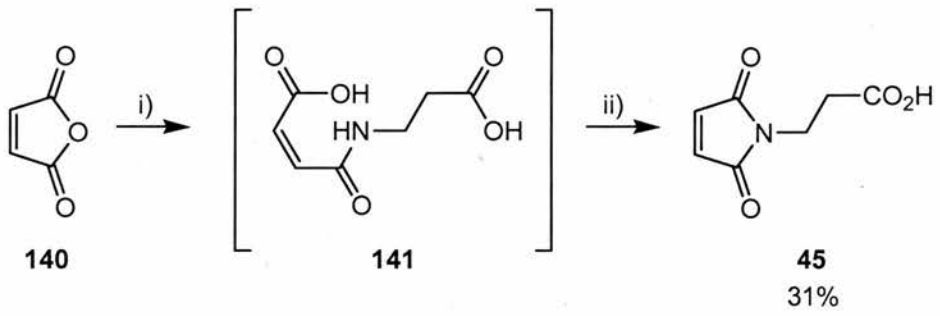

Scheme 31 i) β-alanine, AcOH; ii) Δ.

Following procedures established within the group (Scheme 31), β-alanine and maleic anhydride **140** were dissolved in acetic acid and stirred overnight to form intermediate **141**. The reaction mixture was then heated to reflux for 6 hours, before being purified by vacuum filtration through a short pad of silica gel, to afford cyclised product **45** in 31% yield. The low yield obtained from this reaction is a consequence of the competing polymerisation reaction and is typical for this class of compound.

2.4 Synthesis of Reactants

Organocatalyst **122** was used to accelerate a Diels-Alder cycloaddition, a [3+2] dipolar cycloaddition and a conjugate addition reaction. For the Diels-Alder cycloaddition and conjugate addition reactions, the commercially available reactants furan **142** and thiophenol **143** were used respectively. The [3+2] dipolar cycloaddition reaction required preparation of the reactant. Different alternatives were available; a nitrone and an azide are two possibilities.

Benzyl azide **145** was chosen as the reagent because it can be easily prepared by heating a suspension of benzyl chloride **144** and sodium azide in acetone to reflux for 48 hours (Scheme 32). Azide **145** was obtained in 94% yield.

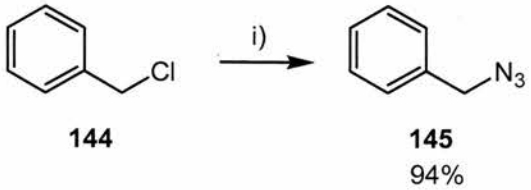

Scheme 32 i) NaN_3, acetone, Δ.

2.5 Characterisation of Reaction Products

The products of all three reactions were also synthesised for characterisation purposes. The cycloadduct of the Diels-Alder reaction **146** was obtained by stirring a solution containing equal equivalents of **45** and **142** in chloroform at 35 °C for two weeks (Scheme 33). The solvent was removed and the product obtained in 74% yield as the *exo* isomer.

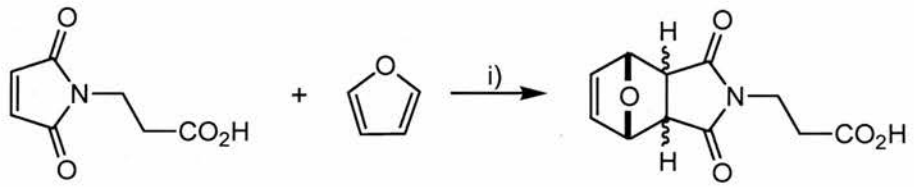

45 **142** **146**

Scheme 33 i) $CHCl_3$.

The [3+2] dipolar cycloaddition reaction cycloadduct **147** was prepared by stirring a solution of **145** and **45** dissolved in chloroform at 35 °C for two weeks (Scheme 34). The solution was filtered and the solvent removed to afford the product in 58% yield.

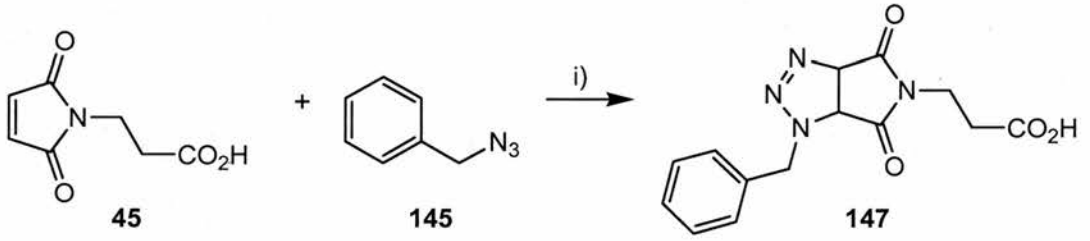

45 **145** **147**

Scheme 34 i) $CHCl_3$.

Preparation of the product from the conjugate addition reaction **148** was conducted in a similar manner (Scheme 35). Maleimide **45** and **143** were dissolved in chloroform and 0.5 equivalents of *t*-butyl pyridine were added. The solution was stirred at room temperature for one week before the product was isolated through recrystallisation from v/v 1:10 DCM:hexane in 62% yield.

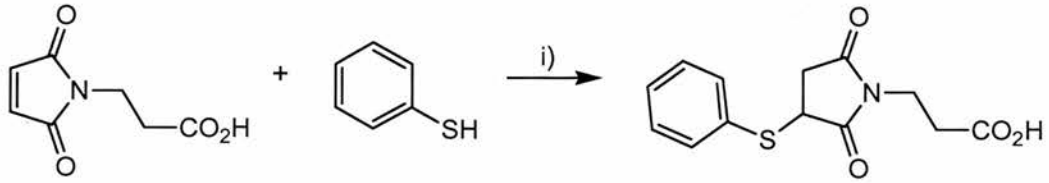

45 **143** **148**
62%

Scheme 35 i) *t*-butyl pyridine, $CHCl_3$.

2.6 Binding Studies

Having prepared all the necessary compounds, it was then possible to carry out tests using **122**. Firstly, it was necessary to establish that **122** did indeed bind **45**. This characterisation was done in two different ways – by 300 MHz ^{1}H NMR titration and by 500 MHz ^{1}H–^{15}N correlation NMR (^{1}H–^{15}N HSQC).

2.6.1 ^{1}H NMR Titration

An accurate way of determining the association constant, K_a, is through NMR titration.[215] The K_a value gives an indication of the strength of the binding capability of the organocatalyst for the substrate. The number of hydrogen bonds involved in binding helps to determine the strength of association. The more hydrogen bonds responsible for binding leads to a higher K_a value being observed.

In order to calculate the association constant, K_a, for **45** binding to **122**, a ^{1}H NMR titration experiment was conducted. The concentration of **122** was maintained at 10 mM and ^{1}H NMR spectra were recorded for samples containing **122** with concentrations of **45** ranging from 0 to 100 mM. The resulting spectra allow plots of chemical shift change vs substrate concentration to be constructed. If there is strong binding then a chemical shift change is observed in all protons around the hydrogen bond and not simply the amide proton.

The ^{1}H NMR titration experiment was carried out by recording 300 MHz ^{1}H NMR spectra at 25 °C. The samples prepared contained 10 mM **122** dissolved in $CDCl_3$ with 0, 1, 2, 5, 7, 10, 15, 20, 30, 40, 60, 80 or 100 mM **45** added. Once all spectra had been recorded, the chemical shift change between the spectrum containing only **122** and those with the addition of **45** for each proton in **122** was calculated. The data allowed graphs showing chemical shift change vs concentration of **45** to be drawn for each proton in **122**. The experimental data could then be used to calculate K_a.

K_a is calculated by non-linear curve fitting of the data. Figure 41 shows the graphs obtained from fitting the data, shown in Table 2, for one proton in **122**. Figure 41(a) shows the graph before the data has been fitted, with the experimental data shown in blue and the fitted line in red, whilst Figure 41(b) shows the results obtained when the experimental data has been correctly fitted. This process was repeated for all organocatalyst protons.

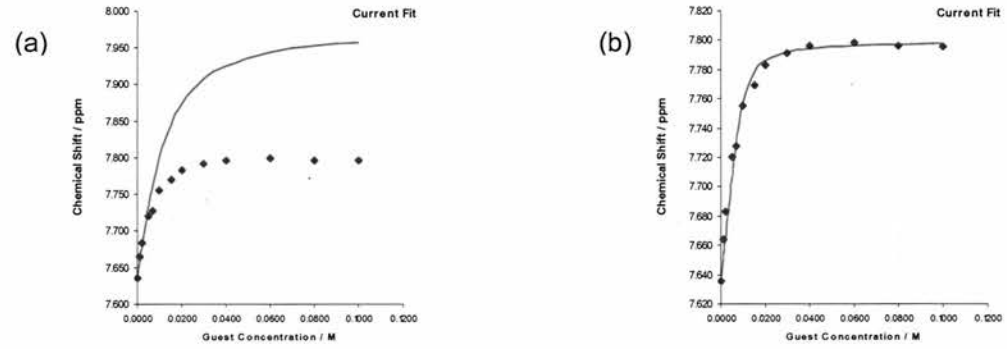

Figure 41 (a) Graph before non-linear curve fitting. (b) Correctly fitted line giving K_a value. The experimental results are shown in blue and the fitted line is shown in red.

Table 2 Table showing the results from the binding study for one proton within the **122**.

Sample Number	[Guest]	δ_{obs}	δ_{calc}	Residual	SR		
1	0	7.635	7.635	0	0.00E+00		
2	0.001	7.664	7.65	0.0141	2.00E-04		
3	0.002	7.683	7.664	0.0186	3.45E-04		
4	0.005	7.72	7.705	0.0146	2.13E-04	**Δδ(sat)**	**0.164**
5	0.007	7.727	7.729	-0.0021	4.44E-06	**[Host]**	**0.01**
6	0.01	7.755	7.756	-0.0009	8.20E-07	**T/K**	**293**
7	0.015	7.769	7.778	-0.0087	7.55E-05	**Ka**	**1080**
8	0.02	7.783	7.786	-0.0028	7.70E-06		
9	0.03	7.791	7.792	-0.0006	3.78E-07		
10	0.04	7.796	7.794	0.0021	4.60E-06		
11	0.06	7.798	7.796	0.0023	5.09E-06		
12	0.08	7.796	7.797	-0.0006	3.33E-07		

From all of the data recorded, an average K_a value of 750 M^{-1} was obtained which allows the calculation of ΔG – in this instance ΔG = -16.4 kJ mol^{-1}. The K_a data obtained are consistent with the results expected for three hydrogen bonds. Previously within the group, the association constants for the binding of **119** and **45** to amidopyridine derivative **149** were calculated (Figure 42). From these data it can be seen that, on average, one hydrogen bond contributes around ΔG = -5.7 kJ mol^{-1} which means that **122** is in fact better than expected. The K_a values previously recorded are much lower than those observed for **122**, showing that **122** is a good fit for **45** and binds it well.

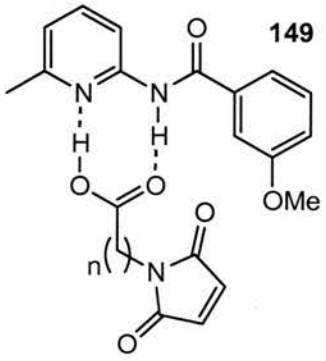

n=1, **119** K_a = 115 M^{-1}; ΔG = -12.7 kJ mol^{-1}

n=2, **45** K_a = 45 M^{-1}; ΔG = -10.2 kJ mol^{-1}

Figure 42 Association constant, K_a, and ΔG values for amidopyridine derivative **149** binding **119** and **45**.

2.6.2 $^{1}H - {}^{15}N$ Correlation NMR

In order to prove the presence of the internal hydrogen bond, a 500 MHz $^{1}H-{}^{15}N$ NMR correlation experiment ($^{1}H-{}^{15}N$ HSQC) was performed. There are three amide groups in **122**: one in the binding site, one in the polarisation site and one involved in the internal hydrogen bond. If all three hydrogen bonds are formed upon complexation with **45**, we should observe a shift in both the ^{1}H and the ^{15}N dimensions when comparing the spectrum of a 1:1 mixture of **122**:**45** with a spectrum containing only **122**. The spectra have been overlaid and are shown in Figure 43, the spectrum for 7 mM **122** is shown in blue, and the spectrum for a mixture of 7 mM **122** with 7 mM **45** is shown in red. It can be seen that all three amide peaks shift in both dimensions – in the case of the binding site amide it shifts off the scale.

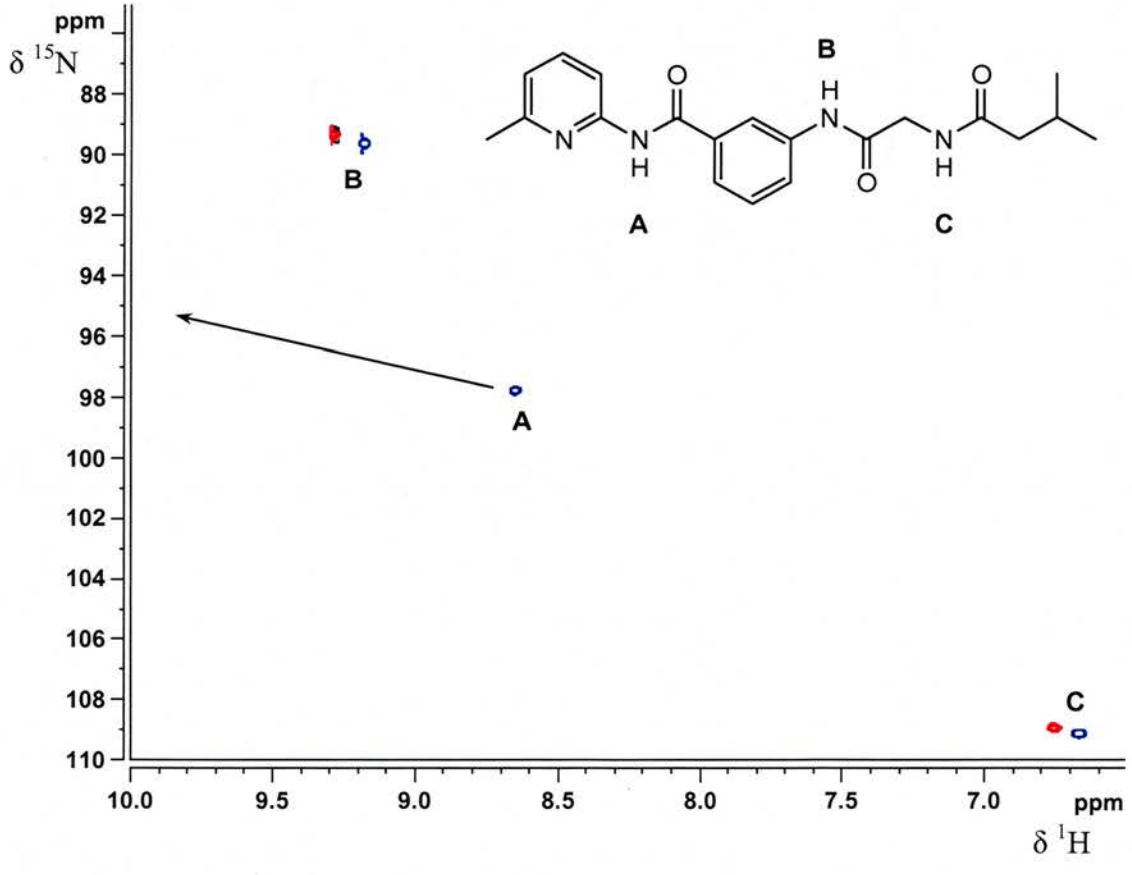

Figure 43 500 MHz $^{1}H-{}^{15}N$ NMR correlation results showing the spectrum of 7 mM **122** in blue with the spectrum of a mixture of 7 mM **45** with 7 mM **122** shown in red. The peak labelled **A** corresponds to the binding site amide, **B** is the internal hydrogen bond and **C** is the polarisation site amide.

The amides are assigned as follows: the peak at 8.6 ppm is the binding site amide which H-bonds to the carboxylic acid group, labelled **A**; the peak at 9.2 ppm is the amide group involved in forming the internal hydrogen bond, labelled **B**; and the peak at 6.7 ppm is the polarisation site amide which H-bonds to the maleimide carbonyl group, labelled **C**. The

shifts for all three peaks indicates that three amide hydrogen bonds are present which is consistent with the K_a data obtained which also indicates the presence of three hydrogen bonds.

2.7 Determining Reaction Conditions

Prior to conducting kinetic experiments, test reactions were conducted to investigate the optimum reaction conditions which could be used for all three reaction types, giving measurable reaction rates for the control reactions without the reactions proceeding too quickly. The control reactions were performed by mixing a solution of **45** (0.5 mL) dissolved in $CDCl_3$, with an equal volume of reactant solution dissolved in $CDCl_3$ to give equal initial concentrations of **45** and reagent.

The extent of reaction was determined in each case by using the deconvolution tool in 1D WinNMR. Deconvolution allows the area of a peak to be determined by fitting the peak to a Lorenzian curve. It is a more accurate method than integration. Resonances are selected from the starting material and products that correspond to protons at the reactive centre. For example, the resonance at 6.7 ppm corresponds to the two CH double bond protons on the maleimide ring in the starting material. This resonance decreases in size as the reaction proceeds and maleimide is converted into product. Figure 44 shows a partial 500 MHz ^{1}H NMR spectrum of the product resonances for the conjugate addition reaction in blue with the results from the deconvolution overlaid. It can be seen that an accurate fit is obtained.

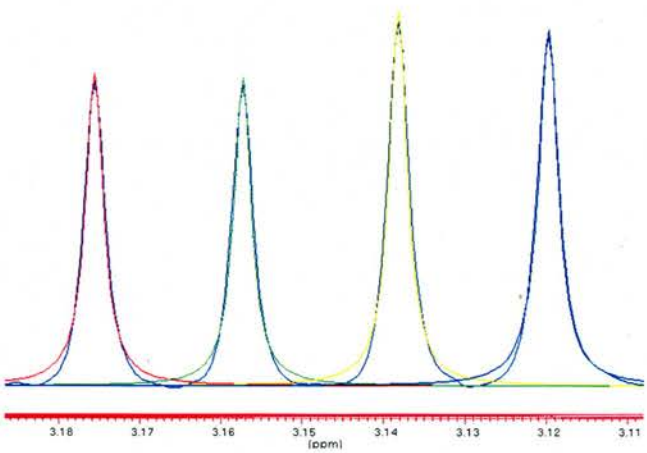

Figure 44 Partial 500 MHz ^{1}H NMR spectrum showing resonances for one proton in the product of the conjugate addition reaction in blue with the results from deconvolution overlaid.

2.7.1 Diels-Alder reaction

For the Diels-Alder reaction, test reactions were carried out at both 25 °C and 35 °C with an overall concentration of 25, 50 or 75 mM for **45** and **142**. The solutions were prepared as described in Section 2.7 and left to react for 16 hours in a water bath at the desired temperature. After this time, 300 MHz ^{1}H NMR spectra were collected. The extent of reaction was calculated through determining the concentration of **146** formed with respect to the starting materials by deconvolution. The results for the different reaction conditions are shown in Table 3.

Table 3 Table showing the results from the percentage conversion of reactants into **146** for the test reactions at two temperatures and three starting concentrations of **142** and **45**.

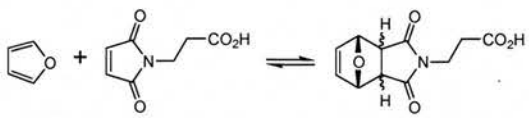

144 **45** **146**

Temperature	% Conversion		
	25 mM	50 mM	75mM
25 °C	8%	17%	24%
35°C	13%	27%	35%

The bridgehead protons on **146** give distinctive resonances between 5.33 and 5.25 ppm which can be used for deconvolution to determine the extent of reaction (Figure 45). It is possible to calculate the product concentrations for both *exo* and *endo* isomers, but because **122** is not designed to alter the stereochemical outcome of the reaction, only the total product concentration of **146** has been used for clarity. Later we will see that, deconvoluting for both isomers in fact shows that the stereoselectivity of the reaction is not altered by **122** as expected.

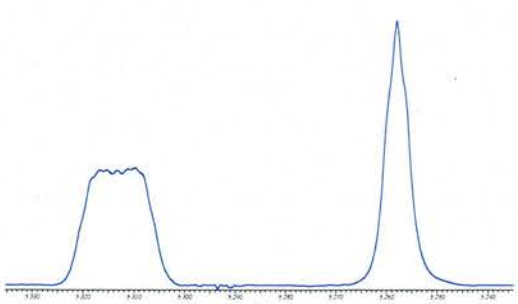

Figure 45 Partial 300 MHz ^{1}H NMR spectrum of the *exo* and *endo* isomers of **146** recorded in $CDCl_3$ showing resonances corresponding to the bridgehead protons in **146** used for deconvolution.

2.7.2 [3+2] Dipolar Cycloaddition Reaction

The reaction conditions for the [3+2] dipolar cycloaddition reaction were probed using the same conditions described for the Diels-Alder reaction. Samples were prepared containing overall concentrations of 25, 50 and 75 mM of **45** and **145** dissolved in $CDCl_3$ and allowed to react at 25 or 35 °C for 16 hours. Results for the extent of the reaction under the different reaction conditions are shown in Table 4.

Table 4 Table showing the results from the percentage conversion of reactants into **147** for the test reactions at two temperatures and three starting concentrations of **145** and **45**.

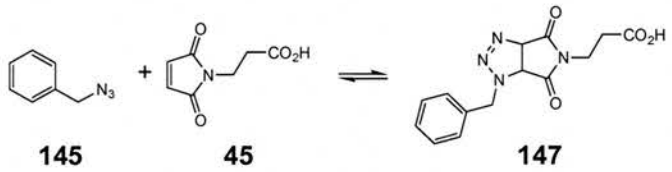

145 **45** **147**

Temperature	% Conversion		
	25 mM	50 mM	75mM
25 °C	1%	7%	11%
35°C	4%	10%	18%

The resonances used for deconvolution, between 4.76 and 4.71 ppm, are shown in Figure 46, corresponding to one proton in **147**. The results must be scaled to account for the fact the maleimide resonance represents two protons.

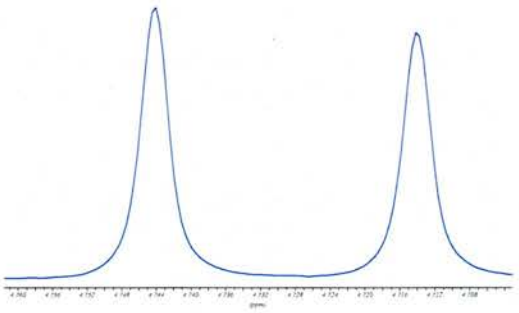

Figure 46 Partial 300 MHz ^{1}H NMR spectrum of **147** recorded in $CDCl_3$ showing resonances corresponding to one proton in the product used for deconvolution.

2.7.3 Conjugate Addition Reaction

Two different thiols and bases were tested for the conjugate addition reaction. Firstly, reactions were conducted using heptanethiol **150** with imidazole acting as the base. Test reactions were conducted at 15 °C and 25 °C using an overall concentration of 25, 50 and 75

mM **150** and **45** with one equivalent of base. Analysis showed that no reaction had occurred overnight; however, white crystals had precipitated. A 300MHz ^{1}H NMR spectrum of these crystals dissolved in methanol was recorded which showed that they were in fact **45**. It appeared that imidazole had deprotonated the carboxylic acid leading to precipitation of **45** as a salt instead of deprotonating **150**.

These test reactions were then repeated using 0.5 and 1 equivalents of 4-*t*-butylpyridine as a base at the same concentrations and temperatures as indicated previously. The spectra obtained from these test reactions did not show any formation of **148** or precipitation of **45**. These results indicate that 4-*t*-butylpyridine is not capable of deprotonating **45**. The results are promising, despite the absence of reaction occurring. The next step was to use an alternative thiol which is more acidic than **150**. It was decided to use another commercially available thiol, this time thiophenol **143**.

Test reactions were repeated with **143**, this time using 25 or 50 mM overall concentration of **143** and **45** with 0.1, 0.5 or 1 equivalents of 4-*t*-butylpyridine at 25 °C. The solutions were warmed at 25 °C for 16 hours before 300 MHz ^{1}H NMR spectra were recorded.

The resonances from **148** used in deconvolution are shown in Figure 47. In this case the four resonances between 3.19 and 3.11 ppm correspond to one proton in **148** and must be scaled to account for the two protons in the maleimide resonance.

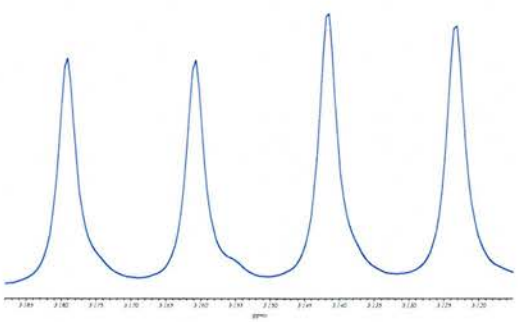

Figure 47 Partial 300 MHz ^{1}H NMR spectrum of the conjugate addition product **148** recorded in $CDCl_3$ showing the resonances corresponding to one proton in **148** used for deconvolution.

Results showed that using **143** with 4-*t*-butylpyridine does indeed lead to the formation of **148** (Table 5).

Table 5 Table showing the percentage conversion of starting materials **143** and **45** into **148** for two different starting concentrations of **143** and **45** and three different base concentrations.

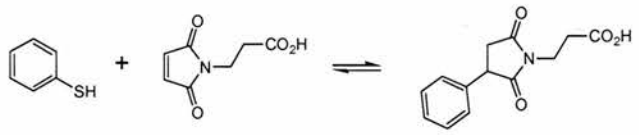

143 **45** **148**

Reactant Concentration / mM	Base / eq	% Conversion
25	0.1	3%
25	0.5	16%
25	1	23%
50	0.1	5%
50	0.5	27%
50	1	44%

After comparing the results obtained for the various reaction conditions used across all three reaction types, it was decided that the optimum conditions to use in our studies were: 50 mM overall concentrations for **45** and **142**, **143**, or **145** at 35 °C with the addition of 0.5 equivalents of 4-*t*-butylpyridine in the conjugate addition reaction. Under these reaction conditions, the [3+2] dipolar cycloaddition reaction is fairly slow, whereas the conjugate addition control reaction is slightly faster than would normally be required in a control reaction. However, it is anticipated that **122** will have the greatest effect on the conjugate addition reaction and a dramatic change will be observed.

2.7.4 Organocatalyst Reactions

In order to investigate the effect of **122** and its potential for turnover, it was proposed to carry out the reactions with varying concentrations of **122**. However, as a consequence of the poor solubility of **122** in $CDCl_3$, the maximum concentration possible is 10 mM which corresponds to a catalyst loading of 20 mol%.

2.8 Kinetic Experiments

Once the optimum reaction conditions had been investigated, it was then possible to conduct kinetic experiments which allowed the product concentration to be monitored against reaction time. These studies were performed by monitoring the reaction by 500 MHz ^{1}H NMR spectroscopy. A 500 MHz ^{1}H NMR spectrum is recorded every 30 minutes over the course of

16 hours, which allows the cycloadduct concentration to be determined through deconvolution, leading to the preparation of a concentration-time profile.

The effect of **122** on the different reaction types was determined by comparing the profile obtained for the control reactions with the profile for reactions containing **122**. For each reaction type two experiments were performed. Firstly, a control reaction was performed which did not contain **122** to give the bimolecular reaction rate. Secondly, the reaction was performed with 10 mM (20 mol%) **122** added.

2.8.1 Diels-Alder Reaction

The results from the reaction between **142** and **45** are shown in Figure 48 where data from the control reaction are shown in red and data from the reaction with **122** added are shown in blue.

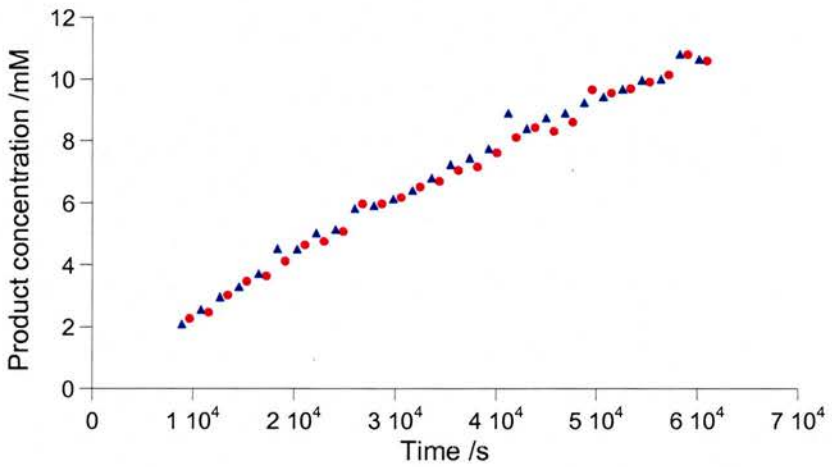

Figure 48 Kinetic data for the reaction between 50 mM **142** and **45** at 35 °C showing total concentration of **146** against time. Red circles indicate the control reaction in the absence of **122**. Blue triangles show the results when 10 mM **122** is added.

It can be seen that **122** has little effect on the rate of the reaction. The best measure of the efficiency of the catalyst is to calculate the rate of the catalysed reaction divided by the rate of the uncatalysed reaction, k_{cat}/k_{uncat}. The concentration-time profile can be used to determine the rates of the uncatalysed and catalysed reactions. The kinetic simulation program Simfit[216] is used for this purpose. The kinetic simulation procedure is outlined in Figure 49.

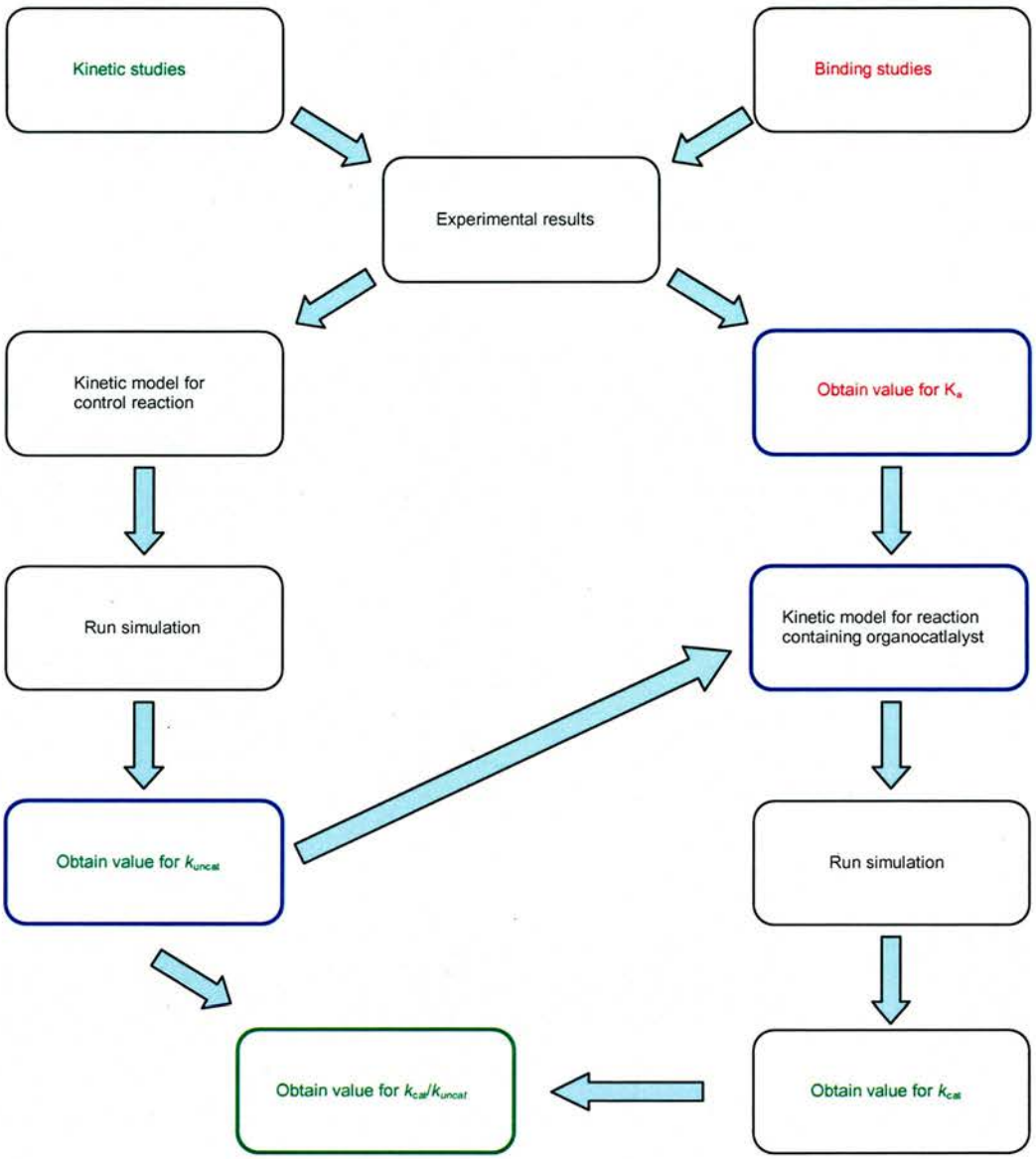

Figure 49 Schematic representation of kinetic simulation procedure. The experimental data for the control reaction is used to obtain a value of k_{uncat}. This value is then inserted into the model for the catalysed reaction along with the K_a value obtained from the binding study giving k_{cat}.

In order to fit the data, several pieces of information are required: the association constant data obtained from the binding study and the results from the kinetic experiments for both the control and catalysed reactions. The control reaction is considered first because the kinetic model is much simpler for this process and a value for k_{uncat} is required for the model of the catalysed reaction. The model for the uncatalysed reaction is shown in Figure 50. The Diels-Alder reaction is reversible; therefore we must consider both the forward and reverse reaction rates. In this case the value of k_{uncat} required is the rate of the forward reaction, $k_{uncatfwd}$.

Uncatalysed reaction:

$$\text{Diene + Dienophile} \xrightarrow{k_{\text{uncatfwd}}} \text{Product}$$

$$\text{Product} \xrightarrow{k_{\text{uncatrev}}} \text{Diene + Dienophile}$$

Figure 50 The kinetic model for the uncatalysed reaction between furan and C-2 maleimide where diene represents **142**, dienophile represents **45** and product is **146**.

The results of the kinetic simulation for the control reaction are shown in Figure 51 and the values obtained for k_{uncatfwd} and k_{uncatrev} are 9.08 x10^{-5} M^{-1} s^{-1} and 6.03 x10^{-7} s^{-1} respectively. These values are then used in the kinetic model for the catalysed reaction.

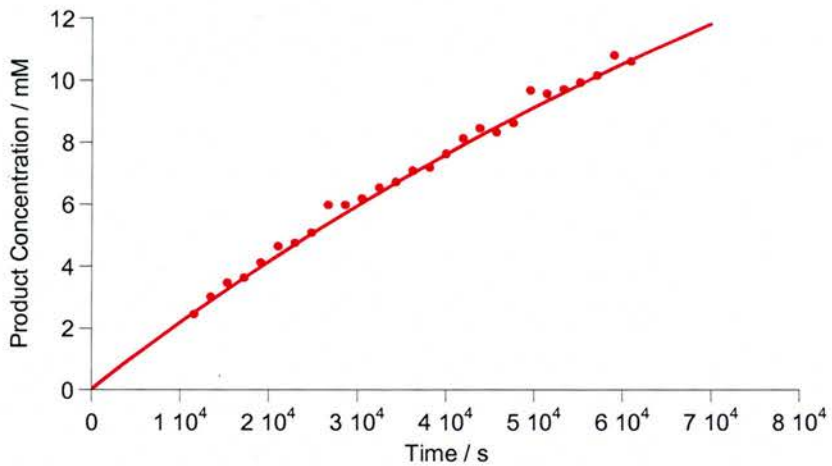

Figure 51 Results of kinetic simulation for the control data, with the experimental data shown as red circles and the fitted data as a solid line.

Fitting the data for the catalysed reaction is more complicated, as shown by the model in Figure 52. The values obtained for the reaction rates of the control reaction are fixed in the model. Values for the association and dissociation of the substrate and catalyst, k_{assoc} and k_{dissoc}, are derived from the K_a value obtained from the binding study are also fixed. The equilibrium for product dissociation from the catalyst is assumed to be the same as the values calculated for substrate binding. The only variables being calculated by the program are the rate constants for k_{catfwd} and k_{catrev}.

Catalysed reaction:

$$\text{Diene + Dienophile} \xrightarrow{k_{uncatfwd}} \text{Product}$$

$$\text{Product} \xrightarrow{k_{uncatrev}} \text{Diene + Dienophile}$$

$$\text{Dienophile + Catalyst} \xrightarrow{k_{assoc}} \text{[Dienophile•Catalyst]}$$

$$\text{[Dienophile•Catalyst]} \xrightarrow{k_{dissoc}} \text{Dienophile + Catalyst}$$

$$\text{[Dienophile•Catalyst] + Diene} \xrightarrow{k_{catfwd}} \text{[Product•Catalyst]}$$

$$\text{[Product•Catalyst]} \xrightarrow{k_{catrev}} \text{[Dienophile•Catalyst] + Diene}$$

$$\text{[Product•Catalyst]} \xrightarrow{k_{dissoc}} \text{Product + Catalyst}$$

$$\text{Product + Catalyst} \xrightarrow{k_{assoc}} \text{[Product•Catalyst]}$$

Figure 52 The kinetic models used for the catalysed reaction. Diene represents **142**, dienophile represents **45**, product represents **146** and catalyst represents **122**.

The results obtained for simulation of the catalysed reaction are shown in Figure 53. In this case the values obtained for k_{catfwd} and k_{catrev} are 1.92 x10^{-4} M^{-1} s^{-1} and 4.47 x10^{-5} s^{-1} respectively.

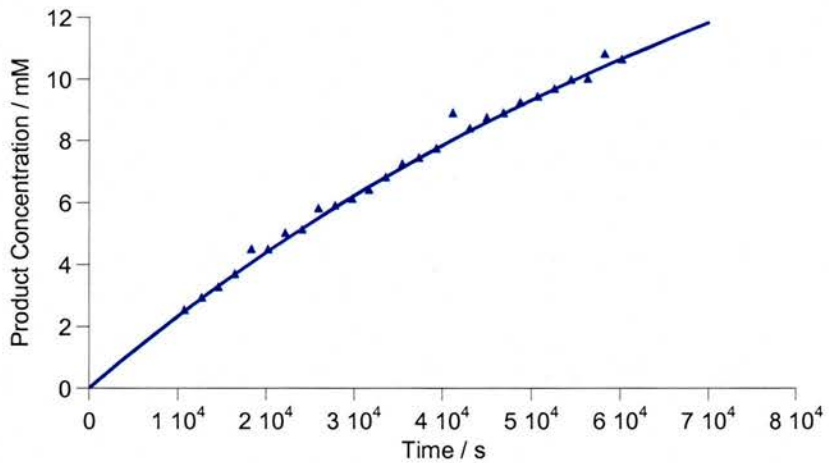

Figure 53 Results of kinetic simulation for the reaction containing **122**, with the experimental data shown as blue triangles and the fitted data as a solid line.

Having calculated the rate constants for both the catalysed and uncatalysed reactions it is now possible to obtain a measure of rate acceleration achieved by the **122**, k_{cat}/k_{uncat}, or in this case $k_{catfwd}/k_{uncatfwd}$. The calculation is shown in Equation 2. For the Diels-Alder reaction, a value of k_{cat}/k_{uncat} = 0.5 was obtained, which indicates that the reaction goes more slowly in the presence of the organocatalyst. It is possible that the organocatalyst could be inhibiting the

reaction. There may be steric interactions which make it more difficult for the Diels-Alder reaction to occur when **45** is bound to **122**.

$$\frac{k_{catfwd}}{k_{uncatfwd}} = \frac{9.08x10^{-5}}{1.92x10^{-4}} = 0.5$$

Equation 2 Calculation of the ratio of catalysed and uncatalysed reaction rates for the Diels-Alder reaction.

2.8.2 [3+2] Dipolar Cycloaddition Reaction

Figure 54 shows the results for the control reaction in red, and the results for the catalysed reaction between **145** and **45** in blue.

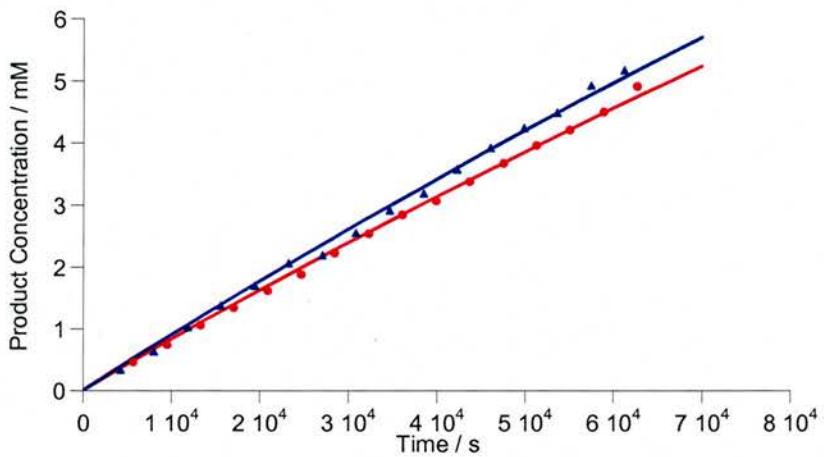

Figure 54 Kinetic data for the reaction between 50 mM **145** and **45** at 35 °C showing **147** concentration against time. Red circles indicate the control reaction in the absence of **122**. Blue triangles show the results when 10 mM **122** is added. Kinetic simulation results are shown as solid lines where red is the uncatalysed reaction and blue is the catalysed reaction.

In the case of the [3+2] dipolar cycloaddition reaction, it appears that **122** is having an effect on the reaction rate. The reaction rates were obtained by kinetic simulation as before, using the models shown in Figure 55. This time the reaction is not reversible so an equilibrium situation does not have to be considered. Results from the simulations give a value of $k_{cat}/k_{uncat} = 1.5$, indicating that **122** is having a slight effect on the rate of the reaction. It is not a particularly large rate acceleration but it has been obtained using only 20 mol% **122**. It is probable that a higher concentration of **122** would lead to greater rate acceleration.

Uncatalysed reaction:

$$\text{Azide + Dipolarophile} \xrightarrow{k_{uncat}} \text{Product}$$

Catalysed reaction:

$$\text{Azide + Dipolarophile} \xrightarrow{k_{uncat}} \text{Product}$$

$$\text{Dipolarophile + Catalyst} \xrightarrow{k_{assoc}} \text{[Dipolarophile•Catalyst]}$$

$$\text{[Dipolarophile•Catalyst]} \xrightarrow{k_{dissoc}} \text{Dipolarophile + Catalyst}$$

$$\text{[Dipolarophile•Catalyst] + Diene} \xrightarrow{k_{cat}} \text{[Product•Catalyst]}$$

$$\text{[Product•Catalyst]} \xrightarrow{k_{dissoc}} \text{Product + Catalyst}$$

$$\text{Product + Catalyst} \xrightarrow{k_{assoc}} \text{[Product•Catalyst]}$$

Figure 55 Kinetic model used for the [3+2] dipolar cycloaddition reaction. Azide represents **145**, dipolarophile represents **45**, catalyst represents **122** and product represents **147**.

2.8.3 Conjugate Addition Reaction

Results for the conjugate addition reaction (Figure 56) show a marked difference in reaction rates between the control reaction, shown in red, and the catalysed reaction, shown in blue.

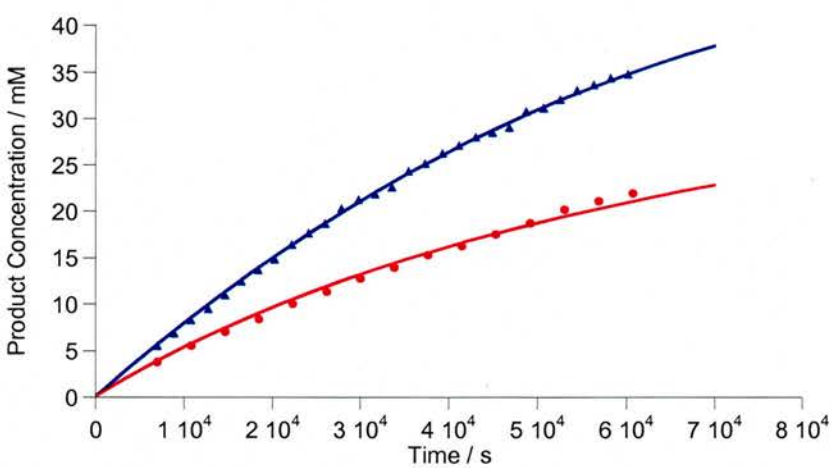

Figure 56 Kinetic data for the reaction between 50 mM **143** and **45** at 35 °C showing **148** concentration against time. Red circles indicate the control reaction in the absence of **122**. Blue triangles show the results when 10 mM **122** is added. Kinetic simulation results are shown as solid lines where red is the uncatalysed reaction and blue is the catalysed reaction.

It is clear from Figure 56 that **122** has a significant effect on the reaction rate for the conjugate addition reaction. The rate constants for the reactions were obtained through kinetic simulation as before. The model becomes more complicated in this instance as the equilibrium between free thiol and disulfide must also be considered. In the uncatalysed reaction model, all three rate constants are simulated. The model is shown in Figure 57.

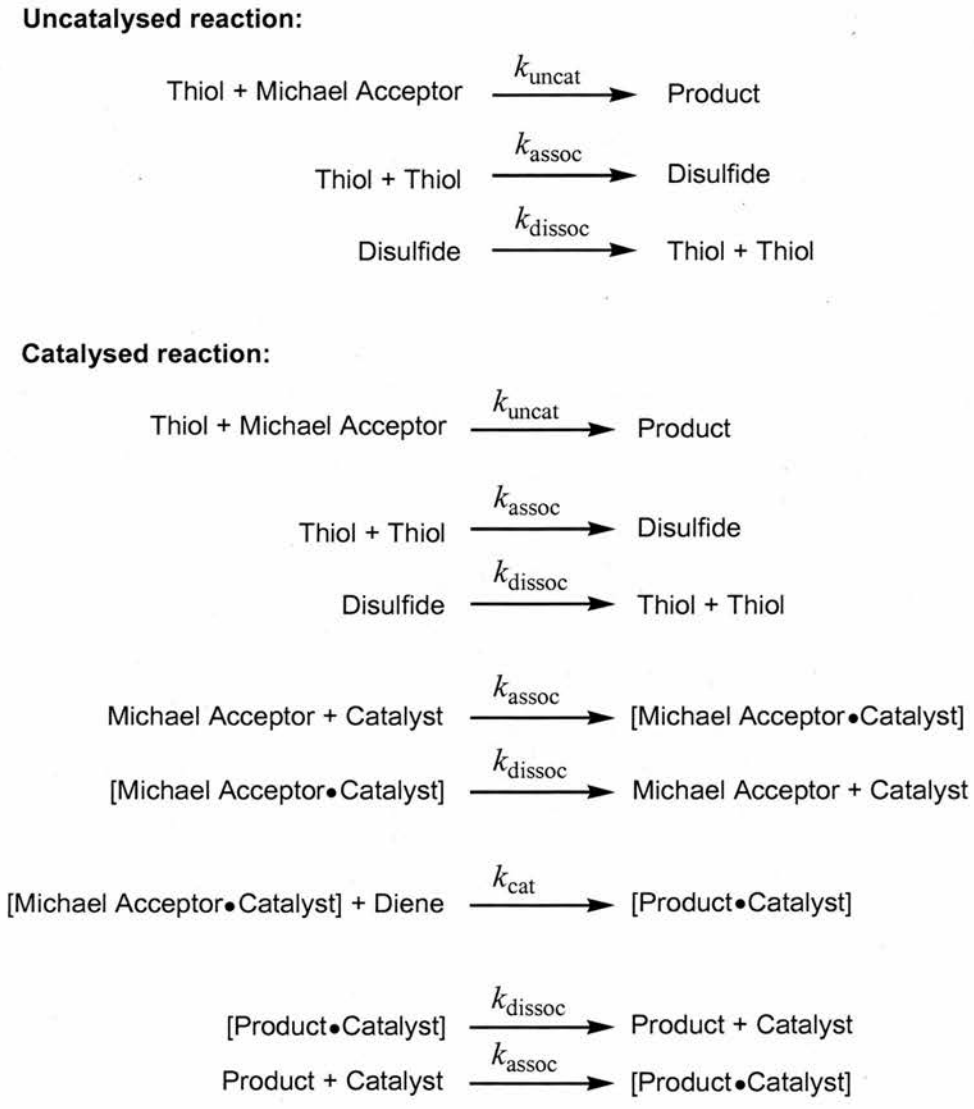

Figure 57 Kinetic model used for the conjugate addition reaction. Thiol represents **143**, Michael Acceptor represents **45**, disulfide represents the dimer of **143**, catalyst represents **122** and product represents the **148**.

The values for the rates of k_{assoc} and k_{dissoc} for the equilibrium between free thiol and disulfide are obtained in the simulation for the control reaction and these values are then fixed when the simulation for the catalysed reaction is run. The reaction rates obtained give a value of K = 0.06 M^{-1} which shows that the equilibrium lies towards the free thiol. Therefore, it is valid to include this equilibrium in the model. For comparison, Figure 58 shows the simulation results

when the equilibrium between free thiol and disulfide is not included. It can be seen that now the simulation does not match the experimental data. For this reaction type, $k_{cat}/k_{uncat} = 37$.

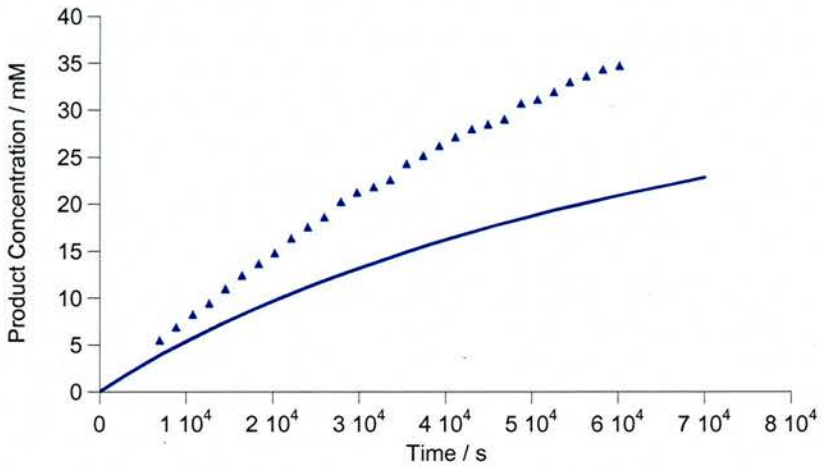

Figure 58 Results of the kinetic simulation when the thiol to disulfide equilibrium is not included in the model. Blue triangles show the experimental data for the catalysed reaction and the solid line is the fitted line.

Having obtained experimental rate acceleration data it is now possible to return to the graph in Figure 35(a) and compare transition state charge with rate acceleration. In order to plot the graph, we must now consider quantifying transition state charges.

It is difficult to quantify transition state charges – there are several different ways that could be chosen. For ionic bonds the matter is simple, one species has a full positive charge whilst the other carries a full negative charge. However, once covalent bonds are considered the matter becomes more complicated. For example, when considering methyl lithium, $Me^{-}Li^{+}$, it would be incorrect to assign a full positive charge to lithium and a full negative charge to the carbon atom of the methyl group because it is not an ionic bond that forms. The question then is to find a method of assigning the charges to each species.

The simplest method was developed by Mulliken[217] whereby the covalent bond is divided in half and the charge that lies to each side of the divide is allocated to the atom on that side as illustrated more clearly in Figure 59. Using this method, lithium is given a value of +0.85 and the carbon atom of the methyl group is given a value of -0.85.

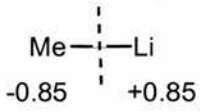

Figure 59 Values for the charges on carbon and lithium in methyl lithium as determined by the Mulliken method. The bond is divided in half and the charge that lies to the left is assigned to carbon whereas the charge that lies to the right is assigned to lithium.

The Mulliken method is only one method of calculating charges for a covalently bonded species. The charges could be calculated in a variety of ways depending on the criteria chosen. When moving towards calculating transition state charges there are more factors to consider and the problem becomes considerably more complicated. For example, the transition state of an S_N2 reaction is shown in Figure 60 which illustrates the different factors to be considered. Partial negative charges are assigned to the approaching nuclophile and the leaving group. However, it is not only these charges which must be considered, the extent of the reaction must also be known so that the length of the bonds being broken and formed can be calculated. This illustrates the importance of considering synchronous and asynchronous reactions (see Section 1.3.2 p.9).

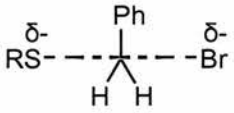

Figure 60 When considering the charge in a transition state, for example an S_N2 reaction, the partial charges on the nucleophile and leaving group are not the only factors to use in calculations. The extent of the reaction must also be considered so the lengths of the bonds, shown in dashed lines, are known.

Calculating charges for transition states is problematic because an accurate model of the transition state in solvent is required. Determining the exact nature of transition states accurately is very difficult. For this reason, we have chosen to concentrate on one atom of the transition state: the oxygen atom of the carbonyl group at the polarisation site. The charge is calculated at the oxygen in the ground state when it is bound to **122** and then recalculated for the transition state of all three reaction types. The percentage change in transition state is then calculated. The reason that the change in charge at the polarisation site was calculated is that it gives results which can be directly compared across the reaction types. For example, in the Diels-Alder reaction there are two reactive sites and in the conjugate addition reaction the sulfur possesses a formal negative charge which would all obscure the results. The results obtained by electronic structure calculations for the three reaction types are shown in Table 6.

Table 6 Results for percentage change in charge at the polarisation site obtained for each reaction type.

Reaction Type	% Change in Charge
Diels-Alder	3
[3+2] Dipolar Cycloaddition	11
Conjugate Addition	86

The values for percentage change in charge at the polarisation site allows the graph shown in Figure 61 to be plotted.

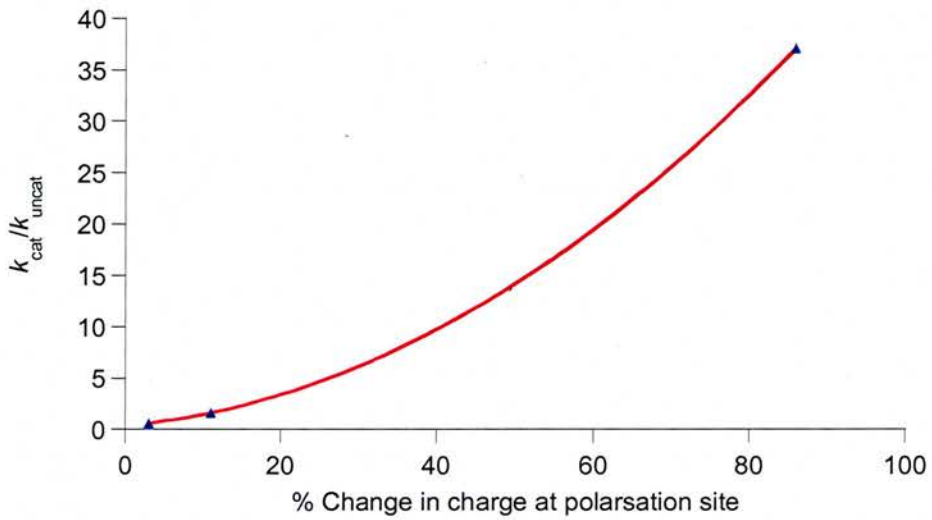

Figure 61 Graph showing rate acceleration, k_{cat}/k_{uncat}, against % change in charge at the polarisation site across the three reaction types. Experimental data is shown in blue triangles and a smooth curve is fitted in red.

From this graph it would appear that a slight increase in transition state charge does not give a disproportionately large rate acceleration (line (ii) in Figure 35(a)) and it also seems unlikely that rate acceleration and charge are directly proportional. It is more likely that the relationship between transition state charge and rate acceleration is closer to line (iii) in Figure 35(a), where significant transition state charge is required before any rate acceleration is observed. Given the differences observed for rate accelerations in enzymes and catalytic antibodies for non-polar reactions, these results are not unexpected.

The graph in Figure 61 only consists of three points which makes it very difficult to make any specific conclusions. In order to definitively establish the relationship between rate acceleration and transition state charge at least two more points on the graph are required. The problem is that we are limited by the number of reactions it is possible to perform using the substrate.

2.9 Conclusions

Natural systems often use biosynthetic strategies which contain a series of polar reactions when the corresponding total synthesis strategies used by chemists may contain non-polar reactions such as the Diels-Alder reaction. Nature will catalyse non-polar reactions in cases where an equivalent polar reaction is not acceptable or in cases where catalysis can be achieved simply. For example, in the case of chorismate mutase (Section 1.4.4) the enzyme holds chorismate in the correct orientation but the reaction is already intramolecular and will occur spontaneously.

In order to establish the relationship more definitively, more points on the graph are required. Now that a method for determining a measure of charges has been established, it should be possible to identify other reactions to investigate and add to the graph. We can now screen reactions that can be carried out using a maleimide substrate to find those with 20-60% change in charge at the polarisation site. For example, we could find that a [3+2] dipolar cycloaddition reaction using a nitrone instead of an azide may lie in this region. This study has allowed us to identify exactly which reaction types we need to study in order to truly establish the relationship between rate acceleration and transition state charge.

From all the data obtained, **122** is most effective at catalysing a polar reaction, which is to be expected from the manner in which the substrate is polarised. Figure 62 shows the two tautomeric forms that **45** can adopt as the two extremes of polarisation.

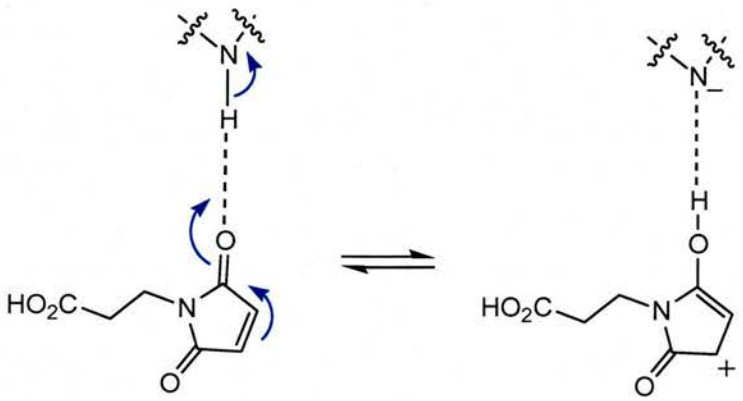

Figure 62 Conjugation of the double bond in **45** through to the polarisation site. Two extreme states are shown.

From Figure 62 it can be clearly seen that the substrate is more suitable for nucleophilic attack as in a conjugate addition reaction than any other reaction type. In order to accelerate a Diels-

Alder reaction, the double bond needs to be evenly activated by polarising both carbonyl groups equally.

2.10 Future Directions

There is the potential for carrying out many more experiments using organocatalyst **122**. A more in depth comparison of the relationship between rate acceleration and the change in charge at the polarisation site is required in order to determine which functional form depicted in Figure 35 most closely matches the experimental data.

There are several features of **122** which could be improved upon.

(i) In order to accelerate a Diels-Alder reaction, the double bond should be evenly activated.

Diels-Alder reactions are catalysed by lowering the energy of the LUMO of the diene and this can be done by polarisation. By removing electron density from both ends of the double bond, the LUMO energy should be lowered and the situation described in Figure 62 avoided. The potential for this activation already exists within the maleimide substrate because it contains carbonyl groups conjugated to both ends of the double bond. Designing an organocatalyst capable of hydrogen bonding to both carbonyl groups, as shown in Figure 63, should remove electron density equally from both sides of the double bond.

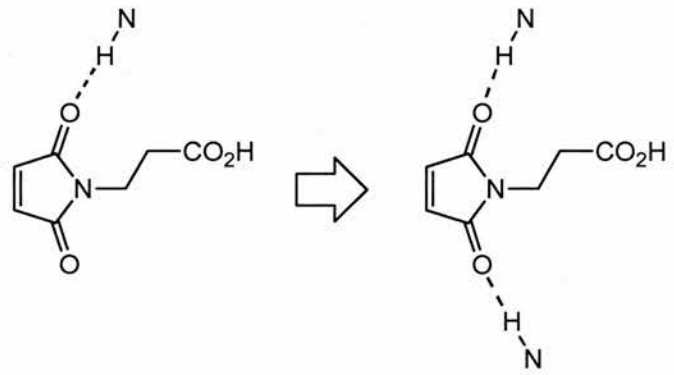

Figure 63 Moving from a situation where only one carbonyl is involved in hydrogen bonding to a situation where both carbonyl groups are hydrogen bonded should give equal polarisation of the double bond making catalysis of a Diels-Alder reaction possible.

(ii) Polarisation could be increased by activating the substrate with more than one hydrogen bond.

Organocatalysts **117** and **118** (Section 2.1) use urea derivatives to polarise the substrate which means there are two hydrogen bonds used to activate the substrate. Increasing the number of hydrogen bonds should lead to an increase in the activation of the maleimide substrate (Figure 64).

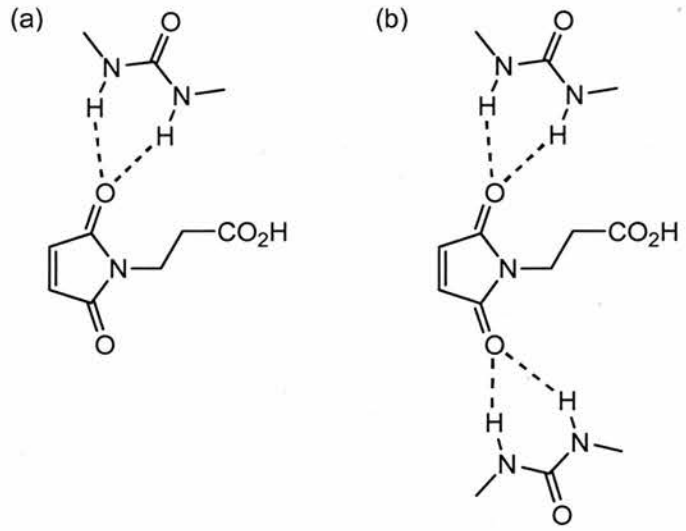

Figure 64 (a) Using a urea in the polarisation site will activate the substrate with two hydrogen bonds which should be more effective. (b) A bis urea organocatalyst should be more effective at accelerating a Diels-Alder reaction than an organocatalyst containing a single urea polarisation site.

(iii) The solubility of the organocatalyst could be improved in order to use higher catalyst loadings.

It would be worthwhile testing a variety of capping groups to determine their effect on the solubility of the organocatalyst. An isovaleryl group was chosen in this instance but there are many other capping groups which could have been used as alternatives such as *tert*-butyl groups or other alkyl chains. Molecular modelling studies of organocatalysts containing different capping groups, to assess their impact on substrate binding and polarisation, should allow suitable groups to be identified and synthesised.

(iv) The organocatalyst only binds one of the reactants which means that the target reaction is still an intermolecular process.

The Introduction has shown that one of the most important features of enzyme catalysis is intramolecularity. In order to approach an enzyme-like situation, the organocatalyst must bind both substrates for the reaction, holding them in close proximity to give rate acceleration through *pseudo*-intramolecularity. Developing an organocatalyst with two binding sites, for

the maleimide and the reaction type specific reactants, and also introducing complementary recognition sites to all reactant molecules will allow the effect of proximity to be examined.

(v) Adapting the synthetic strategy will allow the organocatalyst to be immobilised upon solid support.

Immobilising the organocatalyst upon solid support gives several advantages. It allows the organocatalyst to be easily separated from the reaction mixture which enables recycling. There are also synthetic advantages to using solid-phase chemistry. Adapting the synthetic strategy for use on solid support gives the potential for the rapid synthesis of a range of different organocatalysts. The organocatalyst contains several amide bonds which means that it could be comprised of a variety of different amines and carboxylic acid derivatives.

Originally it was proposed to incorporate an amino acid into the organocatalyst backbone instead of just a CH_2 group. In order to create many different organocatalysts with different amino acid residues easily, it would be advantageous to use combinatorial chemistry techniques. These involve immobilising the organocatalyst upon solid support. For example, in Figure 65(a) the R group indicates an amino acid residue. Conducting the organocatalyst synthesis upon solid support would allow the synthesis of organocatalysts containing any amino acid.

The synthesis could be further adapted by extending the chain length to incorporate two or three amino acid residues (Figure 65(a) and (b)). Extending the chain length allows extra polarisation sites to be introduced and enables the organocatalyst to bind different substrates. Different combinations of amino acids should also give interesting results for reactions that produce different cycloadduct isomers. Adjusting the organocatalyst in this manner should allow the selection of one isomer and the organocatalyst can be tailored to produce a specific product.

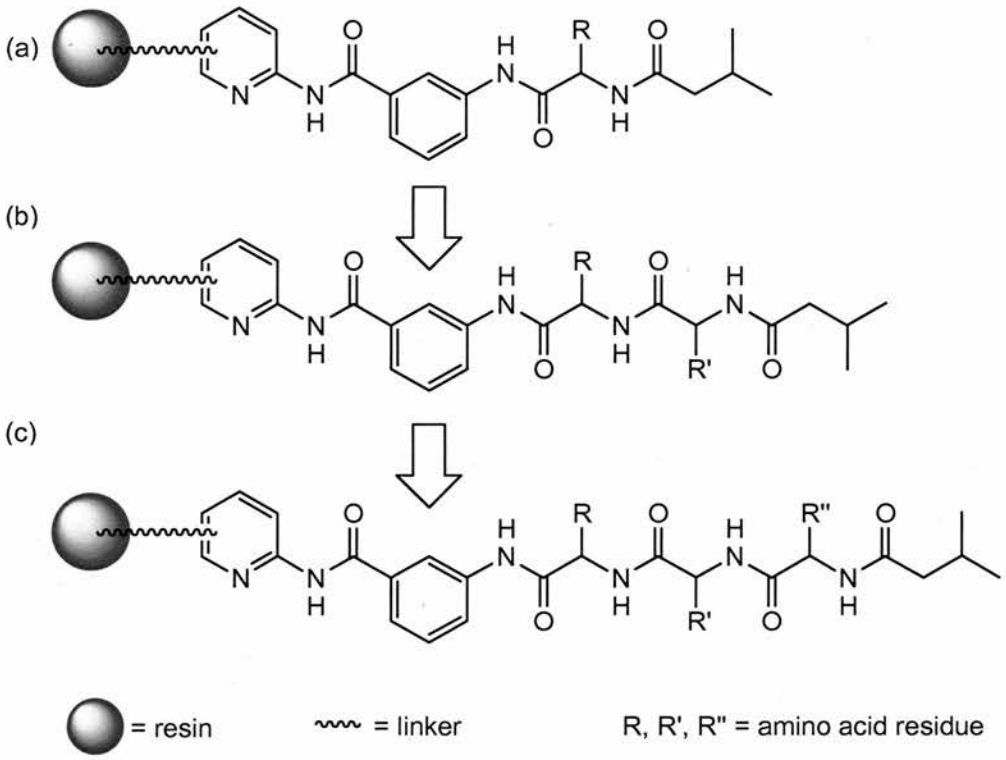

Figure 65 Immobilising the organocatalyst upon solid support introduces a simple method for developing a vast array of different organocatalysts by simply using different amino acids.

It is difficult to envisage a simple modification of the existing synthetic strategy to attach the organocatalyst to a solid support. A different design strategy is required to incorporate solutions to the limitations discussed previously and also improve solubility.

(vi) Adapting the synthetic strategy to incorporate different amino acids introduces chirality and will allow investigations into altering the stereochemical outcome of reactions to be investigated.

The original synthetic strategy involved using the amino acid glycine to introduce the CH_2 group into **122**. Only the Boc group has been tried as a protecting group. It would be worthwhile investigating alternative protecting groups to allow the use of other amino acids which would introduce chirality at the polarisation site. Using amino acids also provides a simple method of extending the length of the organocatalyst backbone to adjust the position of the polarisation site or introduce multiple polarisation sites. Changing the amino acid also allows for great diversity to be introduced, leading to the production of many organocatalysts (Figure 65).

3. Rate Acceleration through Proximity

3.1 Introduction

One of the factors not addressed by the design of organocatalyst **122**, described in Chapter 2, is rate acceleration by locating reaction substrates in close proximity to each other and therefore rendering the reaction *pseudo*-intramolecular. Section 1.6.2 discussed examples of supramolecular catalysis achieved through ABC methodology. ABC methodology is one of the simplest ways to achieve rate acceleration by proximity through using a reaction template as demonstrated by the examples discussed previously. The ABC methodology can be applied to other reaction types and need not involve metal cations as reaction templates.

Another example[218] from the laboratory of Philp and co-workers involves the acceleration of cycloaddition reactions with an organic molecule acting as the reaction template. Selecting cycloaddition reactions also allows another interesting feature to be investigated – the effect of the template upon the stereochemical outcome of the reaction can be determined. Binding reactants **A** and **B** by reaction template **C** should give some degree of control of the orientation of the reactants as they enter the transition state and therefore influence the stereochemistry of the product.

The reactive partners chosen are shown in Figure 66, they contain identical amidopyridine recognition sites capable of forming an **[A•B•C]** complex with a dicarboxylic acid reaction template.

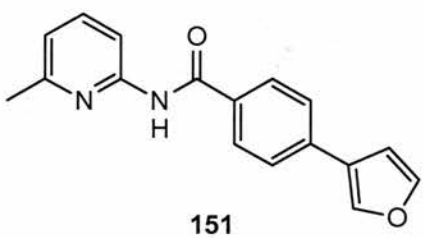

151

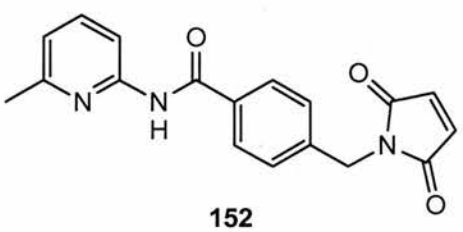

152

Figure 66 Structures of diene **151** and dienophile **152** used as substrates for a Diels-Alder cycloaddition reaction to examine ABC methodology.

The cycloaddition reaction being investigated was the Diels-Alder reaction which gives two possible cycloadduct products, *exo*-**153** or *endo*-**154** (Figure 67).

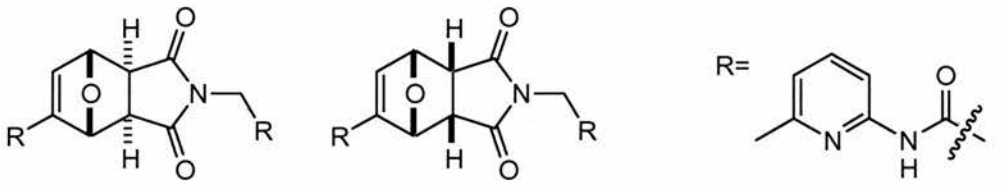

153 *exo* **154** *endo*

Figure 67 Structures of the two isomer cycloadduct products obtained from the Diels-Alder reaction.

Four different reaction templates **155** to **158** were used in these studies (Figure 68). It was found that glutaric acid **155** was the best reaction template; the other templates studied contain two *geminal* non-hydrogen substituents on the central carbon atom which leads to steric crowding in the **[A•B•C]** complex, therefore leading to destabilisation of the transition state.

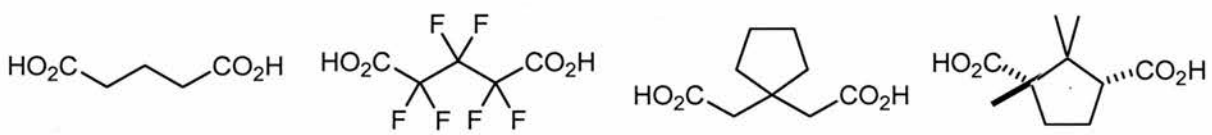

155 **156** **157** **158**

Figure 68 Structures of the four different reaction template molecules investigated, including glutaric acid **155**.

Experiments were carried out using 20 mM solutions of **151** and **152** in $CDCl_3$ at 50 °C with one equivalent of reaction template. The product concentration after 10 hours was calculated and used to compare the bimolecular reaction in the absence of template, and the **[A•B•C]** complex-mediated reaction. It was found that the addition of **155** leads to a 40% increase in product concentration. More interestingly, the stereochemical outcome of the reaction is altered in the presence of **155**.

In the bimolecular reaction, the ratio of *exo*-**153** to *endo*-**154** formed is approximately 1:1. When **155** is added to the reaction there is an 80% enhancement in the formation of *exo*-**153**, whereas there is a 4% suppression in the formation of *endo*-**154**. Thus, adding **155** to the reaction mixture gives a 3:1 selectivity for *exo* over *endo*. These results are consistent with molecular modelling calculations which show that the largest proportion of reactive co-conformations favour the formation of *exo*-**153**.

Molecular modelling studies also determined that although the system does not tolerate *geminal* substitution at the central carbon atom, substitution of one of the hydrogens should not cause steric crowding. One major problem with using **155** as a reaction template is its

poor solubility. Reaction template **159**, shown in Figure 69, was developed because it should be much more soluble as a result of the *t*-butylbenzyl group. Another advantage of using **159** is that the *t*-butyl group can be replaced by an oxygen atom to create an ether linkage to a solid support.

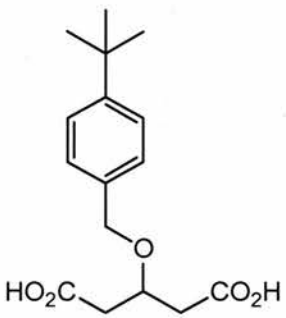

159

Figure 69 The structure of new reaction template **159** containing a solubilising *t*-butyl group.

Initial studies using **159** gave promising results; therefore, it lends itself to further studies. However, there are features of the original reaction that can be improved upon. Dienophile **152** is difficult to synthesise and is not easy to adapt to allow the introduction of synthetic flexibility. It is also possible to use a more reactive diene than **151**. For these reasons, we have decided to use the reactive partners shown in Figure 70.

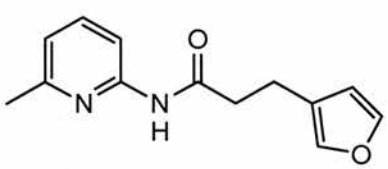

160

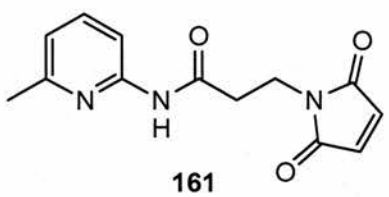

161

Figure 70 Structures of the new target reactive partners for use with reaction template **159** in an ABC system.

In this case diene **160** is more reactive and dieneophile **161** is easier to synthesise and the chain lengths of both molecules can be readily altered. With this system, it is possible to explore the reactivity of the system to determine the effect of **159**. Another advantage of using alkyl spacers as opposed to phenyl spacer units is apparent when considering the removal of recognition. After the reaction is complete, the recognition sites can be removed by cleaving at the amide bond. The resulting bicyclic product with only alkyl groups is of more synthetic use than the corresponding product with phenyl groups attached.

We were interested to see if reaction template **159** is capable of turnover and can therefore be used in less than stoichiometric amounts. The effect of **159** on the stereochemical outcome of

the reaction can also be determined and compared with the previous system. Molecular modelling indicates that *exo* isomer **162** will be favoured over *endo*-**163** (Figure 71) because both recognition groups on **159** are involved in binding *exo*-**162** compared to only one for *endo*-**163**.

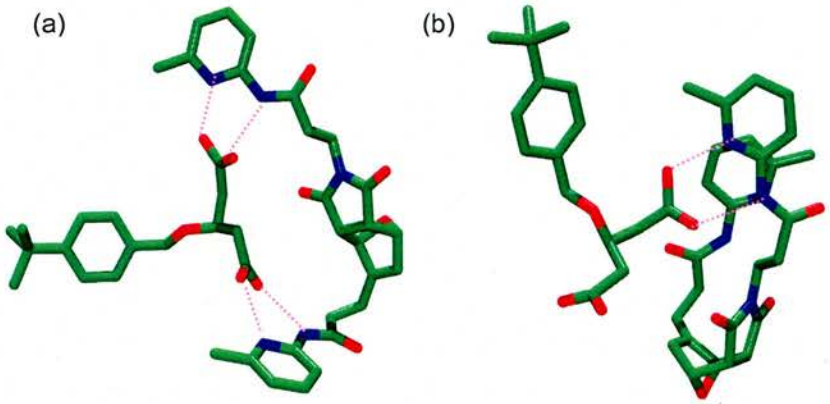

Figure 71 Calculated structures (MMFFs forcefield/GBSA solution model for $CHCl_3$) of (a) [*exo*-**162•159**] and (b) [*endo*-**163•159**]. Hydrogen bonds are shown as dashed lines and hydrogen atoms are omitted for clarity.

Ultimately, it is hoped that it will be possible to immobilise **159** upon a solid support for use in a continuous flow system, as illustrated in Figure 72. The reaction conditions for the system must be carefully controlled in order to obtain the highest yields of the desired product. We want to determine if it is possible to model the system to predict the optimum reaction conditions.

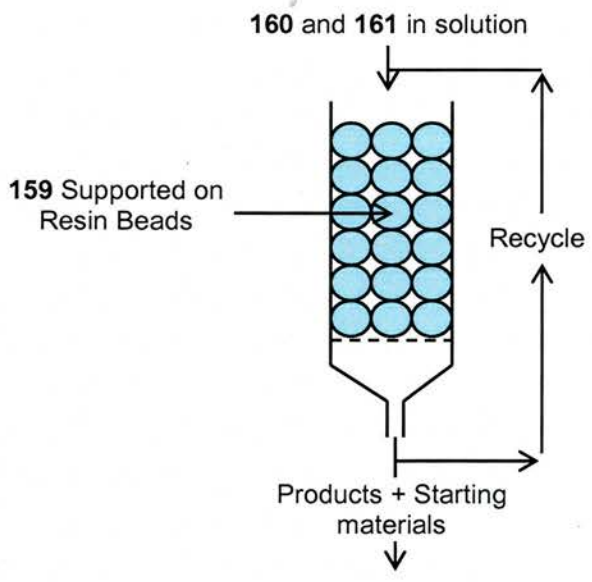

Figure 72 Illustration of a continuous flow system. Reaction template **159** is immobilised upon resin beads and a solution containing **160** and **161** are passed through the vessel. Some of the solution obtained is recycled through the system whilst the remainder is collected. With careful optimisation of conditions the reaction can be controlled to produce only one isomer.

We hope to use the model to predict which reaction conditions will give maximum rate acceleration and compare this to experimental results. The advantage of using this type of system is that extensive studies have already been carried out on similar molecules. From these results, we have an indication of the way the system should behave, and this should simplify the number and type of experiments required. The results should also give an indication of the sensitivity of the reaction to the different conditions. It may be that the reaction requires all factors to be carefully tuned in order to achieve good rate accelerations and selectivities. On the other hand, the reaction may be more tolerant to the conditions, giving good rate accelerations and selectivities over a range of conditions.

3.2 Synthesis of Substrates 160 and 161

The two reactants were synthesised in similar ways. Diene **160** was synthesised according to the pathway shown in Scheme 36. *Trans*-3-furanacrylic acid **164** was reduced by hydrogenation using 10% Pd/C to give 3-furan-3-yl propionic acid **165** in 29% yield. The reaction is low yielding because it is difficult to monitor the end point of the reaction. The product is slightly less UV active than the starting material allowing the end point to be roughly determined by tlc. Formation of some fully reduced 3-(tetrahydrofuran-3-yl)propionic acid is always observed in addition to **165**. Acid **165** was initially purified by Kugelrohr distillation before the fully reduced product was removed by repeated recrystallisations from boiling hexane. Any fully reduced product still remaining is easily removed at the next stage.

Acid **165** was then converted into acid fluoride **166** using cyanuric fluoride and immediately coupled to **126**. Acid fluorides are unstable to heat; therefore, when solvent is removed *in vacuo*, care must be taken to maintain the water bath on the rotary evaporator below 30 °C. Coupled product **160** was obtained in 54% yield after purification by column chromatography.

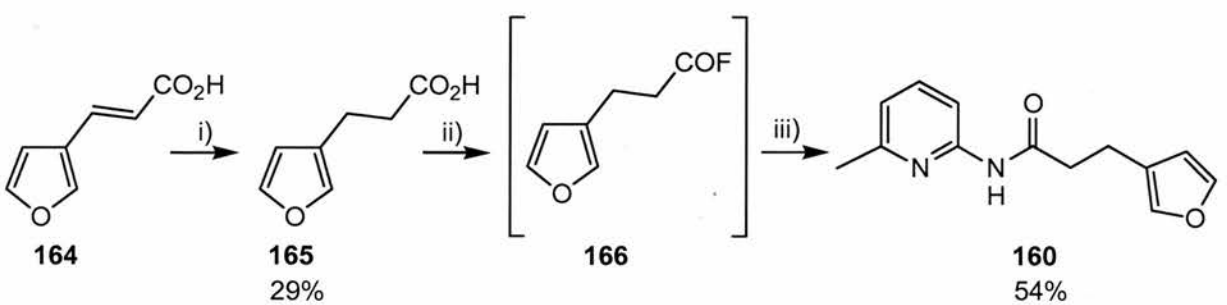

164 **165** 29% **166** **160** 54%

Scheme 36 i) 10% Pd/C, H_2 (g), MeOH; ii) cyanuric fluoride, pyridine, MeCN, 0 °C; iii) **126**, DCM.

Dienophile **161** was synthesised in a similar manner to **160** (Scheme 37). Maleimide **45** was converted into acid fluoride **167** using cyanuric fluoride and reacted immediately with **126** overnight, to give **161** in 48% yield after purification by column chromatography.

The reaction time is critical in this instance. Maleimide **45** was reacted with cyanuric fluoride at 0 °C for 6 minutes, then allowed to stir at room temperature for a further 6 minutes before work up. If the reaction time is not carefully monitored then it leads to ring opening of the maleimide.

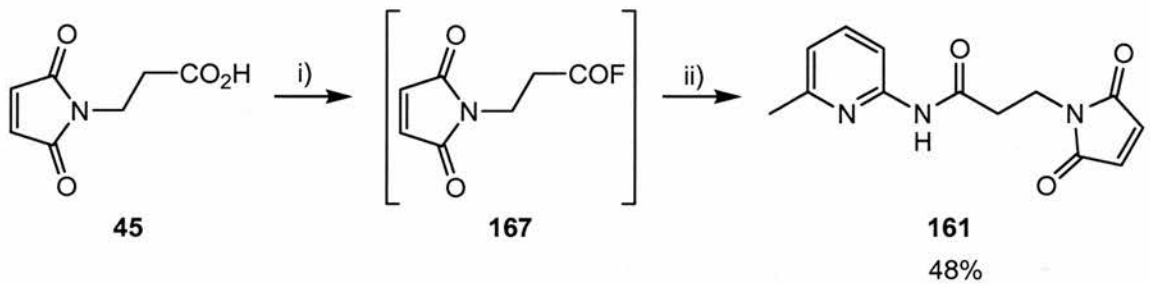

45 **167** **161**

48%

Scheme 37 i) cyanuric fluoride, pyridine, MeCN, 0 °C; ii) **126**, DCM.

3.3 Synthesis of Reaction Template 159

Reaction template **159** was synthesised according to the reaction scheme shown in Scheme 38. 4-*tert*-Butylbenzyl alcohol **168** was converted into the corresponding trichloroacetimidate **169** by a base-catalysed condensation reaction with trichloroacetonitrile to give **169** in 90% yield after purification by vacuum filtration through a short pad of silica gel. The second step in the reaction sequence was more problematic.

The coupling reaction between **169** and diethyl-3-hydroxyglutarate was carried out according to an adapted literature procedure[219] several times with variable results. The reaction was optimised to give good yields. In order to obtain good yields of **170**, cyclohexane must be dried over molecular sieves for 48 hours before use, fresh $BF_3.Et_2O$ was also used and the reaction was stirred overnight. Optimisation of the reaction allowed diester **170** to be obtained in 98% yield after purification by column chromatography. The final step in the reaction scheme is a base-catalysed ester hydrolysis reaction to give **159** in 62% yield after recrystallisation from v/v 1:10 DCM:hexane.

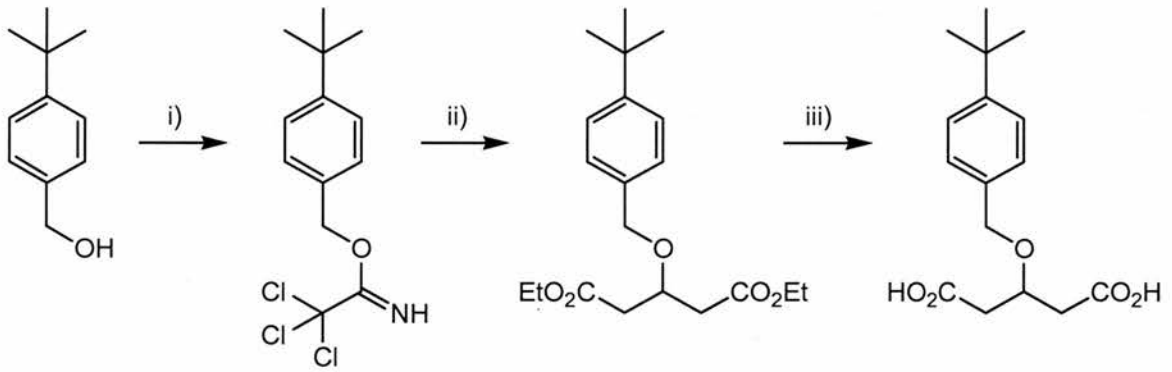

168 **169** 90% **170** 98% **159** 62%

Scheme 38 i) $[CH_3(CH_2)3]_4N(HSO_4)$, trichloroacetonitrile, DCM, 50% KOH, -15 °C (aq); ii) diethyl-3-hydroxyglutarate, $BF_3.Et_2O$, cyclohexane, DCM; iii) 1M NaOH (aq), EtOH.

3.4 Characterisation of Reaction Products

Exo-**162** and *endo*-**163**, the products of the reaction, were prepared for characterisation purposes (Scheme 39). The cycloadducts were prepared by mixing solutions of **160** and **161** dissolved in chloroform at room temperature for two weeks. Cycloadducts *exo*-**162** and *endo*-**163** were separated by column chromatography using v/v 2:1 ethyl acetate:hexane to afford *exo*-**162** in 36% yield and *endo*-**163** in 23% yield.

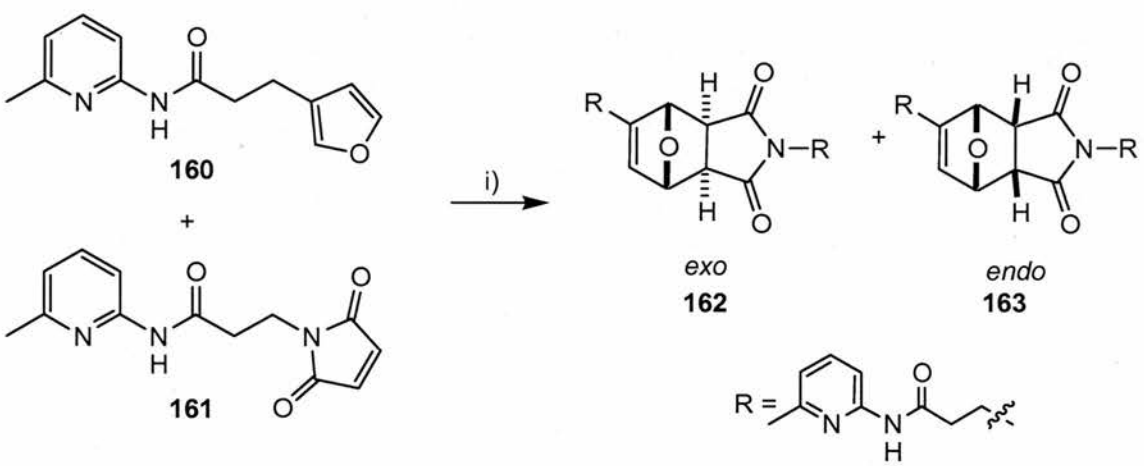

exo **162** *endo* **163**

Scheme 39 i) $CHCl_3$.

3.5 Matrix Experiments

The matrix experiments were conducted in a similar manner to the experiments described in Section 2.7, whereby solutions of **160** and **161** dissolved in $CDCl_3$ were mixed and left overnight at the desired temperature. Samples were then analysed by recording 300 MHz ^1H NMR spectra and the extent of the reaction determined through deconvolution of the appropriate resonances in the ^1H NMR spectrum. The different reaction conditions investigated are shown in Table 7.

Table 7 Table showing the different reaction conditions tested in the matrix experiments.

Conditions	Variations				
Initial Concentration of **160** and **161** / mM	25	50	75		
159 Concentration / mol%	0	10	25	50	100
Temperature / °C	25	35	45		

When deconvolution was performed, the product concentrations for both *exo*-**162** and *endo*-**163** were calculated in order to see the effect of **159** upon the stereochemical outcome of the reaction. The results obtained are very interesting and can be analysed in a number of different ways. Both the overall reaction conversion and stereoselectivity of the reaction can be analysed separately. Tables showing the full results obtained can be found in Appendix 1.

Figure 73 shows the results obtained at 25 °C for total percentage conversion of reactants into products – both *exo* and *endo* – against concentration of **159**. These results are consistent with results expected intuitively, where increasing the reagent concentration from 25 to 75 mM leads to an increase in the percentage conversion for the reaction. This result is as a consequence of increasing the rate of the bimolecular reaction and would be expected to occur in the absence of any recognition-mediated processes as demonstrated by the results shown at 0 mol% **159**.

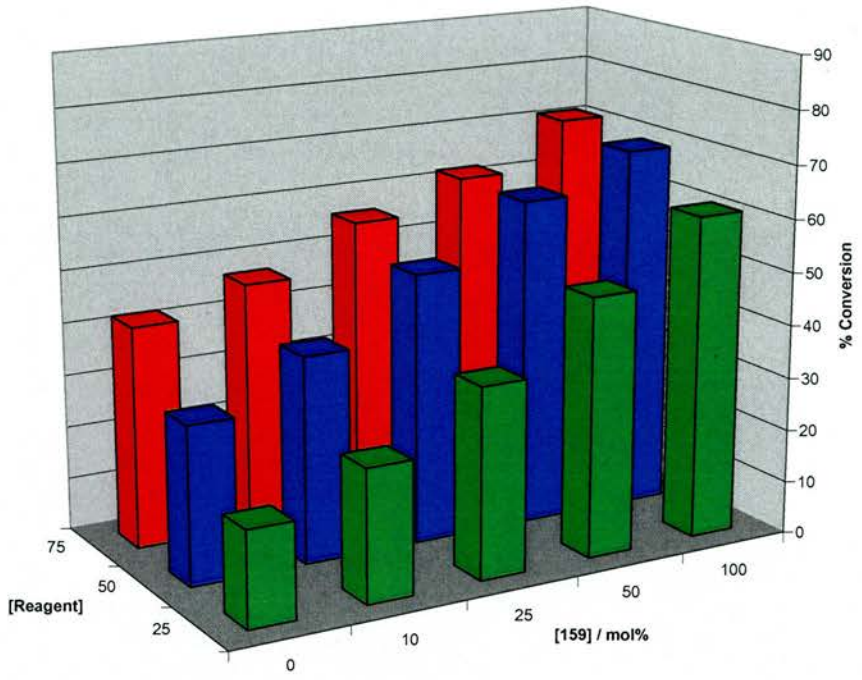

Figure 73 Graph showing a comparison of percentage conversion against [**159**] for the three different concentrations of **160** and **161** at 25 °C. Results shown in green are for a reagent concentration of 25 mM, blue shows the results at 50 mM and the results at 75 mM are shown in red.

However, we can see that recognition does play an important role in the reaction when comparing the results obtained in the absence of **159** with those containing 100 mol% **159**. Dramatic differences are observed for all three initial reagent concentrations. At 25 mM, the control reaction gives a total conversion of 18% and the reaction containing 100 mol% **159** gives a total conversion of 61%. Therefore, the addition of one equivalent of **159** leads to rate enhancement by a factor of 3.4 (Equation 3).

$$\text{Rate Enhancement} = \frac{61}{18} = 3.4$$

Equation 3 Calculation of Rate Enhancement from % conversion of control and catalysed reactions.

The effect decreases with increasing reagent concentration as the bimolecular reaction becomes more important. At 50 mM, the control reaction gives 30% conversion whereas the recognition mediated reaction containing 100 mol% **159** gives 69% conversion, corresponding to a 2.3 fold rate enhancement. Similarly at 75 mM, the control reaction gives 42% conversion and the reaction containing 100 mol% **159** gives 71% conversion which corresponds to rate enhancement by a factor of 1.7 with the addition of one equivalent of **159**.

Figure 74 shows the results obtained at 35 °C on the same scale as the results in Figure 73. From these results it is clear that a similar pattern of results is obtained to those recorded at 25 °C. However, as expected the percentage conversions observed are higher than those recorded at a lower temperature as a result of the faster bimolecular reaction. In this case the difference between the control reaction at 75 mM reagent concentration and the reaction containing 100 mol% **159** is much smaller. The control reaction gives 61% conversion after 16 hours and the corresponding reaction containing **159** gives 80% conversion over the same time period. Therefore, the addition of one equivalent of **159** leads to rate enhancement by a factor of 1.3 at 75 mM which is much smaller than the rate enhancements observed at a lower temperature.

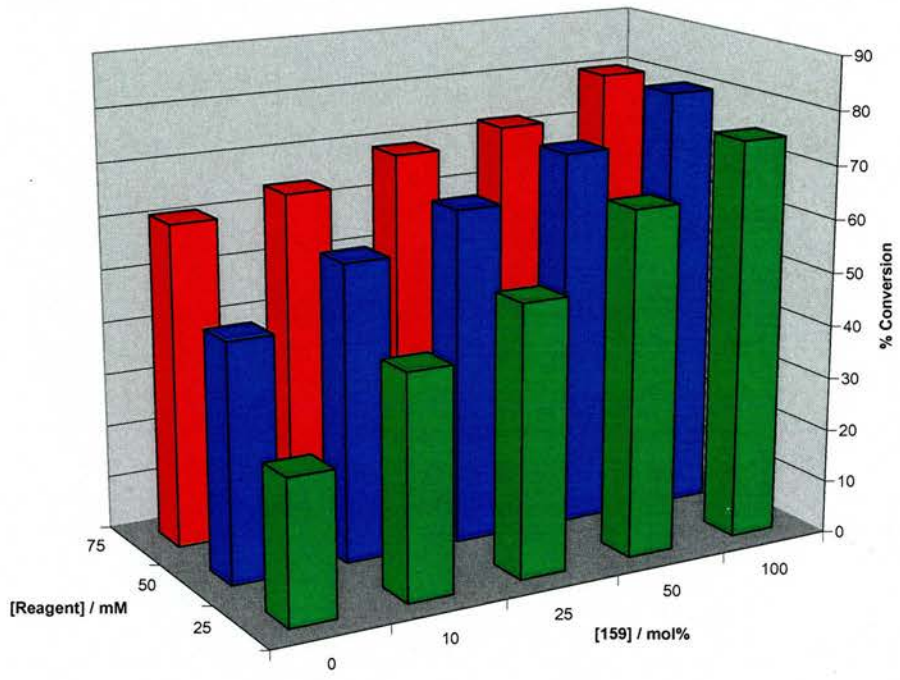

Figure 74 Graph showing a comparison of percentage conversion against [**159**] for the three different concentrations of **160** and **161** at 35 °C. Results shown in green are for a reagent concentration of 25 mM, blue shows the results at 50 mM and the results at 75 mM are shown in red.

The results obtained at 45 °C are shown in Figure 75 and again follow the same trend. Recognition-mediated processes are more important at 25 mM reagent concentration than 75 mM because increasing the temperature has increased the rate of the bimolecular reaction and higher temperatures also leads to the disruption of recognition.

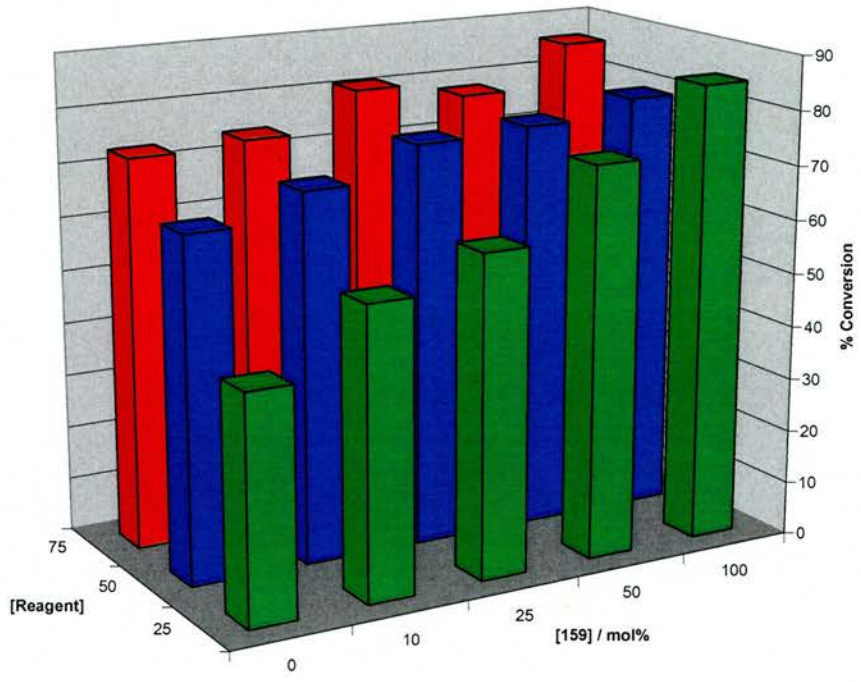

Figure 75 Graph showing a comparison of percentage conversion against [**159**] for the three different concentrations of **160** and **161** at 45 °C. Results shown in green are for a reagent concentration of 25 mM, blue shows the results at 50 mM and the results at 75 mM are shown in red.

The effects of temperature can be seen more clearly when considering the changes observed at each starting reagent concentration. A rate enhancement factor can be calculated by dividing the percentage conversion recorded for the reaction containing 100 mol% **159** with the percentage conversion recorded for the control reaction which does not contain **159**. Figure 76 shows the relationship between rate enhancement factor and temperature for each of the three reagent concentrations.

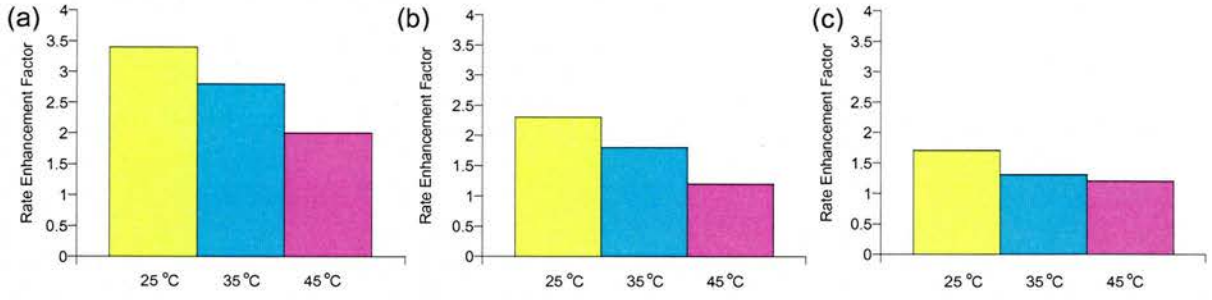

Figure 76 (a) Graph showing the relationship between rate enhancement factor against changes in temperature for 25 mM reagent concentration. (b) Graph showing the relationship between rate enhancement factor against changes in temperature for 50 mM reagent concentration. (c) Graph showing the relationship between rate enhancement factor against changes in temperature for 75 mM reagent concentration. Rate enhancement factor is calculated by dividing the percentage conversion recorded for 100 mol% **159** by the percentage conversion recorded in the absence of **159**.

These results once again demonstrate the importance of temperature and initial reagent concentrations upon rate acceleration. The largest rate enhancements are recorded at 25 °C

with an initial reagent concentration of 25 mM. Under these conditions the bimolecular reaction is slow and the effects of recognition are enhanced.

All of these results display the importance of controlling concentration and temperature in order to achieve good rate accelerations by simple recognition-mediated processes. These results do not give any indication of their effects on the selectivity of the reaction. Therefore, the diastereomeric ratio (*dr*) must now be considered.

The results for diastereomeric ratio show the dramatic effect that recognition can have upon the stereoselectivity of a reaction. Molecular modelling results predict that *exo* isomer **162** will be favoured over *endo*-**163**. Figure 77 shows a comparison between the diastereomeric ratio of *exo*-**162**:*endo*-**163** versus the concentration of **159** added for three different concentrations of the reagents **160** and **161** at 25 °C.

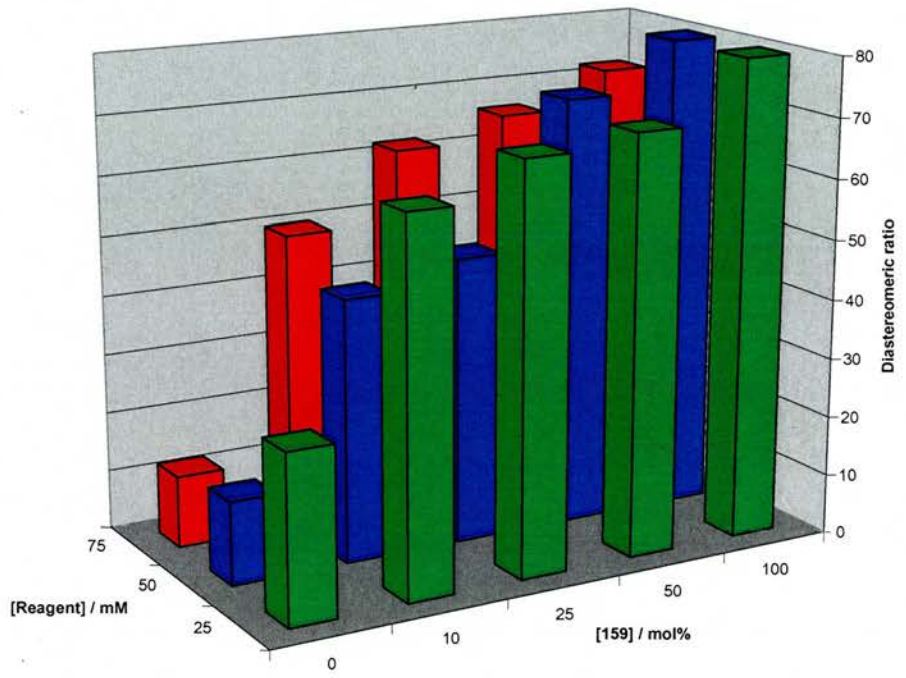

Figure 77 Graph showing a comparison of diastereomeric ratio (*dr*) against [**159**] for three different concentrations of **160** and **161** at 25 °C. Results shown in green are for a reagent concentration of 25 mM, blue shows the results at 50 mM and the results at 75 mM are shown in red.

It appears that the maximum *dr* possible is 80% with the addition of 100 mol% **159** which means that the addition of **159** leads to 9:1 selectivity of *exo*-**162**:*endo*-**163**. These results also demonstrate the efficiency of the recognition-mediated process because the addition of just 10 mol% leads to a dramatic increase in *dr*. At 25 mM the *dr* increases from 28% to 68% which changes the selectivity of the reaction from 1.8:1 *exo*-**162**:*endo*-**163** to 4.3:1 with 10

mol% **159**. Similarly at 50 mM, 10 mol% **159** increases the selectivity of the reaction from 1.3:1 in the absence of **159** to 2.6:1 and at 75 mM the selectivity increases from 1.3:1 to 3:1.

Increasing the concentration leads to a decrease in the *dr* observed because the bimolecular reaction makes more of a contribution. The low results at 10 and 25 mol% **159** for 50 mM when compared to the same results at 75 mM are probably a result of experimental error.

Figure 78 shows the results at 35 °C and, as expected, a similar trend is observed. In this case the *dr* values for the control reaction appear to be lower than expected. It is not clear what the reason for this is but it leads to an artificial increase in selectivities. The same general pattern is observed where increasing the concentration of **159** leads to an increase in *dr*. However, increasing the concentrations of **160** and **161** does not appear to have a great effect on *dr*.

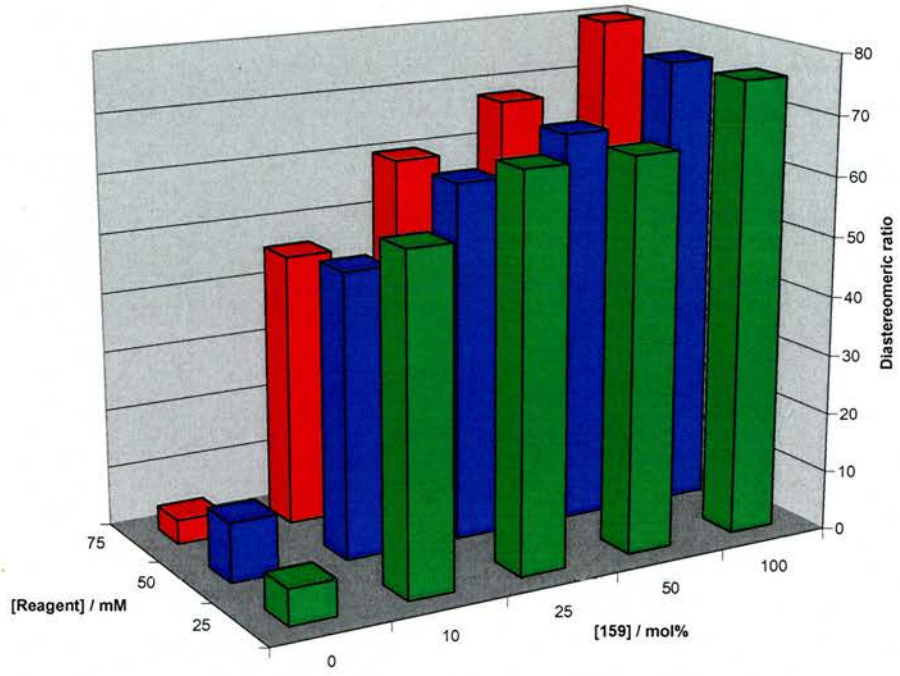

Figure 78 Graph showing a comparison of diastereomeric ratio (*dr*) against [**159**] for three different concentrations of **160** and **161** at 35 °C. Results shown in green are for a reagent concentration of 25 mM, blue shows the results at 50 mM and the results at 75 mM are shown in red.

Figure 79 shows the results recorded at 45 °C and this time the overall *dr* values observed are lower than previously recorded. The maximum *dr* value recorded is no longer 80% but now it has been reduced to 72%. The results at 50 and 75 mM follow the same general patterns as those recorded at 25 and 35 °C. Interestingly, the results at 25 mM appear to show a maximum *dr* when the concentration of **159** is 25 mol% and then decrease with at higher concentrations of **159**.

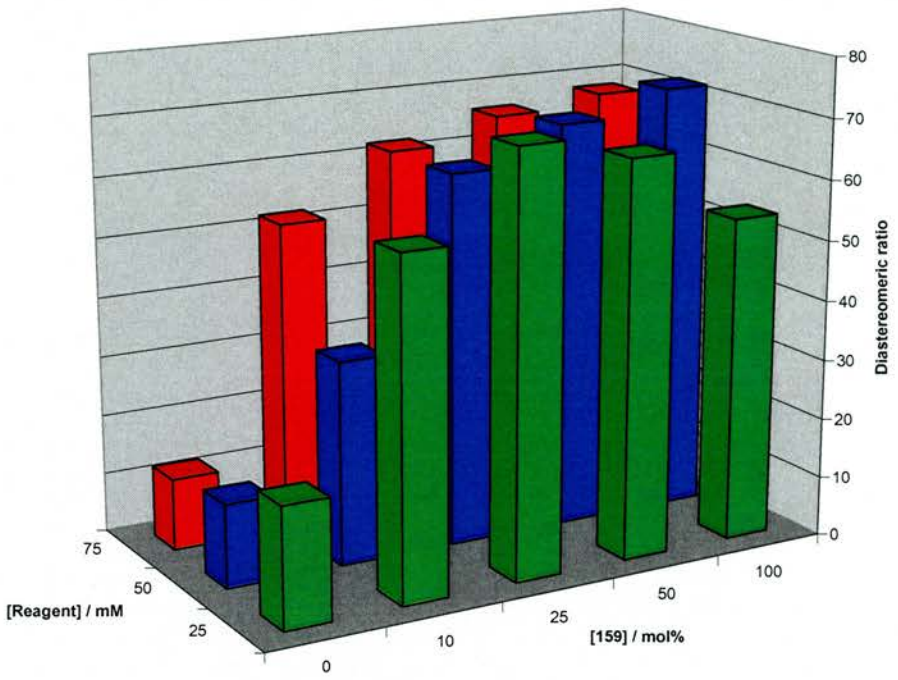

Figure 79 Graph showing a comparison of diastereomeric ratio (*dr*) against [**159**] for three different concentrations of **160** and **161** at 45 °C. Results shown in green are for a reagent concentration of 25 mM, blue shows the results at 50 mM and the results at 75 mM are shown in red.

3.6 Simulation Experiments

The main aim of investigating this system was to compare experimental results with those predicted using simulation software. SIMFIT-32[216] can be used for fitting kinetic data to a model or it can be used to simulate the results expected for a given model. The model for ABC methodology used in the simulation is shown in Figure 80 illustrating the different associations and reactions present.

When running the simulation, there are a number of assumptions which are required and different constants which can be varied. There is a balance between the K_a for the individual associations, of **A** or **B** to **C** with the dissociation of product from **C,** and the effective molarity (EM) of the complex. The advantage of simulating this system is that we know that the assumptions made are valid based upon previous results. The association and dissociation constants have not been measured experimentally for this system but we know the range which they should fall within. This knowledge reduces the number of simulations required and lends validity to the results.

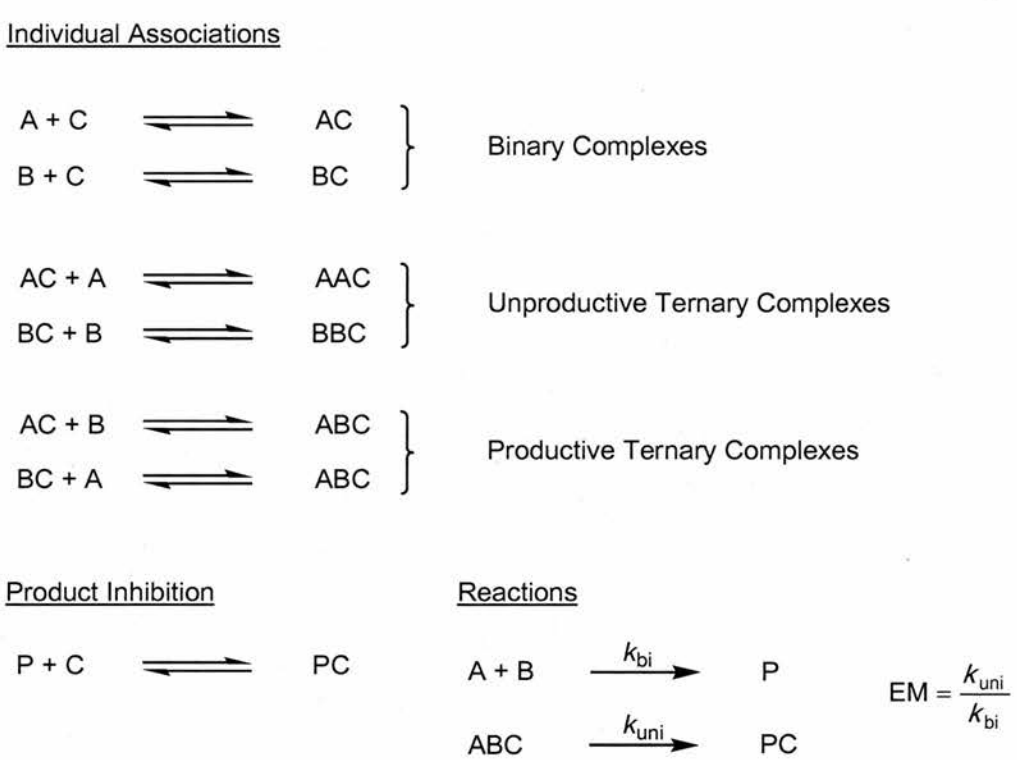

Figure 80 Model used for simulation of results, where A represents **160**, B represents **161**, C represents **159** and P represents total product. Effective molarity is the ratio of the unimolecular rate constant/bimolecular rate constant.

SIMFIT is used to generate and solve the complicated differential equations for the ABC model shown below:

$$\frac{d[A]}{dt} = -k_1[A][C] + k_2[AC] - k_3[A][AC] + k_4[AAC] - k_{11}[A][BC] + k_{12}[ABC] - k_{15}[A][B]$$

$$\frac{d[C]}{dt} = -k_1[A][C] + k_2[AC] - k_7[C][B] + k_8[BC] + k_{13}[PC] - k_{14}[C][P]$$

$$\frac{d[AC]}{dt} = +k_1[A][C] - k_2[AC] - k_3[A][AC] + k_4[AAC] - k_5[AC][B] + k_6[ABC]$$

$$\frac{d[AAC]}{dt} = +k_3[A][AC] - k_4[AAC]$$

$$\frac{d[B]}{dt} = -k_5[AC][B] + k_6[ABC] - k_7[C][B] + k_8[BC] - k_9[B][BC] + k_{10}[BBC] - k_{15}[A][B]$$

$$\frac{d[ABC]}{dt} = +k_5[AC][B] - k_6[ABC] + k_{11}[A][BC] - k_{12}[ABC] - k_{16}[ABC]$$

$$\frac{d[BC]}{dt} = +k_7[C][B] - k_8[BC] - k_9[B][BC] + k_{10}[BBC] - k_{11}[A][BC] + k_{12}[ABC]$$

$$\frac{d[BBC]}{dt} = +k_9[B][BC] - k_{10}[BBC]$$

$$\frac{d[PC]}{dt} = -k_{13}[PC] + k_{14}[C][P] + k_{16}[ABC]$$

$$\frac{d[P]}{dt} = +k_{13}[PC] - k_{14}[C][P] + k_{15}[A][B]$$

Two different types of simulation experiment were conducted: one varying EM and the other varying K_a for product inhibition. The command file used and the data file from one of the simulations are shown in Appendix 2.

The first simulations conducted involved varying product inhibition K_a values whilst keeping all other individual association constants at 100 M^{-1} and EM = 1 M (k_{uni} = 1 x10^{-4} s^{-1} and k_{bi} = 1 x10^{-4} M^{-1} s^{-1}) . Simulation results recorded after 16 hours for K_a = 100 M^{-1} are shown in Figure 81. The rate enhancement is calculated by comparing the initial rates of the control reaction and catalysed reactions which are calculated using the data obtained after 2000s. It can be seen that increasing the concentration of **159** leads to an exponential increase in rate enhancement.

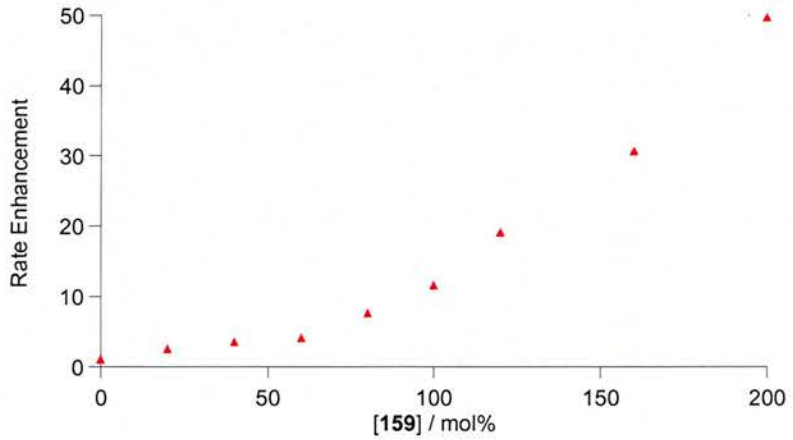

Figure 81 Simulation results after 16 hours for K_a = 100 M^{-1} showing rate enhancement where the control reaction has a rate enhancement factor of one.

Another simulation was performed where the product inhibition K_a = 1000 M^{-1} for two different initial reagent concentrations and the results are shown in Figure 82, 25 mM is shown in red and 75 mM is shown in blue. In this case the results show that rate enhancement reaches a maximum when the concentration of **159** is around 100 mol%, which is one equivalent. These results are more probable than those recorded at K_a = 100 M^{-1} because a drop in rate enhancement with increasing concentration of **159** is expected. Higher concentrations of **159** leads to an increase in substrate bound to **159** which decreases the likelihood of forming the ABC ternary complex. The results shown in Figure 82 are consistent with the experimental data which showed that increasing the reagent concentration led to a decrease in the rate enhancement.

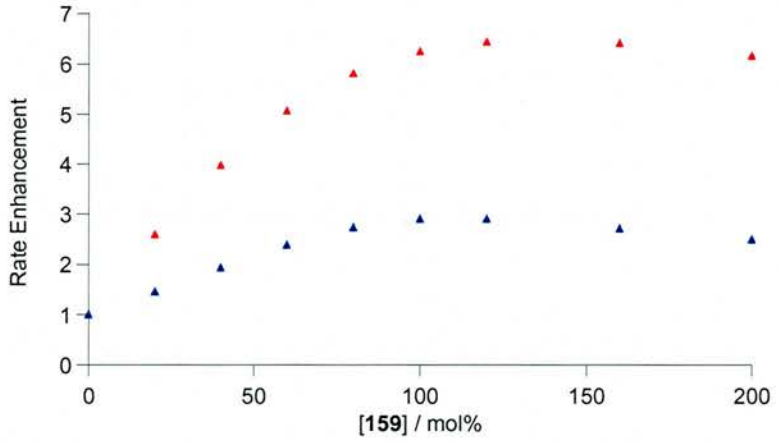

Figure 82 Simulation results after 16 hours when K_a = 1000 M^{-1}. Results shown in red are for 25 mM reagent concentration and results in blue are for 75 mM reagent concentration.

The results obtained are also consistent with reciprocal replication results[220] obtained by Rebek and co-workers. Figure 83 shows a plot of experimentally observed rate acceleration against the number of equivalents of template added. The experimental data are shown as filled square and the three lines indicate the simulation results for K_a values ranging from 5000 M^{-1} to 45000 M^{-1}. In this case it was found that the line which matched experimental data most clearly occurred when a value of K_a = 14000 M^{-1} was used.

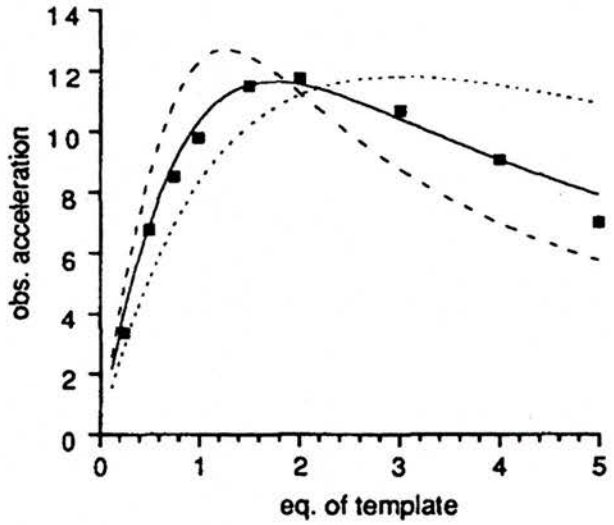

Figure 83 Plot of experimentally observed rate acceleration against the number of equivalents of template added to the reaction with different fitted lines. Experimental data are shown in filled squares. The solid line indicates the fit obtained when K_a = 14000 M^{-1}, dashed line indicates the fit for K_a = 45000 M^{-1} and the dotted line is the fit for K_a = 5000 M^{-1}. Taken from ref 220.

The results also show that maximum rate accelerations are observed with two equivalents of template added. Increasing the amount of template above two equivalents leads to a decrease in rate acceleration because the reaction substrates become bound to the template in AC or BC type complexes which leads to a decrease in the formation of the ternary complex.

The other factor simulated was the effect of EM on product concentration after 16 hours. In this simulation K_a was fixed at K_a = 1000 M^{-1} because it gave the best results from the previous simulations. EM values between 100 mM and 10 M were simulated and results predicted for product concentrations after 16 hours were used to plot the graph shown in Figure 84. The simulations used 25mM as the initial concentrations of the reagents with 100 mol% **159**.

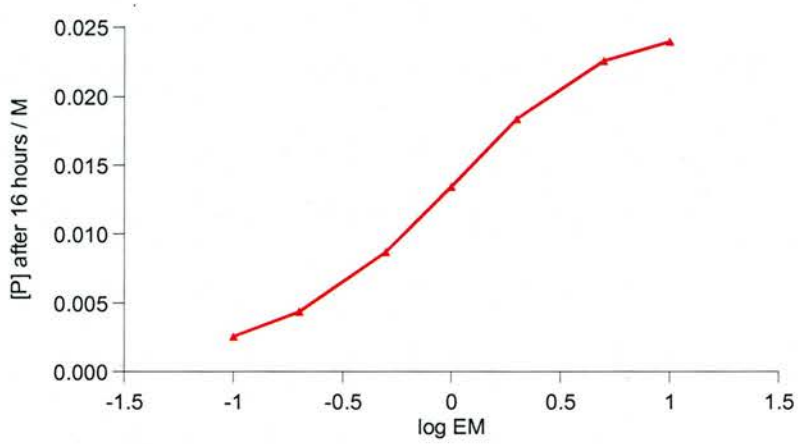

Figure 84 Results for simulations where EM values are varied from 100 mM to 10 M and K_a **P•159** = 1000 M^{-1}. Reagent concentrations are 25 mM with 50 mol% **159**.

Having evaluated the effects of changing EM and K_a values, it was then possible to compare results obtained from the simulations with experimental data recorded from the matrix experiments. Figure 85 shows results at 25 °C for 25 mM **160** and **161** as blue triangles and the results from the simulation are shown as the solid red line. The parameters used for the simulation are EM = 800 mM, K_a = 1000 M^{-1} for the product to **159** association, K_a = 100 M^{-1} for all other associations and the bimolecular reaction rate = 1.5 x 10^{-4} M^{-1} s^{-1}.

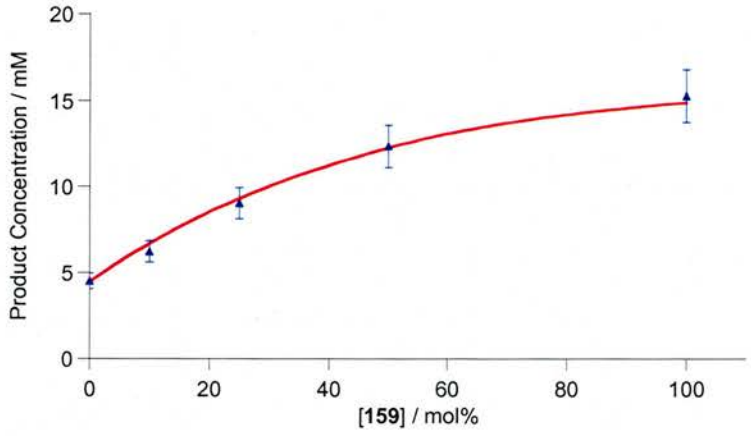

Figure 85 Experimental data at 25 mM reagent concentration at 25 °C are shown in blue. Simulated data are shown as a solid red line. The simulation results were obtained when the K_a for P + C = 1000 M^{-1}, all other K_a values = 100 M^{-1}, EM = 800 mM and k_{bi} = 1.5 x 10^{-4} M^{-1} s^{-1}, k_{uni} = 1.2 x10^{-4} s^{-1}. Error bars show deviations of 10%.

The simulated results and experimental data show good correlation. In order to obtain absolute results for both EM and K_a then full kinetic experiments should be performed alongside NMR titration experiments to calculate K_a using the product and **159**.

3.7 Conclusions

The simulated results show that it is not always necessary to perform full kinetic studies in order to model a system in detail. Good correlations between simulated data and experimental results have been obtained. All values are linked so minor adjustments to one value will affect the others, but the simulated results fall within expected ranges.

The results from the matrix experiments show that the system is ideal for testing in a continuous flow unit. Catalyst loadings on solid supports are often low but this should not have an adverse effect for this reaction because the reaction template is effective at accelerating the reaction and giving good stereochemical control – even at low concentrations.

The system has also shown that it will tolerate changes in the reaction conditions to a degree and slight variations in concentration and temperature will still lead to good rate accelerations and stereochemical control. The diastereomeric ratio relies on the recognition-mediated process for good stereoselectivity. Therefore, in order to maximise the *dr* conditions should be used which favour the recognition-mediated pathway and minimise the contributions from the bimolecular pathway.

3.8 Future Directions

Extensive investigations have been carried out using reaction template **159** to accelerate the Diels-Alder reaction between **160** and **161**, and the next step would be to immobilise **159** on solid support. Attaching the organocatalyst onto solid support allows investigations into catalyst recycling to be carried out before using the catalyst in a continuous flow system, as shown in Figure 72.

Molecular modelling and experimental results have shown that the *t*-butyl group on **159** does not have an adverse effect on its ability to accelerate the reaction and also give *exo* selectivity. Therefore, introducing a site for attachment onto solid support in place of the *t*-butyl group would seem to be the most logical location (Figure 86). The phenyl group of **159** also acts as

a spacer unit to separate the recognition sites from the point of resin attachment which means that the linker unit between the resin and **159** should not be a factor in rate acceleration.

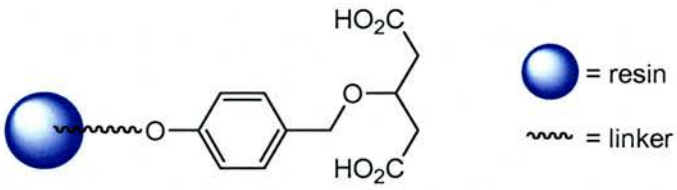

Figure 86 Schematic representation of one possible method of attaching **159** to a resin solid support.

The synthetic strategy used to make **159** also provides an advantage when attaching it to a solid support because the changes can be monitored by IR spectroscopy. It is possible to conduct the synthesis on solid support instead of synthesising the full molecule and then attaching it at the final step. For example, the appearance of the C=N-H peaks at 3344 and 1665 cm^{-1} indicate the formation of trichloroacetimidate **169**, which upon formation of diester **170** are replaced by the distinctive C=O stretching peak at 1736 cm^{-1}. In this manner synthesis of **159** can be monitored easily.

In order for the reaction template to be useful for synthesising bicyclic systems, it is necessary to investigate methods of cleaving the recognition groups. The ultimate goal of creating a recognition-mediated organocatalyst is to develop a system where recognition-mediated processes are used to accelerate the reaction and control the stereochemistry of the product before the recognition sites are removed and the product used as desired.

Reaction template **159** is effective at accelerating a Diels-Alder reaction, giving *exo* selectivity and has the potential for being successfully attached onto solid support. Therefore, investigations into removing the amidopyridine recognition groups will prove valuable when considering the usefulness of organocatalysts such as **159** for synthesising bicyclic systems. One obvious starting point would be to cleave the amide bonds as shown in Figure 87.

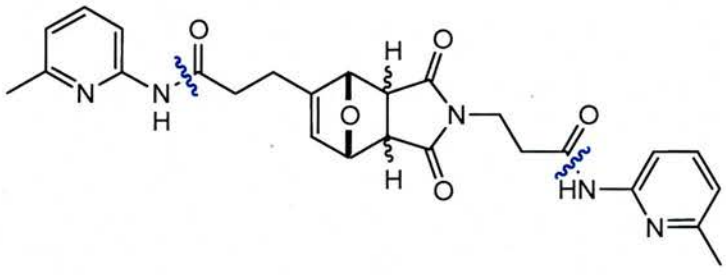

Figure 87 Removing the recognition groups from the product after **159** has been used as an organocatalyst could be achieved by cleaving the amide bonds shown in blue.

4. Combining Polarisation and Proximity

4.1 Introduction

Having investigated the effects of both activation of a substrate through polarisation, and proximity upon rate acceleration, the next step is to investigate combining both effects. It also gives us the opportunity to address the limitations observed for **122** (Chapter 2). It is anticipated that using more than one hydrogen bond to activate the substrate will give an enhanced polarisation effect. It is also hoped that hydrogen bonding to both carbonyl groups of the maleimide ring will result in the organocatalyst accelerating a non-polar reaction. There is also the opportunity, at the design stage, to introduce a site on the molecule that can be deprotected and used to link the organocatalyst to a solid support.

With these features in mind, organocatalysts **171** and **172**, shown in Figure 88, were proposed as the new targets. The molecule can be separated into three different segments: the site of resin attachment is shown in red, the fragment for binding one of the reactants is shown in black, and the fragment for binding and activating the other reactant through polarisation is shown in blue.

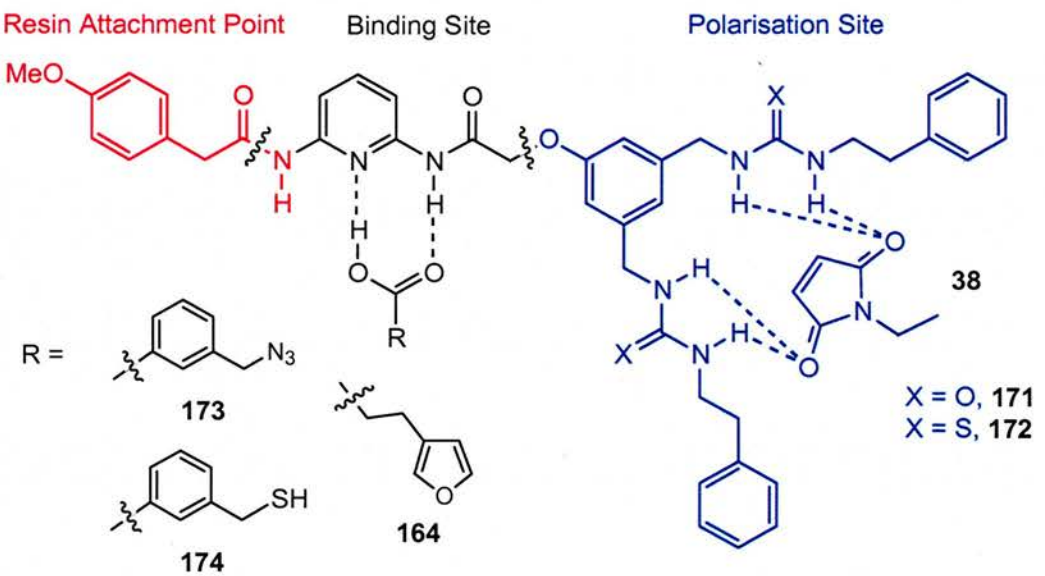

Figure 88 Structure of the new organocatalysts, urea derivative **171** and thiourea derivative **172**, showing the three different sections. The resin attachment fragment is shown in red, the binding site for reagents **164, 173** and **174** containing carboxylic acid recognition groups is shown in black and the polariation site for activating maleimide substrate **38** is shown in blue.

In **171** and **172**, the double bond of *N*-ethylmaleimide **38** is activated by four hydrogen bonds from the bis urea and thiourea moieties. Binding both carbonyl groups of **38** also means that

the entire double bond is activated by electron withdrawal as opposed to one end, which should allow **171** and **172** to be effective in accelerating the Diels-Alder reaction. The amidopyridine-carboxylic acid interaction is now used for binding **164**, **173** and **174**, the reactants specific for each reaction type. Deprotection of the methoxy group gives an ideal attachment point for immobilising **170** and **171** upon solid support.

The molecular modelling pictures shown in Figure 89 illustrate more clearly how **171** holds the two reaction substrates in close proximity. Organocatalyst **171** is shown in green, the Diels-Alder substrate **164** is shown in red, and for clarity maleic anhydride **140** is shown bound in the polarisation site in blue. Figure 89(a) shows the four hydrogen bonds from the bis urea segment of **171** binding **175** in the correct orientation and also in close proximity to **164**. Measurements show that the reactive sites are held approximately 4 Å apart. Figure 89(b) shows the hydrogen bonds between the binding site and **164** more clearly. The molecular models also show that the ethyl substituent on the nitrogen of maleimide **38** will be oriented away from the organocatalyst and not disrupt recognition. Organocatalysts **171** and **172** are carefully designed to give a degree of flexibility to accommodate the different substrates, whilst also being rigid enough to hold the correct shape for aligning the reactive centres.

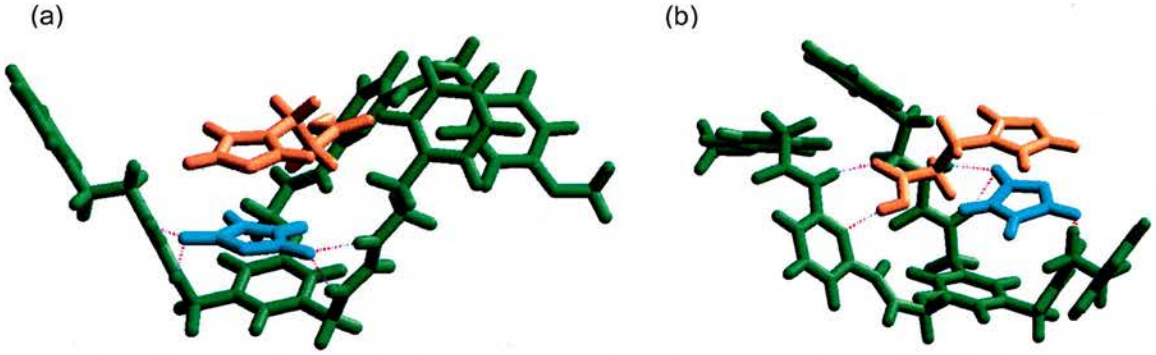

Figure 89 (a) Molecular modelling picture of organocatalyst **171**, in green, binding to Diels-Alder reaction substrate **164**, in red, and maleic anhydride **140** is shown in blue binding to the bisurea of the polarisation site. The four hydrogen bonds holding the polarisation site substrate in position can be clearly seen. (b) Diels-Alder reaction substrate **164** is bound by two hydrogen bonds in the binding site. Measurements show the reactive centres are held approximately 4 Å apart.

Another design feature of **171** and **172** means that the effects of each portion of the organocatalysts can be independently studied. Disconnection of the ether linkage leads the synthesis of control compounds **175-177**, shown in Figure 90. The control compounds allow the effect of binding the carboxylic acid – which is not expected to have any effect on the reaction – and the effect of polarising both ends of the substrate double bond to be determined

individually. Results from **176** and **177** can be directly compared with results obtained for experiments using **122** as described in Chapter 2. From these results, we should see if it is possible to accelerate a non-polar reaction using a simple organocatalyst capable of activating a substrate through polarisation.

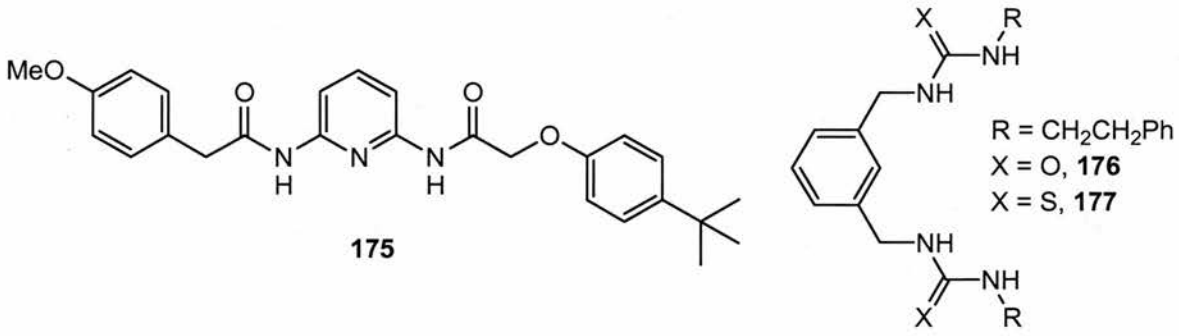

Figure 90 Structure of control compounds: **175** is the control for the binding site, **176** and **177** are controls for the polarisation sites.

4.2 Synthesis of Binding Site Fragment

The synthetic scheme used to obtain the key intermediate **182** for both **175** and the binding site fragment of **171** and **172** is shown in Scheme 40. 4-Methoxyphenylacetic acid **178** was converted into acid fluoride **180** under standard conditions using cyanuric fluoride. Acid fluoride **179** was then immediately reacted with 2,6-diaminopyridine **180** which had been previously purified by vacuum filtration through a pad of celite using DCM as the eluent. The resulting amine **181** was obtained in 39% yield after purification by column chromatography using v/v 5:1 DCM:diethyl ether as the eluent. Key intermediate **182** was obtained in 49% yield through an amide coupling reaction between **181** and chloroacetyl chloride **125**.

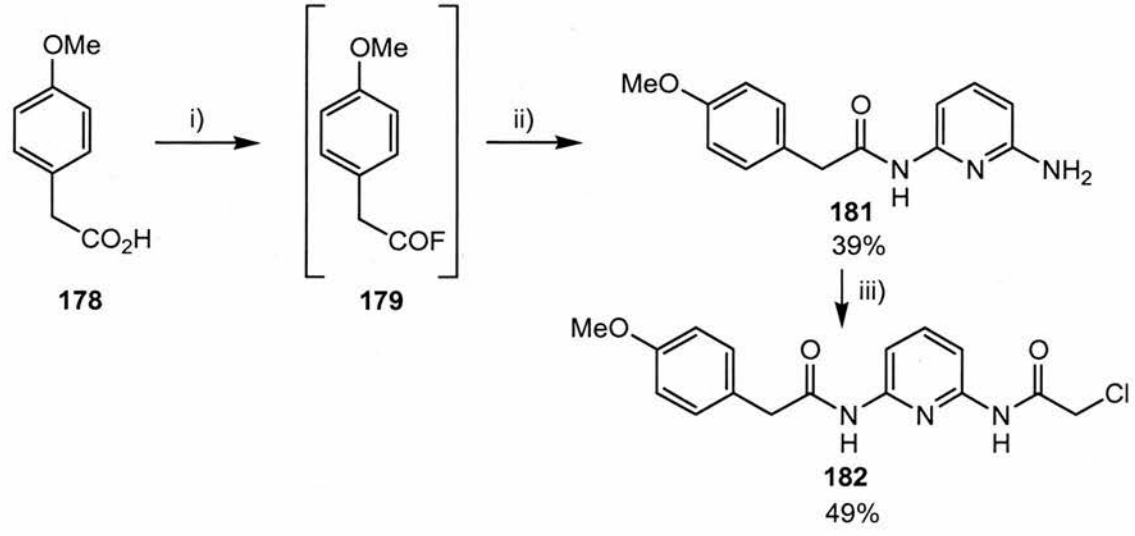

Scheme 40 i) cyanuric fluoride, pyridine, MeCN, 0 °C; ii) **180**, DCM; iii) **125**, DCM.

4.2.1 Synthesis of the Binding Site Control Compound 176

Control **175** was prepared by coupling **182** to *t*-butylphenol **183** as shown in Scheme 41. The reaction is slow and the solution must be heated for several days in order to obtain moderate yields of **175**. Chloride **182** is sparingly soluble in acetonitrile but this does not appear to adversely affect the reaction because the procedure requires slow addition of **182** which means that any **182** that is present in solution reacts immediately to form **175** which prevents over-alkylation by deprotonation of the amide.

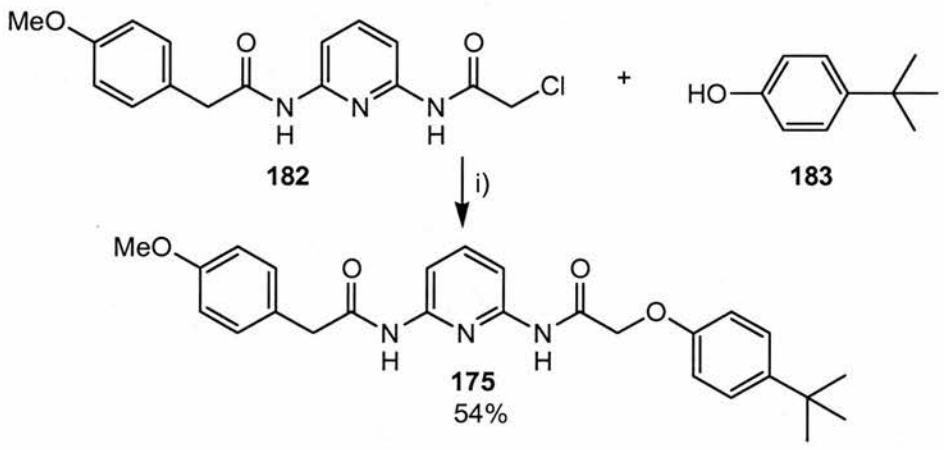

Scheme 41 i) K_2CO_3, MeCN, 80 °C.

4.3 Synthesis of Polarisation Site Fragment

Synthesis of the polarisation site fragment was attempted in different ways. All synthetic strategies were dependent upon the synthesis of the key intermediate **188**. The synthesis of **188** is shown in Scheme 42.

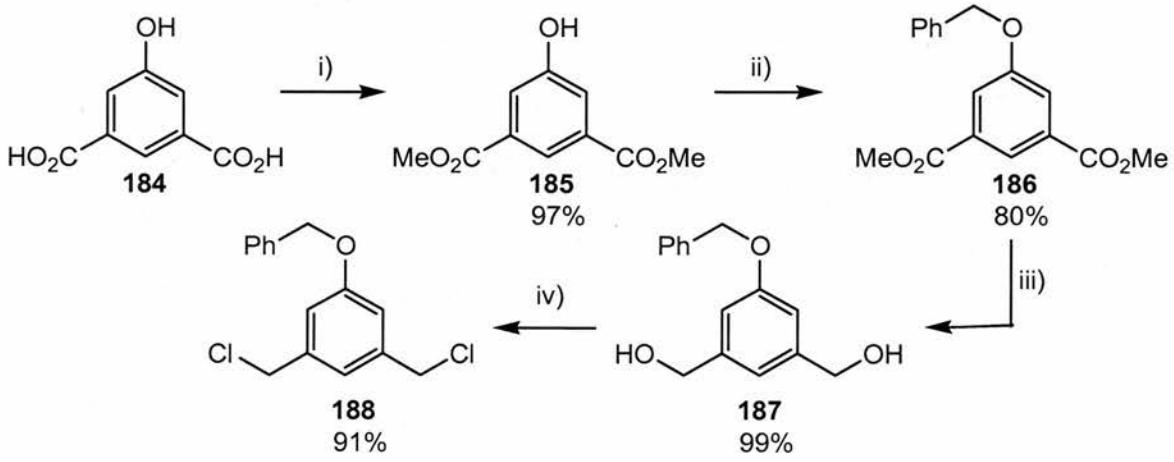

Scheme 42 i) H_2SO_4, MeOH, Δ; ii) benzyl bromide, K_2CO_3, acetone, Δ; iii) $LiAlH_4$, THF, 0 °C; iv) PBu_3, CCl_4, MeCN, 0 °C.

5-Hydroxyisophthalic acid **184** was converted into the dimethyl ester under standard conditions to give **185** in 97% yield. Phenol **185** was then protected using benzyl bromide affording **186** in 80% yield, without the need for further purification. Diol **187** was obtained by reducing **186** with $LiAlH_4$ to rapidly produce **187** almost quantitatively, again without requiring further purification.

Conversion of **187** into **188** required optimisation. Two different phosphines were used in the reaction. The reaction was conducted by cooling a solution of phosphine and **187** dissolved in freshly distilled acetonitrile in an ice bath before adding carbon tetrachloride dropwise. The solution was then allowed to warm to room temperature whilst the reaction was monitored by tlc. Tlc analysis showed the production of both **188** and the intermediate mono-chlorinated species. None of the compounds were very UV active, so the presence of mono-chlorinated product was detected by staining the plates with PMA to ensure the formation of **188**.

Triphenylphosphine was the first phosphine tested in the reaction. Results showed that it was difficult to get the reaction to go to completion, leading to the isolation of mainly the mono-chlorinated compound. The solution also turned black once it reached room temperature. Alternatively, tributylphosphine was used more successfully. Using this phosphine resulted in the isolation of minimal quantities of mono-chlorinated compound. Throughout the reaction the solution remained pale yellow as opposed to turning black. It is proposed that tributylphosphine is better at regulating the temperature of the reaction than triphenylphosphine which minimises the dark by-products formed by the phosphine reacting with carbon tetrachloride.

Chlorination was also attempted using *N*-chlorosuccinimide as a chlorinating agent. However, in this case very little **188** was obtained from the reaction. It appears to be easy to chlorinate the molecule once but more difficult to obtain the desired dichlorinated compound.

After successfully completing the synthesis of **188**, a series of functional group interconversions were required in order to obtain **190** which is necessary for reaction with isocyanates and isothiocyanates to give the final product. Synthesis of diamine **190** synthesis was attempted in two different ways. The first method shown in Scheme 43, is the Gabriel amine synthesis where **188** was converted into phthalimide derivative **189** which upon deprotection yields **190**.

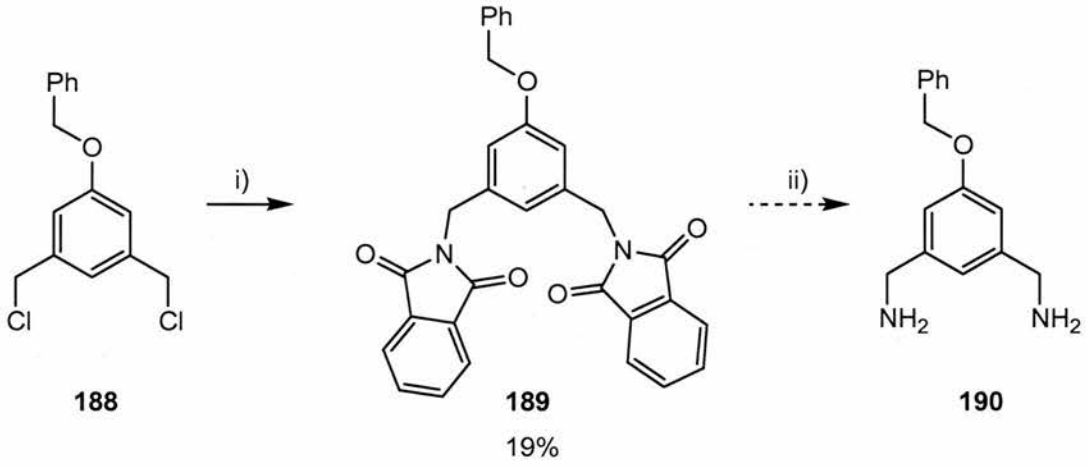

188 **189** **190**

19%

Scheme 43 i) potassium phthalimide, K_2CO_3, MeCN, Δ; ii) hydrazine hydrate, EtOH.

This method was chosen because it would not remove the benzyl protecting group and therefore give a suitable control compound for the polarisation site fragment. Unfortunately, the phthalamide synthesis proved unreliable giving low yields and mixtures of the monochlorinated species along with the desired product. No effective method for purifying the mixture was found and as a result the deprotection using hydrazine hydrate was not attempted.

An alternative method for producing **190** is shown in Scheme 44. In this case, **188** is converted into **191**, a diazide. Azide synthesis is straightforward, high yielding and only requires filtration as a method of purification. Accordingly, **191** was obtained in 97% after heating to reflux for 48 hours. A variety of methods can be used to convert azides into amines. The first method attempted used triphenylphosphine for reduction because this leaves the benzyl protecting group in place. Consequently, **192** the hydrochloride salt of **190** was obtained in apparent 83% yield. However, it was not possible to remove all traces of triphenylphosphine oxide and this route was abandoned.

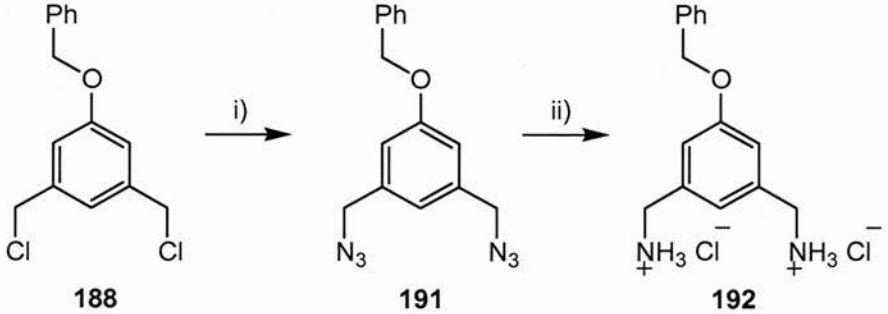

188 **191** **192**

97% 83%

Scheme 44 i) NaN_3, acetone, Δ; ii) PPh_3, H_2O, THF.

Following the disappointing results using triphenylphosphine, it was decided to use another method of converting **191** into **190**. The alternative synthetic strategy is shown in Scheme 45. This time **191** was reduced using palladium catalysed hydrogenation. Hydrogenation also leads to deprotection of the benzyl group to give **193**. Diamine **193** then can be used directly in the synthesis of the full organocatalysts or it can be reprotected for use as a control compound. The hydrogenation reaction was slow and required 7 days to reach completion before fully deprotected **193** was obtained in 97% yield.

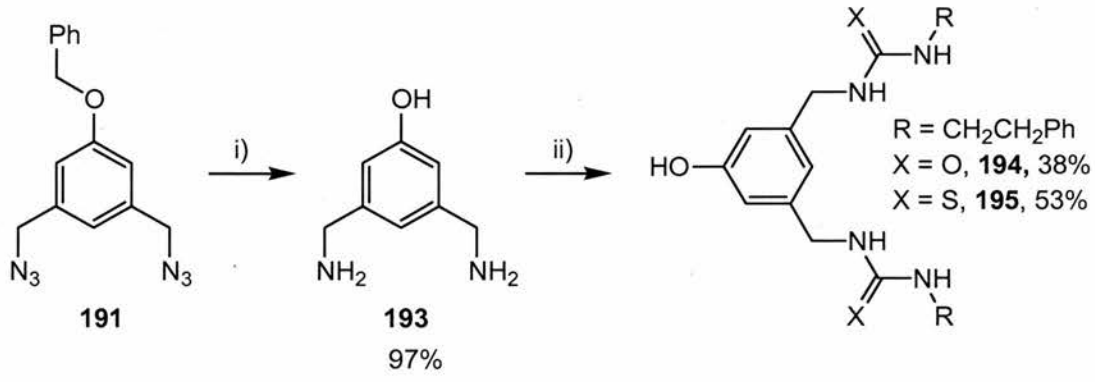

Scheme 45 i) 10% Pd/C, H_2 (g), MeOH; ii) for **194** X = O: phenethyl isocyanate, DMF; for **195** X = S: phenethyl isothiocyante, DMF.

Having successfully obtained **193**, it was then converted into bisurea **194** or bisthiourea **195** by reaction with phenethyl isocyanate or phenethyl isothiocyanate respectively. Bisurea **194** was obtained in 38% yield as a precipitate which is only sparingly soluble in DMSO. The crude product could not be purified and was used in the synthesis of **171** directly. Bisthiourea **195** was obtained in 53% yield as a more soluble waxy solid and was used without further purification in the synthesis of **172**.

4.3.1 Synthesis of the Polarisation Site Control Compounds 176 and 177

Control compounds **176** and **177** were synthesised according to Scheme 46, whereby *m*-xylylenediamine **196** was dissolved in dry DCM and cooled on an ice bath before phenthyl isocyanate or phenethyl isothiocyanate was added dropwise, resulting in the precipitation of the product. Bisurea **176** was obtained in 98% yield and **177** was obtained in 96% yield after filtration. Bisurea **176** was insoluble in a wide range of solvents tested, whereas **177** was soluble in $CDCl_3$. This result means that **176** can be used as a control compound for kinetic studies whereas **177** is unsuitable.

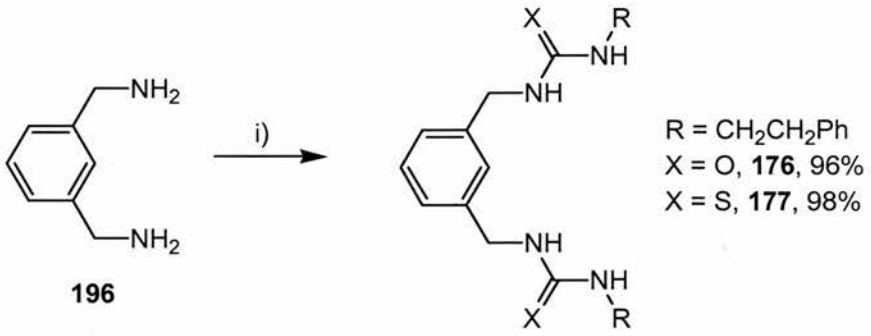

Scheme 46 For X = O, **176**: i) phenethyl isocyanate, DCM, 0 °C. For X = S, **177**: i) phenethyl isothiocyanate, DCM, 0 °C.

Following these results, bisurea compounds **197** and **198**, shown in Figure 47, were prepared in order to test their solubility, and therefore, their suitability for use as control compounds. It was hoped that the alkyl chains would lead to an increase in solubility of the molecule. Unfortunately, this was not the case and both bisureas are very insoluble in a range of solvents tested. In fact, it was not possible to purify the *n*-octylbisurea derivative **197** and it remained a mixture of mono- and bisureas.

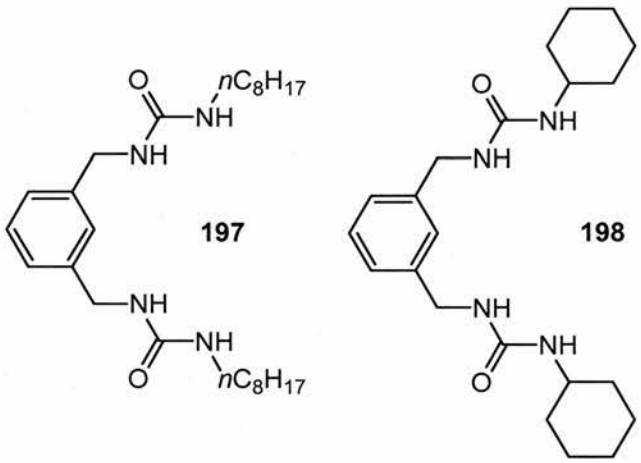

Figure 47 Structures of two alternative bisurea derivatives synthesised to test their solubility and therefore, their suitability as control compounds for the polarisation site.

4.4 Synthesis of Organocatalysts 171 and 172

Having successfully synthesised **182** and crude polarisation site fragments **194** and **195**, the coupling reaction shown in Scheme 48 was attempted. As a consequence of the insolubility of **194**, the coupling reaction was carried out using DSMO as the solvent, whereas the coupling reaction with more soluble **195** was conducted using acetonitrile.

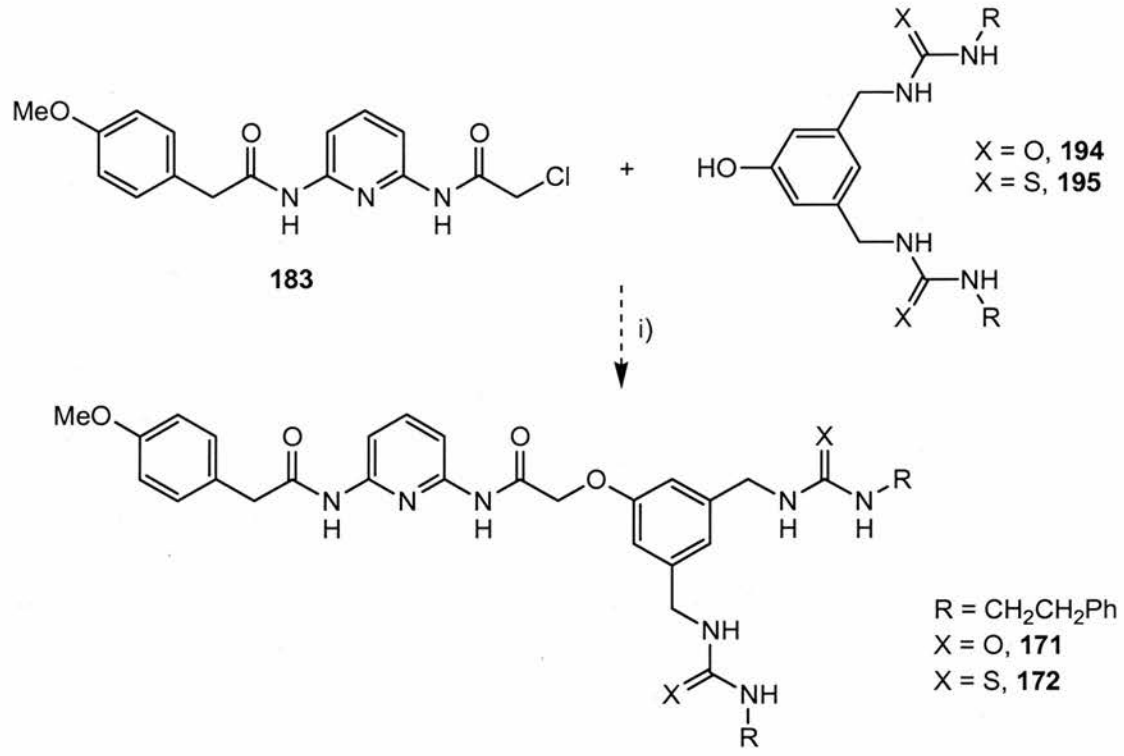

Scheme 48 For X = O, **171**: i) K_2CO_3, DMSO; for X = S, **172**: i) K_2CO_3, MeCN.

Each coupling reaction was only attempted once as a result of time constraints, but unfortunately it was not possible to isolate **171** or **172** from the reaction mixtures. The reactions need to be optimised. Altering the amount of base, solvent, reaction time and the temperature to which the reaction is heated should all be attempted in order to give indications of the best reaction conditions to use. It should then be possible to obtain both **171** and **172**.

Once the ideal coupling reaction conditions have been determined, it should also be possible to synthesise a soluble polarisation site control compound by protecting the phenol with a solubilising group, for example using 4-*t*-butylbenzyl bromide. Alternatively, another option would be to use different isocyanates and isothiocyanates for the formation of bisureas and bisthioureas to find more soluble compounds. Compounds with greater solubilities would make purification simpler and make coupling reactions easier.

4.5 Synthesis of Reactants

The three different reaction types require the synthesis of reactants containing the carboxylic acid recognition moiety. Maleimide **38** is commercially available, soluble and ideal as a substrate for the polarisation site. The three reactants required for the three different reaction

types are shown in Figure 90. The reaction types chosen are the same as those in Chapter 2: the Diels-Alder reaction, [3+2] dipolar cycloaddition and conjugate addition.

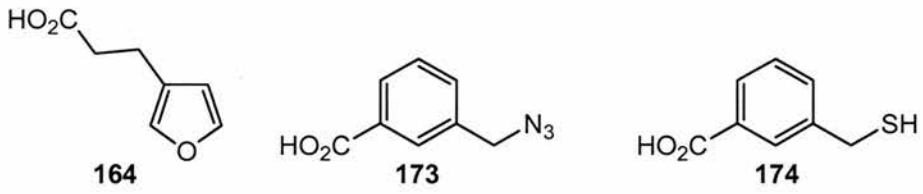

Figure 90 Structure of the reagents for the different reaction types containing the carboxylic acid recognition moiety. Diene **164** is the Diels-Alder reaction reagent, azide **173** is the [3+2] dipolar cycloaddition reaction reagent and thiol **174** is the conjugate addition reaction reagent.

The reactant for the Diels-Alder reaction, 3-furan-3-yl propionic acid **164**, was prepared as described in Section 3.2. Synthesis of **173**, the reactant for the [3+2] dipolar cycloaddition reaction was attempted following synthetic Scheme 49. A suspension of **199** and sodium azide were heated to reflux for 24 hours before being cooled and filtered.

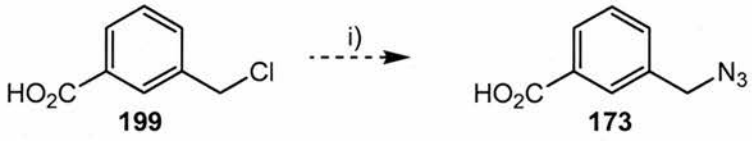

Scheme 49 i) NaN_3, acetone, Δ.

However, it was not possible to isolate **173**. When the reaction mixture was heated to reflux for 16 hours, there was still more than 50% of **199** present according to ^{1}H NMR analysis. The reaction was allowed to reflux for a longer period of time but this only resulted in decomposition. It is not clear what effect the carboxylic acid group has on reactivity, but the best method for obtaining **173** may be through protecting the acid group before conversion into the azide. Deprotection of the acid would then afford the desired product.

Two different strategies were used to attempt to synthesise **174** (Scheme 50).

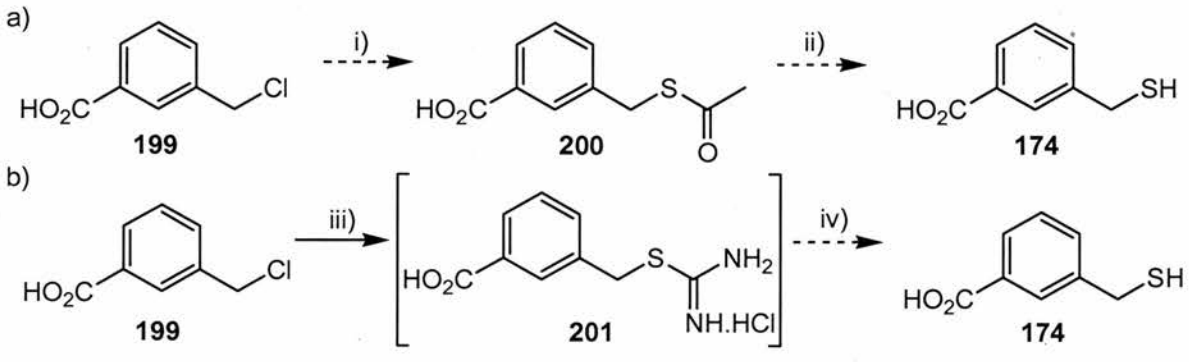

Scheme 50 i) CH_3COSK, acetone; ii) 1M KOH (aq), MeOH; iii) thiourea, acetone, Δ; iv) $Na_2S_2O_5$, H_2O, Δ.

Strategy a) failed to yield the thioacetate product **200**. The second method used to synthesise **174** involved the formation of thiouronium salt intermediate **201**. In this case, preparation of **201** appeared to be successful but there were problems with deprotection as a consequence of insolubility. It was difficult to determine the end point of the reaction because **201** and **174** did not remain in solution. There was also a problem with extracting the thiol from the aqueous phase. The organic solvent used was DCM but no significant quantities of **174** were isolated. In order for this method to be used successfully, optimisation of the deprotection step is required and a variety of solvents should be screened to improve the extraction process.

An alternative strategy for synthesising **174** may be to use hexamethyldisilathiane which has been previously used in the group with varying degrees of success. Another possibility is that in order to successfully synthesise **174**, the carboxylic acid group must first be protected because it appears to hinder the reaction and also causes solubility problems.

Following the failure of the synthesis of **171** and **172**, it was decided to perform matrix experiments using only the control compounds in order to obtain preliminary results. For this reason, thiophenol **143** and benzyl azide **145** were used as substrates for the [3+2] dipolar cycloaddition and conjugate addition reactions because the carboxylic acid recognition group is not required. Substrates **143** and **145** do not possess the required carboxylic acid recognition group required to hydrogen bond to the binding site (Scheme 51). Therefore, addition of **175** should not have any effect on the reaction rate.

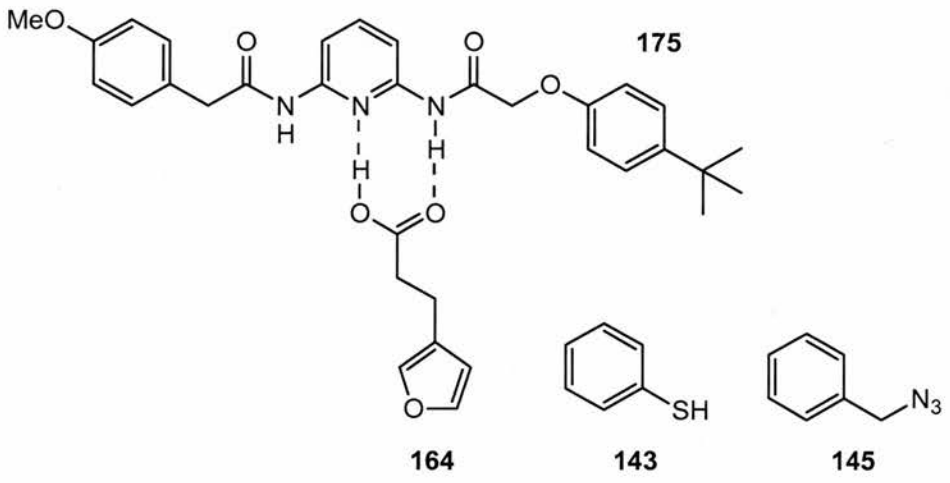

Scheme 51 Reactions using binding site control **175** were carried out using **164** which contains the correct recognition group along with substrates **143** and **145** which are not capable of hydrogen bonding to **175**.

Control **175** is not expected to have any effect upon the reaction rate which will be demonstrated in the reaction with **164**. For the reaction containing polarisation site control **177**, there is no requirement for the carboxylic acid recognition group (Scheme 52). Therefore, **143** and **145** can be used in preliminary investigations to allow comparisons to be made with results obtained for **122** (Chapter 2). If preliminary results are promising, then different strategies for synthesising both organocatalysts **171** and **172**, and also reaction substrates **173** and **174** which contain recognition, can be adopted.

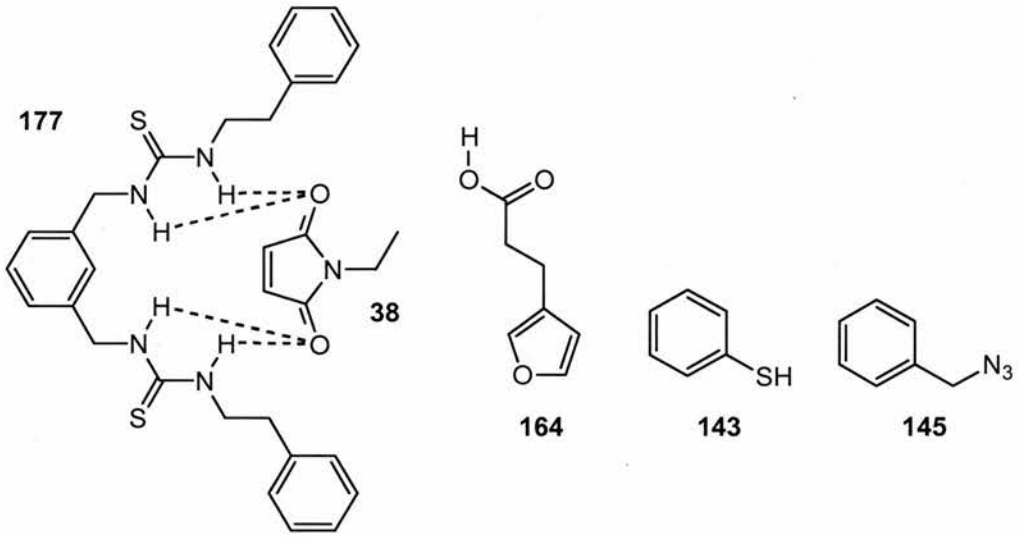

Figure 52 Reactions using **177** do not require recognition groups on reaction substrates **143** and **145**. Results obtained from these reactions can be directly compared with organocatalyst **122** from Chapter 2.

4.6 Synthesis of Reaction Products

The products of all three reactions were prepared for characterisation purposes. Cycloadduct product **202** of the Diels-Alder reaction was synthesised as shown in Scheme 53. Diene **162** and **38** were dissolved in $CDCl_3$ and warmed to 35 °C on a water bath for two weeks. The *exo* isomer was obtained by removing the solvent *in vacuo*.

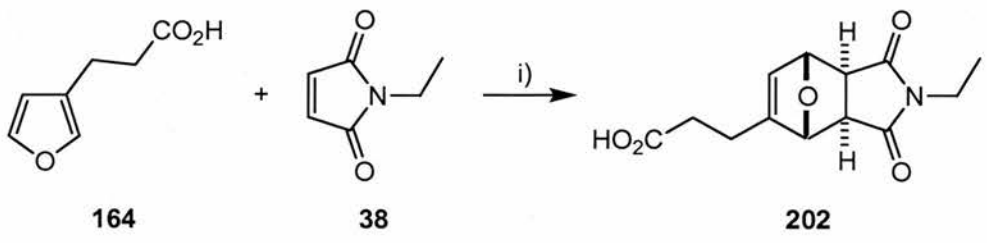

Scheme 53 i) $CDCl_3$.

The [3+2] dipolar cycloaddition reaction is slow. Therefore, the [3+2] dipolar cycloaddition reaction product **203** was prepared by warming a solution of **145** and **38** dissolved in $CDCl_3$ to 50 °C for three weeks (Scheme 54). The product was obtained by removing the solvent *in vacuo* after filtration.

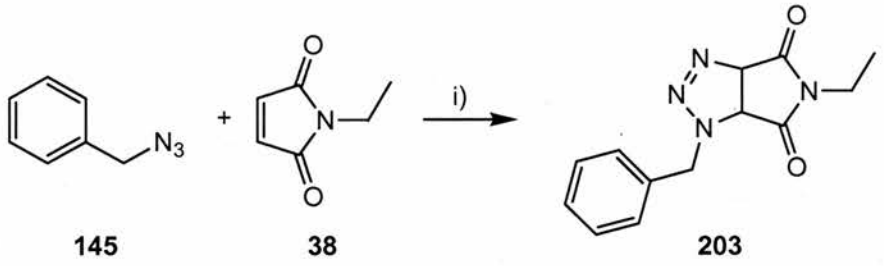

145 **38** **203**

Scheme 54 i) $CDCl_3$.

The product of the conjugate addition reaction **204** was prepared by dissolving **143** and **38** in $CDCl_3$ using 4-*t*-butylpyridine as a base (Scheme 55). The solution was warmed on a water bath at 35 °C for one week before the solution was washed with water, dried and **204** was obtained by removing the solvent *in vacuo*.

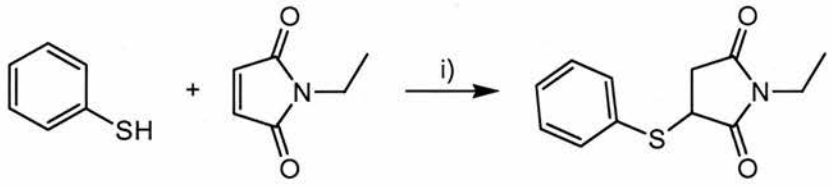

143 **38** **204**

Scheme 55 i) $CDCl_3$, 4-*t*-butylpyridine.

4.7 Binding Studies

Controls **175** and **177** were used in the binding studies. The two binding studies were conducted as described in Section 2.6.1. A 300 MHz ^{1}H NMR titration experiment was conducted using **175** with **164** to calculate the strength of the amidopyridine-carboxylic acid interaction. All 300 MHz ^{1}H NMR spectra were recorded at 35°C containing 10 mM **175** with the addition of 0, 5, 10, 15, 25, 50 or 100 mM **164**. Results from the titration experiment gave an average K_a value of 29 M^{-1} and ΔG = -8.6 kJ mol^{-1}. These results are consistent with those previously obtained within the group (see Figure 42, p. 70).

This process was repeated for **177**. 300 MHz ^{1}H NMR spectra were recorded at 35 °C for solutions of 10 mM **177** with the addition of 0, 5, 10, 15, 25, 50 or 100 mM **38**. Results did

not show any significant chemical shift for any protons in **177**. The titration experiment was repeated again; this time 75.5 MHz ^{13}C NMR spectra were recorded. Unfortunately, there were still no significant chemical shift changes recorded.

4.8 Matrix Experiments

Preliminary matrix experiments were conducted to see the effect of **175** and **177** on all three reaction types. In order to make a direct comparison with results obtained for **122**, described in Chapter 2, the same reaction conditions were used. Initial concentrations of 50 mM solutions of **38** and **164**, **143** or **145** were used. All reactions were carried out at 35 °C with the addition of 0.5 equivalents of 4-*t*-butylpyridine as a base in the conjugate addition reaction. The solutions were maintained at 35 °C on the water bath for 16 hours before the extent of the reaction was calculated through deconvolution of 300 MHz ^{1}H NMR spectra.

Three solutions were prepared for each reaction type: one containing only the reactants, one with the addition of **175** and finally one with the addition of **177**. A summary of the results obtained can be seen in Figure 91. The results for the native reaction, containing no control compounds, can be seen in white; the results for the reaction containing **175** can be seen in blue; and the results for the reaction containing **177** are shown in red.

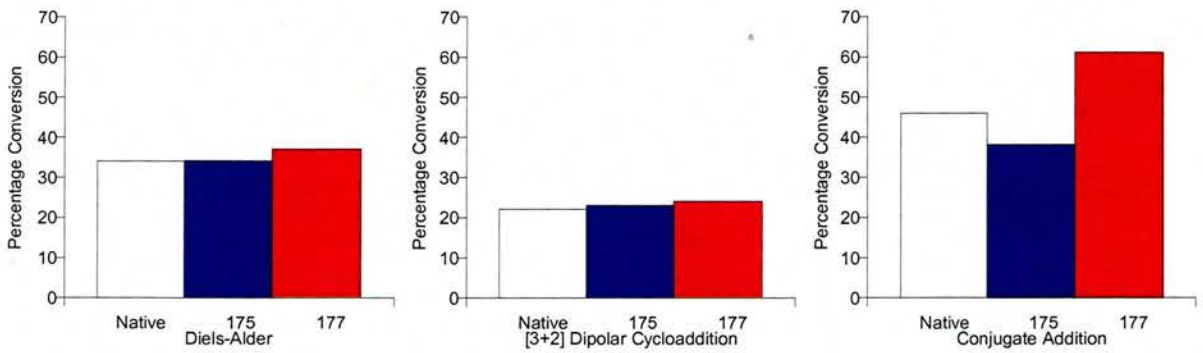

Figure 91 (a) Summary of the results obtained for the Diels-Alder reaction showing the percentage conversion after 16 hours for the native reaction in white, percentage conversion with the addition of binding site control **175** in blue, and the percentage conversion with the addition of polarisation site control **177** in red. (b) Summary of the results obtained for the [3+2] dipolar cycloaddition reaction. (c) Summary of the results obtained for the conjugate addition reaction.

4.9 Conclusions

Preliminary results using the control compounds are interesting. Control **175** does not appear to enhance the reaction, but it would be interesting to perform kinetic experiments to truly see its effect. The results from the conjugate addition reaction containing **175** should be repeated to see if it really is able to slow the reaction. It is not clear what effect **175** could have upon the reaction rate – particularly as **143** does not contain the carboxylic acid recognition moiety.

In the Diels-Alder reaction, **164** was used which does contain the correct recognition elements. The results obtained in this case are consistent with predictions – **175** has no effect on percentage conversion of reactants to products over 16 hours. It is also promising to observe a slight increase in percentage conversion when **177** was added. It is essential to perform kinetic experiments for this system to verify these results. Kinetic experiments also allow kinetic modelling to be performed using Simfit which provides reaction rates. The Simfit results are crucial for determining the extent of catalysis (k_{cat}/k_{uncat}).

The [3+2] dipolar cycloaddition reaction is slow, giving low conversion over 16 hours. The low conversion rates make it difficult to distinguish the effects of **175** and **177** on rate acceleration. Further studies are required before the true effects of the control compounds are known. After kinetic experiments and kinetic modelling have been conducted, the effects of the control compounds will be clearer. It would also be worthwhile to extend the reaction time, and monitor the reaction over 24 or 48 hours as opposed to 16 hours as previously used.

Addition of **177** to the conjugate addition reaction leads to a much higher conversion after 16 hours. The magnitude of this effect can be determined after kinetic studies have been performed and the data fitted to the kinetic model. The resulting reaction rates will indicate if **177** is better than **122** for accelerating conjugate addition reactions.

Although the binding study failed to show significant binding between **177** and **38**, the results indicate that **177** does indeed bind **38** because there is such a dramatic difference in the percentage conversions for the conjugate addition reaction. The difference observed in percentage conversions obtained for the control reaction and the reaction with **177** added indicate that maleimide **38** must be bound to **177**.

4.10 Future Directions

The results presented for these systems are merely a beginning. Preliminary results using **175** and **177** are promising. However, there are many more experiments which should be performed in order to fully understand the effects of combining proximity and polarisation on rate acceleration.

Different synthetic strategies are required in order to find solutions to the various problems encountered. Firstly, different polarisation site control compounds should be investigated with a wider range of isocyanates. The synthetic strategy for obtaining **193** works well but subsequent steps are problematic as a consequence of poor solubility. Screening different control compounds (Scheme 56) will indicate if it is possible to synthesise a more soluble bis urea.

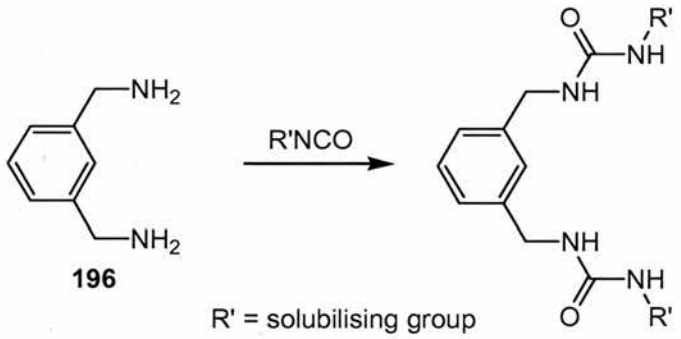

Scheme 56 Screening different isocyanates will determine if it is possible to synthesise a soluble bis urea control compound.

Another option would be to optimise the reduction of **191** using triphenylphosphine to determine if the bis ureas formed from **192** are soluble with the addition of the benzyl group. These compounds could then be used as control compounds. If the resulting compounds are more soluble than those formed from **196**, there is also the possibility of using other protecting groups for the phenol moiety which would further increase solubility (Scheme 57).

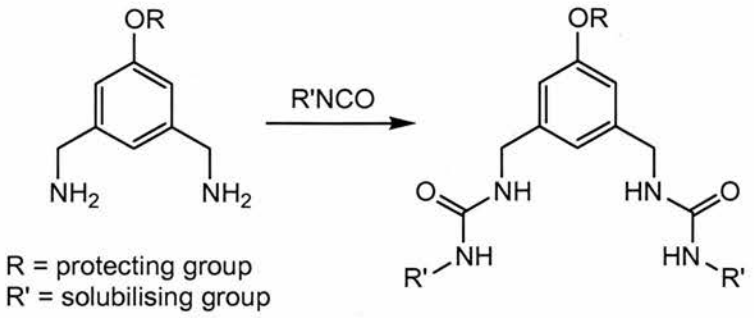

Scheme 57 Reduction of diazide **191** using triphenylphosphine leaves the phenol protecting group intact and should form a soluble diamine and enable the reaction with an isocyanate to be conducted more easily. Leaving the protecting group intact also leads to the production of a suitable control. Altering the protecting group should lead to the formation of a soluble control.

There are several factors which can be varied to optimise the coupling reaction used to synthesise **171** and **172**. These include adjusting the solvent, number of equivalents of base, the base used, the reaction time and temperature. It would be invaluable to carry out several small scale reactions which test these various possibilities in order to determine the optimum reaction conditions. If a clean, soluble bis urea or thiourea can be obtained then will also aid in the synthesis of the full organocatalysts.

Once **171** and **172** have been succesfully obtained, there is a requirement to produce reactants containing the carboxylic acid recognition site. The addition of protection and deprotection steps for the carboxylic acid group when synthesising **173** and **174** should lead to a more successful synthetic strategy (Scheme 58). It would also be worthwhile exploring the synthesis of alternative reagents which incorporate the carboxylic acid recognition site, such as a nitrone for the [3+2] dipolar cycloaddition reaction or an amine for conjugate addition.

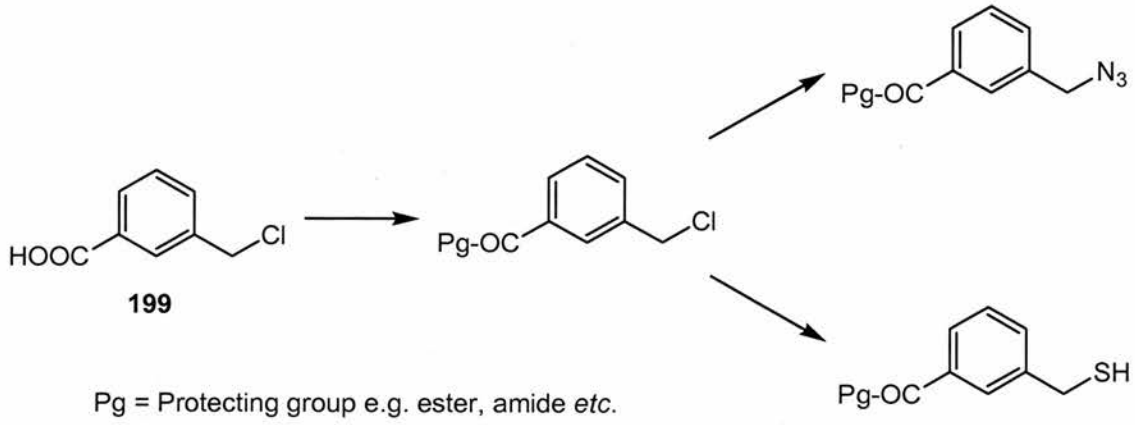

Scheme 58 One method of successfully synthesising **173** and **174** may be through prior protection of the acid group.

Organocatalysts **171** and **172** have been designed with a resin attachment point already on the molecule. After deprotecting the methoxy group, the organocatalyst can then be attached to solid support (Figure 92).

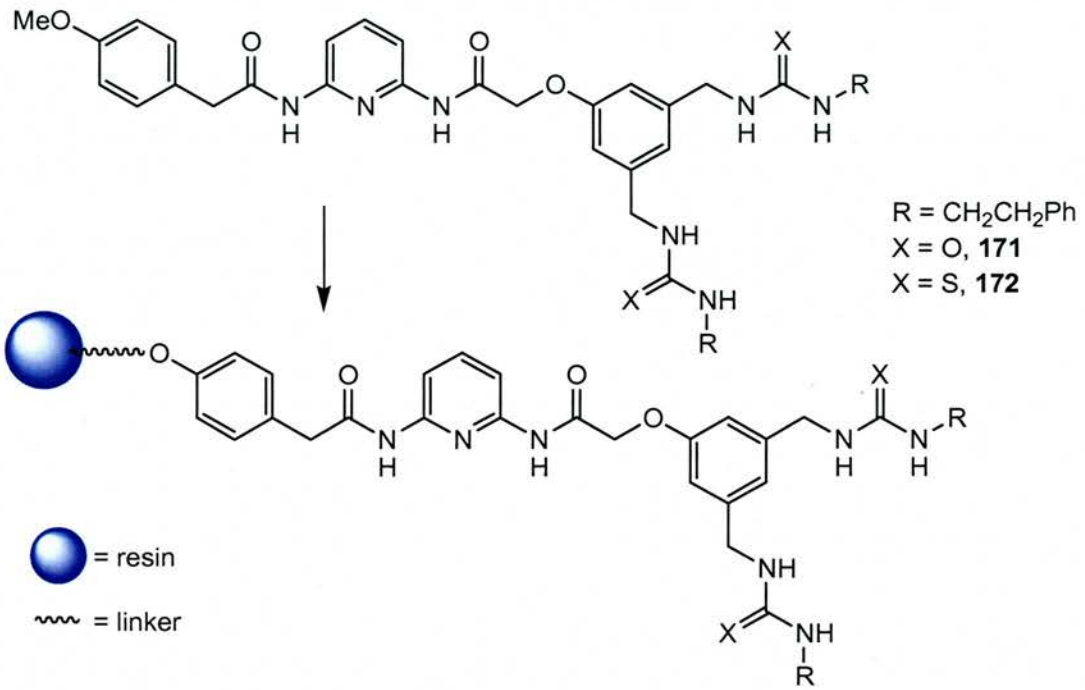

Figure 92 Deprotecting the methoxy group of organocatalysts **171** and **172** provides an ideal site for resin attachment.

With the organocatalyst immobilised on solid support, a number of experiments can be conducted. Firstly, the kinetic experiments performed previously should be repeated to determine if the solid support inhibits the reaction. If there is a decrease in reaction rate when using the immobilised organocatalyst then optimisation of the linker may be required. By extending the linker unit, the distance between the resin and the organocatalyst is increased which should reduce the possibility of there being any interaction.

Having established that the organocatalyst is capable of accelerating reactions whilst immobilised on solid support, it is then possible to carry out continuous flow experiments (Figure 93). A continuous system allows the turnover of the organocatalyst to be investigated and also provides information about the stability of the organocatalyst when immobilised. If there is leaching of the organocatalyst then this will also be detected when the product is isolated.

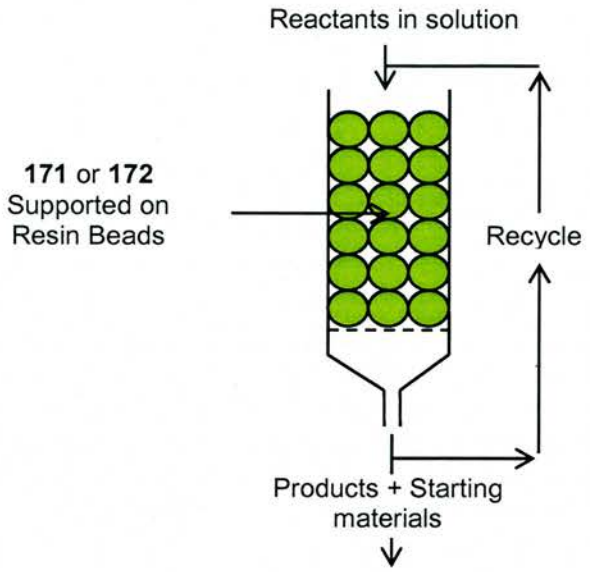

Figure 93 Schematic representation of a continuous flow system. A solution of reactants is passed through a column containing organocatalyst immobilised on solid support. The output containing product and starting materials can be analysed and reaction conditions altered to give the optimum yields of desired product.

The continuous flow system would also benefit from using the prediction techniques described in Section 3.6. Modelling the system will allow the optimum reaction conditions to be determined without the need for extensive matrix testing.

5. Conclusions

Catalysts are vital for many different purposes. Life itself would not exist without natural catalysts enabling essential reactions to proceed with shorter half-lives and a high degree of specificity. Natural catalysts have evolved to catalyse specific reactions very efficiently and some have been adapted for use by synthetic chemists.

However, the true potential of natural catalysts has not yet been exploited and may never be fully realised. Enzyme purification is often troublesome, yielding a very small amount of pure catalyst which is not feasible for use in industrial processes. It is also not possible to find a naturally occurring catalyst for any given reaction, because they are generally limited to accelerating reactions of naturally occurring substrates. It is difficult to produce a tailor-made enzyme which will accept any given substrate. The alternative is to develop new catalysts.

Industry is dependent on the development of new and better catalysts in order to improve synthetic processes to give higher yields at lower costs. Traditionally these processes have involved using homogeneous or heterogeneous metal-based catalysts. In order to reduce costs and move towards more environmentally friendly catalysts, new strategies are required. For this reason, it is useful to study natural catalysts to develop new methods of catalysing reactions using mechanisms perfected by evolution.

Recognition-mediated processes play a key role in enzyme catalysis and can be successfully used to accelerate a range of different reactions. Supramolecular chemistry uses recognition as the basis of many different types of system, from self-assembly through to catalysis and self-replication. The design of such systems is crucial in order to achieve maximum rate accelerations, stereochemical control and catalytic turnover. In this way it is possible to investigate the different techniques used in Nature for rate accelerations and adapt them for use in unnatural reactions.

One interesting feature noted is that very few natural systems are capable of accelerating non-polar reactions. Our results have given an indication of a possible explanation for this observation. Rate acceleration can be easily achieved by the stabilisation of charges and in non-polar reactions there is likely to be only slight differences in charge which makes this difficult. In this manner, chemists can improve on Nature. Much research is based upon

accelerating cycloaddition reactions and good results have been reported. Large rate accelerations have been achieved through careful design using only hydrogen bonds.

The work presented has shown that it is possible to develop a broad spectrum organocatalyst suitable for testing rate accelerations of different reaction types. Activation of a substrate through polarisation can effectively accelerate polar reactions and also shows potential for accelerating non-polar reactions. Proximity is very important in enzyme catalysis and can also be used successfully to control the stereochemistry of chemical reactions. Combining both factors shows great potential for developing organocatalysts based on enzyme methodologies.

6. Experimental Procedures

6.1 General Procedures

Chemicals and solvents were purchased from Acros, Aldrich, Avocado or Fluka and were used as received unless otherwise stated. Tetrahydrofuran (THF) was dried by heating to reflux with sodium-benzophenone under an N_2 atmosphere and collected by distillation. Acetonitrile and DCM (CH_2Cl_2) were dried by heating under reflux over calcium hydride and distilled under N_2.

Thin-layer chromatography (tlc) was performed on aluminium plates coated with Merck Kieselgel 60 F_{254}. Developed plates were air dried and scrutinised under a UV lamp (366 nm), and where necessary, stained with iodine, phosphomolybdic acid (PMA) or ninhydrin to aid identification.

Melting points were determined using an Electrothermal 9200 melting point apparatus and are uncorrected. Column chromatography was performed using Kieselgel 60 (0.040-0.063 mm mesh, Merck 9385). Microanalyses (CHN) were carried out at the University of St Andrews. Infra-red Spectra (IR) were recorded as KBr discs or thin films using a Perkin Elmer Paragon 1000 spectrometer.

^{1}H Nuclear magnetic resonance (NMR) spectra were recorded on a Bruker Avance 300 (300.1 MHz), a Varian Gemini 2000 (300.0 MHz), a Bruker Avance 500 (500.0 MHz) or a Varian UNITYplus 500 (500.0 MHz) spectrometer using the deuterated solvent as the lock and the residual solvent as the internal reference in all cases. ^{13}C NMR spectra using the PENDANT sequence were recorded on a Bruker Avance 300 (75.5 MHz) spectrometer. All other ^{13}C spectra were recorded on a Varian Gemini 2000 (75.5 MHz) spectrometer using composite pulse ^{1}H decoupling. ^{19}F NMR spectra were recorded on a Bruker Avance 300 (282.3 MHz) spectrometer using the deuterated solvent as the lock and the residual solvent as the internal reference. All spectra are recorded at 298 K unless otherwise stated. All coupling constants are quoted to the nearest 0.1 Hz. In the assignment of ^{1}H NMR spectra the symbols b, s, d, t, q, and m denote broad, singlet, doublet, triplet, quartet and multiplet respectively.

Electron impact mass spectrometry (EIMS) and high-resolution mass spectrometry (HRMS) were carried out on a VG AUTOSPEC mass spectrometer or on a Micromass GCT orthogonal

acceleration time of flight mass spectrometer. Chemical Ionisation Mass Spectrometry (CIMS) was carried out on a VG AUTOSPEC instrument or on a Micromass GCT orthogonal acceleration time of flight mass spectrometer. Electrospray mass spectrometry (ESMS) and high-resolution mass spectrometry (HRMS) was carried out on a Micromass LCT orthogonal time of flight mass spectrometer.

6.2 Procedure for Kinetic Experiments

Stock solutions were prepared by dissolving the appropriate amount of reagent in $CDCl_3$ using Volac 5 mL ± 0.025 mL or 2 mL ± 0.015 mL volumetric flasks. Reagents were measured using a Sartorius BP 211D balance (± 0.01 mg) or by using a 25 μL Hamilton gas tight syringe. Solutions were pre-equilibrated to the appropriate temperature on a water bath. The reaction mixture was prepared by mixing a fixed amount of the appropriate stock solution with the addition of solid organocatalyst. The organocatalyst was weighed using a Sartorius BP 211D balance (± 0.01 mg) and all solutions measured using a 1000 μL or 500 μL Hamilton gas tight syringe. The solution was then filtered into a Wilmad 528pp NMR tube which was subsequently fitted with a polyethylene pressure cap to minimise solvent evaporation. Reaction mixtures were then monitored by 500 MHz ^{1}H NMR over 16 hours with spectra recorded every 30 minutes.

6.3 Procedures for Binding Studies

K_a values were determined by the ^{1}H NMR titration method.[215] A stock solution of the appropriate amount of organocatalyst dissolved in $CDCl_3$ was prepared as described above. The organocatalyst solution was mixed with the appropriate amount of guest molecule. On average ten samples were prepared for each binding study with a constant organocatalyst concentration and guest concentrations ranging from 0 to 100 mM. 300 MHz ^{1}H NMR spectra were recorded for each solution and the chemical shift changes for each proton in the organocatalyst molecule were monitored. The data were then used to calculate K_a and ΔG of association using a custom written non-linear fitting spreadsheet in Excel (Version 10, Microsoft Corp., 2002).

6.4 Procedures for Matrix Experiments

Stock solutions of reaction substrates in $CDCl_3$ were prepared as described above. The appropriate amount of solution was mixed using a 1000 μL or 500 μL Hamilton gas tight syringe to give the reaction mixture. In catalysed reactions, the appropriate amount of solid organocatalyst was added. The reaction mixture solution was then filtered into a Wilmad 507PP NMR tube. The NMR tubes were fitted with a polyethylene pressure cap and further sealed with Nescofilm before they were placed in a water bath at the appropriate temperature and left for 16 hours. NMR tubes were then cooled on a dry ice/acetone bath to prevent further reaction. Random batches of three tubes were warmed to room temperature and thoroughly mixed before ^1H NMR spectra were recorded.

6.5 Procedures for Deconvolution and Simulation

The extent of reaction for kinetic and matrix experiments was determined using the deconvolution tool available in 1D WINNMR (version 6.2.0.0, Bruker Daltonik GmbH, Germany, 2000). Kinetic simulation and fitting of the resultant data to the appropriate kinetic models was achieved using the fitting mode of SIMFIT-32.[216] The rate of reaction in the absence of any organocatalyst was assumed to be identical to the background rate in the catalysed reaction. The prediction simulation experiments described in Chapter 3 were conducted using the simulation mode of SIMFIT-32.

6.6 Molecular Modelling Procedures

Electronic structure calculations were performed on a Silicon Graphics Octane2 workstation using the AM1 semi-empirical method as implemented in SPARTAN (Wavefunction Inc, Irvine, CA, USA, version 5.1.3, 1999). Electrostatic potential surfaces were visualised using the same software and are plotted on a common scale of –70 to +45 kcal.

Changes in charge at the polarisation site for the reactions discussed in Chapter 2 were calculated using GAMESS[221] (Version 19 May 2004 R4). The carbonyl charge on the maleimide ring in the ground state was calculated at the HF/6-31G(d) level of theory. The appropriate transition state structure for the reaction was calculated and the charge on the same carbonyl oxygen determined. A percentage change was then calculated by comparing charges on the maleimide carbonyl oxygen atoms in the ground state and the transition state.

6.7 Experimental Procedures

Preparation of 3-Maleimidopropanoic acid 45

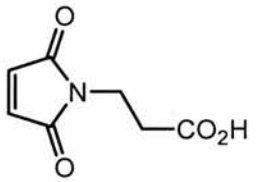

β-Alanine (4.91 g, 55.1 mmol) and maleic anhydride **140** (5.00 g, 51.0 mmol) were dissolved in acetic acid (80 mL) and left to stir under a positive pressure of nitrogen overnight before the solution was heated to reflux for 8 hours. The solvent was removed *in vacuo* affording the crude product as a yellow solid which was purified by vacuum filtration through a short pad of silica gel using v/v 95:5 DCM:acetic acid as the eluent to afford **45** as a colourless solid. Mp 108-110 °C (lit.[222] 105-105.5 °C) (2.64 g, 31%). ^{1}H NMR (300.1 MHz, $CDCl_3$) δ 6.66 (2H, s, CH), 3.77 (2H, t, $^{3}J_{H,H}$ 7.2, N-CH_2) and 2.66 (2H, t, $^{3}J_{H,H}$ 7.2 Hz, CH_2-CO_2H). ^{13}C NMR (75.5 MHz, $CDCl_3$) δ 176.7 (C=O), 170.7 (2 x C=O, ring), 134.6 (2 x CH, ring), 33.6 (CH_2) and 32.9 (CH_2). EIMS m/z 169 (M^+, 4%), 151 (17%), 123 (100%) and 110 (99%). Anal. Calcd. for $C_7H_7NO_4$: C, 49.7; H, 4.17; N, 8.28. Found: C, 49.9; H, 4.03; N, 8.28.

Preparation of 3-Amino-*N*-(6-methylpyridin-2-yl) benzamide 123

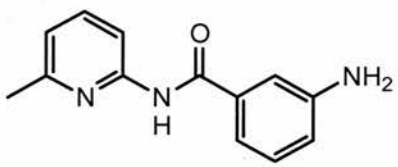

Method A: A saturated solution of $Cu(acac)_2$ in methanol (30 mL) was added to a solution of *N*-(6-methyl-pyridin-2-yl)-3-nitro-benzamide **128** (1.00 g, 3.9 mmol) in methanol (150 mL) before sodium borohydride (0.88 g, 23.3 mmol) was added portionwise and the reaction mixture stirred for 1 hour. The reaction mixture was then extracted with DCM (2 x 100 mL), washed with saturated sodium hydrogen carbonate solution (2 x 100 mL) and then washed with ammonia (2 x 100 mL) before the aqueous layer was dried using $MgSO_4$ and the solvent removed *in vacuo* to afford the crude product as a brown oil. The product was then purified *via* recrystallisation from v/v 1:5 chloroform:hexane to afford **123** as a pale brown solid (240 mg, 27%). When this method was repeated the product could not always be isolated as a

crystalline solid. The procedure often resulted in the production of a crude brown oil that could not be purified.

Method B: **128** (2.00 g, 7.8 mmol) and 5% Pd/C (168 mg) were degassed under nitrogen for 30 minutes before the solvent, methanol (30 mL), was added. The flask was then flushed with hydrogen and a hydrogen balloon fitted before the solution was left to stir overnight. The reaction mixture was then filtered through a pad of celite before being dried with $MgSO_4$ and the solvent removed *in vacuo* to afford a yellow oil. This procedure resulted in a mixture of products that could not be separated.

Method C: Benzyl[3-(6-Methylpyridin-2-ylcarbamoyl)phenyl] carbamate **132** (1.35 g, 3.70 mmol) was dissolved in 30% HBr in acetic acid (15 mL, 5.60 mmol) and stirred overnight under a $CaCl_2$ guard tube. The solution was then diluted with diethyl ether (20 mL) to afford a colourless precipitate which was filtered and dissolved in minimum volume of water. The pH of the solution was then adjusted to 9 using 2M NaOH solution to afford **123** as a colourless solid.

Mp 64-66 °C (0.74 g, 87%). ^{1}H NMR (300.1 MHz, $CDCl_3$) δ 8.52 (1H, bs, NH), 8.17 (1H, d, $^3J_{H,H}$ 7.9 Hz, Ar-H), 7.64 (1H, dd, $^3J_{H,H}$ 7.9 Hz, $^3J_{H,H}$ 7.9 Hz, Ar-H), 7.25-7.23 (3H, m, Ar-H), 6.92 (1H, d, $^3J_{H,H}$ 7.9 Hz, Ar-H), 6.86-6.82 (1H, m, Ar-H), 3.85 (2H, bs, NH_2) and 2.46 (3H, s, CH_3). ^{13}C (75.5 MHz, $CDCl_3$) δ 166.3 (C=O), 157.2 (quat, Ar), 151.2 (quat, Ar), 147.4 (quat, Ar), 139.2 (CH, Ar), 135.9 (quat, Ar), 130.0 (CH, Ar), 119.7 (CH, Ar), 119.0 (CH, Ar), 117.1 (CH, Ar), 114.2 (CH, Ar), 111.3 (CH, Ar) and 24.4 (CH_3). IR (KBr, cm^{-1}) 3386, 2946, 2882, 1683, 1601 and 1580. CIMS *m/z* 228 ([M^++H], 100%), 109 (35%), 75 (25%) and 56 (37%). HRMS (CI^+, *m/z*) calcd for $C_{13}H_{14}N_3O$ 228.1137, found 228.1143.

Preparation of *N*-(6-Methylpyridin-2-yl)-3-nitrobenzamide 128

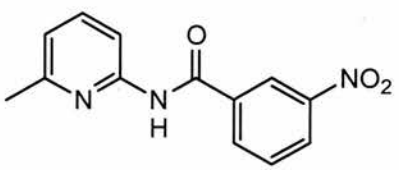

2-Amino-6-methylpyridine **126** (13.98 g, 129.3 mmol) was added to a solution of 3-nitrobenzoyl chloride (12.00 g, 64.7 mmol) in diethyl ether (300 mL) and stirred overnight. The resulting precipitate was filtered and washed with cold diethyl ether before being

dissolved in DCM (300 mL) and washed with 10% HCl (aq) (2 x 100 mL). The organic layer was then dried using $MgSO_4$ and the solvent removed *in vacuo* to afford a colourless solid. This was then purified *via* recrystallisation from v/v 1:10 DCM:hexane to afford **128** as a colourless solid. Mp 128-130 °C (lit.[223] 128.0-130.8 °C) (16.08 g, 97%). ^{1}H NMR (300.1 MHz, $CDCl_3$) δ 12.40 (1H, bs, NH), 9.00 (1H, t, $^4J_{H,H}$ 1.9 Hz, Ar-H), 8.79-8.75 (1H, m, Ar-H), 8.71 (1H, d, $^3J_{H,H}$ 8.8 Hz, Ar-H), 8.43-8.38 (1H, m, Ar-H), 8.10 (1H, m, Ar-H), 7.74 (1H, dd, $^3J_{H,H}$ 7.9 Hz, $^3J_{H,H}$ 7.9 Hz, Ar-H), 7.19-7.16 (1H, m, Ar-H) and 2.75 (3H, s, CH_3). ^{13}C NMR (75.5 MHz, $CDCl_3$) δ 164.1 (C=O), 151.3 (quat, Ar), 149.3 (quat, Ar), 149.0 (quat, Ar), 146.4 (CH, Ar), 134.1 (CH, Ar), 133.9 (quat, Ar), 130.9 (CH, Ar), 128.1 (CH, Ar), 124.7 (CH, Ar), 120.6 (CH, Ar), 114.6 (CH, Ar) and 20.4 (CH_3). CIMS *m/z* 258 ([M^++H], 100%), 228 (14%), 168 (7%).

Preparation of 3-Benzyloxycarbonylaminobenzoic acid 130

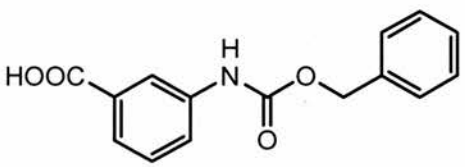

Benzyl chloroformate (11.82 mL, 82.8 mmol) was dissolved in dry THF (30 mL) and added to a solution of 3-aminobenzoic acid **129** (10.00 g, 74.6 mmol) and pyridine (8.00 mL, 99.4 mmol) in dry THF (200 mL) under a positive pressure of nitrogen and stirred for 3 hours. The solvent was removed *in vacuo* before the reactant mixture was triturated with water and acidified using hydrochloric acid to afford a colourless precipitate. The crude product could not be purified *via* column chromatography or recrystallisation, therefore, the crude product was dried *in vacuo* affording **130** as a grey solid which was used without further purification (20.00 g, 89%). ^{1}H NMR (300.1 MHz, d_6-acetone) δ 8.84 (1H, bs, NH), 8.18 (1H, t, $^4J_{H,H}$ 1.8 Hz, Ar-H), 7.72-7.67 (1H, m, Ar-H), 7.60-7.56 (1H, m, Ar-H), 7.34-7.20 (6H, m, Ar-H), 5.07 (2H, s, CH_2) and 2.94 (1H, bs, OH).

Preparation of Benzyl (3-fluorocarbonylphenyl) carbamate 131

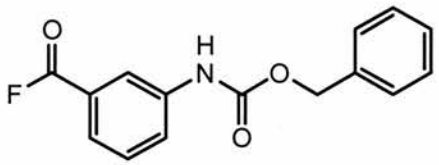

130 (2.00 g, 7.40 mmol) and pyridine (0.59 mL, 7.40 mmol) were dissolved in dry ethyl acetate (50 mL) and cooled in an ice bath before cyanuric fluoride (0.59 mL, 4.40 mmol) was added. The reaction mixture was stirred for 15 minutes before it was diluted with DCM (2 x 50 mL) and washed with water (2 x 50 mL). The organic layer was then dried using $MgSO_4$ and the solvent removed *in vacuo* to afford **131** as a yellow oil which was used without further purification. ^{19}F NMR (282.3 MHz, $CDCl_3$) δ 18.4 (1F, s, acyl-F).

Preparation of Benzyl [3-(6-methylpyridin-2-yl carbamoyl)phenyl] carbamate 132

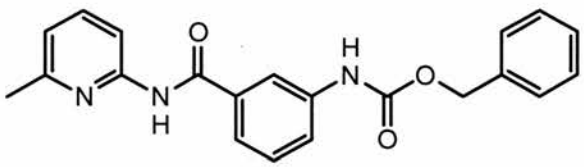

126 (0.79 g, 7.30 mmol) was added to a solution of **130** (2.00 g, 7.30 mmol) in DCM (5 mL) and stirred overnight under a positive pressure of nitrogen before the solvent was removed *in vacuo* to afford a brown oil. The product was purified *via* flash column chromatography (SiO_2; v/v 2:1 hexane:EtOAc) to afford **132** as a pale yellow solid. Mp 73-75 °C (1.10 g, 42%). ^1H NMR (300.1 MHz, $CDCl_3$) δ 8.54 (1H, bs, NH), 8.32 (1H, bs, NH), 8.17-8.14 (1H, m, Ar-H), 7.90-7.88 (1H, m, Ar-H), 7.70 (1H, d, $^3J_{H,H}$ 7.8 Hz, Ar-H), 7.63 (1H, dd, $^3J_{H,H}$ 7.8 Hz, $^3J_{H,H}$ 7.8 Hz, Ar-H), 7.60-7.59 (1H, m, Ar-H), 7.57-7.34 (5H, m, Ar-H), 6.94-6.90 (2H, m, Ar-H), 5.22 (2H, s, CH_2) and 2.47 (3H, s, CH_3). ^{13}C NMR (75.5 MHz, $CDCl_3$) δ 165.9 (C=O), 157.2 (quat, Ar), 153.8 (quat, Ar), 151.1 (C=O), 139.2 (CH, Ar), 139.0 (quat, Ar), 136.3 (quat, Ar), 135.5 (quat, Ar), 129.9 (CH, Ar), 129.0 (2 x CH, Ar), 128.8 (CH, Ar), 128.6 (CH, Ar), 122.6 (2 x CH, Ar), 122.3 (CH, Ar), 119.9 (CH, Ar), 117.9 (CH, Ar), 111.6 (CH, Ar), 67.5 (CH_2) and 24.3 (CH_3). IR (KBr, cm^{-1}) 3319, 3034, 2945, 1738, 1658, 1548 and 1456. CIMS *m/z* 362 ([M^++H], 24%), 254 (65%) and 228 (25%).

Preparation of *tert*-Butoxycarbonylamino acetic acid 133

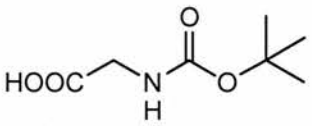

BOC-ON (7.39 g, 30.0 mmol) was added to a solution of glycine **124** (2.25 g, 30.0 mmol) and triethylamine (6.32 mL, 45.0 mmol) in dioxane (20 mL) and water (20 mL) and stirred for 2 hours. Water (50 mL) and ethyl acetate (50 mL) were then added and the aqueous layer was washed with ethyl acetate (50 mL) and the aqueous layer retained. The aqueous layer was then acidified with 5% citric acid solution to pH 4 before being extracted with ethyl acetate (2 x 50 mL). The organic layer was then dried using $MgSO_4$ and the solvent removed *in vacuo* to afford the crude product as a colourless solid. The product was then purified *via* recrystallisation from v/v 1:5 ethyl acetate:hexane to afford **133** as a colourless solid. Mp 87-89 °C (lit.[224] 90 °C) (4.24 g, 81%). ^{1}H NMR (300.1 MHz, $CDCl_3$) δ 10.00 (1H, bs, OH), 6.70 (1H, bs, NH), 3.89 (2H, d, $^3J_{H,H}$ 5.6 Hz, CH_2), 1.38 (9H, s, CH_3). ^{13}C NMR (75.5 MHz, $CDCl_3$) δ 175.1 (C=O), 156.4 (C=O), 80.8 (quat), 42.6 (CH_2), 28.6 (3 x CH_3). IR (KBr, cm^{-1}) 2980, 1749, 1670, 1538, 1410 and 1198. CIMS *m/z* 120 ([M^++2H –C_4H_9], 100%), 102 (13%), 76 (36%), 43 (6%). Anal. Calcd. for $C_7H_{13}NO_4$: C, 48.0; H, 7.48; N, 8.00. Found: C, 48.2; H, 7.83; N, 7.87.

Preparation of *tert*-Butyl fluorocarbonylmethylcarbamate 134

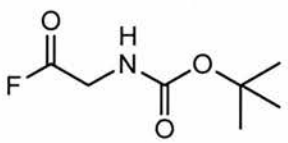

133 (0.70 g, 4.0 mmol) and pyridine (0.33 mL, 2.4 mmol) were dissolved in dry acetonitrile (40 mL) and cooled in an ice bath before cyanuric fluoride (0.20 mL, 4.0 mmol) was added. The reaction mixture was stirred for 15 minutes before being extracted with DCM (2 x 50 mL) and washed with water (2 x 50 mL). The organic layer was then dried using $MgSO_4$ and the solvent removed *in vacuo* to afford **133** as a yellow oil which was used without further purification. ^{19}F NMR (282.3 MHz, $CDCl_3$) δ 31.2 (1F, t, $^3J_{H,F}$ 4.3 Hz, acyl-F).

Preparation of *tert*-Butyl {[3-(6-methylpyridin-2-ylcarbamoyl)phenylcarbamoyl]methyl} carbamate 135

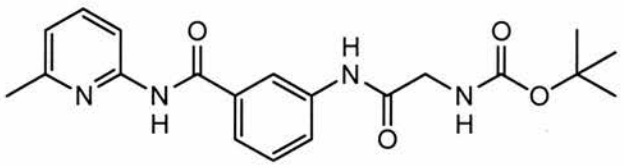

123 (0.25 g, 1.1 mmol) was added to **134** (0.70 g, 4.0 mmol) in dichloromethane (50 mL) and stirred overnight under nitrogen. The solvent was removed *in vacuo* to give a yellow oil which was purified *via* recrystallisation from methanol to afford **135** as a colourless solid. Mp 94-96 °C (0.16 g, 38%). ^{1}H NMR (300.1 MHz, $CDCl_3$) δ 8.62 (1H, bs, NH), 8.32 (1H, bs, NH), 8.11 (1H, d, $^{3}J_{H,H}$ 8.2 Hz, Ar-H), 8.10 (1H, t, $^{4}J_{H,H}$ 1.8 Hz, Ar-H), 7.89-7.84 (1H, m, Ar-H), 7.74-7.68 (2H, m, 2 x Ar-H), 7.39 (1H, dd, $^{3}J_{H,H}$ 8.2 Hz, $^{3}J_{H,H}$ 8.2 Hz, Ar-H), 6.88 (1H, d, $^{3}J_{H,H}$ 8.2 Hz, Ar-H), 3.90 (2H, d, $^{3}J_{H,H}$ 6.1 Hz, CH_2), 2.42 (3H, s, CH_3), 1.42 (9H, s, CH_3). ^{13}C NMR (75 MHz, $CDCl_3$) δ 172.8 (C=O), 169.2 (C=O), 160.2 (C=O), 157.1 (quat, Ar), 152.4 (quat, Ar), 144.6 (quat, Ar), 139.0 (CH, Ar), 136.1 (quat, Ar), 130.2 (CH, Ar), 119.8 (CH, Ar), 118.7 (CH, Ar), 117.4 (CH, Ar), 113.9 (CH, Ar), 111.4 (CH, Ar), 79.5 (quat), 40.3 (CH_2), 28.4 (3 x CH_3) and 24.2 (CH_3). CIMS *m/z* 385 ([M^++H], 100%), 329 (36%), 311 (40%), 285 (71%), 109 (62%), 71 (65%).

Preparation of 3-(2-Chloroacetylamino)-*N*-(6-methylpyridin-2-yl) benzamide 137

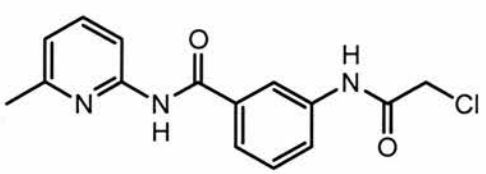

123 (3.30 g, 14.5 mmol) and triethylamine (2 mL, 14.5 mmol) were dissolved in dry DCM (2 mL) before chloroacetyl chloride **125** (1.2 mL, 14.5 mmol) was added dropwise under a positive pressure of nitrogen. The reaction mixture was then stirred overnight before it was diluted with DCM (100 mL) and washed with water (2 x 50 mL) and sodium bicarbonate solution (50 mL). The organic layer was then dried using $MgSO_4$ and the solvent removed *in vacuo*. The product was purified through recrystallisation using hexane/DCM to afford **137** as a colourless solid. Mp 137-139 °C (3.30 g, 75%). ^{1}H NMR (300.1 MHz, $CDCl_3$) δ 8.67 (1H, bs, NH), 8.40 (1H, bs, NH), 8.20-8.17 (1H, m, Ar-H), 8.03 (1H, t, $^{4}J_{H,H}$ 1.9 Hz, Ar-H),

7.95-7.90 (1H, m, Ar-H), 7.75-7.71 (1H, m, Ar-H), 7.70-7.65 (1H, m, Ar-H), 7.50 (1H, dd, $^{3}J_{H,H}$ 7.8 Hz, $^{3}J_{H,H}$ 7.8 Hz, Ar-H), 6.95 (1H, d, $^{3}J_{H,H}$ 7.8 Hz, Ar-H), 4.23 (2H, s, CH_2) and 2.49 (3H, s, CH_3). ^{13}C NMR (75.5 MHz, $CDCl_3$) δ 165.5 (C=O), 164.6 (C=O), 157.3 (quat, Ar), 151.0 (quat, Ar), 139.3 (CH, Ar), 137.8 (quat, Ar), 135.7 (quat, Ar), 130.1 (CH, Ar), 124.0 (CH, Ar), 123.9 (CH, Ar), 120.0 (CH, Ar), 119.3 (CH, Ar), 111.5 (CH, Ar), 43.3 (CH_2) and 24.3 (CH_3). IR (KBr, cm^{-1}) 3385, 3311, 2885, 1674, 1558 and 1456. ESMS *m/z* 304 ([M^+ ^{37}Cl], 36%), 302 ([M^+ ^{35}Cl], 100%), 282 (29%), 266 (6%), 252 (6%) and 212 (10%).

Preparation of 3-(2-Azidoacetylamino)-*N*-(6-methylpyridin-2yl) benzamide 138

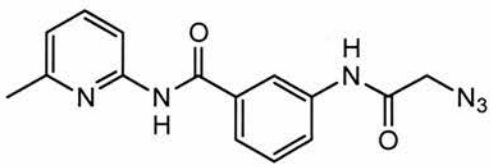

137 (3.00 g, 9.90 mmol) and sodium azide (2.57 g, 39.5 mmol) were dissolved in acetone (60 mL) and heated under reflux for 24 hours before the solution was filtered and the solvent removed *in vacuo*. The crude product was then redissolved in DCM (50 mL) and washed with water (3 x 50 mL). The organic layer was then dried using $MgSO_4$ and the solvent removed *in vacuo* to afford **138** as a colourless solid. Mp 123 – 125 °C (2.02 g, 66%). ^{1}H NMR (300.1 MHz, $CDCl_3$) δ 8.66 (1H, bs, NH), 8.31 (1H, bs, NH), 8.14 (1H, d, $^{3}J_{H,H}$ 7.9 Hz, Ar-H), 8.02 (1H, t, $^{4}J_{H,H}$ 1.9 Hz, Ar-H), 7.90-7.86 (1H, m, Ar-H), 7.70-7.61 (1H, m, Ar-H), 7.45 (2H, m, 2 x Ar-H), 6.92 (1H, d, $^{3}J_{H,H}$ 7.9 Hz, Ar-H), 4.16 (2H, s, CH_2) and 2.62 (3H, s, CH_3). ^{13}C NMR (75.5 MHz, $CDCl_3$) δ 165.4 (C=O), 165.2 (C=O), 157.3 (quat, Ar), 151.0 (quat, Ar), 139.2 (CH, Ar), 137.8 (quat, Ar), 135.7 (quat, Ar), 130.1 (CH, Ar), 123.9 (CH, Ar), 123.7 (CH, Ar), 120.0 (CH, Ar), 119.2 (CH, Ar), 111.4 (CH, Ar), 53.3 (CH_2) and 24.4 (CH_3). IR (thin film, cm^{-1}) 2105, 1701, 1664, 1564, 1455 and 1227. ESMS *m/z* 309 ([M^+-H], 100%), 252 (6%) and 226 (22%). HRMS (ES, *m/z*) calcd for $C_{15}H_{13}N_6O_2$ 309.1100, found 309.1095.

Preparation of [3-(6-Methylpyridin-2-ylcarbamoyl) phenyl carbamoyl] methyl ammonium chloride 139

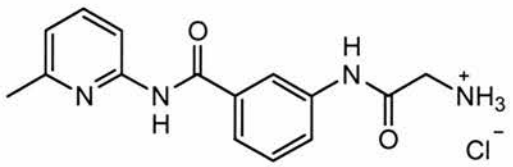

138 (1.50 g, 4.80 mmol) was dissolved in dry THF (30 mL) and water (0.1 mL, 5.81 mmol) before triphenylphosphine (1.27 g, 4.80 mmol) was added portionwise and stirred overnight. The solvent was then removed *in vacuo* and the pale yellow oil was redissolved in ethanol (5 mL). Hydrochloric acid was added dropwise to precipitate the hydrochloride salt. This was left overnight before crude **139** was filtered and reacted through to the next step without further purification. (1.55 g, quant.)

Preparation of 3-[2-(3-Methylbutyrylamino) acetylamino]-*N*-(6-methylpyridin-2-yl) benzamide 122

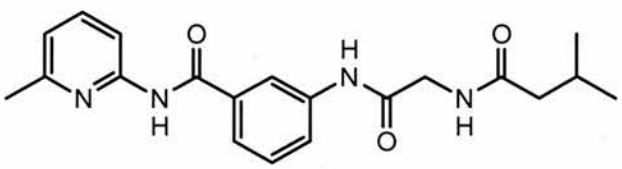

Crude [3-(6-Methylpyridin-2-ylcarbamoyl) phenylcarbamoyl] methyl ammonium chloride **139** (3.38 g) and triethylamine (3.20 mL, 23.2 mmol) were dissolved in DCM (5 mL) then isovaleryl chloride (1.30 mL, 10.6 mmol) in DCM (1 mL) was added dropwise under a positive pressure of nitrogen and the reaction mixture left to stir overnight. The solution was then diluted with DCM (30 mL) and washed with brine (3 x 30 mL) before the organic layer was dried using $MgSO_4$ and the solvent removed *in vacuo*. The product was purified through recrystallisation from 5:1 DCM:hexane to afford **122** as a colourless solid. Mp 161 – 163 °C (1.15 g, 57%). ^{1}H NMR (300.1 MHz, $CDCl_3$) δ 9.26 (1H, bs, NH), 8.67 (1H, bs, NH), 8.14 (1H, d, $^3J_{H,H}$ 7.9 Hz, Ar-H), 8.04 (1H, t, $^4J_{H,H}$ 1.8 Hz, Ar-H), 7.85-7.80 (1H, m, Ar-H), 7.66-7.61 (2H, m, 2 x Ar-H), 7.41 (1H, dd, $^3J_{H,H}$ 7.9 Hz, $^3J_{H,H}$ 7.9 Hz, Ar-H), 6.92 (1H, d, $^3J_{H,H}$ 7.9 Hz, Ar-H), 6.73 (1H, bt, $^3J_{H,H}$ 5.1 Hz, NH), 4.20 (1H, d, $^3J_{H,H}$ 5.1, CH_2), 2.46 (3H, s, CH_3), 2.22-2.15 (3H, m, CH_2, CH), 0.98 (3H, s, CH_3) and 0.96 (3H, s, CH_3). ^{13}C NMR (75.5 MHz, $CDCl_3$) δ 174.0 (C=O), 167.6 (C=O), 165.3 (C=O), 156.8 (quat, Ar), 150.6 (quat, Ar), 138.8

(CH, Ar), 138.4 (quat, Ar), 135.2 (quat, Ar), 129.5 (CH, Ar), 123.4 (CH, Ar), 122.8 (CH, Ar), 119.5 (CH, Ar), 118.5 (CH, Ar), 111.0 (CH, Ar), 45.6 (CH_2), 44.7 (CH_2), 26.2 (CH), 23.9 (CH_3) and 22.4 (2 x CH_3). IR (KBr, cm^{-1}) 3285, 2958, 1680, 1643 and 1549. ESMS *m/z* 367 ([M^+-H], 100%) and 212 (3%). Anal. Calcd for $C_{20}H_{24}N_4O_3$: C, 65.20; H, 6.57; N, 15.21. Found: C, 64.82; H, 6.54; N, 15.21.

Preparation of Benzyl Azide 145

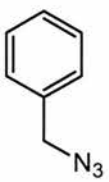

Benzyl chloride **144** (1.82 mL, 15.8 mmol) was dissolved in acetone (80 mL) before sodium azide (3.08 g, 47.4 mmol) was added and the reaction mixture was heated to reflux for 48 hours. The solution was then allowed to cool before it was filtered and the solvent removed *in vacuo* to afford **145** as a pale yellow oil (1.98 g, 94%). ^{1}H NMR (300.1 MHz, $CDCl_3$) δ 7.44 – 7.29 (5H, m, Ar-H) and 4.35 (2H, s, CH_2). ^{13}C NMR (75.5 MHz, $CDCl_3$) δ 135.8 (quat, Ar), 128.9 (2 x CH, Ar), 128.3 (CH, Ar), 128.2 (2 x CH, Ar) and 54.8 (CH_2). IR (KBr, cm^{-1}) 3033, 2097, 1496, 1455, 1256, 877 and 669. CIMS *m/z* 133 (M^+, 3 %), 91 ([M^+-N_3], 100 %). HRMS (CI^+, *m/z*) Calcd for $C_7H_7N_3$, 133.0640, found 133.0643.

Preparation of *exo*- and *endo*- 3-(3,5-Dioxo-10-oxa-4-azatricyclo[5.2.1.$0^{2,6}$]dec-8-en-yl)propionic acid 146

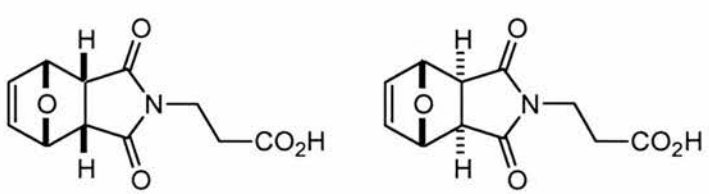

Furan **142** (0.43 mL, 5.92 mmol) and **45** (1.00 g, 5.92 mmol) were dissolved in chloroform (10 mL) and stirred at 35 °C for two weeks. The solvent was then removed *in vacuo* to give a pale yellow oil which was purified by recrystallisation from v/v 5:1 hexane:DCM to afford only the *exo* isomer of **146** as a colourless solid. Mp 132-134 °C (1.04 g, 74%) ^{1}H NMR (300.1 MHz, d_4-MeOD) δ 6.50-6.49 (2H, m, 2 x CH alkene), 5.11-5.10 (2H, m, 2 x CH bridgehead), 3.75-3.62 (2H, m, CH_2), 2.88-2.86 (2H, m, 2 x CH) and 2.59-2.44 (2H, m, CH_2).

^{13}C NMR (75.5 MHz, d_4-MeOD) δ 178.2 (C=O),174.3 (C=O), 172.2 (C=O), 137.6 (2 x CH, alkene), 82.3 (2 x CH), 42.9 (2 x CH), 35.5 (CH_2) and 32.6 (CH_2). ESMS *m/z* 236 ([M^+-H], 100%) and 164 (58%). HRMS (ES^-, *m/z*) calcd for $C_{11}H_{10}NO_5$ 236.0562, found 236.0559.

Preparation of 3-(1-Benzyl-4,6-dioxo-3a, 4, 6, 6a-tetrahydro-1*H*-pyrrolo[3,4-*d*][1,2,3]triazol-5-yl)propionic acid 147

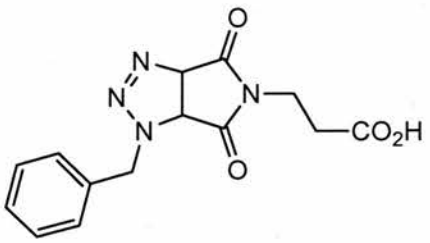

Benzyl azide **145** (15.2 mg, 0.1 mmol) and **45** (16.9 mg, 0.1 mmol) were dissolved in $CDCl_3$ (1 mL) and warmed on a water bath to 50 °C for two weeks. The solution was filtered and the fitrate concentrated *in vacuo* to afford **147** as a colourless oil. ^{1}H NMR (300.1 MHz, $CDCl_3$) δ 7.43-7.29 (5H, m, Ar-H), 5.43 (1H, d, $^3J_{H,H}$ 10.9 Hz, CH), 4.34 (2H, s, CH_2), 4.10 (1H, d, $^3J_{H,H}$ 10.9 Hz, CH), 3.59-3.55 (2H, m, CH_2) and 2.70-2.62 (2H, m, CH_2). ^{13}C NMR (75.5 MHz, $CDCl_3$) δ 174.1 (C=O), 170.9 (C=O), 166.2 (C=O), 134.5 (quat, Ar), 127.8 (2 x CH, Ar). 127.2 (2 x CH, Ar), 126.7 (CH, Ar), 84.5 (CH), 55.3 (CH), 53.8 (CH_2), 47.4 (CH_2) and 32.1 (CH_2). ESMS *m/z* 325 ([M^++Na], 100%).

Preparation of 3-(3-Benzylsulfanyl-2,5-dioxopyrrolidin-1-yl)propionic acid 148

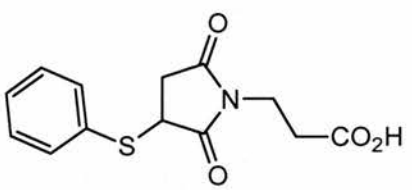

Thiophenol **143** (0.61 mL, 5.92 mmol), *t*-butylpyridine (0.44 mL, 2.96 mmol) and **45** (1.00 g, 5.92 mmol) were dissolved in chloroform (10 mL) and stirred at room temperature for one week. The solvent was then removed *in vacuo* to give an orange oil which was purified by recrystallisation from v/v 5:1 hexane:DCM to afford 3-(3-benzylsulfanyl-2,5-dioxopyrrolidin-1-yl)propionic acid as a pale yellow solid. Mp 143-145 °C (1.02 g, 62%) ^{1}H NMR (300.1 MHz, DMSO-d_6) 12.42 (1H, bs, OH), 7.49-7.34 (5H, m, Ar), 4.38 (1H, dd, $^3J_{H,H}$ 9.1 Hz, $^4J_{H,H}$ 4.0 Hz, CH), 3.50 (2H, t, $^3J_{H,H}$ 7.6 Hz, CH_2), 3.23 (1H, dd, $^3J_{H,H}$ 18.4 Hz, $^4J_{H,H}$ 9.1 Hz, CH),

2.59 (1H, dd, $^{3}J_{H,H}$ 18.4 Hz, $^{4}J_{H,H}$ 4.0 Hz, CH) and 2.32 (2H, $^{3}J_{H,H}$ 7.6 Hz, CH_2). ^{13}C NMR (75.5 MHz, DMSO-d_6) 175.8 (C=O), 174.9 (C=O), 172.2 (C=O), 132.9 (2 x CH, Ar), 131.8 (quat, Ar), 129.7 (2 x CH, Ar), 128.7 (CH, Ar), 43.4 (CH), 36.2 (CH_2), 34.6 (CH_2) and 31.7 (CH_2). IR (KBr, cm^{-1}) 2863, 1769, 1707, 1440, 1400, 1227, 1167, 750 and 699. ESMS *m/z* 278 ([M^+- H], 11%), 168 (100%) and 109 (14%). HRMS (ES^-, *m/z*) calcd for $C_{13}H_{12}NO_4S$ 278.0487, found 278.0483.

Preparation of 3-Furan-3-yl propionic acid 165

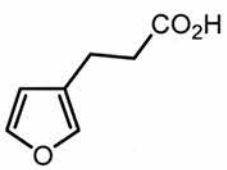

Trans-3-furanacrylic acid **164** (4.00 g, 29.0 mmol) and 10% palladium on carbon (384 mg) were flushed with nitrogen for 10 minutes before methanol (40 mL) was added carefully. The flask was flushed with hydrogen gas and a hydrogen balloon fitted. The reaction mixture was stirred at room temperature for 5 hours before it was filtered through a pad of celite, dried using $MgSO_4$ and the solvent removed *in vacuo* to afford the crude product as a brown oil. The product was purified by Kugelrohr distillation to afford a colourless solid which was further purified by recrystallisation from hexane to afford **165** as a colourless solid. Mp 65-67 °C (lit.[225] 66-67 °C) (1.19 g, 29%). ^{1}H NMR (300.1 MHz, $CDCl_3$) δ 10.34 (1H, bs, OH), 7.37-1.36 (1H, m, furan-H), 7.28-7.26 (1H, m, furan-H), 6.30-6.29 (1H, m, furan-H), 2.78 (2H, t, $^{3}J_{H,H}$ 7.4 Hz, CH_2) and 2.63 (2H, t, $^{3}J_{H,H}$ 7.4 Hz, CH_2). ^{13}C NMR (75.5 MHz, $CDCl_3$) δ 179.4 (C=O), 143.4 (CH, furan), 139.5 (CH, furan), 123.6 (quat, furan), 111.1 (CH, furan), 34.9 (CH_2) and 20.4 (CH_2). IR (KBr, cm^{-1}) 2936, 1699, 1501, 1410, 1214 and 1016. CIMS *m/z* 141 ([M^++H], 19%), 140 (M^+, 22%), 123 ([M^++H-OH], 100%), 95 (36%) and 81 (23%). HRMS (CI^+, *m/z*) calcd for $C_7H_8O_3$ 140.0473, found 140.0470.

Preparation of 3-Furan-3-yl propionyl fluoride 166

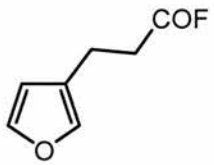

165 (1.00 g, 7.10 mmol) and pyridine (0.57 mL, 7.10 mmol) were dissolved in dry acetonitrile (15 mL) under a positive pressure of nitrogen and cooled on an ice bath before cyanuric fluoride (0.36 mL, 4.30 mmol) was added. The reaction mixture was stirred for 2 hours at 0°C before it was diluted with DCM (20 mL) and washed with brine (20 mL). The organic layer was then dried using $MgSO_4$ and the solvent removed *in vacuo* to afford **166** as a yellow oil which was used without further purification. ^{19}F NMR (282.3 MHz, $CDCl_3$) δ 44.8 (1F, s, acyl-F).

Preparation of 3-Furan-3-yl-*N*-(6-methyl pyridine-2-yl) propionamide 160

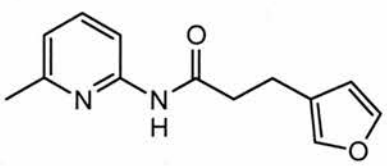

126 (0.76 g, 7.00 mmol) was added to a solution of 3-furan-3-yl propionyl fluoride **166** (1.00 g, 7.00 mmol) in dry DCM (5 mL) under a positive pressure of nitrogen. The reaction mixture was stirred overnight before the solvent was removed *in vacuo* to afford the crude product. The product was then purified *via* flash column chromatography (SiO_2; v/v 1:1 DCM:diethyl ether) to afford **160** as a colourless solid. Mp 48-50 °C (0.87 g, 54%). ^1H NMR (300.1 MHz, $CDCl_3$) δ 8.06 (1H, bs, NH), 8.0 (1H, d, $^3J_{H,H}$ 7.9 Hz, Ar-H), 7.58 (1H, dd, $^3J_{H,H}$ 7.9 Hz, $^3J_{H,H}$ 7.9 Hz, Ar-H), 7.34-7.25 (2H, m, Furan-H), 6.88 (1H, d, $^3J_{H,H}$ 7.9 Hz, Ar-H), 6.28-6.29 (1H, m, Furan-H), 2.85 (2H, t, $^3J_{H,H}$ 7.4 Hz, CH_2), 2.60 (2H, t, $^3J_{H,H}$ 7.4 Hz, CH_2) and 2.43 (3H, s, CH_3). ^{13}C NMR (75.5 MHz, $CDCl_3$) δ 171.1 (C=O), 157.0 (quat, Ar), 151.0 (quat, Ar), 143.4 (CH, Ar), 139.5 (CH, Ar), 139.3 (CH, Ar), 123.8 (quat, Ar), 119.7 (CH, Ar), 111.4 (CH, Ar), 111.2 (CH, Ar), 38.4 (CH_2), 24.2 (CH_2) and 20.8 (CH_3). CIMS *m/z* 231 ([M^++H], 100%). HRMS (CI^+, *m/z*) calcd for $C_{13}H_{15}N_2O_2$ 231.1134, found 231.1136.

Preparation of 3-(2,5-Dioxo-2,5-dihydropyrrol-1-yl) propionyl fluoride 167

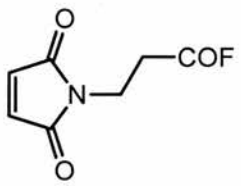

45 (5.00 g, 29.6 mmol) and pyridine (2.39 mL, 29.6 mmol) were dissolved in dry acetonitrile (80 mL) under a positive pressure of nitrogen and cooled on an ice bath before cyanuric fluoride (1.50 mL, 17.8 mmol) was added. The reaction mixture was stirred for 6 minutes at 0°C then stirred for a further 6 minutes at room temperature. The solution was then diluted with DCM (80 mL) and washed with brine (100 mL). The organic layer was then dried using $MgSO_4$ and the solvent removed *in vacuo* to afford **167** as a yellow oil which was used without further purification. ^{19}F NMR (282.3 MHz, $CDCl_3$) δ 49.4 (1F, s, acyl-F).

Preparation of 3-(2,5-Dioxo-2,5-dihydropyrrol-1-yl)-*N*-(6-methyl pyridine-2-yl) propionamide 161

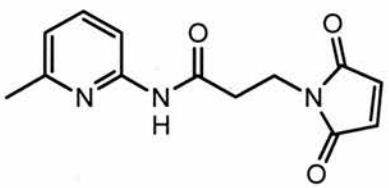

126 (3.16 g, 29.2 mmol) was added to a solution of 3-(2,5-Dioxo-2,5-dihydropyrrol-1-yl) propionyl fluoride **167** (5.00 g, 29.2 mmol) in dry DCM (5 mL) under a positive pressure of nitrogen. The reaction mixture was stirred overnight before the solvent was removed *in vacuo* to afford the crude product. The product was then purified *via* flash column chromatography (SiO_2; v/v 1:1 DCM:diethyl ether) to afford **161** as a colourless solid. Mp 166-168 °C (3.67 g, 48%). ^1H NMR (300.1 MHz, $CDCl_3$) δ 8.13 (1H, bs, NH), 7.96 (1H, d, $^3J_{H,H}$ 8.0 Hz, $^3J_{H,H}$ 8.0 Hz, Ar-H), 5.86 (1H, dd, $^3J_{H,H}$ 8.0 Hz, Ar-H), 6.89 (1H, $^3J_{H,H}$ 8.0 Hz, Ar-H), 6.71 (2H, s, C=C), 3.93 (2H, t, $^3J_{H,H}$ 7.1 Hz, CH_2), 2.73 (2H, t, $^3J_{H,H}$ 7.1 Hz, CH_2) and 2.43 (3H, s, CH_3). ^{13}C NMR (75.5 MHz, $CDCl_3$) δ170.9 (2 x C=O), 168.7 (C=O), 157.1 (quat, Ar), 150.7 (quat, Ar), 139.2 (CH, Ar), 134.6 (2 x CH, ring), 119.8 (CH, Ar), 111.4 (CH, Ar), 35.9 (CH_2), 34.2 (CH_2) and 24.3 (CH_3). IR (KBr, cm^{-1}) 3313, 1765, 1701, 1454, 1297 and 849. CIMS *m/z* 260

([M^++H], 100%). HRMS (CI^+, *m/z*) calcd for $C_{13}H_{14}N_3O_3$ 260.1035, found 260.1029. Anal. Calcd. for $C_{13}H_{13}N_3O_3$: C, 60.22; H, 5.05; N, 16.21. Found: C, 59.83; H, 5.34; N, 16.24.

Preparation of *exo*- 162 and *endo*- 163 *N*-(6-Methyl pyridine-2-yl)-3-{8-[2-(6-methyl pyridine-2-ylcarbamoyl)ethyl]-3,5-dioxo-10-oxa-4-azatricyclo[5.2.1.$0^{2,6}$]dec-8-en-4-yl}propionamide

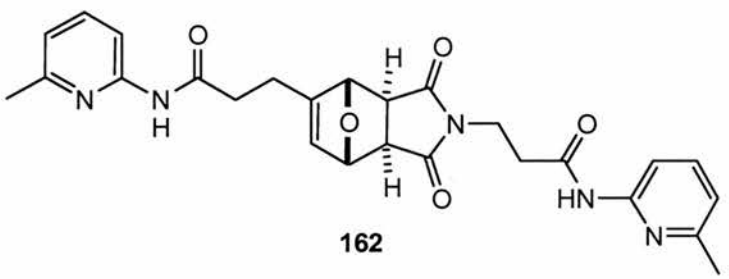

162

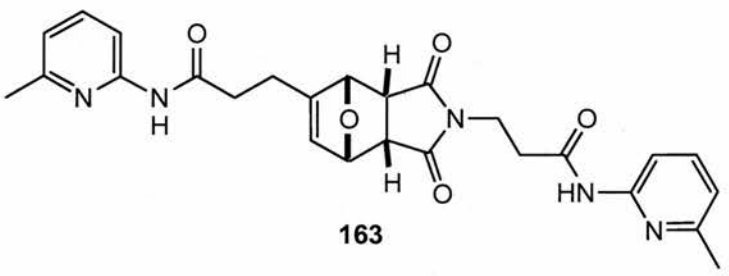

163

160 (173 mg, 0.8 mmol) and **161** (194 mg, 0.8 mmol) were dissolved in $CDCl_3$ (9 mL) and stirred at room temperature for two weeks before the solvent was removed *in vacuo* to give a pale yellow oil. The products were purified *via* column chromatography (SiO_2; v/v 2:1 ethyl acetate:hexane to afford **162** and **163** as colourless oils. (**162**: 140 mg, 36%; **163**: 90 mg, 23%) **162** ^{1}H NMR (300.1 MHz, $CDCl_3$) δ 8.2 (1H, bs, NH), 8.1 (1H, bs, NH), 7.95 (2H, d, $^3J_{H,H}$ 8.2 Hz, Ar-H), 7.62-7.55 (2H, m, Ar-H), 6.92-6.87 (2H, m, Ar-H), 6.06-6.04 (1H, m, CH), 5.20-5.18 (1H, m, CH), 5.07 (1H, s, CH), 3.87 (2H, t, $^3J_{H,H}$ 7.2 Hz, CH_2), 2.97 (1H, d, $^3J_{H,H}$ 6.5 Hz, CH), 2.87 (1H, d, $^3J_{H,H}$ 6.5 Hz, CH), 2.67-2.58 (6H, m, 3 x CH_2), 2.45 (3H, s, CH_3) and 2.43 (3H, s, CH_3). **163** ^{1}H NMR (300.1 MHz, $CDCl_3$) δ 8.76 (1H, bs, NH), 8.43 (1H, bs, NH), 8.08-7.96 (2H, m, Ar-H), 7.61-7.55 (2H, m, Ar-H), 6.91-6.87 (2H, m, Ar-H), 6.01-5.97 (1H, m, CH), 5.27-5.23 (1H, m, CH), 5.13-5.09 (1H, m, CH), 3.87-3.65 (2H, m, CH_2), 3.56 (2H, m, 2 x CH), 2.95-2.88 (6H, m, 3 x, CH_2), 2.45 (3H, s, CH_3), 2.43 (3H, s, CH_3). **162** ^{13}C NMR (75.5 MHz, $CDCl_3$) δ 176.2 (C=O), 176.1 (C=O), 169.8 (C=O), 168.7 (C=O), 156.8 (quat, Ar), 156.7 (quat, Ar), 150.5 (quat, Ar), 150.4 (quat, Ar), 138.9 (CH, Ar), 138.7 (CH, Ar), 129.0 (CH, Ar), 119.4 (CH, Ar), 119.3 (CH, Ar), 111.1 (CH, Ar), 111.0 (CH, Ar), 83.2 (CH, bridgehead), 81.8 (CH, bridgehead), 77.3 (quat, alkene), 49.0 (CH), 47.0 (CH),

35.0 (CH_2), 34.9 (CH_2), 34.5 (CH_2), 23.9 (2 x CH_3) and 22.4 (CH_2). **163** ^{13}C NMR (75.5 MHz, $CDCl_3$) 174.7 (C=O), 174.4 (C=O), 170.1 (C=O), 168.4 (C=O), 156.7 (quat, Ar), 150.5 (quat, Ar), 150.3 (quat, Ar), 149.4 (quat, Ar), 138.9 (CH, Ar), 138.7 (CH, Ar), 126.6 (CH, alkene), 119.5 (CH, Ar), 119.3 (CH, Ar), 111.1 (CH, Ar), 111.0 (CH, Ar), 82.0 (CH, bridgehead), 80.3 (CH, bridgehead), 77.2 (quat, alkene), 47.3 (CH), 46.1 (CH), 35.2 (CH_2), 34.9 (CH_2), 34.5 (CH_2), 34.4 (CH_2), 24.0 (CH_3) and 23.9 (CH_3). IR (KBr, cm^{-1}) 3263, 1701, 1538, 1456, 1138, 769 and 725. ESMS *m/z* 488 ([M^+- H], 100%). HRMS (ES^-, *m/z*) calcd for $C_{26}H_{26}N_5O_5$ 488.1934, found 488.1938.

Preparation of 4-*tert*-Butylbenzyl ester-2,2,2-trichloroacetimidate 169

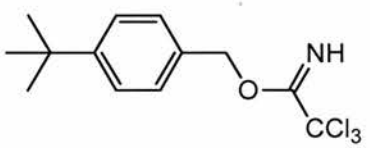

4-*t*-Butylbenzylalcohol **168** (4.68 mL, 26.4 mmol) was dissolved in dry DCM (40 mL) under a positive pressure of nitrogen and cooled on an ice/salt bath before *t*-n-butyl ammonium hydrogen sulfate (0.12 g, 0.40 mmol) and 50% KOH (aq) solution (40 mL) were added. The solution was then stirred at -15 °C for 15 minutes before trichloroacetonitrile (3.17 mL, 31.5 mmol) was added dropwise. The solution was stirred at this temperature for 30 minutes before it was slowly warmed to room temperature and stirred for a further 30 minutes. The organic layer was separated and the aqueous layer extracted with DCM (2 x 30 mL). The combined organic layers were dried using $MgSO_4$ and solvent removed *in vacuo*. The product was then purified by vacuum filtration through a short pad of silica gel using v/v 2.5:1 hexane:ethyl acetate as eluent to afford **169** as a colourless oil (7.29 g, 90%). ^1H NMR (300.1 MHz, $CDCl_3$) δ 8.38 (1H, bs, NH), 7.44-7.34 (4H, m, Ar-H), 5.31 (2H, s, CH_2) and 1.33 (9H, s, 3 x CH_3). ^{13}C NMR (300.1 MHz, $CDCl_3$) δ 163.1 (C=NH), 151.7 (quat, Ar), 132.9 (quat, Ar), 128.0 (2 x CH, Ar), 125.9 (2 x CH, Ar), 91.9 (CCl_3), 71.1 (CH_2), 35.1 (quat, t-Bu) and 31.8 (3 x CH_3). IR (thin film, cm^{-1}) 3344, 2964, 2905, 1665, 1518 and 1079. ESMS *m/z* 307 ([M^+ 3 x ^{35}Cl], 96%), 309 ([M^+ 2 x ^{35}Cl 1 x ^{37}Cl], 100%), 311 ([M^+ 2 x ^{37}Cl 1x ^{35}Cl], 33%) and 313 ([M^+ 3 x ^{37}Cl], 4%). HRMS (ES^+, *m/z*) calcd for $C_{13}H_{16}NO^{35}Cl_3$ 307.0297, found 307.0304.

Preparation of Diethyl-3-(4-*tert*-butyl benzyloxy) pentandioate 170

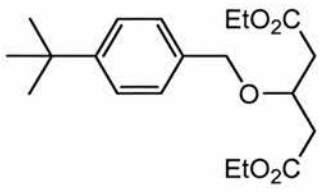

Diethyl-3-hydroxyglutarate (1.39 mL, 11.2 mmol) was added to a solution of **169** (6.90 g, 22.5 mmol) dissolved in cyclohexane (22 mL) under a positive pressure of nitrogen. $BF_3{\cdot}Et_2O$ (0.22 mL, 1.80 mmol) was added to form a colourless precipitate before DCM (11 mL) was added and the solution stirred overnight. Sodium bicarbonate (approx. 0.5 g) was added before the solution was filtered and the solvent removed *in vacuo*. The product was then purified *via* column chromatography (SiO_2; v/v 15:1 hexane:ethyl acetate) to afford **170** as a colourless oil (3.91 g, 98%). ^{1}H NMR (300.1 MHz, $CDCl_3$) δ 7.36-7.33 (2H, m, Ar-H), 7.25-7.22 (2H, m, Ar-H), 4.56 (2H, s, CH_2), 4.38-4.29 (1H, m, CH), 4.14 (4H, q, $^3J_{H,H}$ 7.1 Hz, 2 x CH_2, ethyl), 2.71-2.56 (4H, m, 2 x CH_2), 1.30 (9H, s, 3 x CH_3) and 1.25 (6H, t, $^3J_{H,H}$ 7.1 Hz, 2 x CH_3). ^{13}C NMR (300.1 MHz, $CDCl_3$) δ 171.4 (2 x C=O), 151.1 (quat, Ar), 135.4 (quat, Ar), 128.1 (2 x CH, Ar), 125.7 (2 x CH, Ar), 73.4 (CH), 72.4 (CH_2), 61.0 (2 x CH_2), 40.2 (2 x CH_2), 34.9 (quat, *t*-Bu), 31.7 (3 x CH_3) and 14.6 (2 x CH_3). IR (thin film, cm^{-1}) 2965, 2871, 1736, 1515 and 1190. CIMS *m/z* 350 (M^+, 1%), 147 ([M^+-$C_9H_{15}O_5$, 100%). HRMS (CI^+, *m/z*) calcd for $C_{20}H_{30}O_5$ 350.2093, found 350.2092.

Preparation of 3-(4-*tert*-Butyl benzyloxy) pentanedioic acid 159

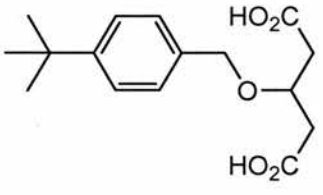

1M NaOH (aq) (6 mL) was added to a solution of diethyl-3-(4-*tert*-butyl benzyloxy) pentandioate **170** (250 mg, 0.70 mmol) in ethanol (6.25 mL) and the reaction mixture stirred overnight at room temperature. The reaction mixture was quenched by adjusting the pH to 1 using 1M HCl (aq). The organic layer was then extracted using ethyl acetate (2 x 10 mL), washed with brine (2 x 10 mL), dried using $MgSO_4$ and the solvent removed *in vacuo* to afford the crude product. The product was purified through recrystallisation in v/v 1:10

DCM:hexane to afford **159** as a colourless solid. Mp 104-106 °C (130 mg, 62%). ^{1}H NMR (300.1 MHz, $CDCl_3$) δ 10.24 (2H, bs, 2 x OH), 7.38-7.34 (2H, m, Ar-H), 7.26-7.24 (2H, m, Ar-H), 4.58 (2H, s, CH_2), 4.35-4.27 (1H, m, CH), 2.82-2.64 (4H, m, 2 x CH_2) and 1.30 (9H, s, 3 x CH_3). ^{13}C NMR (75.5 MHz, $CDCl_3$) δ 177.4 (2 x C=O), 151.4 (quat, Ar), 134.8 (quat, Ar), 128.2 (2 x CH, Ar), 125.8 (2 x CH, Ar), 72.4 (CH_2), 72.3 (CH), 34.8 (quat, *t*-Bu) 39.6 (2 x CH_2) and 31.7 (3 x CH_3). IR (thin film, cm^{-1}) 2953, 2345, 1706, 1515, 1406 and 1076. CIMS *m/z* 294 (M^+, 5%), 163 (22%) and 147 (100%). HRMS (CI^+, *m/z*) calcd for $C_{16}H_{22}O_5$ 294.1467, found 294.1473. Anal. Calcd. for $C_{16}H_{22}O_5$: C, 65.29; H, 7.53. Found: C, 65.58; H, 7.78.

Preparation of 3-Azidomethylbenzoic acid 173

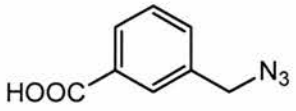

Sodium azide (2.29 g, 35.2 mmol) was added to a solution of 3-(chloromethyl)benzoic acid **199** (2.00 g, 11.7 mmol) dissolved in acetone (30 mL) and refluxed for 16 hours. The solution was then cooled and filtered before the solvent was removed *in vacuo* to afford a pale yellow oil. Analysis by 300 MHz ^{1}H NMR did not reveal the presence of any **173**.

Preparation of 3-Mercaptomethylbenzoic acid 174

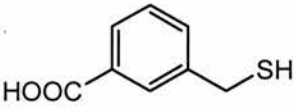

Thiourea (0.45 g, 5.9 mmol) was added to a solution of 3-(chloromethyl)benzoic acid **199** (1.00 g, 5.9 mmol) dissolved in acetone (20 mL) and heated to reflux for 2 hours. The solution was then allowed to cool at -18 °C for 18 hours before hexane was added to precipitate the thiouronium salt intermediate **201**. Thiouronium salt **201** was filtered under reduced pressure and used immediately. Sodium metabisulfite (2.23 g, 11.7 mmol) was added to a solution of **201** dissolved in water (10 mL) and heated to reflux for 10 minutes. The product was then extracted into DCM (10 mL) but unfortunately it was not possible to isolate **174** as a consequence of the insolubility of **201** and **174**.

Preparation of 1-Phenethyl-3-[3-(3-phenethyl ureidomethyl)benzyl] urea 176

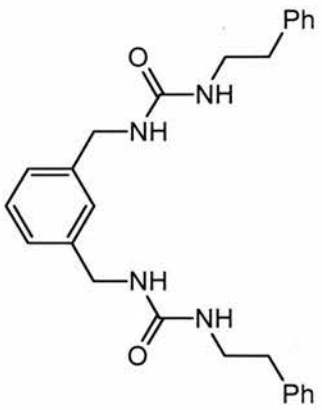

Phenethyl isocyanate (3.00 mL, 22.0 mmol) was added dropwise to a solution of *m*-xylylenediamine **196** (0.97 mL, 7.34 mmol) in dry DCM (15 mL) cooled on an ice bath. The solution was stirred overnight before the resulting precipitate was filtered and dried under vacuum to afford **176** as an insoluble colourless solid. Mp 187-189 °C (3.10 g, 98%) IR (KBr, cm^{-1}) 3328, 3026, 2935, 1623, 1243 and 1068. Anal. Calcd. for $C_{26}H_{30}N_4O_2$: C, 72.53; H, 7.02; N, 13.01. Found: C, 72.65; H, 7.26; N, 12.91.

Preparation of 1-Phenethyl-3-[3-(3-phenethyl thioureidomethyl)benzyl] thiourea 177

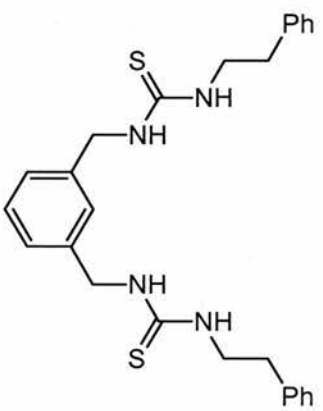

Phenethyl isothiocyanate (3.30 mL, 22.0 mmol) was added dropwise to a solution of **196** (0.97 mL, 7.34 mmol) in dry DCM (15 mL) cooled on an ice bath. The solution was stirred overnight before the resulting precipitate was filtered and dried under vacuum to afford **177** as a colourless solid. Mp 147-148 °C (3.27 g, 96%). ^{1}H NMR (300.1 MHz, $CDCl_3$) 7.67 (2H, bs, 2 x NH), 7.42 (2H, bs, 2 x NH), 7.33-6.97 (14H, m, Ar-H), 4.90 (4H, bs, CH_2), 3.05 (4H,

bs, CH_2) and 2.50 (4H, t, $^3J_{H,H}$ 6.9 Hz, CH_2). ^{13}C NMR (75.5 MHz, $CDCl_3$) 182.6 (2 x C=S), 138.9 (2 x quat, Ar), 138.3 (2 x quat, Ar), 128.8 (2 x CH, Ar), 128.6 (4 x CH, Ar), 128.5 (4 x CH, Ar), 126.5 (3 x CH, Ar), 126.3 (CH, Ar), 48.0 (2x CH_2), 45.8 (2 x CH_2) and 34.9 (2 x CH_2). IR (KBr, cm^{-1}) 3233, 3059, 1560, 1379 and 1349. ESMS *m/z* 461 ([M^+- H], 100%). Anal. Calcd. for $C_{26}H_{30}N_4S_2$: C, 67.49; H, 6.54; N, 12.11. Found, C, 67.46; H, 6.57; N, 12.17.

Preparation of (4-Methoxyphenyl acetyl) fluoride 179

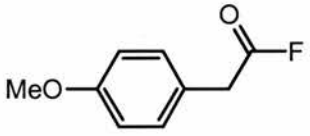

4-Methoxyphenylacetic acid **178** (2.00 g, 12.0 mmol) and pyridine (0.97 mL, 12.0 mmol) were dissolved in dry acetonitrile (40 mL) under a positive pressure of nitrogen and cooled on an ice bath before cyanuric fluoride (0.61 mL, 7.20 mmol) was added. The reaction mixture was stirred overnight then diluted with DCM (50 mL) and washed with brine (2 x 50 mL). The organic layer was then dried using $MgSO_4$ and the solvent removed *in vacuo* to afford **179** as a pale yellow oil which was used without further purification. ^{19}F NMR (282.3 MHz, $CDCl_3$) δ 43.6 (1F, t, $^3J_{H,F}$ 2.2 Hz, acyl-F).

Preparation of *N*-(6-Aminopyridin-2-yl)-2-(4-methoxyphenyl) acetamide 181

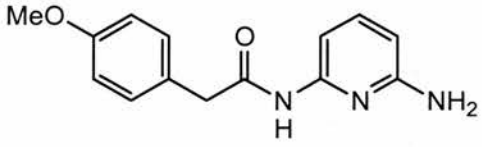

2,6-Diaminopyridine **180** (1.42 g, 13.0 mmol) was added to a solution of **179** (2.00 g, 13.0 mmol) in dry DCM (10 mL) under a positive pressure of nitrogen. The reaction mixture was stirred overnight before the solvent was removed *in vacuo* to afford the crude product. The product was then purified *via* flash column chromatography (SiO_2; v/v 5:1 DCM:diethyl ether) to afford **181** as a colourless solid. Mp 148-150 °C (1.19 g, 36%). ^1H NMR (300.1 MHz, $CDCl_3$) δ 7.51-7.57 (2H, m, NH, Ar-H), 7.4 (1H, dd, $^3J_{H,H}$ 7.9 Hz, $^3J_{H,H}$ 7.9 Hz, Ar-H), 7.25-7.20 (2H, m, Ar-H), 6.93-6.88 (2H, m, Ar-H), 6.23-6.20 (1H, m, Ar-H), 4.27 (2H, bs, NH_2), 3.81 (3H, s, CH_3) and 3.65 (2H, s, CH_2). ^{13}C NMR (75.5 MHz, $CDCl_3$) δ 169.6 (C=O), 159.1 (quat, Ar), 156.8 (quat, Ar), 149.4 (quat, Ar), 140.3 (CH, Ar), 130.6 (2 x CH, Ar), 126.0

(quat, Ar), 114.6 (2 x CH, Ar), 104.4 (CH, Ar), 103.1 (CH, Ar), 55.3 (OMe) and 44.1 (CH_2). IR (KBr, cm^{-1}) 3450, 3402, 2835, 1697, 1513 and 1070. CIMS *m/z* 258 ([M^++H], 100%) and 240 (6%). HRMS (CI^+, *m/z*) calcd for $C_{14}H_{16}N_3O_2$ 258.1243, found 258.1243.

Preparation of *N*-[6-(2-Chloroacetylamino) pyridine-2-yl]-2-(4-methoxyphenyl) acetamide 182

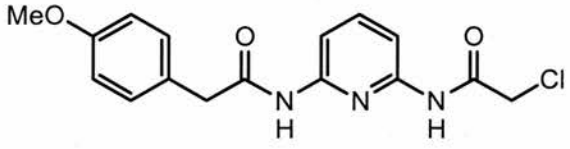

A solution of chloroacetyl chloride **125** (0.28 mL, 3.50 mmol) dissolved in dry DCM (20 mL) was added dropwise to **181** (0.91 g, 3.5 mmol) and *N,N*-diisopropylethyl amine (1.24 mL, 7.10 mmol) under a positive pressure of nitrogen. The solution was stirred overnight before it was diluted with DCM (20 mL) and washed with brine (20 mL). The organic layer was then dried using $MgSO_4$ and the solvent removed *in vacuo* to afford the crude product. The product was purified *via* column chromatography (SiO_2; v/v 12:1 DCM:diethyl ether) to afford **182** as a colourless solid. Mp 137-139 °C (0.76 g, 64%). ^{1}H NMR (300.1 MHz, $CDCl_3$) δ 8.51 (1H, bs, NH), 7.98 (1H, d, $^3J_{H,H}$ 8.1 Hz, Ar-H), 7.86 (1H, d, $^3J_{H,H}$ 8.1 Hz, Ar-H), 7.72 (1H, t, $^3J_{H,H}$ 8.1 Hz, Ar-H), 7.55 (1H, bs, NH), 7.27-7.23 (2H, m, Ar-H), 6.98-6.93 (2H, m, Ar-H), 4.16 (2H, s, CH_2), 3.84 (3H, s, CH_3) and 3.70 (2H, s, CH_2). ^{13}C NMR (75.5 MHz, $CDCl_3$) δ 170.2 (OMe), 164.6 (C=O), 159.6 (C=O), 149.8 (quat, Ar), 148.7 (quat, Ar), 141.4 (CH, Ar), 131.1 (2 x CH, Ar), 126.1 (quat, Ar), 115.2 (2 x CH, Ar), 110.6 (CH, Ar), 110.0 (CH, Ar), 55.8 (OMe), 44.5 (CH_2) and 43.1 (CH_2). IR (KBr, cm^{-1}) 3270, 3039, 2841, 1689, 1661, 1538 and 801. CIMS *m/z* 336 ([M^++H ^{37}Cl], 34%) and 334 ([M^++H ^{35}Cl], 100%). HRMS (CI^+, *m/z*) $C_{16}H_{17}N_3O_3{}^{35}Cl$ 334.0958, found 334.0959.

Preparation of 2-(4-*tert*-Butylphenoxy)-*N*-{6-[2-(4-methoxyphenyl) acetylamino] pyridine-2-yl} acetamide 175

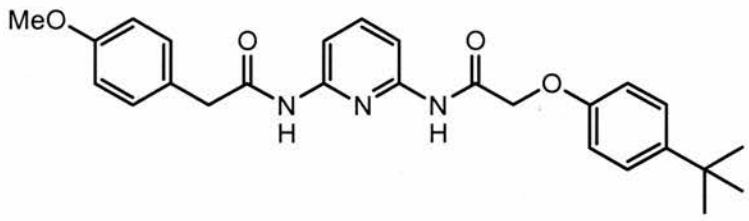

t-Butylphenol (0.23 g, 1.50 mmol) and potassium carbonate (1.24 g, 9.00 mmol) were dissolved in dried and degassed acetonitrile (10 mL) and the solution warmed to 80 °C for 20 minutes. A solution of **182** (0.5 g, 1.50 mmol) dissolved in dry acetonitrile (20 mL) was then added dropwise and the resulting mixture heated to reflux for 72 hours. The solution was then cooled and filtered before the solvent was removed *in vacuo* to afford the crude product. The product was purified *via* column chromatography (SiO_2; v/v 25:1 DCM:diethyl ether) to afford **175** as a colourless solid. Mp 131-133 °C (0.36 g, 54%) ^{1}H NMR (300.1 MHz, $CDCl_3$) δ 8.61 (1H, bs, NH), 7.98-7.94 (2H, m, Ar-H), 7.72 (1H, dd, $^3J_{H,H}$ 8.1 Hz, Ar-H), 7.59 (1H, bs, NH), 7.38-7.32 (2H, Ar-H), 7.27-7.23 (2H, m, Ar-H), 6.97-6.89 (4H, m, Ar-H), 4.57 (2H, s, CH_2), 3.83 (3H, s, CH_3), 3.69 (2H, s, CH_2) and 1.31 (9H, s, *t*-Bu). ^{13}C NMR (75.5 MHz, $CDCl_3$) δ 169.8 (C=O), 166.9 (C=O), 159.2 (quat, Ar), 154.2 (quat, Ar), 149.4 (quat, Ar), 148.5 (quat, Ar), 145.4 (quat, Ar), 140.9 (CH, Ar), 130.7 (2 x CH, Ar), 126.7 (2 x CH, Ar), 125.8 (quat, Ar), 114.7 (2 x CH, Ar), 114.4 (2 x CH, Ar), 110.0 (CH, Ar), 109.8 (CH, Ar), 67.8 (CH_2), 55.3 (OMe), 44.1 (CH_2), 34.2 (quat, *t*-Bu) and 31.5 (3 x CH_3, *t*-Bu). IR (KBr, cm^{-1}) 3403, 1707, 1586, 1513, 1451, 1243 and 805. CIMS *m/z* 448 ([M^++H], 100%) and 447 (M^+, 24%). HRMS (CI$^+$, *m/z*) calcd for $C_{28}H_{30}N_3O_4$ 448.2236, found 448.2244.

Preparation of Dimethyl-5-hydroxy isophthalate 185

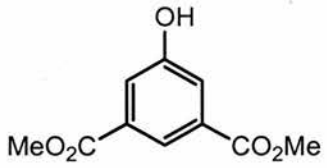

5-Hydroxyisophthalic acid **184** (10.00 g, 54.9 mmol) and concentrated sulfuric acid (6 mL) were dissolved in methanol (120 mL) and heated to reflux for 48 hours. The solution was cooled and poured into water (50 mL) and extracted into ethyl acetate (2 x 50 mL). The

combined organic layers were dried using $MgSO_4$ and the solvent removed *in vacuo* to afford **185** as a colourless solid. Mp 161-163 °C (lit.[226] 162-163.5 °C) (11.21 g, 97%). ^{1}H NMR (300.1 MHz, d_6-acetone) δ 9.17 (1H, bs, OH), 8.11 (1H, t, $^4J_{H,H}$ 1.5 Hz, Ar-H), 7.68 (2H, d, $^4J_{H,H}$ 1.5 Hz, Ar-H) and 3.91 (6H, s, 2 x CH_3). ^{13}C NMR (75.5 MHz, d_6-acetone) δ 166.8 (2 x C=O), 159.0 (quat, Ar), 133.3 (2 x quat, Ar), 122.5 (CH, Ar), 121.5 (2 x CH, Ar) and 53.0 (2 x CH_3). IR (KBr, cm^{-1}) 3361, 3013, 2963, 1704 and 1600. CIMS *m/z* 211 ([M^++H], 100%), 179 (15%), 167 (6%). HRMS (CI^+, *m/z*) calcd for $C_{10}H_{11}O_5$ 211.0606, found 211.0609. Anal. Calcd. for: $C_{10}H_{10}O_5$: C, 57.14; H, 4.80. Found: C, 56.93; H, 4.60.

Preparation of Dimethyl-5-benzyloxy isophthalate 186

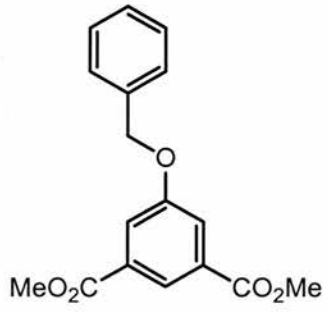

Potassium carbonate (13.16 g, 95.2 mmol) was added to a solution of **185** (5.00 g, 23.8 mmol) dissolved in acetone (100 mL) and heated to reflux for 1 hour before benzyl bromide (2.83 mL, 23.8 mmol) was added. The resulting solution was then refluxed overnight before it was filtered and the solvent removed *in vacuo* to afford **186** as a colourless solid. Mp 93-95 °C (lit.[227] 94-95 °C) (6.50 g, 91%). ^{1}H NMR (300.1 MHz, $CDCl_3$) δ 8.29 (1H, t, $^4J_{H,H}$ 1.4 Hz, Ar-H), 7.84 (2H, $^4J_{H,H}$ 1.4 Hz, Ar-H), 7.47-7.31 (5H, m, Ar-H), 5.14 (2H, s, CH_2) and 3.93 (6H, s, 2 x CH_3). ^{13}C NMR (75.5 MHz, $CDCl_3$) δ 166.5 (2 x C=O), 159.2 (quat, Ar), 136.5 (2 x quat, Ar), 132.2 (quat, Ar), 129.1 (2 x CH, Ar), 128.7 (CH, Ar), 128.0 (2 x CH, Ar), 123.6 (CH, Ar), 120.6 (2 x CH, Ar), 70.9 (CH_2) and 52.8 (2 x CH_3). IR (KBr, cm^{-1}) 3007, 2954, 1718, 1596 and 1080. CIMS *m/z* 301 ([M^++H], 100%) and 91 (46%). HRMS (CI^+, *m/z*) calcd for $C_{17}H_{17}O_5$ 301.1076, found 301.1072. Anal. Calcd. for $C_{17}H_{16}O_5$: C, 67.99; H, 5.37. Found: C, 68.27; H, 5.17.

Preparation of 3-(Benzyloxy-5-hydroxymethyl phenyl) methanol 187

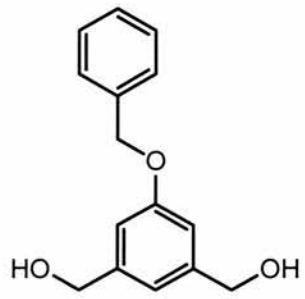

A solution of **186** (5.00 g, 16.7 mmol) in dry THF (40 mL) was added dropwise to a suspension of lithium aluminium hydride (1.27 g, 33.4 mmol) in dry THF (50 mL) under a positive pressure of nitrogen. The solution was stirred for 3 hours, diluted with ethyl acetate (50 mL), water (30 mL) and acidified to pH 1 using 2M HCl (aq). The aqueous layer was then extracted using ethyl acetate (50 mL) before the combined organic layers were dried using $MgSO_4$ and solvent removed *in vacuo* to afford **187** as a colourless solid. Mp 62-64 °C (lit.[228] 64.8-65.2 °C) (4.01 g, 99%). ^{1}H NMR (300.1 MHz, $CDCl_3$) δ 7.45-7.32 (5H, m, Ph), 6.96-6.91 (3H, m, Ar-H), 5.08 (2H, s, CH_2), 4.67 (4H, s, 2 x CH_2) and 1.69 (2H, bs, 2 x OH). ^{13}C NMR (75.5 MHz, $CDCl_3$) δ 159.5 (quat, Ar), 143.2 (2 x quat, Ar), 137.2 (quat, Ar), 129.0 (2 x CH, Ar), 128.4 (CH, Ar), 127.9 (2 x CH, Ar), 118.2 (CH, Ar), 112.8 (2 x CH, Ar), 70.4 (CH_2) and (2 x CH_2). IR (thin film, cm^{-1}) 3304, 1598, 1454, 1302, 1165 and 1019. CIMS *m/z* 245 ([M^++H], 3%), 227 ([M^+-OH], 100%), 91 (22%). HRMS (CI^+, *m/z*) calcd for $C_{15}H_{17}O_3$ 245.1178, found 245.1170. Anal. Calcd. for $C_{15}H_{16}O_3$: C, 73.75; H, 6.60. Found: C, 73.93; H, 6.58.

Preparation of 1-Benzyloxy-3,5-bis chloromethyl benzene 188

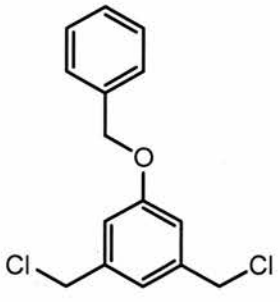

Method A: *N*-Chlorosuccinimide (0.77 g, 5.7 mmol) was added to a solution of **187** (0.5 g, 2.1 mmol) and triphenylphosphine (1.35 g, 5.1 mmol) dissolved in distilled THF (20 mL) and

stirred under a positive pressure of nitrogen overnight. The solution was then diluted with DCM (20 mL) and washed with water (2 x 20 mL). The combined organic layers were then dried with $MgSO_4$ and the solvent removed *in vacuo*. The product was purified *via* column chromatography (SiO_2; v/v 12:1 DCM:petroleum ether) to afford the product as a colourless solid containing a mixture of **188** and mono-chlorinated product which could not be separated.

Method B: Carbon tetrachloride (1.74 mL, 18.0 mmol) was added dropwise *via* syringe to a solution of **187** (1.00 g, 4.10 mmol) and triphenylphosphine (4.73 g, 18.0 mmol) in dry acetonitrile (20 mL) cooled on an ice bath under a positive pressure of nitrogen. The solution was stirred at 0 °C for 2 hours before it was warmed to room temperature and stirred overnight. The solution turned black when it reached room temperature. The solvent was removed *in vacuo* to afford a yellow oil which was purified *via* column chromatography (SiO_2; v/v 10:1 hexane:ethyl acetate) to afford the product as a colourless solid containing a mixture of **188** and mono-chlorinated product which could not be separated.

Method C: Carbon tetrachloride (1.74 mL, 18.0 mmol) was added dropwise *via* syringe to a solution of **187** (1.00 g, 4.10 mmol) and tributylphosphine (4.50 mL, 18.0 mmol) in dry acetonitrile (20 mL) cooled on an ice bath under a positive pressure of nitrogen. The solution was stirred at 0 °C for 2 hours before it was warmed to room temperature and stirred overnight. The solvent was removed *in vacuo* to afford a yellow oil which was purified *via* column chromatography (SiO_2; v/v 29:1 petroleum ether:ethyl acetate) to afford **188** as a colourless solid. (1.05 g, 91%).

Mp 85-86 °C. ^{1}H NMR (300.1 MHz, $CDCl_3$) δ 7.46-7.32 (5H, m, Ph), 7.02-6.98 (3H, m, Ar-H), 5.08 (2H, s, CH_2) and (4H, s, 2 x CH_2). ^{13}C NMR (75.5 MHz, $CDCl_3$) δ 159.3 (quat, Ar), 139.4 (2 x quat, Ar), 136.5 (quat, Ar), 128.7 (2 x CH, Ar), 128.2 (CH, Ar), 127.6 (2 x CH, Ar), 121.1 (CH, Ar), 115.0 (2 x CH, Ar), 70.2 (CH_2) and 45.8 (2 x CH_2). IR (KBr, cm^{-1}) 3125, 2448, 1596, 1325, 1039, 856 and 843. CIMS *m/z* 284 ([M^+ 2 x ^{37}Cl], 1%), 282 ([M^+ ^{35}Cl^{37}Cl], 4%), 280 ([M^+ 2 x ^{35}Cl], 7%), 247 (36%), 245 (100%) and 91 (58%). HRMS (Cl^+, *m/z*) calcd for $C_{15}H_{14}O^{35}Cl_2$ 280.0422, found 280.0425. Anal. Calcd. for $C_{15}H_{14}OCl_2$: C, 64.07; H, 5.02. Found: C, 64.36; H, 4.92.

Preparation of Diphthalamide protected 3-Aminomethyl-5-benzyloxy benzylamine 189

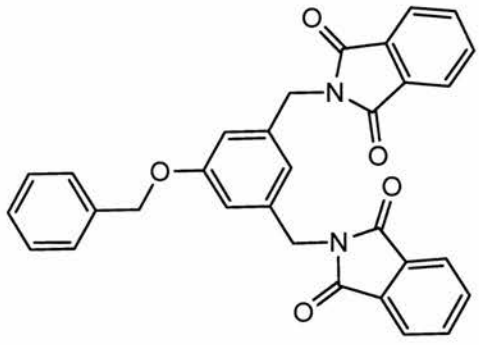

Potassium carbonate (0.25 g, 1.8 mmol) and potassium phthalamide (1.52 g, 8.2 mmol) were added to a solution of **188** (0.5 g, 2.1 mmol) dissolved in freshly distilled acetonitrile under a positive pressure of nitrogen. The solution was then heated to reflux for 24 hours before being cooled the product filtered. The product was then washed with water and dried under vacuum to afford **189** as a colourless solid. The product obtained was a mixture of mono- and di- phthalamide protected derivatives which could not be separated.

Preparation of 1,3-Bisazidomethyl-5-benzyloxy benzene 191

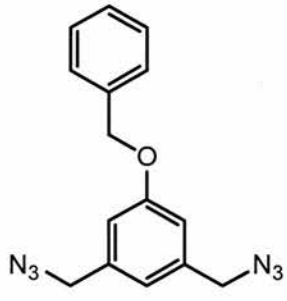

Sodium azide (9.59 g, 147.5 mmol) was added to a solution of **188** (6.91 g, 24.6 mmol) dissolved in acetone (100 mL) and refluxed for 48 hours. The solution was then cooled and filtered before the solvent was removed *in vacuo* to afford **191** as a pale yellow oil. (7.02 g, 97%). ^{1}H NMR (300.1 MHz, $CDCl_3$) δ 7.46-7.32 (5H, m, Ph), 6.92-6.87 (3H, m, Ar-H), 5.09 (2H, s, CH_2) and 4.33 (4H, s, 2 x CH_2). ^{13}C NMR (75.5 MHz, $CDCl_3$) δ 159.9 (quat, Ar), 138.0 (2 x quat, Ar), 136.9 (quat, Ar), 129.1 (2 x CH, Ar), 128.6 (CH, Ar), 128.0 (2 x CH, Ar), 120.6 (CH, Ar), 114.7 (2 x CH, Ar), 70.6 (CH_2) and 54.9 (2 x CH_2). IR (KBr, cm^{-1}) 2930, 2099, 1596 and 1155. CIMS *m/z* 295 ([M^++H], 1%), 252 ([M^++H-N_3], 100%), 239 (24%) and 91 (15%). HRMS (CI^+, *m/z*) calcd for $C_{15}H_{15}N_6O$ 295.1307, found 295.1313.

Preparation of 3-Aminomethyl-5-benzyloxy benzylamine dihydrochloride salt 192

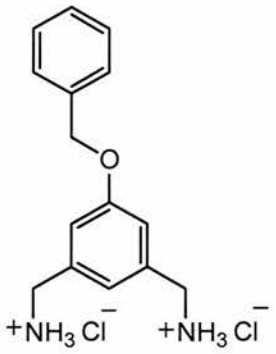

Triphenylphosphine (0.68 g, 2.6 mmol) was added portionwise to a solution of **188** (0.38 g, 1.3 mmol) dissolved in distilled THF (9 mL) and water (30 μL) and the solution stirred overnight. The solvent was then removed *in vacuo* and the resulting pale yellow oil was redissolved in ethanol (1.5 mL). Hydrochloric acid was added dropwise to precipitate the hydrochloride salt. It was not possible to remove all traces of triphenylphosphine from crude **192** obtained.

Preparation of 3,5-Bisaminomethylphenol 193

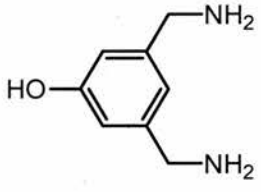

191 (4.00 g, 13.6 mmol) and 10% palladium on carbon (256 mg) were flushed with nitrogen for 10 minutes before methanol (60 mL) was added carefully. The flask was flushed with hydrogen gas and a hydrogen balloon fitted. The reaction mixture was stirred at room temperature for 7 days before being filtered through a pad of celite, dried using $MgSO_4$ and the solvent removed *in vacuo* to afford crude **193** as an insoluble brown oil which was used without further purification. (2.00 g, 97%) ^{1}H NMR (300.1 MHz, d_4-MeOD) δ 6.87 (2H, s, Ar-H), 6.86 (1H, s, Ar-H) and 3.73 (4H, s, 2 x CH_2).

Preparation of 1-[3-Hydroxy-5-(3-phenethyl ureidomethyl)benzyl]-3-phenethyl urea 194

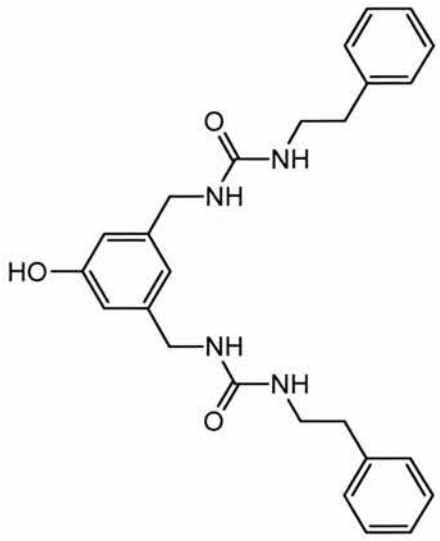

Phenethylisocyanate (7.50 mL, 54.2 mmol) was added dropwise to a solution of **193** (2.06 g, 13.6 mmol) dissolved in DMF (dried over mol. sieves) (10 mL). The solution was stirred overnight and the resulting precipitate filtered under reduced pressure to afford impure **194** as an insoluble colourless solid which was used without further purification. Mp 207-209 °C (2.28 g, 38%)

Preparation of 2-[3,5-Bis(3-phenethyl ureidomethyl)phenoxy]-*N*-{6-(4-methoxy phenyl)-acetylamino]pyridine-2-yl}acetamide 171

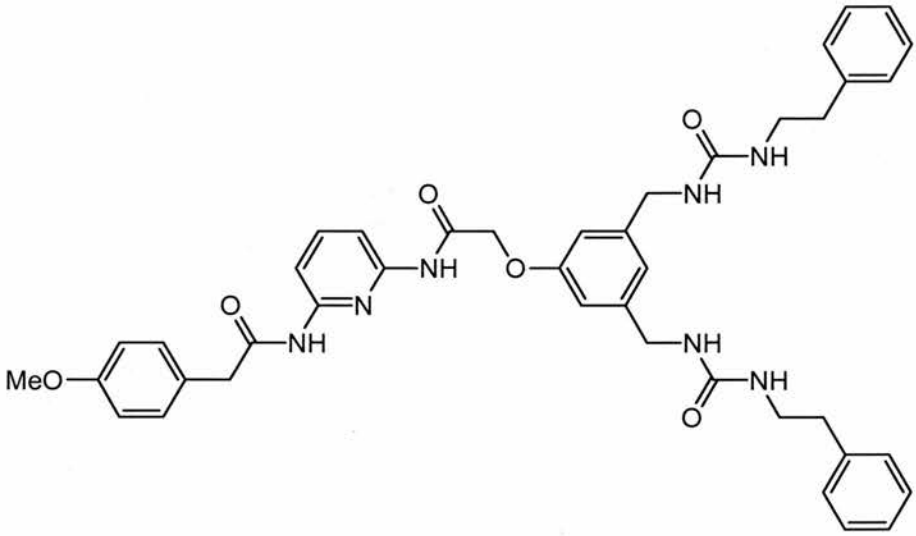

Potassium carbonate (0.46 g, 3.36 mmol) was added to a solution of 1-[3-hydroxy-5-(3-phenethyl ureidomethyl)benzyl]-3-phenethyl urea **194** (0.5 g, 1.12 mmol) dissolved in DMSO

(5 mL) and heated to 80 °C for one hour. A solution of *N*-[6-(2-chloroacetylamino) pyridine-2-yl]-2-(4-methoxyphenyl) acetamide **182** (0.38 g, 1.12 mmol) dissolved in DMSO (10 mL) was added dropwise and the resulting solution was maintained at 80 °C for 3 days. The solution was then cooled, diluted with DCM (30 mL) and washed with brine (3 x 30 mL) before the organic layer was dried using $MgSO_4$ and solvent removed *in vacuo* to afford the crude product. It was not possible to separate **171** from the crude mixture.

Preparation of 1-[3-Hydroxy-5-(3-phenethyl thioureidomethyl)benzyl]-3-phenethyl thiourea 195

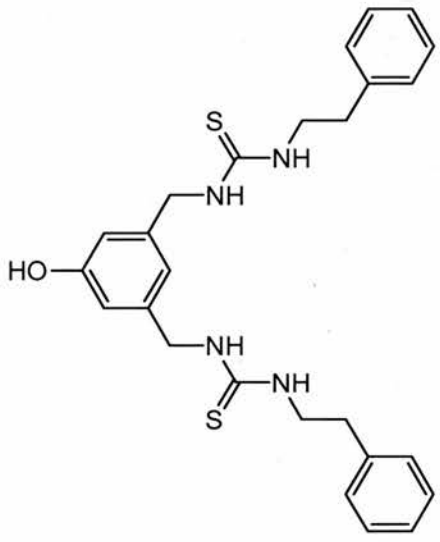

Phenethylisothiocyanate (8.40 mL, 56.5 mmol) was added dropwise to a solution of **193** (2.86 g, 18.8 mmol) dissolved in DMF (10 mL). The solution was stirred overnight and the resulting precipitate filtered under reduced pressure to afford impure **195** as waxy pale orange solid which was used without further purification. (4.76 g, 53%)

Preparation of 2-[3,5-Bis(3-phenethyl thioureidomethyl)phenoxy]-*N*-{6-(4-methoxy phenyl)-acetylamino]pyridine-2-yl}acetamide 172

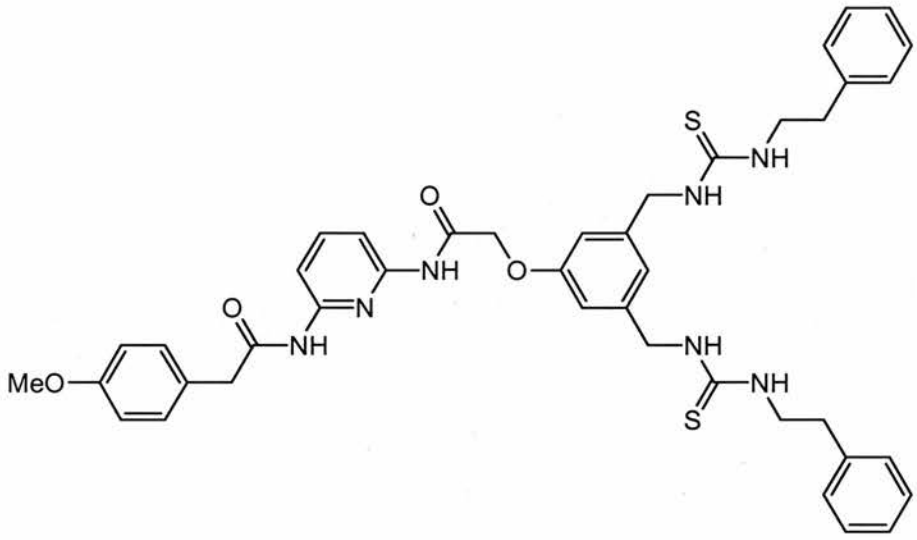

Potassium carbonate (1.73 g, 12.5 mmol) was added to a solution of 1-[3-hydroxy-5-(3-phenethyl thioureidomethyl)benzyl]-3-phenethyl thiourea **195** (1.00 g, 2.09 mmol) dissolved in acetonitrile (10 mL) and heated to 80 °C for one hour. A solution of **182** (0.70 g, 2.09 mmol) dissolved in acetonitrile (10 mL) was added dropwise and the resulting solution was maintained at 80 °C for 3 days. The solution was then cooled, diluted with DCM (40 mL) and washed with brine (3 x 40 mL) before the organic layer was dried using $MgSO_4$ and solvent removed *in vacuo* to afford the crude product. It was not possible to separate **172** from the crude mixture.

Preparation of 1-Octyl-3-{3-[(3-octyl ureido)methyl]benzyl} urea 197

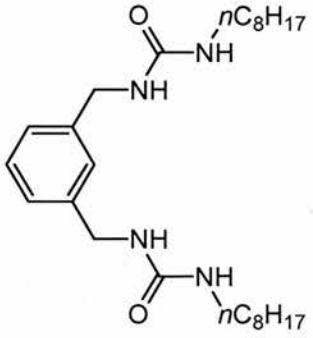

Octylisocyanate (3.90 mL, 22.0 mmol) was added dropwise to a solution of **196** (0.97 mL, 7.34 mmol) in dry DCM (15 mL) cooled on an ice bath. The solution was stirred overnight

before the resulting precipitate was filtered and dried under vacuum to afford **197** as an insoluble colourless solid which could not be purified. Mp 175-177 °C (3.20 g, 98 %) IR (KBr, cm^{-1}) 3334, 2925, 2853, 1623, 1576, 1248 and 1068.

Preparation of 1-Cyclohexyl-3-[3-(3-cyclohexyl ureidomethyl)benzyl] urea 198

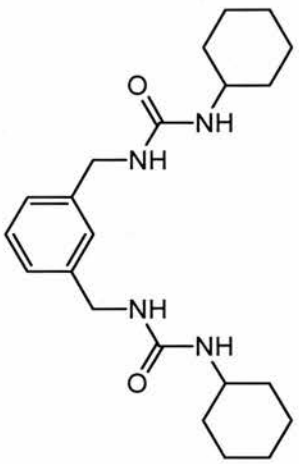

Cyclohexylisocyanate (2.80 mL, 22.0 mmol) was added dropwise to a solution of **196** (0.97 mL, 7.34 mmol) in dry DCM (15 mL) cooled on an ice bath. The solution was stirred overnight before the resulting precipitate was filtered and dried under vacuum to afford **198** as an insoluble colourless solid. Mp 241-243 °C (2.80 g, 99%) IR (KBr, cm^{-1}) 3315, 2928, 2852, 1626, 1575 and 1076. Anal. Calcd. for $C_{22}H_{34}N_4O_2$: C, 68.36; H, 8.87; N, 14.49. Found: C, 68.43; H, 9.06; N, 14.46.

Preparation of 3-Acetylsulfanylmethylbenzoic acid 201

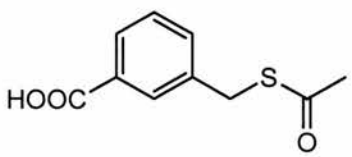

199 (1.00 g, 5.9 mmol) and potassium thioacetate (2.01 g, 17.6 mmol) were dissolved in acetone (100 mL) and the solution was stirred overnight. The solution was then diluted with DCM (100 mL) and washed with 10% $NaHSO_4$ (aq) (2 x 100 mL). The organic layer was decolourised with charcoal, dried using $MgSO_4$ and the solvent removed *in vacuo*. Removal of the solvent did not lead to the isolation of any **201**.

Preparation of *exo*- 3-(4-Ethyl-3,5-dioxo-10-oxa-4-aza tricycle[5.2.1.$0^{2,6}$]dec-8-en-8-yl)propionic acid 202

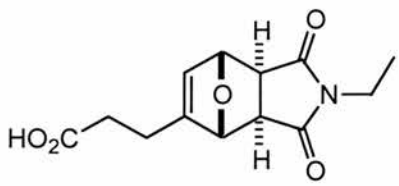

163 (14.0 mg, 0.1 mmol) was added to a solution of **38** (16.9 g, 0.1 mmol) dissolved in $CDCl_3$ and the solution warmed at 50 °C for two weeks. The solvent was removed *in vacuo* to afford **202** as a colourless oil as the *exo* isomer. ^{1}H NMR (300.1 MHz, $CDCl_3$) δ 6.06-6.05 (1H, m, CH alkene), 5.20-5.19 (1H, m, CH bridgehead), 5.04 (1H, s, CH bridgehead), 3.61-3.48 (4H, m, 2 x CH_2), 2.88-2.86 (2H, m, 2 x CH), 2.61-2.54 (2H, m, CH_2) and 1.21-1.12 (3H, m, CH_3). ^{13}C NMR δ 178.7 (C=O), 178.5 (C=O), 176.4 (C=O), 152.1 (quat), 130.0 (CH, alkene), 84.5 (CH), 83.1 (CH), 50.4 (CH), 48.4 (CH), 34.6 (CH_2), 32.6 (CH_2), 23.4 (CH_2) and 13.1 (CH_3). ESMS 288 ([M^++Na], 100%), 179 (17%) and 163 (57%). HRMS (ES^+, *m/z*) calcd for $C_{13}H_{15}NO_5Na$ 288.0848, found 288.0844.

Preparation of 1-Benzyl-5-ethyl-3a,6a-dihydro-1*H*-pyrrolo[3,4-*d*][1,2,3]triazole-4,6-dione 203

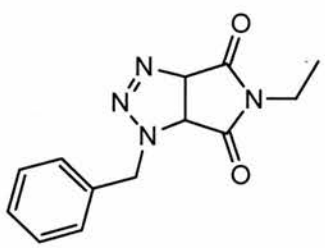

145 (13.3 mg, 0.1 mmol) was added to a solution of **38** (16.9 mg, 0.1 mmol) dissolved in $CDCl_3$ (1 mL) and the solution warmed at 50 °C for two weeks. The solvent was removed *in vacuo* to afford **203** as a yellow oil. ^{1}H NMR (300.1 MHz, $CDCl_3$) δ 7.42-7.30 (5H, m, Ar-H), 4.73 (1H, d, $^3J_{H,H}$ 10.9 Hz, CH), 4.34 (2H, s, CH_2), 4.07 (1H, d, $^3J_{H,H}$ 10.9 Hz, CH), 3.61-3.51 (2H, m, CH_2) and 1.21-1.12 (3H, m, CH_3). ^{13}C NMR δ 170.7 (C=O), 169.7 (C=O), 133.1 (quat, Ar), 128.0 (2 x CH, Ar), 127.9 (2 x CH, Ar), 127.5 (CH, Ar), 80.3 (CH), 55.4 (CH), 51.7 (CH_2), 33.4 (CH_2) and 11.8 (CH_3). ESMS *m/z* 281 ([M^++Na], 100%) and 259 ([M^++H] 8%). HRMS (ES^+, *m/z*) calcd for 281.1004, found 281.1014.

Preparation of 1-Ethyl-3-phenylsulfanyl pyrrolidine-2,5-dione 204

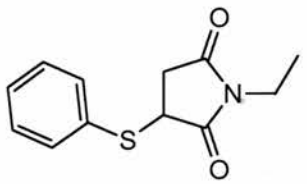

143 (10.1 μL, 0.1 mmol) was added to a solution of **38** (12.6 mg, 50 μmol) and 4-*t*-butylpyridine (7.3 μL, 50 μmol) dissolved in $CDCl_3$ (1 mL) and the solution warmed at 35 °C on a water bath for one week. The solution was then washed with water (0.5 mL), dried using $MgSO_4$ and the solvent removed *in vacuo* to afford **204** as an orange oil. ^{1}H NMR (300.1 MHz, $CDCl_3$) δ 7.57-7.34 (5H, m, Ar-H), 4.02 (1H, dd, $^3J_{H,H}$ 4.0 Hz, $^4J_{H,H}$ 9.2 Hz, CH), 3.49 (2H, q, $^3J_{H,H}$ 7.2 Hz, CH_2), 3.15 (1H, dd, $^3J_{H,H}$ 9.2 Hz, $^4J_{H,H}$ 18.8 Hz, CH), 2.73 (1H, $^3J_{H,H}$ 4.0 Hz, $^4J_{H,H}$ 18.8 Hz, CH) and 1.06 (3H, t, $^3J_{H,H}$ 7.2 Hz, CH_3). ^{13}C NMR (75.5 MHz, $CDCl_3$) δ 174.3 (C=O), 173.3 (C=O), 133.6 (2 x CH, Ar), 129.2 (quat, Ar), 128.3 (2 x CH, Ar), 126.5 (CH, Ar), 42.9 (CH), 35.2 (CH_2), 33.7 (CH_2, ring) and 11.73 (CH_3). ESMS *m/z* 258 ([M^++Na], 20%).

7. References

1. Fischer, E. *Chem. Ber.* **1894**, *27*, 2985-2993.
2. Koshland, D. E. Jr. *Angew. Chem. Int. Ed. Engl.* **1994**, *33*, 2375-2378.
3. Pauling, L. *Nature* **1948**, *161*, 707-709.
4. Kirby, A. J. *Phil. Trans. R. Soc. Lond. A* **1993**, *345*, 67-76.
5. Benkovic, S. J.; Hammes-Schiffer, S. *Science* **2003**, *301*, 1196-1202.
6. Suckling, C. J. *Chem. Soc. Rev.* **1984**, *13*, 97-129.
7. Menger, F. M. *Biochemistry* **1992**, *31*, 5368-5373.
8. Koshland, D. E. Jr. *J. Theoret. Biol.* **1962**, *2*, 75-86.
9. Page, M. I. *Angew. Chem. Int. Ed. Engl.* **1977**, *16*, 449-459.
10. Bruice, T. C.; Turner, A. *J. Am. Chem. Soc.* **1970**, *92*, 3422-3428.
11. Bruice, T. C. *Annu. Rev. Biochem.* **1976**, *45*, 331-373.
12. Kirby, A. J. *Acc. Chem. Res.* **1997**, *30*, 290-296.
13. Houk, K. N.; Tucker, J. A.; Dorigo, A. E. *Acc. Chem. Res.* **1990**, *23*, 107-113.
14. Hur, S.; Bruice, T. C. *J. Am. Chem. Soc.* **2003**, *125*, 10540-10542.
15. Kirby, A. J. *Adv. Phys. Org. Chem.* **1980**, *17*, 183-278.
16. Dafforn, A.; Koshland, D. E. Jr. *Proc. Natl. Acad. Sci. USA* **1971**, *68*, 2463-2467.
17. Lightstone, F. C.; Bruice, T. C. *J. Am. Chem. Soc.* **1996**, *118*, 2595-2605.
18. Page, M. I.; Jencks, W. P. *Proc. Natl. Acad. Sci. USA* **1971**, *68*, 1678-1683.
19. Bruice, T. C. *Acc. Chem. Res.* **2002**, *35*, 139-148.
20. Villà, J.; Štrajbl, M.; Glennon, T. M.; Sham, Y. Y.; Chu, Z. T.; Warshel, A. *Proc. Natl. Acad. Sci. USA* **2000**, *97*, 11899-11904.
21. Storm, D. R.; Koshland, D. E. Jr. *J. Am. Chem. Soc.* **1972**, *94*, 5805-5814.
22. Storm, D. R.; Koshland, D. E. Jr. *J. Am. Chem. Soc.* **1972**, *94*, 5815-5825.
23. Mesecar, A. D.; Stoddard, B. L.; Koshland, D. E. Jr. *Science* **1997**, *277*, 202-206.
24. Hoare, D. G. *Nature* **1972**, *236*, 437-440.
25. Bruice, T. C.; Brown, A.; Harris, D. O. *Proc. Natl. Acad. Sci. USA* **1971**, *68*, 658-661.

26. Pauling, L. *J. Am. Chem. Soc.* **1931**, *53*, 1367-1400.

27. Menger, F. M.; Glass, L. E. *J. Am. Chem. Soc.* **1980**, *102*, 5404-5406.

28. Scheiner, S.; Lipscomb, W. N.; Kleier, D. A. *J. Am. Chem. Soc.* **1976**, *98*, 4770-4777.

29. Menger, F. M. *Acc. Chem. Res.* **1985**, *18*, 128-134.

30. Menger, F. M. *Acc. Chem. Res.* **1993**, *26*, 206-212.

31. Beesley, R. M.; Ingold, C. K.; Thorpe, J. F. *J. Am. Chem. Soc.* **1915**, *107*, 1081-1106.

32. Bruice, T. C.; Pandit, U. K. *Proc. Natl. Acad. Sci. USA* **1960**, *46*, 402-404.

33. Jung, M. E.; Gervay, J. *Tetrahedron Lett.* **1988**, *29*, 2429-2432.

34. von R. Schleyer, P. *J. Am. Chem. Soc.* **1961**, *83*, 1368-1373.

35. Bruice, T. C.; Pandit, U. K. *J. Am. Chem. Soc.* **1960**, *82*, 5858-5865.

36. Jung, M. E.; Gervey, J. *J. Am. Chem. Soc.* **1991**, *113*, 224-232.

37. Jung, M. E.; Kiankarimi, M. *J. Org. Chem.* **1998**, *63*, 2968-2974.

38. Lightstone, F. C.; Bruice, T. C. *J. Am. Chem. Soc.* **1996**, *118*, 2595-2605.

39. Lightstone, F. C.; Bruice, T. C. *J. Am. Chem. Soc.* **1997**, *119*, 9103-9113.

40. Lightstone, F. C.; Bruice, T. C. *Bioorg. Chem.* **1998**, *26*, 193-199.

41. Bruice, T. C.; Lightstone, F. C. *Acc. Chem. Res.* **1999**, *32*, 127-136.

42. Bruice, T. C.; Benkovic, S. J. *Biochemistry* **2000**, *39*, 6267-6274.

43. Koshland, D. E. Jr.; Neet, K. E. *Annu. Rev. Biochem.* **1968**, *37*, 359-410.

44. McMurry, J. *Organic Chemistry*, 4th Ed, Brooks/Cole, California, **1996**.

45. Dewar, M. J. S.; Pierini, A. B. *J. Am. Chem. Soc.* **1984**, *106*, 203-208.

46. Dewar, M. J. S. *J. Am. Chem. Soc.* **1984**, *106*, 209-219.

47. Pohnert, G. *ChemBioChem* **2001**, *2*, 873-875.

48. Laschat, S. *Angew. Chem. Int. Ed. Engl.* **1996**, *35*, 289-291.

49. Katayama, K.; Kobayashi, T.; Oikawa, H.; Honma, M.; Ichihara. A. *Biochem. Biophys. Acta* **1998**, *1384*, 387-395.

50. Oikawa, H.; Kobayashi, T.; Katayame, K.; Suzuki, Y.; Ichihara, A. *J. Org. Chem.* **1998**, *63*, 8748-8756.

51. Oikawa, H.; Katayama, K.; Suzuki, Y.; Ichihara, A. *J. Chem. Soc., Chem. Commun.* **1995**, 1321-1322.

52. Breslow, R. *Acc. Chem. Res.* **1991**, *24*, 159-164.

53. Moore, R. N.; Bigan, G.; Chan, J. K.; Hogg, A. M.; Nakashima, T. T.; Vederas, J. C. *J. Am. Chem. Soc.* **1985**, *107*, 3694-3701.

54. Yoshizawa, Y.; Witter, D. J.; Liu, Y.; Vederas, J. C. *J. Am. Chem. Soc.* **1994**, *116*, 2693-2694.

55. Witter, D. J.; Vederas, J. C. *J. Org. Chem.* **1996**, *61*, 2613-2623.

56. Wagschal, K. Yoshizawa, Y.; Witter, D. J.; Liu, Y.; Vederas, J. C. *J. Chem. Soc., Perkin Trans. 1* **1996**, 2357-2363.

57. Hendrickson, L.; Davis, C. R.; Roach, C.; Nguyen, D. K.; Aldrich, T.; M^{c}Ada, P. C.; Reeves, C. D. *Chem. Biol.* **1999**, *6*, 429-439.

58. Auclair, K.; Sutherland, A.; Kennedy, J.; Witter, D. J.; van den Heever, J. P.; Hutchinson, C. R.; Vederas, J. C. *J. Am. Chem. Soc.* **2000**, *122*, 11519-11520.

59. Watanabe, K.; Mie, T.; Ichihara, A.; Oikawa, H.; Honma, M. *J. Biol. Chem.* **2000**, *275*, 38393-38401.

60. Oikawa, H.; Watanabe, K.; Yagi, K.; Ohashi, S.; Mie, T.; Ichihara, A.; Honma, M. *Tetrahedron Lett.* **1999**, *40*, 6983-6986.

61. Watanabe, K.; Mie, T.; Ichihara, A.; Oikawa, H.; Honma, M. *Tetrahedron Lett.* **2000**, *41*, 1443-1446.

62. Ose, T.; Watanabe, K.; Mie, T.; Honma, M.; Watanabe, H.; Yao, M.; Oikawa, H.; Tanaka, I. *Nature* **2003**, *422*, 185-189.

63. Wolfe, S. L. *Molecular and Cellular Biology*, Wadsworth, California, **1993**.

64. Lee. A. Y.; Stewart. J. D.; Clardy, J.; Ganem, B. *Chem. Biol.* **1995**, *2*, 195-203.

65. Martí, S.; Andres, J.; Moliner, V.; Silla, E.; Tunon, I.; Bertran, J. *J. Phys. Chem. B* **2000**, *104*, 11308-11315.

66. Kast, P.; Tewari, Y. B.; Wiest, O.; Hilvert, D.; Houk, K.; Goldberg, R. N. *J. Phys. Chem. B* **1997**, *101*, 10976-10982.

67. Lee, A. Y.; Stewart, J. D.; Clardy, J.; Ganem. B. *Chem. Biol.* **1995**, *2*, 195-203.

68. Görisch, H. *Biochemistry* **1978**, *17*, 3700-3705.

69. Chook, Y. M.; Ke, H.; Lipscomb, W. N. *Proc. Natl. Acad. Sci. USA* **1993**, *90*, 8600-8603.

70. Chook, Y. M.; Gray, J. V.; Ke, H.; Lipscomb, W. N. *J. Mol. Biol.* **1994**, *240*, 476-500.

71. Kast, P.; Grisostomi, C.; Chen. I. A.; Li. S.; Krengel. U.; Xue. Y.; Hilvert. D. *J. Biol. Chem.* **2000**, *275*, 36832-36838.

72. Gustin, D. J.; Mattei, P.; Kast, P.; Wiest, O.; Lee, L.; Cleland, W. W.; Hilvert, D. *J. Am. Chem. Soc.* **1999**, *121*, 1756-1757.

73. Gajewski, J. J.; Conrad, N. D. *J. Am. Chem. Soc.* **1979**, *101*, 6693-

74. Gajewski, J. J.; Emrani, J. *J. Am. Chem. Soc.* **1984**, *106*, 5733-5734.

75. Kupczyk-Subotkowska, L.; Saunders, W. H.; Shine, H. J.; Subotkowski, W. J. *J. Am. Chem. Soc.* **1993**, *115*, 5957-5961.

76. Wiest, O.; Houk, K. N. *J. Am. Chem. Soc.* **1995**, *117*, 11628-11639.

77. Yoo, H. Y.; Houk, K. N. *J. Am. Chem. Soc.* **1994**, *116*, 12047-12048.

78. Worthington, S. E.; Roitberg, A. E.; Krauss, M. *J. Phys. Chem. B* **2001**, *105*, 7087-7095.

79. Martí, S.; Moliner, V.; Tuñón, I.; Williams, I. H. *Org. Biomol. Chem.* **2003**, *1*, 483-487.

80. Lee. A. Y.; Karplus, P. A.; Ganem, B.; Clardy, J. *J. Am. Chem. Soc.* **1995**, *117*, 3627-3628.

81. Edwards, J. M.; Jackman, L. M. *Aust. J. Chem.* **1965**, *18*, 1227-1239.

82. Marti, S.; Andres, J.; Moliner, V.; Silla, E.; Tunon, I.; Bertran, J.; Field, M. J. *J. Am. Chem. Soc.* **2001**, *123*, 1709-1712.

83. Ranaghan, K. E.; Ridder, L.; Szefczyk, B.; Solkalski, W. A.; Hermann, J. C.; Mulholland, A. J. *Org. Biomol. Chem.* **2004**, *2*, 968-980.

84. Hur, S.; Bruice, T. C. *J. Am. Chem. Soc.* **2003**, *125*, 1472-1473.

85. Guo, H.; Cui, Q.; Lipscomb, W. N.; Karplus, M. *Proc. Natl. Acad. Sci. USA* **2001**, *98*, 9032-9037.

86. Campbell, A. P.; Tarasow, T. M.; Massefski, W.; Wright, P. E.; Hilvert, D. *Proc. Natl. Acad. Sci. USA* **1993**, *90*, 8663-8667,

87. Hur, S.; Bruice, T. C. *Proc. Natl. Acad. Sci. USA* **2003**, *100*, 12015-12020.

88. Hur, S.; Bruice, T. C. *J. Am. Chem. Soc.* **2003**, *125*, 5964-5972.

89. Hur, S.; Bruice, T. C. *Proc. Natl. Acad. Sci. USA* **2002**, *99*, 1176-1181.

90. Campbell, N. A. *Biology*, 4th Ed, Benjamin/Cummings, California, **1996**.

91. Benkovic, S. J. *Annu. Rev. Biochem.* **1992**, *61*, 29-54.

92. Scanlon, T. S.; Schultz, P. G. *Phil. Trans. R. Soc. Lond. B* **1991**, *332*, 157-164.

93. Kirby, A. J. *Acta Chem. Scand.* **1996**, *50*, 203-210.

94. Wentworth. P. Jr.; Janda, K. D. *Curr. Opin. Chem. Biol.* **1998**, *2*, 138-144.

95. Tramontano, A.; Janda, K. D.; Lerner, R. A. *Science* **1986**, *234*, 1566-1570.

96. Tramontano, A.; Ammann, A. A.; Lerner, R. A. *J. Am. Chem. Soc.* **1988**, *110*, 2282-2286.

97. Haynes, M. R.; Stura, E. A.; Hilvert, D.; Wilson, I. A. *Science* **1994**, *263*, 646-652.

98. Pollack, S. J.; Jacobs, J. W.; Schultz, P. G. *Science* **1986**, *234*, 1570-1573.

99. Smithrud, D. B.; Benkovic, S. J. *Curr. Opin. Biotech.* **1997**, *8*, 459-466.

100. Lerner, R. A.; Benkovic, S. J.; Schultz, P. G. *Science* **1991**, *252*, 659-667.

101. Stewart, J. D.; Benkovic, S. J. *Chem. Soc. Rev.* **1993**, 213-219.

102. Hasserodt, J. *Synlett* **1999**, *12*, 2007-2022.

103. List, B.; Shabat, D.; Barbas III, C. F.; Lerner, R. A. *Chem. Eur. J.* **1998**, *4*, 881-885.

104. Shabat, D.; List, B.; Lerner, R. A.; Barbas III, C. F. *Tetrahedron Lett.* **1999**, *40*, 1437-1440.

105. Taylor, S. V.; Kast, P.; Hilvert, D. *Angew. Chem. Int. Ed.* **2001**, *40*, 3310-3335.

106. Griffiths, A. D.; Tawfik, D. S. *Curr. Opin. Biotechnol.* **2000**, *11*, 338-353.

107. Bornsheuer, U. T. *Angew. Chem. Int. Ed.* **1998**, *37*, 3105-3108.

108. Minshull, J.; Stemmer, W. P. C. *Curr. Opin. Chem. Biol.* **1999**, *3*, 284-290.

109. Reetz, M. T.; Jaeger, K.-E. *Chem. Eur. J.* **2000**, *6*, 407-412.

110. Arnold, F. H.; Volkov, A. A. *Curr. Opin. Chem. Biol.* **1999**, *3*, 54-59.

111. Arnold, F. H. *Acc. Chem. Res.* **1998**, *31*, 125-131.

112. Yano, T.; Oue, S.; Kagamiyama, H. *Proc. Natl. Acad. Sci. USA* **1998**, *95*, 5511-5515.

113. Olsen, M.; Iverson, B.; Georgiou, G. *Curr. Opin. Biotechnol.* **2000**, *11*, 331-337.

114. Hilvert, D. *Annu. Rev. Biochem.* **2000**, *67*, 751-793.

115. Hilvert, D.; Hill, K. W.; Nared, K. D.; Auditor, M.-T. M. *J. Am. Chem. Soc.* **1989**, *111*, 9261-9262.

116. Hilvert, D. *Acc. Chem. Res.* **1993**, *26*, 552-558.

117. Jackson, D. Y.; Jacobs, J. W.; Sugasawara, R.; Reich, S. H.; Bartlett, P.A.; Schultz, P. G. *J. Am. Chem. Soc.* **1988**, *110*, 4841-4842.

118. Cram, D. J. *Angew. Chem. Int. Ed. Engl.* **1988**, *27*, 1009-1112.

119. Pederson, C. J. *Angew. Chem. Int. Ed. Engl.* **1988**, *27*, 1021-1027.

120. Lehn, J. –M. *Angew. Chem. Int. Ed. Engl.* **1988**, *27*, 89-112.

121. Philp, D.; Stoddart, J. F. *Angew. Chem. Int. Ed. Engl.* **1996**, *35*, 1154-1196.

122. Greig, L. M.; Philp, D. *Chem. Soc. Rev.* **2001**, *30*, 287-302.

123. Fyfe, M. C. T.; Stoddart, J. F. *Acc. Chem. Res.* **1997**, *30*, 393-401.

124. Mascal, M. *Contemp. Org. Synth.* **1994**, *1*, 31-46.

125. Lindsey, J. S. *New J. Chem.* **1991**, *15*, 153-180.

126. Lehn, J. -M. *Rep. Prog. Phys.* **2004**, *67*, 249-265.

127. Menger, F. M. *Proc. Natl. Acad. Sci. USA* **2002**, *99*, 4818-4822.

128. Sanders, J. K. M. *Chem. Eur. J.* **1998**, *4*, 1378-1383.

129. Hartley, J. H.; James, T. D.; Ward, C. J. *J. Chem. Soc., Perkin Trans. 1* **2000**, 3155-3184.

130. Yatsimirsky, A.; Schneider, H. J. *Principles and Methods in Supramolecular Chemistry* Wiley & Sons: Chichester, 2000.

131. Robertson, A.; Philp, D.; Spencer, N. *Tetrahedron* **1999**, *55*, 11365-11384.

132. Booth, C. A.; Philp, D. *Tetrahedron Lett.* **1998**, *39*, 6987-6990.

133. Philp, D.; Robertson, A. *Chem. Commun.* **1998**, 879-880.

134. Howell. S. J.; Spencer, N.; Philp, D. *Tetrahedron* **2001**, *57*, 4945-4954.

135. Bennes, R.; Babiloni, M. S.; Hayes, W.; Philp, D. *Tetrahedron Lett.* **2001**, *42*, 2377-2380.

136. Tecilla, P.; Hamilton, A. D. *J. Chem. Soc., Chem. Commun.* **1990**, 1232-1234.

137. Tecilla, P.; Jubian, V.; Hamilton, A. D. *Tetrahedron* **1995**, *51*, 435-448.

138. Pearson, R. J.; Kassianidis, E.; Philp, D. *Tetrahedron Lett.* **2004**, *45*, 4777-4780.

139. Seeman, J. I. *Chem. Rev.* **1983**, *83*, 83-134.

140. Winstein, S.; Holness, N. J. *J. Am. Chem. Soc.* **1955**, *77*, 5562-5578.

141. Goodwin, J. T.; Lynn, D. G. *J. Am. Chem. Soc.* **1992**, *114*, 9197-9198.

142. Roigk, A.; Schneider, H. –J. *Eur. J. Org. Chem.* **2001**, 205-209.

143. Huc, I.; Pieters, R. J.; Rebek, J. Jr. *J. Am. Chem. Soc.* **1994**, *116*, 10296-10297.

144. Kelly, T. R.; Bridger, G. J.; Zhao. C. *J. Am. Chem. Soc.* **1990**, *112*, 8024-8034.

145. Howell, S. J.; Ashton, P. R.; Spenser, N.; Philp, D. *Org. Lett.* **2001**, *3*, 353-356.

146. Schreiner, P. R. *Chem. Soc. Rev.* **2003**, *32*, 289-296.

147. Clarke, M. L. *Letters in Organic Chemistry* **2004**, *1*, 292-296.

148. Puglisi, A.; Benaglia, M.; Cinquini, M.; Cozzi, F.; Celentano, G. *Eur. J. Org. Chem.* **2004**, 567-573.

149. Dalko, P. I.; Moisan, L. *Angew. Chem. Int. Ed.* **2004**, *43*, 5138-5175.

150. Jarvo, E. R.; Miller, S. J. *Tetrahedron* **2002**, *58*, 2481-2495.

151. Hartikka, A.; Arvidsson, P. I. *Tetrahedron: Assymmetry* **2004**, *15*, 1831-1834.

152. Nakadai, M.; Saito, S.; Yamamoto, H. *Tetrahedron* **2002**, *58*, 8167-8177.

153. Pihko, P. M. *Angew. Chem. Int. Ed.* **2004**, *43*, 2062-2064.

154. Benaglia, M.; Puglisi, A.; Cozzi, F. *Chem. Rev.* **2003**, *103*, 3401-3429.

155. Dalko, P. I.; Moisan, L. *Angew. Chem. Int. Ed.* **2001**, *40*, 3726-3748.

156. Northrup, A. B.; MacMillan, D. W. C. *J. Am. Chem. Soc.* **2002**, *124*, 6798-6799.

157. Paras, N. A.; MacMillan, D. W. C. *J. Am. Chem. Soc.* **2002**, *124*, 7894-7895.

158. Alcázar, V.; Morán, J. R.; de Mendoza, J. *Tetrahedron Lett.* **1995**, *36*, 3941-3944.

159. Fenniri, H.; Lehn, J. –M.; Marquis-Rigault, A. *Angew. Chem. Int. Ed. Engl.* **1996**, *35*, 337-339.

160. Fenniri, H.; Dallaire, C.; Funeriu, D. P.; Lehn, J. –M. *J. Chem. Soc., Perkin Trans. 2* **1997**, 2073-2081.

161. Crego, M.; Raposo, C.; Mussons, M. L.; Caballero, M. C.; Morán, J. R. *Tetrahedron Lett.* **1994**, *35*, 1929-1932.

162. Kavallieratos, K.; Crabtree, R. H. *Chem. Commun.* **1999**, 2109-2110.

163. List, B.; Lerner, R. A.; Barbas III, C. F. *J. Am. Chem. Soc.* **2000**, *122*, 2395-2396.

164. Bui, T.; Barbas III, C. F. *Tetrahedron Lett.* **2000**, *41*, 6951-6954.

165. Fehr, C.; Stempf, I.; Galindo, J. *Angew. Chem. Int. Ed. Engl.* **1993**, *32*, 1042-1044.

166. Fehr, C.; Stempf, I.; Galindo, J. *Angew. Chem. Int. Ed. Engl.* **1993**, *32*, 1044-1046.

167. Page, P. C. B.; Barros, D.; Buckley, B. R.; Ardakani, A.; Marples, B. A. *J. Org. Chem.* **2004**, *69*, 3595-3597.

168. Page, P. C. B.; Rassias, G. A.; Barros, D.; Ardakani, A.; Bethell, D.; Merifield, E. *Synlett* **2002**, *4*, 580-582.

169. Kang, J.; Hilmersson, G.; Santamaría, J.; Rebek, J. Jr. *J. Am. Chem. Soc.* **1998**, *120*, 3650-3656.

170. Kang, J.; Santamaría, J.; Hilmersson, G.; Rebek, J. Jr. *J. Am. Chem. Soc.* **1998**, *120*, 7389-7390.

171. Lutter, H. –D.; Diederich, F. *Angew. Chem. Int. Ed. Engl.* **1986**, *25*, 1125-1127.

172. Szejtli, J. *Chem. Rev.* **1998**, *98*, 1743-1753.

173. Breslow, R.; Dong, S. D. *Chem. Rev.* **1998**, *98*, 1997-2011.

174. Harada, A. *Adv. Polym. Sci.* **1997**, *133*, 141-191.

175. Saenger, W. *Angew. Chem. Int. Ed. Engl.* **1980**, *19*, 344-362.

176. Takahashi, K. *Chem. Rev.* **1998**, *98*, 2013-2033.

177. Meyer, A. G.; Easton, C. J.; Lincoln, S. F.; Simpson, G. W. *Chem. Commun.* **1997**, 1517-1518.

178. Tabushi, I.; Kiyosuke, Y, Sugimoto, T.; Yamamura, K. *J. Am. Chem. Soc.* **1978**, *100*, 916-919.

179. Demarco, P.V.; Thakkar, A. L. *Chem. Commun.* **1970**, 2-4.

180. Nakamura, A.; Inoue, Y. *J. Am. Chem. Soc.* **2003**, *125*, 966-972.

181. Wulff, G. *Chem. Rev.* **2002**, *102*, 1-27.

182. Spivak, D.; Shea, K. J. *J. Org. Chem.* **1999**, *64*, 4627-4634.

183. Sellergren, B. *Angew. Chem. Int. Ed.* **2000**, *39*, 1031-1037.

184. Whitcombe, M. J.; Vulfson, E. N. *Adv. Mater.* **2001**, *13*, 467-478.

185. Haupt, K.; Mosbach, K. *Chem. Rev.* **2000**, *100*, 2495-2504.

186. Alexander, C.; Davidson, L.; Hayes, W. *Tetrahedron* **2003**, *59*, 2025-2057.

187. Cunliffe, D.; Pennadam, S.; Alexander, C. *Eur. Polym. J.* **2004**, *40*, 5-25.

188. Sellergren, B.; Karmalkar, R. N.; Shea, K. J. *J. Org. Chem.* **2000**, *65*, 4009-4027.

189. Lavignac, N.; Allender, C. J.; Brain, K. R. *Anal. Chim. Acta* **2004**, *510*, 139-145.

190. Whitcombe, M. J.; Alexander, C.; Vulfson, E. N. *Synlett* **2000**, *6*, 911-923.

191. Simonsen, K. B.; Jørgensen, K. A.; Hu, Q.-S.; Pu, L. *Chem. Commun.* **1999**, 811-812.

192. Visnjevski, A.; Yilmaz, E.; Brüggemann, O. *Appl. Catal. A-Gen.* **2004**, *260*, 169-174.

193. Severin, K. *Curr. Opin. Chem. Biol.* **2000**, *4*, 710-714.

194. Tada, M.; Iwasawa, Y. *J. Mol. Cat. A* **2003**, *199*, 115-137.

195. Sellergren, B.; Karmalkar, R. N.; Shea, K. J. *J. Org. Chem.* **2000**, *65*, 4009-4027.

196. Hirst, S. C.; Hamilton, A. D. *J. Am. Chem. Soc.* **1991**, *113*, 382-383.

197. Wabnitz, T. C.; Saaby, S.; Jørgensen, K. A. *Org. Biomol. Chem.* **2004**, *2*, 828-834.

198. Thadani, A. N.; Stankovic, A. R.; Rawal, V. H. *Proc. Natl. Acad. Sci. USA* **2004**, *101*, 5846-5850.

199. Kim, S. P.; Leach, A. G.; Houk, K. N. *J. Org. Chem.* **2002**, *67*, 4250-4260.

200. Schuster, T.; Kurz, M.; Göbel, M. W. *J. Org. Chem.* **2000**, *65*, 1697-1701.

201. Houk, *Acc. Chem. Res.* **1975**, *8*, 361-369.

202. Ruiz-López, M. F.; Assfield, X.; García, J. I.; Mayoral, J. A.; Salvatella, L. *J. Am. Chem. Soc.* **1993**, *115*, 8780-8787.

203. Blake, J. F.; Lin, D.; Jørgensen, W. L. *J. Org. Chem.* **1994**, *59*, 803-805.

204. Kelly, T. R.; Meghani, P.; Ekkundi, V. S. *Tetrahedron Lett.* **1990**, *24*, 3381-3384.

205. Etter, M. C. *Acc. Chem. Res.* **1990**, *23*, 120-126.

206. Etter, M. C. *J. Phys. Chem.* **1991**, *95*, 4601-4610.

207. Schreiner, P. R.; Wittkopp, A. *Org. Lett.* **2002**, *4*, 217-220.

208. Kinsman, A. C.; Kerr, M. A. *J. Am. Chem. Soc.* **2003**, *125*, 14120-14125.

209. Northrup, A. B.; MacMillan, D. W. C. *J. Am. Chem. Soc.* **2002**, *124*, 2458-2460.

210. Mock, W. L.; Shih, N. –Y. *J. Org. Chem.* **1983**, *48*, 3619-3620.

211. Mock, W. L.; Irra, T. A.; Wepsiec, J. P.; Manimaran, T. L. *J. Org. Chem.* **1983**, *48*, 3619-3620.

212. Rowe, H. L.; Spencer, N.; Philp, D. *Tetrahedron Lett.* **2000**, *41*, 4475-4479.

213. Rowe, H. *PhD Thesis* University of St Andrews, **2002**.

214. Calcagno, P. *PhD Thesis* University of Birmingham, **2001**.

215. Wilcox, C. S. *Frontiers in Supramolecular Organic Chemistry and Photochemistry* VCH:Cambridge, 1991.

216. Sievers, D.; von Kiedrowski, G. *Chem. Eur. J.* **1998**, *4*, 629-641.

217. Jensen, F. *Introduction to Computational Chemistry* Wiley & Sons: Chichester, 1999.

218. Howell, S. J.; Spencer. N.; Philp, D. *Org. Lett.* **2002**, *4*, 273-276.

219. Armstrong, A.; Brackenridge, I.; Jackson, R. F. W.; Kirk, J. M. *Tetrahedron Lett.* **1988**, *29*, 2483-2484.

220. Pieters, R. J.; Huc, I.; Rebek, J. Jr. *Tetrahedron* **1995**, *51*, 485-498.

221. Schmidt, M. W.; Baldridge, K. K.; Boatz, J. A.; Elbert, S. T.; Gordon, M. S.; Jensen, J. H.; Koseki, S.; Matsunaga, N.; Nguyen, K. A.; Su, S. J.; Windus, T. L.; Dupuis, M.; Montgomery, J. A. *J. Comput. Chem.* **1993**, *14*, 1347-1363.

222. Rich, D. H.; Gesellchen, P. D.; Tong, A.; Cheung, A. *J. Med. Chem.* **1975**, *18*, 1004-1010.

223. Booth, C. A. *Ph. D. Thesis*, University of Birmingham, **1999**.

224. Keller, O.; Rudinger, J. *Helv. Chim. Acta.* **1975**, *58*, 531-541.

225. Arena, G.; Cali, R.; Maccarone, E.; Passerini, A. *J. Chem. Soc., Perkin Trans. 2* **1993**, *10*, 1941-1945.

226. Gensler, W. J.; Solomon, P. H. *J. Org. Chem.* **1973**, *38*, 1726-1731.

227. Schwender, C. F.; Sunday, B. R.; Shavel, J.; Giles, R. E. *J. Med. Chem.* **1974**, *17*, 1112-1115.

228. Le Stang, S.; Meier, R.; Rocaboy, C.; Gladysz, J. A. *J. Fluorine Chem.* **2003**, *119*, 141-149.

8. Appendices

8.1 Fitting the Kinetics of the [3+2] Dipolar Cycloaddition Reaction between 45 and 145.

The command file used in SIMFIT-32 for fitting the kinetic data for the control [3+2] dipolar cycloaddition reaction described in Section 2.8.2 is given below:

```
dim (1)                                          * number of rate constants to be fitted

reaction (A + B --> P1)                          * define reaction stoichiometry
reaction (compile)                               * generates the differential equations
reaction (show)                                  * prints the differential equations

constant (1,1.37e-2,1,1,1000)                    * starting value and parameters to vary
                                                   rate constant for bimolecular reaction
constant (show)                                  * show rate constants in context

define (1,P1,p,1) scale (3,1)                    * define monitored species

select (P1)                                      * column in data file containing [Product]
read (Azide)                                     * name of file containing kinetic data

time (sec)                                       * indicates units of time

win (0,70000,10000,200,0,40e-3,2e-3,3e-4)        * sets parameters for the x and y axes

assign (obs, P1 = P1)                            * match species in model to data file
assign (spec, A = #50e-3)                        * concentration of reagent A
assign (spec, B = #50e-3)                        * concentration of reagent B

choose (exp1)
integ (stiff)                                    * select stiff integration of differential
                                                   equations

plot

simplex (plot)                                   * three rounds of Simplex optimisation
simplex (plot)                                   * with screen update
simplex (plot)

newton (plot)                                    * Newton-Raphsan optimisation with
                                                   screen update

plot (file)                                      * generates the output file
```

8.2 Fitting the Kinetics of the [3+2] Dipolar Cycloaddition Reaction between 45 and 145 in the presence of 122.

The command file used in SIMFIT-32 for fitting the kinetic data for the catalysed [3+2] dipolar cycloaddition reaction described in Section 2.8.2 is given below:

```
dim (1)                                          * number of rate constants to be fitted

reaction (A + B --> P1)                          * define reaction stoichiometry
reaction (A + R ==> AR)
reaction (B + AR --> P1R)
reaction (P1R ==> P1 + R)
reaction (compile)                               * generates the differential equations
reaction (show)                                  * prints the differential equations

constant (1,3.3333e-5,0,1,1)                     * bimolecular rate constant from control
                                                   reaction fitting
constant (2,1.2321e8,0,1,1)                      * from Ka obtained by NMR titration
constant (3,1.0957e5,0,1,1)                      * from Ka obtained by NMR titration
constant (4,1.37e-3,3,1,1000)                    * starting value and parameters to vary
                                                   rate constant for catalysed reaction
constant (5,2.7925e5,0,1,1)                      * 1/Ka obtained by NMR titration
constant (6,9.0629e7,0,1,1)                      * 1/Ka obtained by NMR titration
constant (show)                                  * show rate constants in context

define (1,P1,p,1) scale  (3,1)                   * define monitored species

select (P1)                                      * column in data file containing [Product]
read (AzideRec)                                  * name of file containing kinetic data

time (sec)                                       * indicates units of time
win (0,70000,10000,200,0,5e-2,2e-3,3e-4)         * sets parameters for the x and y axes

assign (obs, P1 = P1 + P1R)                      * match species in model to data file
assign (spec, A = #50e-3)                        * concentration of reagent A
assign (spec, B = #50e-3)                        * concentration of reagent B
assign (spec, R = #10e-3)                        * concentration of catalyst

choose (exp1)
integ (stiff)                                    * select stiff integration of differential
                                                   equations

plot

simplex (plot)                                   * three rounds of Simplex optimisation
simplex (plot)                                   * with screen update
simplex (plot)

newton (plot)                                    * Newton-Raphsan optimisation with
                                                   screen update

plot (file)                                      * generates the output file
```

8.3 Output File generated by SIMFIT for [3+2] Dipolar Cycloaddition between 45 and 145.

The output file obtained from fitting the kinetic data for the control [3+2] dipolar cycloaddition reaction described in Section 2.8.2 is given below:

```
  ************************************************************************
  * SimFit (PB/DLL6) 32-bit (10-Feb-2003)  (C) 1989-2001 G. v. Kiedrowski *
  ************************************************************************
This version of SimFit comes with 2 GB variable space.
SF32.INI is currently set to:
100 species,100 reactions,50 iteratable rate constants,
50 observables,20 files,20 experiments/file,50 reaction times/experiment.

DIM (1)

REACTION (a + b --> p1)

REACTION (compile)

REACTION (show)
---------------------------------------
DGLCODER               Version 11.03.93
---------------------------------------

Reactions:
   A + B --> P1

Species found: A  B  P1

Rate equations:
    d[A]/dt =  - k1·[A]·[B]
    d[B]/dt =  - k1·[A]·[B]
   d[P1]/dt =  + k1·[A]·[B]

Jacobian matrix: NJacobi& = 6 JacobiList& = 12
     d(d[A]/dt)/d[A] =  - k1·[B]
     d(d[A]/dt)/d[B] =  - k1·[A]
     d(d[B]/dt)/d[A] =  - k1·[B]
     d(d[B]/dt)/d[B] =  - k1·[A]
    d(d[P1]/dt)/d[A] =  + k1·[B]
    d(d[P1]/dt)/d[B] =  + k1·[A]

CONSTANT (1,1.37e-2,1,1,1000)

CONSTANT (show)
A + B --> P1    k(1) =  1.370E-2  [k1]            Min: 1.370E-5 Max: 1.370E+1

DEFINE (1,p1,p,1)

SCALE (3,1)
p1: K1 * FE

SELECT (p1)

READ (azide)
The following observables found in azide.txt are DEFINEd: p1

TIME (sec)

WIN (0,70000,10000,200,0,40e-3,2e-3,3e-4)

ASSIGN (obs,p1 = p1)

ASSIGN (spec,a = #50e-3)

ASSIGN (spec,b = #50e-3)

CHOOSE (exp1)
INTEG (stiff)

PLOT
```

```
SIMPLEX (plot)
k1_________ R.M.S.[%]
initial values:

  8.2200E-3 1.588E+3
  2.7400E-3 1.357E+3
  2.7400E-3 1.357E+3
  2.7400E-3 1.357E+3
  2.7399E-3 1.357E+3
  2.7398E-3 1.357E+3
  2.7396E-3 1.357E+3
  2.7392E-3 1.357E+3
  2.7383E-3 1.357E+3

sum squares =  2.0530E-2

SIMPLEX (plot)
k1_________ R.M.S.[%]
initial values:

  1.6430E-3 1.199E+3
  5.4767E-4  770.9473
  5.4766E-4  770.9454
  5.4766E-4  770.9414
  5.4765E-4  770.9335
  5.4763E-4  770.9177
  5.4759E-4  770.8860
  5.4750E-4  770.8226
  5.4734E-4  770.6959

sum squares =  6.6236E-3

SIMPLEX (plot)
k1_________ R.M.S.[%]
initial values:

  3.2840E-4  562.5912
  1.0947E-4  202.4227
  1.0947E-4  202.4216
  1.0947E-4  202.4192
  1.0946E-4  202.4144
  1.0946E-4  202.4049
  1.0945E-4  202.3858
  1.0943E-4  202.3476
  1.0940E-4  202.2713

sum squares =  4.5624E-4

SIMPLEX (plot)
k1_________ R.M.S.[%]
initial values:

  6.5640E-5   93.5124
  2.1880E-5   36.8027
  4.3760E-5   31.5623
  3.2820E-5    2.9331
  3.3504E-5    2.3491
  3.3333E-5    2.3327
sum squares =  6.0677E-8

Minmax constraint was active.

NEWTON (plot)
k1_________ R.M.S.[%]
Initial values:----------
  3.3333E-5    2.3327
 ±0.0000E+0

-------------------------
  3.3378E-5    2.3253
 ±1.3661E-7

  3.3378E-5    2.3253
 ±1.3665E-7
sum squares =  6.0294E-8

Covariance Matrix:
        __k1__
    k1   1.000
```

* Final RMS and errors for unimolecular rate constant

```
PLOT (file)
time--------- p1-----------
56.8E+2 45.E-5
94.8E+2 73.E-5
13.28E+3 10.5E-4
17.08E+3 13.3E-4
20.88E+3 16.E-4
24.68E+3 18.7E-4
28.48E+3 22.2E-4
32.28E+3 25.3E-4
36.08E+3 28.3E-4
39.88E+3 30.6E-4
43.68E+3 33.7E-4
47.48E+3 36.6E-4
51.28E+3 39.5E-4
55.08E+3 42.E-4
58.88E+3 44.9E-4
62.68E+3 49.E-4

time--------- p1-----------
00.E-1 00.E-1
35.E+2 28.98438E-5
70.E+2 57.635211E-5
10.5E+3 85.946837E-5
14.E+3 11.39363E-4
17.5E+3 14.160905E-4
21.E+3 16.897044E-4
24.5E+3 19.60257E-4
28.E+3 22.277991E-4
31.5E+3 24.923809E-4
35.E+3 27.540511E-4
38.5E+3 30.128575E-4
42.E+3 32.688467E-4
45.5E+3 35.220647E-4
49.E+3 37.725559E-4
52.5E+3 40.203643E-4
56.E+3 42.655327E-4
59.5E+3 45.08103E-4
63.E+3 47.481162E-4
66.5E+3 49.856127E-4
70.E+3 52.206316E-4
```

8.4 Results from Matrix Experiments for ABC System

A summary of the results obtained at 25 °C for the matrix experiments described in Section 3.5 is given below:

Table 8 Summary of results from matrix experiments showing overall percentage conversion and exo:endo diastereomeric ratio (*dr*) values at 25 °C for three different reagent concentrations and four reaction template concentrations.

[160] / mM	[161] / mM	[159] / mol%	162:163 dr / %	conversion / %
75	75	100	72	71
75	75	50	66	62
75	75	25	62	56
75	75	10	50	47
75	75	0	12	42
50	50	100	80	69
50	50	50	72	62
50	50	25	48	51
50	50	10	44	39
50	50	0	14	30
25	25	100	80	61
25	25	50	70	49
25	25	25	68	36
25	25	10	62	25
25	25	0	28	18

A summary of the results obtained at 35 °C for the matrix experiments described in Section 3.5 is given below:

Table 9 Summary of results from matrix experiments showing overall percentage conversion and exo:endo diastereomeric ratio (*dr*) values at 35 °C for three different reagent concentrations and four reaction template concentrations.

[160] / mM	[161] / mM	[159] / mol%	162:163 *dr* / %	conversion / %
75	75	100	80	80
75	75	50	68	72
75	75	25	60	69
75	75	10	46	64
75	75	0	4	61
50	50	100	76	80
50	50	50	66	71
50	50	25	60	63
50	50	10	48	56
50	50	0	10	45
25	25	100	76	75
25	25	50	66	65
25	25	25	66	51
25	25	10	56	42
25	25	0	6	27

A summary of the results obtained at 25 °C for the matrix experiments described in Section 3.5 is given below:

Table 10 Summary of results from matrix experiments showing overall percentage conversion and exo:endo diastereomeric ratio (*dr*) values at 45 °C for three different reagent concentrations and four reaction template concentrations.

[160] / mM	[161] / mM	[159] / mol%	162:163 *dr* / %	conversion / %
75	75	100	68	86
75	75	50	66	78
75	75	25	62	81
75	75	10	52	74
75	75	0	12	73
50	50	100	72	79
50	50	50	68	76
50	50	25	62	75
50	50	10	34	69
50	50	0	14	64
25	25	100	54	85
25	25	50	66	73
25	25	25	70	60
25	25	10	56	54
25	25	0	20	42

8.5 Command File for ABC Simulation

The command file used in SIMFIT-32 for the simulation of the ABC model described in Section 3.6 is given below:

```
mode (isosim)                                          * indicates simulation mode

reaction (A + C ==> AC,1e11,1e9)                       * binary association, Ka = 100 M-1
reaction (A + AC ==> AAC,1e11,1e9)                     * binary association, Ka = 100 M-1
reaction (B + AC ==> ABC,1e11,1e9)                     * binary association, Ka = 100 M-1
reaction (B + C ==> BC,1e11,1e9)                       * binary association, Ka = 100 M-1
reaction (B + BC ==> BBC,1e11,1e9)                     * binary association, Ka = 100 M-1
reaction (A + BC ==> ABC,1e11,1e9)                     * binary association, Ka = 100 M-1
reaction (PC ==> P + C,1e8,1e11)                       * product dissociation
reaction (A + B --> P,1e-4)                            * bimolecular reaction
reaction (ABC --> PC,1e-4)                             * ABC reaction

reaction (compile)                                     * generates the differential equations
reaction (Show)                                        * prints the differential equations

integ (stiff,1e-11,8)                                  * integration command

numplot (100)                                          * number of points to generate

time (sec)                                             * indicates units of time

win (0,100000,10000,0.1,0,25e-3,2.5e-3,3e-4)           * sets parameters for the x and y axes

init (A,25e-3,2)                                       * initial concentration of A
init (B,25e-3,4)                                       * initial concentration of B
init (C,50e-3,5)                                       * initial concentration of C

plot (file)                                            * generates the data file
```

EM is calculated as bimolecular reaction/ABC reaction.

8.6 Output File generated by SIMFIT for Simulation of ABC model.

The data file obtained from SIMFIT-32 for the simulation of the ABC model described in Section 3.6 is given below:

```
  ************************************************************************
  * SimFit (PB/DLL6) 32-bit (10-Feb-2003)  (C) 1989-2001 G. v. Kiedrowski *
  ************************************************************************
This version of SimFit comes with 2 GB variable space.
SF32.INI is currently set to:
100 species,100 reactions,50 iteratable rate constants,
50 observables,20 files,20 experiments/file,50 reaction times/experiment.

MODE (isosim)

REACTION (a + c ==> ac,1e11,1e9)

REACTION (a + ac ==> aac,1e11,1e9)

REACTION (b + ac ==> abc,1e11,1e9)

REACTION (b + c ==> bc,1e11,1e9)

REACTION (b + bc ==> bbc,1e11,1e9)

REACTION (a + bc ==> abc,1e11,1e9)

REACTION (pc ==> p + c,1e8,1e11)

REACTION (a + b --> p,1e-4)

REACTION (abc --> pc,1e-4)

REACTION (compile)

REACTION (show)
----------------------------------------
DGLCODER                Version 11.03.93
----------------------------------------

Reactions:
    A + C --> AC
       AC --> A + C
   A + AC --> AAC
      AAC --> A + AC
   B + AC --> ABC
      ABC --> B + AC
    B + C --> BC
       BC --> B + C
   B + BC --> BBC
      BBC --> B + BC
   A + BC --> ABC
      ABC --> A + BC
       PC --> P + C
    P + C --> PC
    A + B --> P
      ABC --> PC

Species found: A  C  AC  AAC  B  ABC  BC  BBC  PC  P

Rate equations:
     d[A]/dt =  - k1·[A]·[C] + k2·[AC] - k3·[A]·[AC] + k4·[AAC] - k11·[A]·[BC] +
k12·[ABC] - k15·[A]·[B]
     d[C]/dt =  - k1·[A]·[C] + k2·[AC] - k7·[C]·[B] + k8·[BC] + k13·[PC] -
k14·[C]·[P]
    d[AC]/dt =  + k1·[A]·[C] - k2·[AC] - k3·[A]·[AC] + k4·[AAC] - k5·[AC]·[B] +
k6·[ABC]
   d[AAC]/dt =  + k3·[A]·[AC] - k4·[AAC]
     d[B]/dt =  - k5·[AC]·[B] + k6·[ABC] - k7·[C]·[B] + k8·[BC] - k9·[B]·[BC] +
k10·[BBC] - k15·[A]·[B]
   d[ABC]/dt =  + k5·[AC]·[B] - k6·[ABC] + k11·[A]·[BC] - k12·[ABC] - k16·[ABC]
    d[BC]/dt =  + k7·[C]·[B] - k8·[BC] - k9·[B]·[BC] + k10·[BBC] - k11·[A]·[BC] +
k12·[ABC]
   d[BBC]/dt =  + k9·[B]·[BC] - k10·[BBC]
```

```
    d[PC]/dt =  - k13·[PC] + k14·[C]·[P] + k16·[ABC]
     d[P]/dt =  + k13·[PC] - k14·[C]·[P] + k15·[A]·[B]

Jacobian matrix: NJacobi& = 53 JacobiList& = 124
       d(d[A]/dt)/d[A] =  - k1·[C] - k3·[AC] - k11·[BC] - k15·[B]
       d(d[A]/dt)/d[C] =  - k1·[A]
      d(d[A]/dt)/d[AC] =  + k2 - k3·[A]
     d(d[A]/dt)/d[AAC] =  + k4
       d(d[A]/dt)/d[B] =  - k15·[A]
     d(d[A]/dt)/d[ABC] =  + k12
      d(d[A]/dt)/d[BC] =  - k11·[A]
       d(d[C]/dt)/d[A] =  - k1·[C]
       d(d[C]/dt)/d[C] =  - k1·[A] - k7·[B] - k14·[P]
      d(d[C]/dt)/d[AC] =  + k2
       d(d[C]/dt)/d[B] =  - k7·[C]
      d(d[C]/dt)/d[BC] =  + k8
      d(d[C]/dt)/d[PC] =  + k13
       d(d[C]/dt)/d[P] =  - k14·[C]
      d(d[AC]/dt)/d[A] =  + k1·[C] - k3·[AC]
      d(d[AC]/dt)/d[C] =  + k1·[A]
     d(d[AC]/dt)/d[AC] =  - k2 - k3·[A] - k5·[B]
    d(d[AC]/dt)/d[AAC] =  + k4
      d(d[AC]/dt)/d[B] =  - k5·[AC]
    d(d[AC]/dt)/d[ABC] =  + k6
     d(d[AAC]/dt)/d[A] =  + k3·[AC]
    d(d[AAC]/dt)/d[AC] =  + k3·[A]
   d(d[AAC]/dt)/d[AAC] =  - k4
       d(d[B]/dt)/d[A] =  - k15·[B]
       d(d[B]/dt)/d[C] =  - k7·[B]
      d(d[B]/dt)/d[AC] =  - k5·[B]
       d(d[B]/dt)/d[B] =  - k5·[AC] - k7·[C] - k9·[BC] - k15·[A]
     d(d[B]/dt)/d[ABC] =  + k6
      d(d[B]/dt)/d[BC] =  + k8 - k9·[B]
     d(d[B]/dt)/d[BBC] =  + k10
     d(d[ABC]/dt)/d[A] =  + k11·[BC]
    d(d[ABC]/dt)/d[AC] =  + k5·[B]
     d(d[ABC]/dt)/d[B] =  + k5·[AC]
   d(d[ABC]/dt)/d[ABC] =  - k6 - k12 - k16
    d(d[ABC]/dt)/d[BC] =  + k11·[A]
      d(d[BC]/dt)/d[A] =  - k11·[BC]
      d(d[BC]/dt)/d[C] =  + k7·[B]
      d(d[BC]/dt)/d[B] =  + k7·[C] - k9·[BC]
    d(d[BC]/dt)/d[ABC] =  + k12
     d(d[BC]/dt)/d[BC] =  - k8 - k9·[B] - k11·[A]
    d(d[BC]/dt)/d[BBC] =  + k10
     d(d[BBC]/dt)/d[B] =  + k9·[BC]
    d(d[BBC]/dt)/d[BC] =  + k9·[B]
   d(d[BBC]/dt)/d[BBC] =  - k10
      d(d[PC]/dt)/d[C] =  + k14·[P]
    d(d[PC]/dt)/d[ABC] =  + k16
     d(d[PC]/dt)/d[PC] =  - k13
      d(d[PC]/dt)/d[P] =  + k14·[C]
       d(d[P]/dt)/d[A] =  + k15·[B]
       d(d[P]/dt)/d[C] =  - k14·[P]
       d(d[P]/dt)/d[B] =  + k15·[A]
      d(d[P]/dt)/d[PC] =  + k13
       d(d[P]/dt)/d[P] =  - k14·[C]

INTEG (stiff,1e-11,8)

NUMPLOT (100)

TIME (sec)

WIN (0,100000,10000,0.1,0,25e-3,2.5e-3,3e-4)

INIT (a,25e-3,2)

INIT (b,25e-3,4)

PLOT (file)
```